**University of Strathclyde**

**Strathclyde Institute of Pharmacy and Biomedical Sciences**

# DEVELOPMENT OF NON-IONIC SURFACTANT VESICLES FOR INHALED DRUG DELIVERY

**Mireia Puig i Sellart**

**A thesis presented in fulfilment of the requirements for the degree of Doctor of Philosophy**

**January 2016**

‘This thesis is the result of the author’s original research. It has been composed by the author and has not been previously submitted for examination which has led to the award of a degree.’



Mireia Puig

January 2016

## Acknowledgments

This thesis should start by thanking Dr Chris Carter and Prof Alex Mullen for their supervision and guidance whilst carrying out this work. My grateful thanks are also extended to Prof Linda Harvey for her encouraging words during every report review. I would also like to acknowledge Dr Ibrahim Khadra for his endless kindness and support.

Thanks to Prof Colin Suckling, Dr Fraser Scott and Dr Abedawn Khalaf for letting me collaborate with their promising MGBs research. Special thanks to the I-neb scientific team at Philips Respironics: Lucy Hardaker, Graham Matthews, Dr. Ross Hatley and Sara Byrne for their support with the nebulisation studies.

Thanks to the BPU staff for being always so friendly and helpful: Dr Linda Horan, Lee Wheeler, George Walker, Carol Whitehouse, Kevin O'Halloran, and Steven McDonald. A special appreciation goes to all who have helped me one way or another during my research and scientific development: Dr Steven Fort, Dr Catherine Lawrence, Anne Goudie, John Nevin, Maureen Vass, Lynne Kernweiss and Craig Johnston.

I would also like to thank my academic colleagues: Craig Shaw, Muattaz Hussain, Christopher Farmer, John Carruthers, Pila Akrachalanont, Antonella Cano, Cesar Bellota, Sara Filgueira, Emilio Cortes, Stewart Watts, Zhou Zhou, Toke Jonsson, Michelle Armstrong, Marina Castaño, Stuart Woods, Mariam Badawi and Abiy Desta.

In a more personal level, I would like to especially thank Dr Martin van Zyl, he has been a true inspiration for me and a great support during this journey. And, the most significant of my acknowledgements goes to my mum:

*M'agradaria especialment dedicar aquesta tesis a la meva mare:*
*tot el que sóc i tot el que espero ser algun dia, ho dec al seu incondicional suport.*

## Abstract

Non-ionic surfactant vesicles (NIVs) provide similar bioavailability as liposomes but they are associated with higher stability profiles and reduced production cost. However, NIVs formulations are limited by the stability of the encapsulated drug and little is know about their use for inhaled delivery. Therefore, in this study, NIVs for pulmonary delivery were developed and factors, which affected their efficacy and stability, were determined.

The addition of the cryoprotectant sucrose to NIVs containing amphotericin B (AmB-NIVs) allowed the physicochemical characteristics of the vesicles to be maintained upon freeze-drying and rehydration. Those were proven stable up to 4 months and up to 21 days when reconstituted and stored at 4°C. Pulmonary administration of AmB-NIVs was able to supress the progress of visceral leishmaniasis *in vivo* with larger particles being superior to smaller sizes ($p \leq 0.05$ in the liver and spleen).

Incursion of hydroxypropyl-γ-cyclodextrin (HPγCD), rather than sucrose ($p \leq 0.01$), protected empty-NIVs when freeze-dried and rehydrated with different drugs. Therefore, empty-NIVs rehydrated with drugs such as cisplatin or gemcitabine, could be formulated *in situ* evading undesirable drug instability issues.

The effect of using different types of vibrating-mesh nebulisers (active and passive) on the stability of AmB-NIVs was determined. AmB-NIVs properties, like drug entrapment efficiency, were not critically impaired upon nebulisation. The NIVs viscosity, the type of drug nebulised and the inhaler used affected the final aerosolised outcome i.e. aerosol output and aerosol droplet size.

*In vitro* screening of novel minor binders (MGBs) against B16 F10 cells and *L. donovani* identified potential lead compounds. Studies in a murine model of

visceral leishmaniasis showed that intravenous administration of $MGB_{58}$ encapsulated within NIVs reduced the parasite burdens in the liver ($p \leq 0.05$).

In conclusion, NIVs have been optimised to provide a stable and successful inhaled drug delivery platform with enhanced bioavailability, especially to target intracellular diseases such as leishmaniasis.

# Table of contents

## Abbreviations

| | |
|---|---|
| **AAD** | Adaptive aerosol delivery |
| **Ade** | Amide |
| **Adi** | Amidine |
| **AFM** | Atomic force microscopy |
| **Ake** | Alkene |
| **AmB** | Amphotericin B |
| **AmB-CD** | Amphotericin B with hydroxypropyl-γ-cyclodextrin |
| **AmB-NIVs** | Amphotericin B within non-ionic surfactant vesicles |
| **Ane** | Amine |
| **ANOVA** | Analysis of variance |
| **API** | Active pharmaceutical ingredient |
| **ARRIVE** | Animal research: reporting of *in vivo* experiments |
| **Atm** | Atmosphere |
| **AUC** | Area under the curve |
| **B16-F10-luc** | Luciferase expressing B16-F10 cell line |
| **BLI** | Bioluminescence |
| **CF** | Cystic fibrosis |
| **CFC** | Chlorofluorocarbon |
| **Cis** | Cisplatin |
| **Cis-NIVs** | Cisplatin within non-ionic surfactant vesicles |
| **CLI** | Chemiluminescence |
| **COPD** | Chronic obstructive pulmonary disease |
| **CPP** | Critical packing parameter |
| **Cyg** | Cyanoguanidine |
| **$D_{aer}$** | Aerodynamic diameter |
| **DCP** | Dicetyl phosphate |
| **DDTC** | Sodium diethyldithiocarbamate |
| **$D_g$** | Geometric diameter |
| **Dha** | Dihydroxyalkyl |
| **DLS** | Dynamic light scattering |
| **Dmap** | Dimethylaminopropyl |
| **DMEM** | Dulbecco's modified eagle medium |
| **Dmh** | Dimethylhydrazine |
| **DMSO** | Dimethyl sulfoxide |
| **DPI** | Dry powder inhaler |
| **DRV** | Dehydration-rehydration method |
| **DSC** | Differential scanning calorimetry |
| **EE** | Entrapment efficiency |

| | |
|---|---|
| **ELSD** | Evaporative eight scattering detector |
| **$FEV_1$** | Forced expiratory volume in one second |
| **FFEM** | Freeze fracture electron microscopy |
| **FPF < 5 μm** | Fine particle fraction < 5 μm |
| **Gem** | Gemcitabine |
| **Gem-NIVs** | Gemcitabine within non-ionic surfactant vesicles |
| **GSD** | Geometric standard deviation |
| **HFA** | Hydrofluoroalkan |
| **HLB** | Hydrophilic-lipophilic balance |
| **HP-CD** | Hydroxypropyl-cyclodextrin |
| **HPH** | High-pressure homogenisation |
| **HPLC** | High-performance liquid chromatography |
| **HPαCD** | Hydroxypropyl-α-cyclodextrin |
| **HPβCD** | Hydroxypropyl-β-cyclodextrin |
| **HPγCD** | Hydroxypropyl-γ-cyclodextrin |
| **$IC_{50}$** | Half maximal inhibitory concentration |
| **ICH** | International conference on harmonisation guideline |
| **Ip** | Intraperitoneal |
| **IS** | Internal standard |
| **IV** | Intravenous therapy |
| **LABA** | Long acting $\beta_2$ agonist |
| **LAMA** | Long acting muscarinic antagonist |
| **Luc** | D-luciferin firefly potassium salt |
| **Luc-NIVs** | D-luciferin within non-ionic surfactant vesicles |
| **LV82-luc** | Luciferase expressing *Leishmania donovani* (LV82 strain) |
| **mAU** | Milli absorbance unit |
| **Mdmap** | Methylated dimethylaminopropyl |
| **MGB-NIVs** | Minor grove binder within non-ionic surfactant vesicles |
| **MGBs** | Minor groove binders |
| **MMAD** | Mass median aerodynamic diameter |
| **MMD** | Mass median diameter |
| **Mmor** | Methylated morpholine |
| **Mor** | Morpholine |
| **MPO** | Myeloperoxidase |
| **MSLI** | Multi-stage liquid impinger |
| **n.a.** | Not-applicable |
| **NaCl** | Sodium chloride |
| **Nalk** | Nitro alkene |
| **NaOH** | Sodium hydroxide |
| **NGI** | New generator impactor |
| **$Ni(DDTC)_2$** | Complex between nickel chloride and diethyldithiocarbamate |

| | |
|---|---|
| **$NiCl_2$** | Nickel chloride |
| **NIV** | Non-ionic surfactant vesicle |
| **n.p.** | Not present |
| **NSCLC** | Non-small-cell lung cancers |
| **O** | Oral therapy |
| **Omor** | N-oxide morpholine |
| **PBS** | Phosphate buffer saline pH 7.4 |
| **Pdi** | Polydispersity index |
| **Pip** | Piperazine |
| **PL** | Power level related to I-neb |
| **pMDI** | Pressurised metered-dose inhaler |
| **Pt** | Platinum compound |
| **$Pt(DDTC)_2$** | Complex between cisplatin and diethyldithiocarbamate |
| **Pyol** | Pyrrolidine |
| **Pyr** | Pyrrole |
| **Pyri** | Pyridine |
| **$R^2$** | Correlation coefficient |
| **Rt** | Retention time |
| **SCLC** | Small-cell lung cancer |
| **Sol** | Solution |
| **Surfactant** | Tetra-ethylene glycol mono n-hexadecyl ether |
| **TBM** | Tidal breathing mode |
| **TEM** | Transmission electron microscopy |
| **$T_g$** | Glass transition temperature |
| **$T_g'$** | Glass transition temperature of the maximally freeze-concentration fraction |
| **Thz** | Thiazole |
| **TIM** | Targeted inhalation mode |
| **TMDSC** | Temperature-modulated differential scanning calorimetry |
| **Tm** | Melting temperature |
| **UV** | Ultraviolet detector |
| **WVL** | Wavelength |
| **ZP** | ζ-potential |

# CHAPTER 1. GENERAL INTRODUCTION

## 1.1. Lung related diseases

One in four residents in the United Kingdom is affected by a lung related disease (British Lung Foundation, 2014). The most common lung disorders are asthma, chronic obstructive pulmonary disease (COPD), cystic fibrosis (CF), lung infections and lung cancer. Respiratory diseases are among the most common causes of death and account for 15 % of total deaths in the European Union, following cardiovascular diseases and non-respiratory cancers. In addition, more than 6 million hospital admissions a year are related to respiratory diseases in Europe and their clinical cost exceeded £272 billion in 2012 (European Respiratory Society, 2012).

Asthma is a common heterogeneous group of conditions that result in inflammation of the airways with episodes of bronchial obstruction. The development depends on genetic and/or environmental factors. The exposure to indoor allergens or outdoor air pollutants are thought to have a major impact (Sears, 2014). Patients with asthma may have low forced expiratory volume in one second ($FEV_1$). These levels generally go back to normal after inhalation of a fast-acting inhaled $\beta_2$ agonists, such as salbutamol. Further exacerbations are prevented or ameliorate by inhalation of long-acting corticosteroids, such as budesonide. Alternative treatments are leukotriene receptor antagonists, long acting $\beta_2$ agonists (LABA), theophylline or oral corticosteroids. However, the success of inhaled asthma treatment is limited by the patient adherence to the medication (Martinez and Vercelli, 2013).

COPD is a group of obstructive lung diseases related to degenerative emphysema or chronic asthmatic bronchitis. Exposures to tobacco smoke or air pollutants are the most common causes of COPD. Long-term exposure to these irritants triggers an inflammatory response in the lungs resulting in narrowing or damage to the airways. Chronic bronchitis is a form of COPD characterised with coughing spells that may be accompanied by phlegm production and

breathlessness. COPD is diagnosed when patients present poor spirometry results (low $FEV_1$) and contrary to asthma, the lung function test do not improve after the administration of $\beta_2$ agonists. There is no cure for COPD, however the symptoms can be treated and the progression of the disease delayed (Brody *et al.*, 2012). Decreasing the exposure to the irritant agents is the first step of the treatment, in particularly by smoking cessation. Inhaled treatment with $\beta_2$ agonists and anticholinergics (such as ipratropium) are commonly used. And long acting $\beta_2$ agonists (LABA), such as salmeterol; long acting muscarinic antagonists (LAMA), such as tiotropium bromide; or inhaled corticosteroids are also employed (Graham-Rowe, 2012). The decline in smoking in European and American countries has lowered the prevalence of COPD. However, in parts of the world, such as China, where smoking culture is increasing, the prevalence of COPD is expected to grow (Hughes, 2012).

Cystic fibrosis (CF) is an autosomal recessive genetic disorder that affects the structure of the mucus. It is the most deadly genetic disorder affecting the Caucasian population (O'Sullivan and Freedman, 2009). The mucus in CF patients is thick and sticky, and it blocks different conduits in the body located in the lungs and the digestive system. Mutations in the gene that encodes for the CF transmembrane conductance protein are responsible for the disease. This protein is involved in regulating the levels of sodium and chloride in epithelial and blood cells. Therefore, when this protein is not functional, the mucus secretions become thick. The symptomatology of the disease includes cough, recurring infections and poor weight gain. There is no cure for CF and patients often contract lung infections such as *Pseudomonas aeruginosa*. Those conditions require treatment with antibiotics such as azithromycin or colistin (Collins, 2009). Bronchodilators are often used to expand the patient airways but the ultimate therapeutic option for CF patients with declined lung function is a double lung transplant (Kesser and Geller, 2009).

There are a variety of infections that affect the lungs and respiratory airways, for example pneumonia, aspergillosis or tuberculosis. Pneumonia is an infection of the lungs affecting the alveoli and is commonly caused by bacteria or viruses and less frequently produced by fungi or parasites. The symptomatology associated with pneumonia normally includes chest pain, cough, pyrexia and dyspnea. In the case of bacterial pneumonia, the most important pathogen is *Streptococcus pneumonia*. This infection can sometimes be prevented with vaccination programs (Liesenborghs *et al.*, 2013) or treated with oral antibiotics such as amoxicillin. On the other hand, fungal pulmonary infections often occur when atmospheric infective spores are inhaled. The majority of aspergillosis cases occur in patients with other lung related diseases, such as TB and COPD or if the person is receiving immunosuppressive drugs as part of a chemotherapy for other conditions such as leukaemia or AIDS (Segal, 2009). The fungal infection is firstly visualised when a lung halo appears in a lung X-ray or CT scan and antifungal agents used to treat aspergillosis include voriconazole or amphotericin B (AmB; Beyer *et al.*, 1994).

Tuberculosis (TB) is a type of pneumonia specifically caused by *Mycobacterium tuberculosis*. Yearly, TB causes over 1.7 million deaths worldwide despite the fact that the first anti-TB agents were discovered more than half a century ago (Lawn and Zumla, 2011). The high mortality of the disease is believed to be related with HIV co-infection and drug resistant *Mycobacterium* (Gandhi *et al.*, 2010; Lönnroth *et al.*, 2010). TB is transmitted through airborne droplets produced when people with active pulmonary disease cough, whereas people with latent TB infections are thought to be non-contagious. The symptomatology of TB includes cough with sputum, fever, night sweats and weight loss. The disease treatment is difficult and requires administration of antibiotics daily, usually in combination, for a minimum of 6 months with oral administered drugs such as rifampicin, isoniazid, ethambutol and/or pyrazinamide. Inhaled delivery of anti-TB agents have been under investigation but are yet to be clinically approved (Misra *et al.*, 2011). The disease can also be

prevented by Bacille Calmette-Guérin (BCG) vaccination, which is the most widely used vaccine in the world but only effective up to 80 % of the population (Andersen and Doherty, 2005).

Cancer is considered a major health problem and is responsible for approximately 13 % of the deaths worldwide with an incidence of 13 million new cases every year (World Health Organisation, 2013). Lung cancer is one of the most frequent cancers followed by breast, colorectal, stomach and prostate cancer. In terms of deaths per year, lung cancer causes around 1.4 million deaths/ year worldwide. Lung cancers are divided into two major groups based on features visualised using microscopy: small-cell lung cancer (SCLC) or non-small-cell lung cancer (NSCLC). The later includes squamous-cell carcinomas, adenocarcinomas and large-cell carcinomas. SCLC corresponds to about 20 % of all lung cancers; it is strongly associated with smoking and it is very aggressive, causing early metastasis. Patients with SCLC are normally men, who are older than 70, have been smokers at some point of their life and have a history of pulmonary and/or cardiovascular problems (Van Meerbeeck *et al.*, 2011). The prognosis for SCLC is poor with a median survival without treatment of 2 to 4 months from diagnosis (Hoffman *et al.*, 2000). SCLC tumours typically have a central location in the lungs and are therefore difficult to surgically remove. Only stage I patients (according to the TNM classification; International Union Against Cancer, 2009) might be eligible for surgery and these patients are also given adjuvant chemotherapy (Table 1.1). Patients with stages II to IV of SCLC are mainly treated with chemotherapy and/or radio-chemotherapy. The first-line chemotherapy treatment is a platinum based combination of cisplatin or carboplatin with etoposide or irinotecan (Schmittel *et al.*, 2011). Topotecan is only used as a second-line treatment drug when the disease relapses in the 90 days after the end of the first-line therapy (Ardizzoni *et al.*, 2014).

NSCLCs account for 80 % of all lung cancers cases with adenocarcinomas being the most prevalent (Goldstraw *et al.*, 2011). Commonly, an adenocarcinoma

tumour is symptomless and located in the periphery of the lungs but quickly develops into a metastatic cancer. Adenocarcinoma is not associated with smoking and occurs more frequently in non-smokers. In the contrary, squamous cell carcinomas occur in smokers, are located in the centre of the lungs and have a low metastasis rate. Moreover, squamous cell carcinomas are associated with pneumonia, haemoptysis and lung lobar collapse. Another type of NSLC is large-cell carcinomas which are formed from large rounded cells that group in peripheral masses (Hoffman *et al.*, 2000). Although surgery is considered the first choice of treatment for stage I NSCLC patients, adjuvant chemotherapy is also used. Whereas, for advanced NSCLC, chemotherapy remains the main treatment. For instance, the first-line chemotherapy is a platinum-based combination, using etoposide and cisplatin. Moreover, drug treatments with third generation chemotherapy agents (docetaxel, gemcitabine, paclitaxel or vinorelbine) as a single treatment or in combination with a platinum drug are also used as second line treatment (Table 1.1).

Cisplatin is an inorganic chemotherapy compound composed by two chloride and two ammonia molecules that bind to a central platinum atom. It is the lead treatment for lung cancers and it is also used to treat other types of cancer such as bladder, cervical and testicular cancers. In the extracellular fluid, cisplatin exist in the none-reactive form due to the high concentration of chloride molecules. Cisplatin enters the intracellular matrix by passive diffusion or protein-mediated transport by the copper transporter protein CTR1 (Figure 1.1). Once in the intracellular fluid, the chlorides are sequentially hydrolysed and the resulting positive complex binds to DNA bases in the DNA major groove, specially the N7 position of guanidine. Then, the other chloride ligand hydrolyses and creates a crosslink bound to another guanine. This adduct interferes with cell mitosis or DNA repair causing cell apoptosis within the cell that has taken up the drug (Lippert, 1999). Nonetheless, treatment with cisplatin is limited because of its inherent adverse side effects. The associated nephrotoxicity is commonly monitored with creatinine clearance measures.

Other undesirable effects include nausea, vomiting, ototoxicity, electrolyte distribution, myelotoxicity and anaemia. Initially, a good response is observed with cisplatin treatment but the majority of patients eventually relapse due to development of drug resistances within the tumour cells (Gately and Howell, 1993; Casares *et al.*, 2012). Moreover, another chemotherapy agent used for lung cancer treatment is gemcitabine. This is a nucleoside analogue of deoxycytidine with two extra fluorine atoms. Gemcitabine can have multiple toxic effects on cells, which result in cell apoptosis (Noble and Goa, 1997). For instance, it can replace cytidine molecules of DNA during replication and it can bind to ribonucleotide reductase and inhibit its enzyme activity. Besides, gemcitabine is rarely administered as monotherapy and it is usually given in combination with platinum compounds (Rinaldi *et al.*, 2000; Table 1.1).

Treatment of respiratory diseases by the pulmonary route is beneficial, as it minimised drug exposure of non-target tissues. This is especially important for drugs with inherent toxic side effects or for expensive formulations. The utility of this approach has been demonstrated in asthma and COPD treatment, which both rely on inhaled therapy.

**Table 1.1** Summary of some of the drugs used to treat lung cancers (Pt, platinum compound; SCLC, small-cell lung cancer; NSCLC, non-small-cell lung cancer; IV, intravenous therapy; O, oral therapy).

| Drug | Mechanism of action | Treatment | Regimen | Route | Reference |
|---|---|---|---|---|---|
| **Carboplatin** | Pt compound that blinds to DNA | SCLC and NSCLC | Pt-based doublet, first and second line therapy | IV | (Van Meerbeeck *et al.*, 2011) |
| **Cisplatin** | Pt compound that blinds to DNA | SCLC and NSCLC | Pt-based doublet, first and second line therapy | IV | (Lippert, 1999) |
| **Docetaxel** | Microtubule stabilizing agent | NSCLC | Combined with Pt | IV | (Casal *et al.*, 2011) |
| **Doxorubicin** | Inhibits topoisomerase II | SCLC and NSCLC | Second line treatment | IV | (Singhal *et al.*, 2006) |
| **Etoposide** | Inhibit topoisomerase II | SCLC | First-line combined with Pt (non-Asian patients) | O | (Schmittel *et al.*, 2011) |
| **Gemcitabine** | Nucleoside analog | NSCLC | In combination with Pt | IV | (Rinaldi *et al.*, 2000) |
| **Irinotecan** | Inhibits topoisomerase I | SCLC | First-line combined with Pt (Asian patients) | IV | (Schmittel *et al.*, 2011) |
| **Paclitaxel** | Microtubule stabilizing agent | NSCLC | Frist line treatment single or combined with Pt | IV | (Gridelli *et al.*, 2001) |
| **Topotecan** | Topoisomerase I inhibitor | SCLC | Second line therapy | IV or O | (Ardizzoni *et al.*, 2014) |
| **Vinorelbine** | Microtubule destabilizing agent | NSCLC | First line treatment single or combined with Pt | IV or O | (Sorensen *et al.*, 2015) |

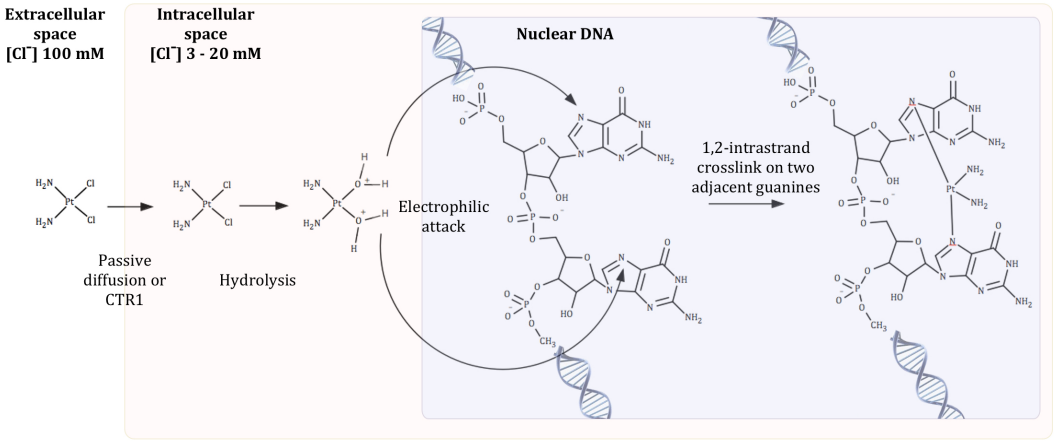


**Figure 1.1** Cisplatin reaction with DNA to form 1,2-intrastrand crosslink on two adjacent guanidines. Inactivated cisplatin (with both chloride molecules) enter the intracellular matrix by passive diffusion or copper transporter protein (CTR1). Due to the low chloride molecule concentration, cisplatin is hydrolysed and the positive complex binds to two adjacent guanidines (N7 location) to form a 1,2-intrastand crosslink adduct (interpreted from Lippert, 1999).

## 1.2. Inhaled therapy

Inhalation therapy has been recognised as a valuable way of administering drugs for a long time. The first reported case dates from the Egyptian civilisation (*c.* 1554 BC) where inhalation of black henbane was used to treat breathless patients (Clarke, 1988; Smyth and Hickey, 2011). Since then, inhalation therapy has been widely used to treat local lung conditions such as asthma or COPD. Furthermore, drug delivery to the lungs for the treatment of systemic diseases has also been investigated (Patton and Byron, 2007).

### 1.2.1. Lung anatomy and physiology

Centric to the respiratory system are the lungs, where the oxygen and carbon dioxide gas-exchange occurs. The lungs act as a ventilating pump, facilitated by the movement of the chest wall and the respiratory muscles. Anatomically, the respiratory system is divided into upper respiratory tract (nasal cavity and pharynx) and lower respiratory tract (larynx, trachea, bronchi, bronchioles and alveoli). However, in terms of physiology, the respiratory tract is divided into two general areas according to conducting or respiratory purposes (Figure 1.2). The conducting airways cover the region from the mouth/nose area to the terminal bronchioles and include the trachea, bronchi and bronchioles. In this area, no gas-exchange occurs since its principal purpose is to transport the air from the environment to the respiratory region. Furthermore, conducting airways modify the humidity and the temperature of the air so that this equilibrates to the respiratory environment conditions. On the other hand, the respiratory airways are made up of terminal bronchioles, respiratory bronchioles and alveolar ducts and sacs, with the primary propose of gas exchange. In this area, oxygen from the air is taken up into the blood and carbon dioxide is released from the body and exported in the opposite direction. The respiratory system is characterised with a high surface area that increases from 2 $m^2$ in the upper airways to 103 $m^2$ in the distal airways. At the same time, the

cell thickness decreases from 60 μm in the bronchi to 0.1 μm in the alveoli (Figure 1.3). These two characteristics (wider surface area and thinner membranes) facilitate the gas-exchange in the alveoli (Groneberg *et al.*, 2003; Smyth and Hickey, 2011). Moreover, the human lung architecture follows a symmetric dichotomously branching model (Figure 1.2). This means that each branch leads to a new generation of airways. For example, the trachea is generation 0 and bifurcates into two bronchi, which are generation 1. This process continues up to generation 17 in the conducting airway and up to generation 23 in the alveoli (Lucangelo *et al.*, 2008). As the branching progresses the surface area increases, the airways diameter decreases and the airflow velocity decelerates.

The pulmonary epithelium contains a variety of cells that are specific to the different regions of the respiratory tract. For instance, the bronchus consists of ciliated, goblet, brush, Clara and serous cells whereas the alveoli epithelium contains type I and type II pneumocytes and macrophages (Figure 1.3). Ciliated cells are predominant in the trachea and bronchi regions and there are approximately 200 cilia per cell. Cilia are hair-like protections that sweep microbes and debris up and out of the lungs. Although the tracheobronchial airways are completely covered with cilia, these are absent in the alveolar region. Moreover, scattered between the cilia, are goblet cells that secrete mucus. This is a complex mixture of lipids and glycoproteins such as mucins, which act as a barrier and protect the airways (Schuster *et al.*, 2013). The most common cells in the alveolar epithelia are pneumocytes type I. Type I pneumocytes are very thin and provide the required surface area for gas-exchange. Whereas type II pneumocytes store, secrete and reutilise pulmonary surfactant. Pulmonary surfactant consists of a mixture of lipoproteins and lipids such as dipalmitoylphosphatidylcholine. Its main propose is to reduce the surface tension throughout the lungs and to help the oxygen penetrate to the blood, whilst protecting the alveoli from collapsing (Hillery *et al.*, 2001). Alveolar macrophages, which make up 3 per cent of alveolar cells, have a key

role in immunosurveillance of the respiratory tract since this is continuously exposed to environmental microbial challenges. Resident alveolar macrophages recognise bacteria using their toll-like receptors and once activated they secrete cytokines that recruit neutrophils to the infection site and aid in pathogen removal (Westphalen *et al.*, 2014). Phagocytosed particles or pathogens are digested and cleared by the lymphatic system or removed via the mucociliary escalator (Landsman and Jung, 2007).

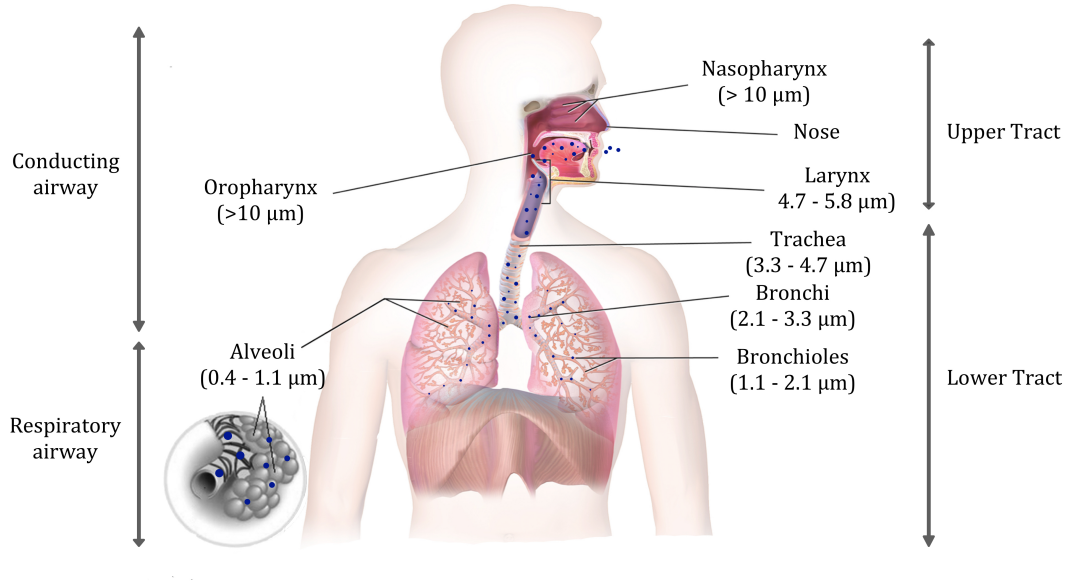


**Figure 1.2** Areas of the respiratory system divided by physiological characteristics (conducting and respiratory airways) or anatomical parts (upper and lower tract). Inhaled aerosols (represented as blue circles) are deposited in different areas of the respiratory system according to their droplet size (in brackets; adapted from Hillery *et al.*, 2001; Patton and Byron, 2007 and Hu *et al.*, 2008).

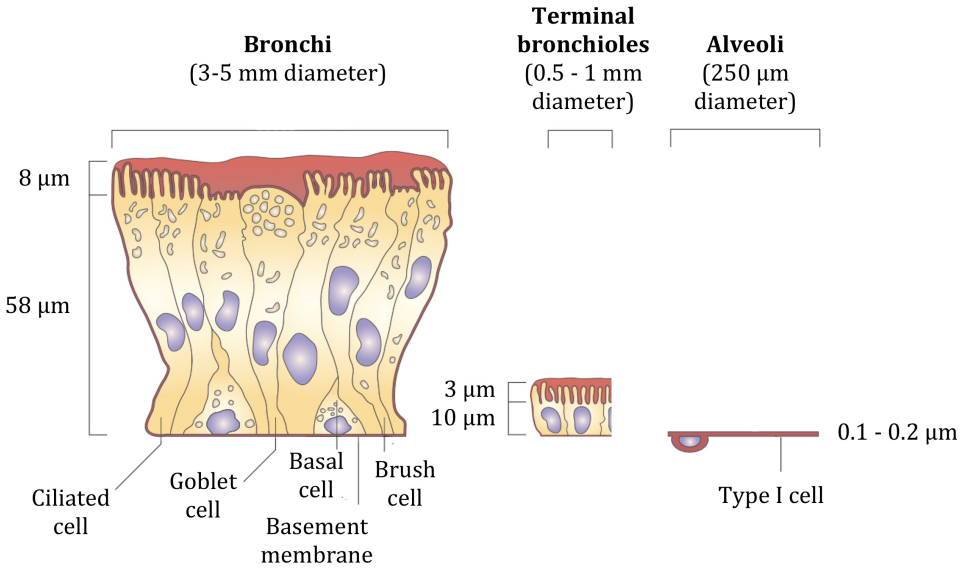


**Figure 1.3** Types of cells present in the different parts of the respiratory system: bronchi, bronchioles and alveoli (adapted from Patton and Byron, 2007).

### 1.2.2. Pulmonary drug delivery

Pulmonary drug delivery presents several advantages over other delivery routes such as oral or intravenous. For example, inhalation of drugs is a non-invasive technique that improves patient compliance by reducing multiple-daily injections. Marcia and Donald (2007) confirmed increased patient treatment satisfaction using inhaled insulin compared to injected formulations. Furthermore, locally acting drugs administered by inhalation require fewer doses to produce the same effect than using oral administration. Hence, reducing the possible side effects associated with a high dose systemic exposure. For example, 2-4 mg of oral salbutamol is therapeutically equivalent to 0.1-0.2 mg of the inhaled compound (Labiris and Dolovich, 2003). Another advantage is the quick onset of action of the inhaled drugs. The drug peak effect occurs much quicker compared to oral treatment due to the wide lung surface and the highly vascular area. Moreover, inhaled therapy is associated with moderate permeability attributable to the thin epithelial barrier (Mathias and Hussain, 2010). Drug delivery to the lungs is amenable to both small molecules and macromolecules and most drugs are not denaturised after pulmonary delivery hence they can be absorbed intact (Hastings *et al.*, 1992). Besides, drugs administered by inhalation avoid first pass metabolism in the liver and the amount of metabolising enzymes such as CYP450 is lower in the lungs compared to other organs (Colombo *et al.*, 2012).

The ability of an aerosol drug particle to deposit into the lungs depends on its capacity of evading the lungs natural defences. This includes, highly branched airway geometry, humidity, mucociliary clearance and alveolar macrophages (Groneberg *et al.*, 2003). Aerosol particle size is a key parameter in defining the final drug location within the lungs (Figure 1.2). Small aerosols are distributed in the peripheral airways whereas larger aerosols are deposited in the central area of the lungs. Depending on their dimensions, aerosol particles can be deposited in the lungs by inertial impaction, gravitational sedimentation or

Brownian diffusion. Inertial impaction predominates in the upper tracheobronchial region for large particles (> 10 μm). Those particles, carrying a big momentum, are not able to follow the fast airflow in the conducting airways and impact into the walls. Particles that impact on the mucus barrier are then cleared by the mucociliary escalator system. This uses the ciliated epithelium to move the mucous and particles towards the pharynx, which are then engulfed or expectorated (Clarke, 1988). Sedimentation of smaller aerosol particles (< 5 μm) is observed in the bronchi and bronchioles. Brownian diffusion, which is the random motion of the particles that occurs after their collision with gas molecules, is observed in the alveoli, where the air velocity is negligible. Although specific prediction of particle deposition is challenging due to variations between individuals, it can be stated that aerosol particles between 1 and 5 μm are likely to reach the lower respiratory system (Byron, 1986). Nonetheless, submicron particles cannot be deposited in the airways as they are easily breathed out (Asking and Olsson, 1997). The direct relationship between aerosol size and drug deposition has also been observed clinically. Zanen *et al.* (1994) aerosolised salbutamol with aerosol particles sizes of 1.5 μm, 2.8 μm and 5.0 μm. Asthmatic patients treated with an aerosol particle size of 2.8 μm obtained a superior vasodilator effect than 5.0 μm or 1.5 μm treatments. Moreover, the optimal site of aerosol deposition also depends on the disease to be targeted. For instance, $\beta_2$ receptors are located in the bronchi and bronchioles whereas the muscarinic M3 receptors are predominant in the conducting airways. Therefore, the $\beta_2$ agonist salbutamol should be delivered to the peripheral areas (Zanen *et al.*, 1994) whereas the muscarinic antagonist ipratropium bromide needs deposition in the conducting airways (Johnson *et al.*, 1989). For the treatment of systemic diseases, the inhaled drug should be deposited in the peripheral areas that are rich in alveoli. In those regions, systemic absorption is facilitated due to a thin alveolar-vascular permeable barrier (Patton and Byron, 2007).

Moreover, drug deposition can be altered by pathological bronchoconstriction, inflammation or airway obstruction. Respiratory diseases, such as CF or lung cancer, change the architecture of the airways. Those abnormal variations have a direct effect on the disposition of aerosol drugs leading to uneven aerosol particle distribution (Dolovich *et al.*, 1976; Nahar *et al.*, 2013).

The development of an effective inhaled therapy depends on the pharmacology of the active ingredient and the aerosolisation characteristics. In particular, the final pulmonary deposition of the aerosol droplets has a strong relation with the type of inhaler device used.

### 1.2.3. Inhalers for pulmonary delivery

Inhaler devices have evolved over time in conjunction with general technology and innovation, this leading to a wide range of pulmonary inhalers on the market (Dolovich and Dhand, 2011). New generation inhalers (i.e. smart nebulisers) are more efficient compared with previous devices (i.e. continuous nebulisers) and they incorporate features such as better portability and ease of use (Lavorini *et al.*, 2014). Aerosol delivery devices can be classified into pressurised metered-dose inhalers (pMDIs), dry powder inhalers (DPIs) and nebulisers.

Pressurised metered-dose inhalers (pMDIs) are the most widely used inhalers for the treatment of asthma or COPD (Graham-Rowe, 2012; Martinez and Vercelli, 2013). They are small in size, economic to produce and the container can incorporate multiple dosing. A pressurised propellant is normally used to generate the aerosol and a mixture of the propellant gas and the drug is transferred from a liquefied canister through a nozzle at high velocity (> 30 m/s; Stein *et al.*, 2014). Then the propellant quickly evaporates and the residual non-volatile drug is inhaled. The first propellants used were chlorofluorocarbons (CFCs) but they were banned due to ozone layer damaging

effects. Hydrofluoroalkanes (HFAs) have substituted CFCs, as they do not contain chlorine. Despite these challenging changes, the redesign of pMDIs to adopt the new environmental laws did not affect the clinical therapeutic outcome (Hawksworth *et al.*, 2002). In general, only around 10 % of the emitted dose by a pMDI is deposited in the lungs. The rest of the aerosol impacts into the oropharyngeal region due to high aerosol velocity and large aerosol size (Newman *et al.*, 1991). Patients are encouraged to use the slow inhalation manoeuvre followed by a breath hold. This is to maximise lung deposition and allow inhaled particles suspended in the airways to settle. One of the drawbacks associated with pMDIs is the requirement for hand-mouth patient coordination. To eliminate these limitations, spacer chambers were developed and categorised as add-on devices (McFadden, 1995). Spacers create a holding chamber that allows the retention of the aerosol for a prolonged time and increase the generation of fine aerosol particles since larger droplets deposit into the chamber walls (Barry and O'Callaghan, 1996). As a result, the use of pMDIs with a spacer chamber is easier for infants and elderly population. Moreover, the production of a breath-actuated pMDIs tackled the problems related to breath-device coordination.

Dry powder inhalers (DPIs) eliminate some of the drawbacks of the pMDIs such as user coordination difficulties and the presence of CFCs. In DPIs, the drug is kept in a loose powder form and only delivered by the force of the patient inspiration. The biggest challenge in DPIs is to formulate the therapeutic powder in an optimal particle size. In order to ease the process, the drug entity is normally mixed with a carrier, with lactose being the most common. Moreover, if the drug powder does not disaggregate properly during inhalation, it could lead to poor lung deposition. To overcome this issue, turbulent airflow to break the aggregates should be created in the container. Or force control agents like magnesium stearate, should be added. However, those high-resistance inhalers might require a strong inspiratory effort from the patient (Kesser and Geller, 2009). There are different types of DPIs on the market:

single-dose charged by the patient (e.g. HandiHaler®), pre-charged multi dose blister pack (e.g. Diskhaler®) and the reservoir type (e.g. Turbohaler®; Dolovich and Dhand, 2011).

Nebulisers are inhalers that convert liquid formulations into an aerosol mist. Therefore, they can aerosolise most of the drugs solutions and suspension with higher deposited doses than pMDIs and DPIs. There is no need for patient breath coordination when nebulisers are used, since the aerosol mist is inhaled during normal tidal breathing. Four main types of nebuliser are commercially available: jet nebulisers, ultrasonic nebulisers, soft mist inhalers and vibrating-mesh nebulisers (Table 1.2). Nebulisers are also preferred in early stages of inhaled formulation development because novel drug solutions and suspension can be nebulised without requiring the same control of particle size necessary for DPIs or working with a pressurised propellant as for pMDIs (Darwis and Kellaway, 2001; Abd-Elbary *et al.*, 2008; Alsaadi *et al.*, 2012; Ong *et al.*, 2014).

Air-jet nebulisers or pneumatic nebulisers require a compressed gas to aerosolise the formulation, either air or oxygen. This gas goes through a narrow orifice and a zone of low pressure is created. This causes the liquid formulation to rise up from the reservoir and aerosol droplets are formed. Air-jet nebuliser performance depends on the design of the device. For example, baffled surfaces within the device are positioned so larger aerosol droplets impinge upon them to produce smaller droplets (Niven and Brain, 1994). Jet nebulisers are bulky and not portable due to the requirement of compressed air to generate the aerosol. In addition, the nebulisation time is the longest of the different types of nebulisers. Moreover, high amounts of drug are lost to the environment during expiration, which might lead to a suboptimal patient dosing and involuntary drug exposure of health professionals. Besides, the high amount of dead volume left in the reservoir is also a concern since this can be as much as 2 ml from a typical 5 ml dose (Hardaker and Hatley, 2010).

Ultrasonic nebulisers contain a piezoelectric crystal that oscillates at high frequencies (> 1 MHz). The oscillator energy generated is transmitted to the liquid formulation and results in the formation of a fine slow-moving mist of aerosolised droplets. The size of the droplets produced is related to the oscillation speed of the nebuliser and the surface tension of the liquid (Smyth and Hickey, 2011). Because these nebulisers do not require compressed air, they are more portable and quieter than air-jet nebulisers. Moreover, the dead volume is smaller and the treatment time is faster. However, one of the main concerns for ultrasonic nebulisers is the temperature rise in the liquid reservoir. This can be up to 20°C above the ambient temperature, which needs to be taken into account when nebulising temperature sensitive drugs (Katial *et al.*, 2000).

Soft mist nebulisers aerosolise the pharmaceutical liquid by extruding it under pressure through an array of holes. The energy required to generate the aerosol is transmitted by the mechanical movement of a spring. For example, AER$_x$™ has been investigation for the use of inhaled insulin (Schuster *et al.*, 1997) and morphine (Dershwitz *et al.*, 2000). Another soft mist nebuliser is Respimat® Soft Mist™, which has already been approved for the inhalation of tiotropium (Dalby *et al.*, 2011). However, Respimat® has been associated with a 30 % increased risk of mortality in patients with COPD compared to similar treatment with HandiHaler®. This suggests that further studies are required to re-establish the dose-efficacy balance for the new soft-mist nebuliser (Verhamme *et al.*, 2013).

Vibrating-mesh nebulisers contain a piezoelectric element synchronised with a laser-bored mesh plate. The microscopic mesh apertures provide the aerosol cloud with a small and homogeneous aerosol particle size. Vibrating-mesh nebulisers are portable, quiet and fast. Moreover, this type of nebuliser results in little drug loss, negligible residual liquid and high lung deposition. Vibrating-mesh nebulisers can operate actively or passively. In the active mode, the vibrational element makes the mesh plate vibrate and pump fluid from a small

volume reservoir throughout the holes (e.g. Aeroneb Go®). The OnQ™ technology from Aerogen® contains over 1,000 holes surrounded by the vibrational element that makes them move up to 128,000 times per second. Each hole acts like a micro pump extruding the liquid through and creating a fine aerosol cloud (Aerogen, 2014). In the passive vibrating-mesh mode, the mesh remains stationary and the piezoelectric element makes a transducer horn that vibrates and pulses the fluid through a mesh (e.g. I-neb® or Omron MicroAir NE-U22®). The vibration of the horn creates an oscillating pressure over the liquid located at the entrance of the trumpet shape nozzles. As a result, the liquid starts flowing through the mesh as an aerosol. In general, vibrating-mesh devices are highly dependent on formulations physicochemical properties such as viscosity or ion concentration (Ghazanfari *et al.*, 2007).

When a nebuliser generates an aerosol in continuous mode, a large proportion of drug is lost during exhalation. This can be solved through coordinating nebulisation with inspiration. For example, in breath-enhanced inhalers drug delivery is increased during inspiration and decreased during exhalation. Other examples are breath-actuated inhalers, where the aerosol is totally turned off during exhalation. These technologies are incorporated to newer generations of smart nebulisers such as the adaptive aerosol delivery inhalers (AAD; Philips Respironics, Chichester, UK). AAD nebulisers administer the dose to a specific portion of the inhalation resulting in increased clinical efficacy and superior patient compliance (Rijnders *et al.*, 2008; Goodman *et al.*, 2010). In addition, the AAD technology also provides feedback information about correct use of the device to the patient and healthcare personal (Dhand, 2010). This has demonstrated excellent patient adherence even in children populations (McNamara *et al.*, 2009). Examples of commercially available AAD nebulisers are the vibrating-mesh I-neb® and the jet nebuliser Pro-dose®. AAD can be used in the tidal breathing mode (TBM) or in the targeted-inhalation mode (TIM; Figure 1.4). In the TBM mode, the AAD nebulisers establishes the shape of the tidal breathing patent of the patient during the first three breaths. Then, uses

this information to nebulise drug only during the first half of each inspiration. This monitoring continues throughout the inhalation treatment and stops the nebulisation when the breathing is interrupted. TIM is similar to TBM but it was additionally refined to slow down the patient's inspiration rates so as to increase distal deposition. For example, in order to decrease the inspiration flow rate to 20 L/min, a high-resistance mouthpiece was incorporated in the I-neb®. With the TIM mode, the patients could inhale for as long as 9 seconds where the nebuliser aerosolised during the first 8 seconds followed by 1 second rest (Figure 1.4). As a result, TIM mode increased lung deposition of an emitted dose compared to TBM mode (Kesser and Geller, 2009). Moreover, the treatment time was reduced by up to 50 % using TIM mode (Denyer *et al.*, 2010).

Apart from the AAD, other smart devices are emerging, like the Flow And VOlume Regulated Inhalation TEchnology (FAVORITE; Vectura, Chippenham, UK). This technology has been introduced to air-jet nebulisers (AKITA® jet) and vibrating-mesh nebulisers (AKITA®2 APIXNEB® and FOX®) to provide controlled aerosolisation. For examples, the AKITA® devices are programmed through a smart card to meet the patient's and the dosage needs. As a consequence, drug deposition can be programmed to impact either in the distal airways or large-airways. Moreover, the AKITA® unit incorporates a flow and volume regulated inhalation technology that encourages the patient to a slow and deep inhalation (Bakker *et al.*, 2011).

Furthermore, due to technology advances associated with inhalers, pulmonary therapy has expanded from localised therapy to the inhaled treatment of systemic diseases.

**Table 1.2** Comparison between different nebulisers (AAD, adaptive aerosol delivery; TBM, tidal breathing mode; TIM, target inhalation mode; n.a, not-applicable).

| Properties | Nebulisers | | | |
|---|---|---|---|---|
| | **Jet nebulisers** | **Ultrasonic nebulisers** | **Vibrating-mesh nebulisers** | **Soft-mist inhalers** |
| **Power** | Compressed gas, electrical mains | Electrical mains or batteries | Electrical mains or batteries | Mechanical energy |
| **Portability** | Restricted | Restricted | Portable | Portable |
| **Aerosol output** | Slow | Medium | High | Very high |
| **Residual formulation** | 2 ml | Variable but low | < 0.2 ml | n.a |
| **Breath-actuated** | Available | No | Available | No |
| **Smart device** | Akita® Jet | No | AAD (TBM or TIM) | No |
| **Cost** | Low | Moderate | High | Low |
| **Major inconvenience** | Portability, drug loss | Increase drug temperature | Cost | Not suitable for large doses |
| **Examples** | AeroEclipse II BAN®, Pari LC Star® | Beurer IH30®, UltraAir NE-U17® | Aeroneb Go®, I-neb® | $AER_x$®, Respimat® |

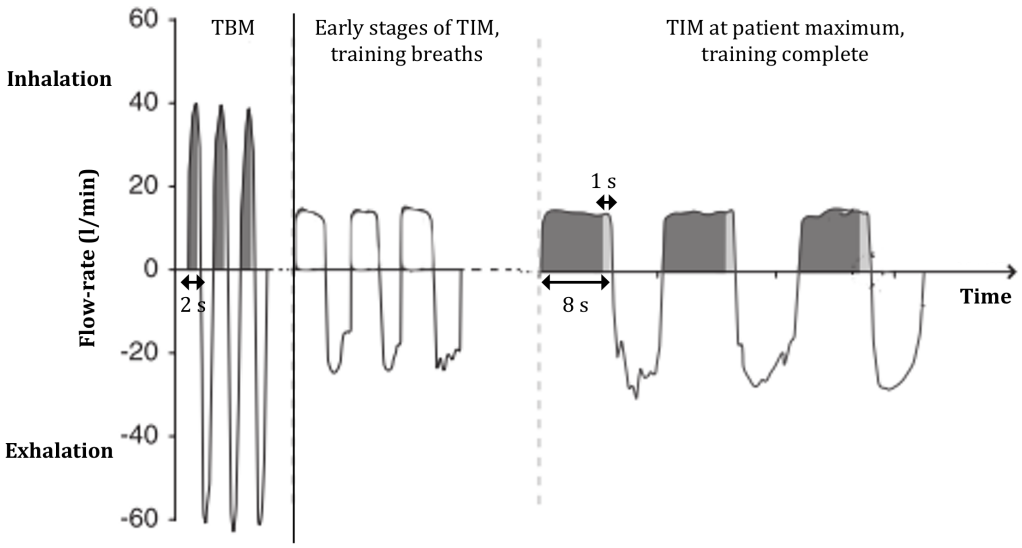


**Figure 1.4** Representation of the two breathing patterns associated with the I-neb adaptive aerosol delivery: tidal breathing mode (TBM) and target inhalation mode (TIM). The graphic represents the patient breathing with both systems. During the first part of the graph, the patient uses normal tidal breath with the TBM mode. In the second part of the graph the TIM system coaches the patient to extend and slow down the breaths. The last part of the graph shows the slow and deep inhalation of the patient. The time when the nebuliser aerosolises is painted in dark grey and the light grey zone indicates nebulisation cessation (adapted from Denyer *et al.*, 2010).

## 1.3. Inhaled therapy to treat systemic diseases

Since the lungs have a wide absorption area, very thin permeability membranes and high blood irrigation; inhaled therapy can also be used to target systemic diseases. The first reported study of drug administration via the lungs for a systemic delivery was described by Gänsslen in 1925. In those studies, it was shown that inhaled insulin lowered the glucose levels in tested subjects. However, this research was overlooked until much later in the century, probably because the research was published in an obscure German journal (Patton and Byron, 2007). Later, other authors detected systemic drug levels of drugs delivered by inhalation. For example, Patton *et al.* (1989) detected human growth hormone in the systemic circulation of rats after inhalation treatment. Since then, the use of inhaled therapy for non-invasive administration of systemic drugs has been widely studied, especially for insulin.

Insulin is normally administered by subcutaneous injection, as proteins are readily degraded in the gastrointestinal tract (Wang *et al.*, 2015). However, subcutaneous administration is associated with low patient adherence and lipohypertrophy (Testa and Simonson, 2007). From all the alternative methods to deliver insulin, inhalation is the most promising since two products have already been approved, e.g. Afrezza® and Exubera® (subsequently removed from the market in 2007; Bailey and Barnett, 2010). Inhaled delivery of insulin increased its bioavailability compared to nasal or oral routes and lung delivered insulin allowed a rapid onset of action (Mastrandrea and Quattrin, 2006). Exubera® was a dry powder insulin formulation which was stable at room temperature. The formulation was withdrawn from the market due to poor sales and poor acceptance. Some of the drawbacks of Exubera® included a complicated dose-equivalent system with its analogous subcutaneous formulations, large dimensions of the inhaler and requirement for multiple inhalations per dose (Santos Cavaiola and Edelman, 2014). More recently, the FDA approved Afrezza® for the treatment of diabetes mellitus type I and type II.

In this powder formulation, insulin is encapsulated in low-density freeze-dried microspheres. When Afrezza® is nebulised, the main excipient (fumaryl diketopiperazine) dissolves resulting in the release of insulin in the lungs, where it is quickly absorbed into the bloodstream. The maximum effect of inhaled insulin is at 50 minutes after inhalation whereas for subcutaneous lispro insulin occurs at 120 minutes after injection (Abramowicz *et al.*, 2015). Insulin in the Afrezza® device is loaded into single dose cartridges and is aerosolised with a small DPI. The most common adverse effect related to using inhaled insulin is a cough. A decline but no progressive variation in the $FEV_1$ is also observed in the first three months of treatment. The mechanism for these changes remains unknown but those are reversible and return to normal levels after discontinuation of the therapy. However, inhaled insulin is not approved for patients with asthma, COPD or cigarette smokers. A small percentage of patients treated with inhaled insulin developed lung cancer (0.13 %) compared to the control group (0.02 %). Despite the fact that those patients had a history of cigarette smoking, the FDA has demanded a longer study to investigate the lung cancer relationship with Afrezza® inhalation (Cassidy *et al.*, 2011).

Other drugs have been studied for their systemic effect after inhaled administration. For example, an $AER_x$ nebuliser was used to deliver morphine with similar onset and duration of the effects as the intravenous administration (Dershwitz *et al.*, 2000). Moreover, comparable equivalences were also perceived for a fentanyl pMDI where a similar control of severe pain was achieved for intravenous and inhaled administration (Mather *et al.*, 1998). Other drugs, such as rizatriptan gave instantaneous systemic action after inhalation. Thus suggesting the suitability of the respiratory route as a non-invasive treatment for migraine treatment (Rabinowitz *et al.*, 2004). In addition, different molecules were also successfully detected in the systemic circulation after inhaled therapy. These include erythropoietin to stimulate the red blood cell production (Bitonti *et al.*, 2004), follicle stimulating hormone for the

treatment of both male and female infertility (Low *et al.*, 2005) and AmB for experiment treatment of visceral leishmaniasis (Alsaadi *et al.*, 2012).

### 1.3.1. Leishmaniasis disease and its treatment with Amphotericin B

Leishmaniasis is a parasitic disease transmitted by the bite of female infected sandfly. It is endemic in 88 nations and more than twelve million people are infected all over the world (World Health Organisation, 2011a). The *Leishmania* parasite has two morphological forms in its life cycle (Figure 1.5), the extracellular promastigote, which exists in the sandfly vector, and the intracellular amastigote in the mammalian host. During a bite from the infected sand fly, promastigotes are deposited into the skin of the host. The parasites are phagocytosed by neutrophils and macrophages where they differentiate into the amastigote form within the parasitophorous vacuole. Inside macrophages, amastigotes divide by binary fission until the cell eventually bursts. The released parasites can then infect more cells within the mononuclear phagocytic system. The parasite life cycle is completed when another sandfly bites an infected host and the vector takes up infected macrophages or free amastigotes. The amastigotes, undergo further development in the vector and the cycle is completed once infective promastigotes are produced (Figure 1.5; Murray *et al.*, 2005; Besteiro *et al.*, 2007).

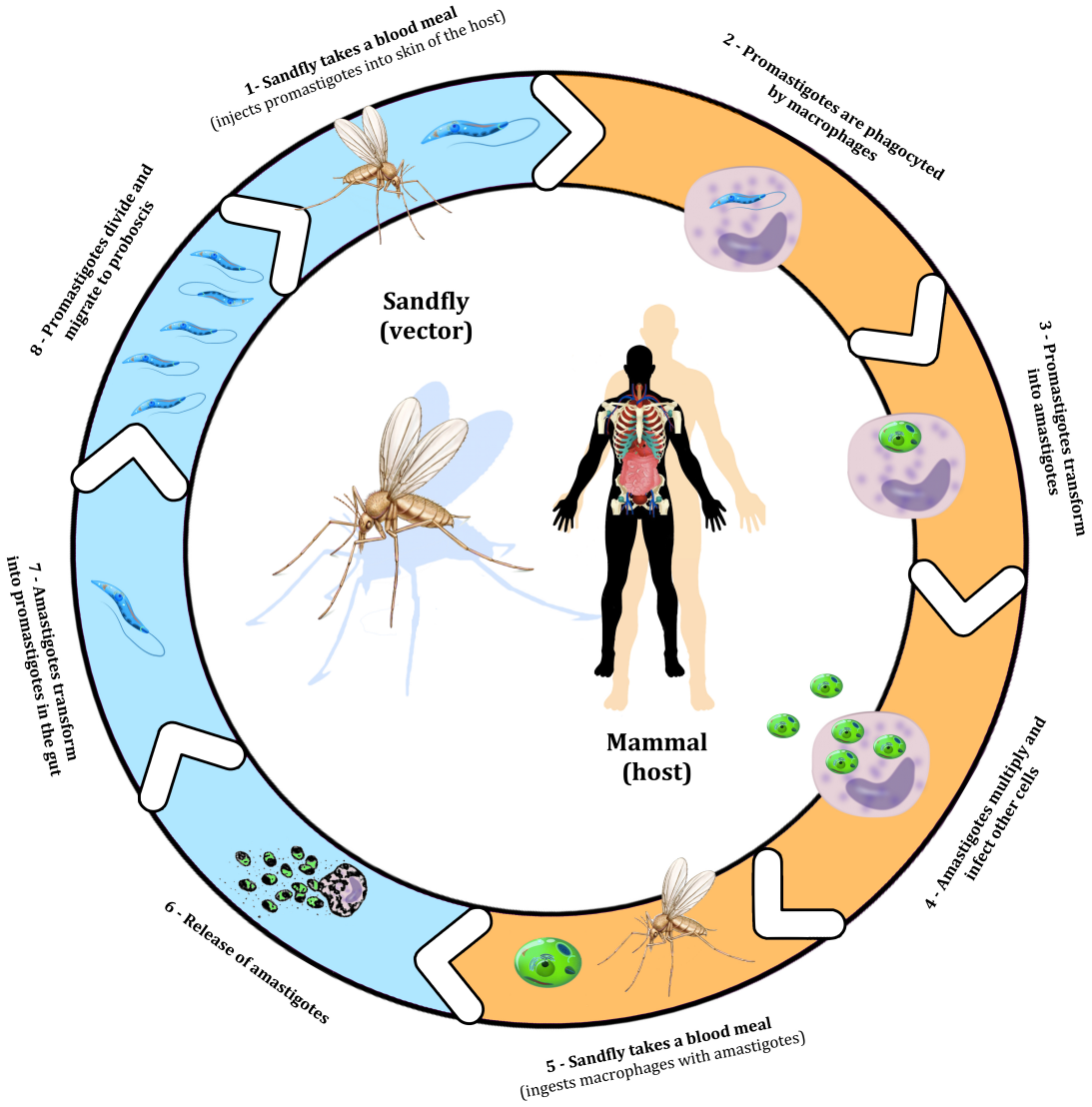


**Figure 1.5** Representation of the leishmaniasis life cycle. (1) When the infected female phlebotomine sandfly bites a mammal, promastigotes are deposited from the vector proboscis to the host skin. (2) Promastigotes are phagocytosed by macrophages and other types of mononuclear phagocytic cells and (3) and then differentiate to amastigotes. (4) The amastigotes multiply by simple division in the macrophages and when the cell burst they are released to infect other cells. (5, 6) Sandflies become infected during blood meal and ingesting infected cells with amastigotes. (7) The amastigotes are transformed to promastigotes in the sandfly gut (8) where they multiply and migrate to the sandfly proboscis. (1) When the infected sandfly bites another host, the cycle is restarted.

Three main clinical types of leishmaniasis occur in humans, divided according to the tropism and the immune response of the host: cutaneous, mucocutaneous and visceral leishmaniasis. Cutaneous leishmaniasis infects 1.5 million people every year and normally presents as a self-healing lesion at the site of the sand fly bite (Llambrich *et al.*, 2009). Cutaneous leishmaniasis is mainly cause by *L. major*, *L. tropicana* or *L. mexicana* species (Desjeux, 1996). Another clinical manifestation is mucocutaneous leishmaniasis, which affects the facial mucous membranes and can lead to oral and pharyngeal cavities destruction. From those, two thirds of mucocutaneous leishmaniasis cases have had a previous history of cutaneous leishmaniasis (Grevelink and Lerner, 1996). However, the most severe form of the parasitic disease is visceral leishmaniasis since it can be fatal if left untreated. Half a million new cases of visceral leishmaniasis occur every year and approximately 50,000 of those result in death (World Health Organisation, 2011a). The disease is caused by infection with *L. donovani*, *L. chagasi* or *L. infantum* species (Guerin *et al.*, 2002). Generally the patient has a history of a cutaneous leishmaniasis and after an incubation period, from weeks to months, the parasite spreads systematically to the liver, spleen, bone marrow and the peripheral lymph nodes (Murray *et al.*, 2005). Visceral leishmaniasis infection is associated with fever, weakness, anorexia, anaemia, hepatosplenomegaly and pancytopenia (Desjeux, 1996). Visceral leishmaniasis can be diagnosed by microscopy observation of the amastigotes in tissue biopsies, antigen dipstick test or polymerase chain reaction (Srividya *et al.*, 2011).

Treatment of *Leishmania* infections has always been a challenge due to the intracellular nature of the parasites. An ideal anti-*Leishmania* therapy should be effective, minimise recurrences, have a low toxicity and be cost-effective. Ideally, a vaccine is required to prevent infection. Although several vaccines against leishmaniasis are under development, none has reached successful clinical trials yet (Singh and Sundar, 2012; Doro, 2014; Kumar and Engwerda, 2014). Treatment with pentavalent antimonials such as sodium stibogluconate

or meglumine antimoniate, have been used since 1940s and they were the first-line treatment for visceral leishmaniasis for many years. Antimonials inhibit the trypanothione reductase enzyme and induce cell apoptosis by multiple effects such as oxidative stress. However, drug resistance in endemic population have limited the clinical utility of these drugs since the 1980s and they are no longer recommended for treatment of visceral leishmaniasis in India (Ritmeijer *et al.*, 2006; Maltezou, 2010). Another anti-leishmaniasis drug is miltefosine, which was the first oral drug recommended for visceral leishmaniasis treatment. However, miltefosine therapy is associated with teratogenicity and therefore is administered with caution to fertile women (Rahman *et al.*, 2011). Pentamidine is also used against cutaneous and visceral leishmaniasis. However, pentamidine intravenous or intramuscular treatment is associated to irreversible insulin dependent side-effects, which limits its use to a second-line drug (Das *et al.*, 2009). Other treatments include paromomycin, but this drug can induce nephrotoxicity and ototoxicity (Musa *et al.*, 2010). Clinical trials with oral sitamiquine have showed promising benefits for the treatment of visceral leishmaniasis (Jha *et al.*, 2005; Wasunna *et al.*, 2005). Nonetheless, despite other treatment options being available, amphotericin B (AmB) is the first-line treatment for visceral leishmaniasis (Sundar *et al.*, 2004).

Amphotericin (AmB) is a polyene macrolide with anti-mycotic properties, widely used to treat life-threating fungal infections (Groll and Walsh, 2002) or visceral leishmaniasis (Sundar *et al.*, 2004). AmB was firstly isolated in 1959 from *Streptomyces nodosus* (Dutcher *et al.*, 1959) and the drug is still extracted from microbiological fermentation on an industrial scale. AmB is a molecule composed by a mycosamine sugar and two amphiphilic sides and it is amphoteric in nature due to a carboxyl and an amine terminal group. Moreover, AmB is an unstable drug and exhibits light sensitivity and is degraded at elevated temperatures (Hung *et al.*, 1988). In addition, it has a low solubility and low permeability profile hence belonging to class IV of the Biopharmaceutics Classification System (Amidon *et al.*, 1995). Due to these properties, AmB has to

be administered intravenously in conjunction with a solubilising agent or encapsulated in a delivery system (Torrado *et al.*, 2008). The mechanism of action of AmB is centred in the formation of pores in fungal or *Leishmania* cell membranes (Figure 1.6). Those result in the release of the intracellular contents and cell apoptosis. Moreover, AmB has a greater affinity for ergosterol compared to cholesterol, which gives its selectivity against fungi and *Leishmania*. Despite this affinity, the use of AmB is associated with nephrotoxicity in mammals; for this reason, treatment with AmB is dose-limited by renal toxicity (Chattopadhyay and Jafurulla, 2011).

AmB solubilised in sodium deoxycholate has been in the market for more than 40 years, branded as Fungizone® (Bristol-Myers Squibb, Nutley, USA). Fungizone® is a freeze-dried product that forms a micellar colloidal complex with sodium deoxycholate when reconstituted with dextrose solution. These complexes dissociate quickly in plasma and perfuse the tissues when the drug is associated with very low-density and low-density lipoproteins. The affiliation of AmB complexes with low-density lipoproteins causes interaction with cholesterol of mammalian cell membranes. Those forming a disorder in the renal electrolyte equilibrium and producing nephrotoxicity (Lemke *et al.*, 2005). Therefore, it is extremely important to monitor renal toxicity during treatment, since up to 30 % of the patient may present acute renal failure (Bates *et al.*, 2001). Nonetheless, fewer side effects are associated with other commercially available AmB formulations such as the liposomal AmBisome® (Gilead Sciences, Foster City, USA), the lipid complex Abelcet® (The Liposome Company, Princeton, USA) and the colloidal dispersion Amphotec® (Kadmon Corporation, New York, USA). Despite their superior efficacy and lower side effects profiles, the high cost of these alternate lipid-based formulations restricts their use in limited resources countries. For example, World Health Organisation, (2010a) estimated that the treatment with a liposomal formulation is 13 times more expensive than treatment with Fungizone®.

The lipid formulation Abelcet® is an AmB lipid complex formulation with particles that resemble ribbons of 1-10 μm. This formulation has a long half-life, suggesting that the delivery systems acts as a depot in tissues where the drug is gradually released (Ng *et al.*, 2003). One more commercialised AmB delivery system is Amphotec®, which is a colloidal dispersion of AmB with cholesteryl sulphate. Amphotec® is composed of particles with a disc structure formation with a thickness of 4 nm and diameter of 100 nm. Other novel AmB drug delivery formulations that are under development are PEG liposomes (Van Etten *et al.*, 1995), polymeric nanoparticles (Italia *et al.*, 2009b), thermo resistant liposomes (Sivak *et al.*, 2011), microemulsions (Brime *et al.*, 2002), nanosuspensions (Kayser *et al.*, 2003) and micelles (Santangelo *et al.*, 2000). Regardless, the most clinically used drug delivery system for AmB is the liposome formulation AmBisome® which is a vesicular system for drug delivery, further described later.

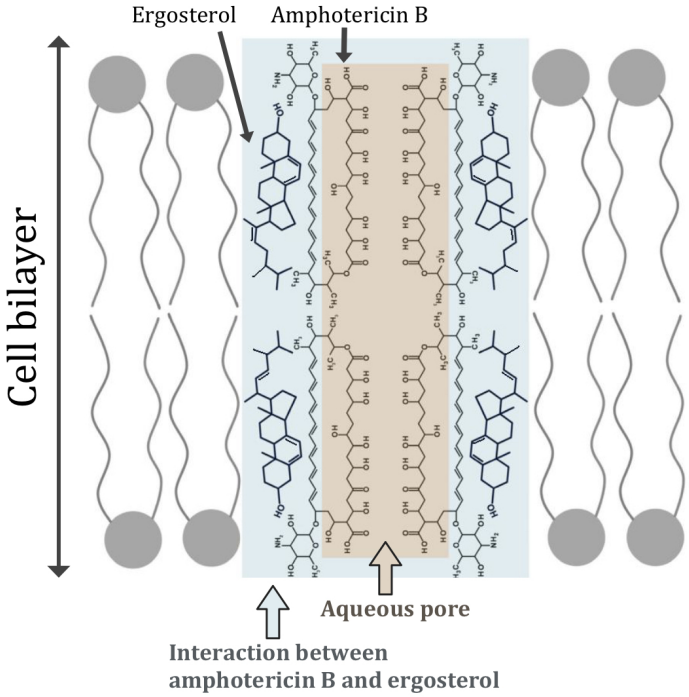


**Figure 1.6** Amphotericin B aqueous pore formed between the cell bilayer. AmB hydrophobic faces interact with the sterol (ergosterol in the figure) with a Van der Walls union while the hydrophilic faces are orientated towards the centre and form a water filled pore (adapted from Chattopadhyay and Jafurulla, 2011 and Puig-Sellart, 2013).

## 1.4. Vesicular systems for drug delivery

Vesicular drug delivery systems are nanostructures that encapsulate drugs and deliver them in a controlled manner. In general, the structures of vesicular systems contain a principal molecule with a hydrophilic head group attached to a hydrophobic tail. The bilayer structure is arranged with the long hydrophobic tails pointing into the interior of the membrane, and the polar head groups facing outwards. Encapsulated hydrophilic drug molecules are found into the aqueous core. On the contrary, lipid-soluble molecules are absorbed in the lipophilic domain of the bilayers. The entrapment efficiency varies depending on the nature of the encapsulated moieties, overall being higher for lipid-soluble molecules than aqueous materials.

The self-assembly of amphiphilic molecules is not spontaneous and an additional energy input is necessary (Gentile *et al.*, 2011b). Generally vesicular systems are prepared by mixing the vesicle composite with the drug followed by a high-shear mixing to produce vesicles of desired dimensions. However, some of those methods rely on the use of organic solvents to create the vesicles, such as ether-injection, thin-film hydration, and reverse phase evaporation. For instance, in the ether-injection method, the lipids and the drug are dissolved in diethyl ether and slowly injected into a warm aqueous phase. This results in ether evaporation in contact with the warm liquid and the formation of unilamellar vesicles. Another method, named as thin-film hydration, consists in dissolving all the structural components in chloroform in a round-bottomed flask. This is generally followed by rotary vacuum evaporation to produce a thin lipidic film around the flask. Then, the drug solution is used to hydrate the dry lipid and form the vesicles (Bayindir and Yuksel, 2010; Tavano *et al.*, 2011; Manca *et al.*, 2014). Further methods, like the reverse phase technique consists in dissolving the lipids in a mixture of ether and chloroform followed by incorporation of the drug in an aqueous solution. Then, the solvents are removed with evaporation under pressure (Abdelkader *et al.*, 2012). Other methods do not require the incorporation of organic solvents. This is

advantageous for formulations intended for human therapeutics. For example, the homogenisation method of melted lipids hydrated with the aqueous drug solution (Carter *et al.*, 1997) or micro fluidization at high pressure (Lo *et al.*, 2010). In seldom occasions the entire drug load is encapsulated in the formed vesicles. Therefore, some authors purify the vesicles and remove unentrapped drug using dialysis, gel filtration or centrifugation methods. Nonetheless, others argue that the use of vesicular systems with encapsulated and free drug may benefit from a biphasic distribution profile and increase sample stability. Consequently, the initial onset of action related to the free drug would be followed by the drug delivery system sustained release (Uchegbu and Vyas, 1998; Marianecci *et al.*, 2014) .

Liposomes are a type of vesicular drug delivery systems, which originated in the research published in 1965 by Dr. Alec Bangham. Since then, liposomes have been extensively investigated as vesicular drug carriers. Liposomes are made of an amphiphilic natural or artificial phospholipid surrounded and entrapped by an aqueous media (Lasic, 1998; Lian and Ho, 2001; Edwards and Baeumner, 2006). Nowadays, there are more than ten approved liposomal products available for clinical use. These include Doxil®, liposomal doxorubicin for the treatment of recurrent ovarian cancer; DaunoXome®, liposomal daunorubicin for the treatment of Kaposi sarcoma; Epaxal®, a hepatitis A vaccine and AmBisome® for the treatment of visceral leishmaniasis. In particular, AmBisome® consists of unilamellar vesicles of 100 nm in diameter containing the drug AmB. AmBisome® is produced by thin-film hydration where all the constituents are dissolved in chloroform and DMSO (AmB, hydrogenated soybean phosphatidylcholine, distearoylphosphatidylglycerol, cholesterol, disodium succinate hexahydrate and alpha-tocopherol) followed with a solvent removal. The resulted lipid film is then rehydrated with a sucrose-buffered solution and homogenised at high-pressure to give small vesicles followed by a terminal aseptic filtration step (Proffitt *et al.*, 1999). The maximum tolerated dose for AmBisome® is 5 times higher than that of Fungizone®, therefore the

liposomal treatment is associated with better efficacy outcomes (Lemke *et al.*, 2005).

Following on from the development of liposomes, the cosmetic industry introduced the concept of non-ionic surfactant vesicles (NIVs; Mahale *et al.*, 2012). NIVs do not use phospholipids as the main amphiphilic molecule instead they use non-ionic surfactants. Those surfactants overcome the drawbacks associated with phospholipids used in liposomes, as they have a greater physical and chemical stability and they are generally cheaper. Other authors denominate NIVs as niosomes, nanoniosomes, polymerosomes or bilosomes (when bile salts are added; Moghassemi and Hadjizadeh, 2014). Despite the promising therapeutics of NIVs, up to this date no NIVs formulation has been approved for clinical use yet.

The main components in NIVs are surfactants with some NIVs having extra sterols or charged species (Figure 1.7). Surfactants, like phospholipids, are amphiphilic molecules that can form lamellar vesicles once hydrated. Moreover, according to the functionally of the hydrophilic head group, surfactants can be classified as anionic, cationic, amphoteric or non-ionic (Schick, 1987). Non-ionic surfactants are part of the category with no charge in their head group, which is less toxic for mammalian cells (Marianecci *et al.*, 2010). However, even though several studies have suggested low cytotoxicity of non-ionic surfactants, the *in vivo* long-term effect remains to be investigated. The most commonly used non-ionic surfactants are alkyl ethers. Those can be divided according to the structure of the hydrophilic head, which could be ethylene oxide subunits (Carter *et al.*, 1997; Gentile *et al.*, 2011a), repeats of glycerol subunits, related isomers or larger sugar molecules (such as sorbitan). Sorbitan based surfactants generate stable NIVs in the form of sorbitan monoesters (Span) or polyethoxylated sorbitan esters (Tween) of different molecular weights. Other amphiphilic molecules are gemini surfactants, with two hydrophilic and two hydrophobic chain linked by a spacer, or bolaamphiphiles surfactants, with

bipolar hydrophilic structures (Mohammed *et al.*, 2012). Others have investigated the formation of NIVs after coating water-soluble drug carriers with surfactant, named as the proniosome technique. The resultant dry composition is hydrated to form NIVs (Abd-Elbary *et al.*, 2008; Elhissi *et al.*, 2013). Nevertheless, the surfactant selection depends on the hydrophilic-lipophilic balance (HLB) and the critical packing parameter (CPP). For example, high HLB surfactant values (HLB = 14 - 16) or smaller values (HLB < 6) would not produce vesicles unless cholesterol is added to increase stability (Pardakhty *et al.*, 2007). Therefore, an ideal HLB between 3 and 8 is desirable to formulate bilayers. Moreover, the CPP of the surfactant can predict the type of vesicle formed such as micelles (CPP ≤ 0.5), spherical bilayer vesicles (CPP = 0.5 – 1.0) or inverted micelles (CPP ≥ 1.0; Marianecci *et al.*, 2014). Another important parameter to describe surfactants is the gel liquid transition temperature ($T_g$), which is when the vesicle components are transformed from gel phase (closely packed) to liquid phase (loosely packed lipids due to molecular rotation of the chains). Particularly, higher drug leakage is observed when lipids are in the liquid phase (Nasseri, 2005). However, the addition of cholesterol to the lipid mixture influences the physical properties and structure of the vesicles due to interaction with the surfactant. Therefore, the incorporation of cholesterol into the vesicle bilayer at low concentrations increases $T_g$ and might also eliminate the phase transition (Lian and Ho, 2001; Puig-Sellart, 2013). Other ingredients commonly found in NIVs are charged molecules such as dicetyl phosphate (DCP), for negative charges; or stearylamine, for positive charges. These molecules induce charge into the vesicle structure, hence to prevent aggregation and increase stability.

NIVs can be used to deliver different types of drugs and can be administered by different routes. The most common route of administration is the intravenous route. However, other non-invasive routes have been examined. NIVs excel in transdermal and dermal delivery. The reason for that is the enhancement of dermal drug penetration through fusion with the stratum corneum (Schreief

and Bouwstra, 1994). Some example of dermal NIVs formulations tested include tretinoin-NIVs (Manca *et al.*, 2014) and capsaicin-NIVs (Tavano *et al.*, 2011). Similar bioavailability enhancement properties were observed for ocular administration of NIVs. Kaur *et al.* (2012) formulated fluconazole deformable NIVs with better ocular penetration profiles than the drug alone. Furthermore, as a non-invasive technique, oral route is the preferred route of administration for most drugs. However, drugs have to overcome the acids and digestive enzymes of the gastrointestinal track before delivering to the mucous membranes. Bayindir and Yuksel (2010) investigated the use of different NIVs to protect paclitaxel upon oral administration. Paclitaxel-NIVs made with span 40 resisted the effect of different pepsin type enzymes specially for alpha-chymotrypsin. Moreover, delivery of NIVs to the brain have been reported for glucose NIVs with the vasoactive intestinal peptide (Dufes *et al.*, 2004). NIVs have also been used as vaccine delivery for rheovirus or small pox vaccine. Due to the fact that NIVs can offer adjuvant properties for vaccine delivery, with similar effects as the currently adjuvants employed for human vaccines i.e. aluminium phosphate (Singh *et al.*, 2011). Following, the use of vesicular systems for inhaled therapy is further reviewed.

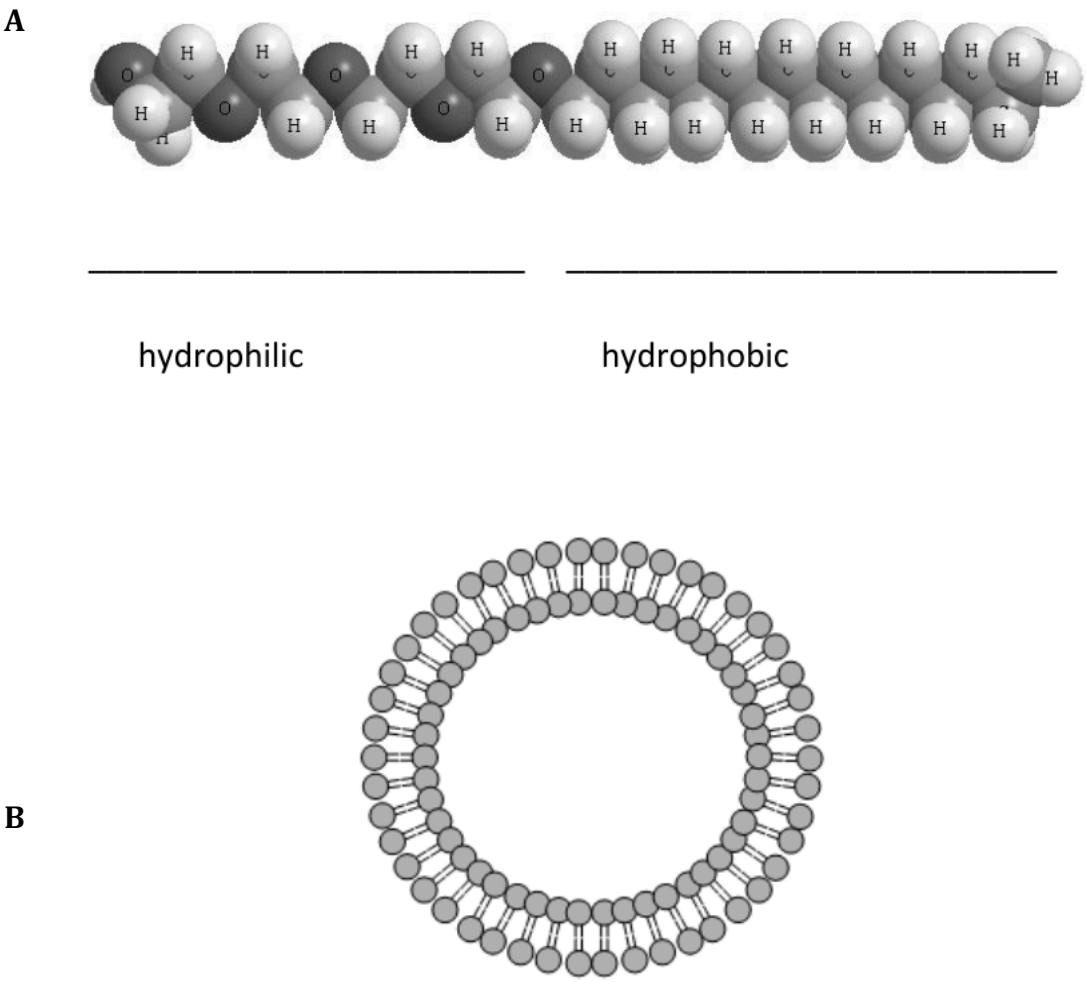


**Figure 1.7** Schematic representation of tetra-ethylene glycol mono hexadecyl ether (surfactant A) and a NIVs vesicle (B, round part of the molecule represents the hydrophilic part and double lines are the hydrophobic side).

### 1.4.1. Inhaled drug delivery of vesicular systems

Vesicular based delivery systems present several advantages on delivering drugs by inhalation. Specially when compared to other aerosol systems such as solutions or dry powders. They provide a sustained release profile of the encapsulated drug while prolonging local therapeutic effect in the lungs. As a consequence, the frequency of local drug dosing is reduced (VanDevanter and Geller, 2011). Apart from localised lung treatment, vesicular systems are also used to provide drug systemic effect (Bai and Ahsan, 2010). Moreover, vesicular systems have a predisposition to target phagocytic cells in the lungs, such as alveolar macrophages (Vyas *et al.*, 2005). Macrophages recognise the colloidal structures as foreigner and phagocyte them. In addition, epithelial lung cells can also be targeted by vesicular systems attached to specific surface receptors (Schreier *et al.*, 1993). Another advantage of vesicular systems is protection effect of the encapsulated drug. For instance, loaded peptides are protected from enzymatic degradation in the lungs. Some of the studied inhaled peptide-containing liposomes include insulin (Chono *et al.*, 2009) or vasoactive intestinal peptide (Hajos *et al.*, 2008).

For a successful inhaled vesicular delivery system, the particles should be robust to the inhalation process. Ideally, the entrapment efficiency and the vesicle size should not change after aerosolisation. Nonetheless for the majority of inhaled vesicular delivery systems, this is not the case (Elhissi *et al.*, 2007, 2012; Manca *et al.*, 2012b; Lehofer *et al.*, 2014). Only a few studies have reported maintenance of physicochemical properties upon nebulisation (Gaspar *et al.*, 2010). A review by Cipolla *et al.*, (2013) investigated the effect of using liposomes for inhaled therapy and the effect of various forms of nebulisation on the release of encapsulated drug as a function of liposome vesicle size. Unilamellar vesicles with high content of cholesterol were found to be the most robust upon nebulisation. Furthermore, the type of inhalation device was found to influence the stability of the vesicles. Vibrating-mesh nebulisation was less

disruptive to salbutamol sulphate liposomes compared with air-jet or ultrasonic nebulisers (Elhissi *et al.*, 2012).

Liposomes have been investigated as inhaled drug delivery carriers (Anabousi, 2006; Manca *et al.*, 2012a; Jain *et al.*, 2014). Despite several liposome formulations being approved for intravenous clinical use, none is specifically labelled for inhaled delivery. Nevertheless, inhaled liposomal AmB formulations have been used off-label to treat invasive pulmonary aspergillosis (Rijnders *et al.*, 2008; Fauvel *et al.*, 2012) and as a prophylactic treatment to prevent fungal infections in lung transplant patients (Perfect *et al.*, 2004). Only two liposomal formulations are in the last stages of clinical trials for inhaled therapy: a liposomal amikacin for the treatment of CF with Pseudomonas infection (Clancy *et al.*, 2013) and a liposomal ciprofloxacin in non-CF bronchiectasis (Serisier *et al.*, 2013). Liposomes are believed to be safe for lung delivery due to the biocompatibility of the ingredients with the lung environment. The lungs contain airway fluid with phospholipids and cholesterol (Wauthoz and Amighi, 2014). Particularly relevant for biocompatibility characteristics with the lung fluids are liposomes made with DPPC phospholipid since this compound is also the main component of the lung surfactant. However, contrary to liposomes, that were firstly developed for intravenous administration and then studied for inhaled delivery; lipid microparticles were specifically developed with pulmonary applications in mind. Lipid microparticles are low-density high porosity particles formulated with a large geometric diameter in order to avoid phagocytosis. However, due to the low density of particles the aerodynamic aerosol size is ideal for airways deposition. Tobramycin lipid microparticles, named PulmoSphere® are already approved for clinical use in CF patients under the name of TOBI Podhaler® (VanDevanter and Geller, 2011).

As mentioned previously, NIVs have higher stability properties than liposomes and can be used for inhaled administration of drugs. The use of NIVs to deliver glucocorticoids for asthma and COPD patients has been described in different

publications. Terzano *et al.* (2005) demonstrated that beclomethasone dipropionate-NIVs could successfully penetrate the mucus layer and therefore reach the receptors localised in the epithelial cells. Marianecci *et al.* (2010) confirmed the tolerability of the beclomethasone-NIVs with insignificant cytotoxicity against human lung fibroblast. Other beclomethasone proniosomes were successfully nebulised with air jet and vibrating-mesh nebulisers with high fine particle fraction (Elhissi *et al.*, 2005, 2013). Moreover, the addition of antibiotics in NIVs has also been described for pulmonary delivery. For example, ciprofloxacin-NIVs presented good inhalation characteristics whilst providing lower cytotoxicity than the drug alone (Moazeni *et al.*, 2010). In addition, encapsulated all-trans-retinoic acid in NIVs also presented less toxicity than the drug alone with good inhalation characteristics (Desai and Finlay, 2002). Finally, Alsaadi *et al.*, (2012) investigated the AmB-NIVs potential of targeting a systemic disease such as leishmaniasis by inhalation (Alsaadi *et al.*, 2012). However, further investigations of formulation stability, *in vitro* aerosol size and efficacy are required.

## 1.5. Study outline

The use of NIVs to enhance drug delivery has outclassed the liposomes technology in terms of increased stability and reduced cost. However, the majority of NIVs formulations produced are limited to the intravenous administration and by encapsulated drug stability. This has encouraged the investigation of NIVs delivery by other non-invasive routes such as inhalation. The objective of this study is to characterise the use of NIVs to deliver different drugs with particular emphasis in the pulmonary delivery route. Therefore the aims of this project were:

- Produce a stable AmB-NIVs formulation for the treatment of visceral leishmaniasis (Chapter 3).

- Develop a freeze-dried NIV platform able to encapsulate various drugs and to be used for different applications (Chapter 4).

- Characterize the nebulisation properties of NIVs formulations with different vibrating-mesh nebulisers (Chapter 5).

- Study of novel minor grove binders compounds to treat visceral leishmaniasis and lung cancer and the effect of using a NIVs formulation (Chapter 6).

# CHAPTER 2. MATERIALS AND METHODS

## 2.1. Materials

Deoxycytidine, cisplatin, α-naphthol, dimethyl sulfoxide (DMSO), hydroxypropyl -α-cyclodextrin (HPαCD), hydroxypropyl-γ-cyclodextrin (HPγCD), sucrose, luminol and Triton™ X-100 were purchased from Sigma-Aldrich (Gillingham, UK). Hydroxypropyl-β-cyclodextrin (HPβCD) was obtained from International Speciality Products (Köln, Germany). Cholesterol was acquired from Croda Chemicals (East Yorkshire, UK). Dicetyl phosphate (DCP) was supplied from Fine Chemical Products (Earley, UK). Tetra-ethylene glycol mono n-hexadecyl ether (surfactant) was purchased from Nikkol chemicals (Tokyo, Japan). Calcium acetate trihydrate HPLC grade and glucose were obtained from Fisher Chemical (Loughborough, UK). Trehalose was a kind gift from Hayashibara (Okayama, Japan). Dulbecco's Modified Eagle Medium (DMEM), Phosphate buffer saline pH 7.4 (PBS) and penicillin streptomycin were acquired from Invitrogen (Paisley, UK). Foetal bovine serum was received from Biosera (Uckfield, UK). Amphotericin B (AmB) and gemcitabine, both pharmaceutical-grade, were supplied from Sequoia Research Products (Pangbourne, UK). Prednisolone was purchased from ICN Biomedical (Aurora, USA). Isoflurane 100 % was received from Abbott (Maidenhead, UK). D-luciferin firefly potassium salt (Luc) was supplied from Life Silences, PerkinElmer (Massachusetts, USA). Hypnovel® was purchased from Roche Pharma (Burgess Hill, UK) and Hypnorm® from VetaPharma Ltd (Sherburn-in-Elmet, UK). All distilled water used was filtered using a Purite® system (Ondeo IS, Oxon, UK). Other reagents used were analytical grade.

I-neb passive vibrating-mesh nebuliser was leased from Philips Respironics (Chichester, UK). It was used in continuous mode with 0.5 ml metric chamber and power level (PL) 6 or 10, as stated. Aeroneb Go and Aeroneb Lab were both from Aerogen (Galway, Ireland). The unit used in the Aeroneb Lab had a small diameter with a stated particle size of 2.4 to 4.0 μm. Specially made adaptors

made in collaboration with Mr. Nevin (University of Strathclyde) were used to connect the nebulisers to the particle size measurement devices.

Bioware® B16-F10-luc-G5 mouse melanoma cell line was purchased from Caliper Life Sciences (Hopkinton, USA). Three types of *Leishmania donovani* strains were used in this studies, LV82 (MHOM/ET/67:LV82), luciferase expressing strain LV82-luc (Mißlitz *et al.*, 2000; Alsaadi *et al.*, 2012) and the clinical isolate 200015 strain (Carter *et al.*, 2001).

All animal studies were carried out in accordance with the Animals (Scientific Procedures) Act, amended 2012 (Home Office, 2014). The studies were approved by the UK Home Office and also had local ethical approval from the University of Strathclyde. This research is described following the animal research ARRIVE guidelines (Animal Research: Reporting of *In Vivo* Experiments; Kilkenny *et al.*, 2010). BALB/c mice, Sprague Dawley and Golden Syrian hamsters (*Mesocricetus auratus*) were in-house, in-bred. Male and female age matched subjects were used as specified.

## 2.2. High-performance liquid chromatography (HPLC) quantification of drug levels in samples

HPLC methods were used in this study using ultraviolet detection (UV) or an evaporative light scattering detection (ELSD). All the methods were adapted and validated for the specific analyte quantified, i.e. amphotericin B, cisplatin, gemcitabine, D-luciferin, surfactant, cholesterol or dicetyl phosphate.

The amount of amphotericin B, cisplatin or gemcitabine in samples was determined using reverse HPLC with UV detection. A Dionex P680 HPLC System was equipped with a P680 pump, an ASI-100 automated sample injector, an UVD170V photodiode diode-array UV detector (Dionex, Thermo Scientific, Warrington, UK) and a CE1160 column oven 1100 series (Cecil Instruments,

Cambridge, UK). In all methods the mobile phase was filtered before use with a Millipore vacuum filtration kit (Watford, UK) fitted with a 0.22 µm Phenomenex membrane filter (Macclesfield, UK). The resulted chromatograms were analysed using Chromeleon (version 6.80 SR10, Dionex, Thermo Scientific, Warrington, UK). Moreover, all HPLC-UV methods were validated according to precision, sensitivity, accuracy, linearity, range and specificity parameters described in the International Conference on Harmonisation guidelines (ICH; European Medicines Agency, 1995). For instance, peaks were analysed by recording retention time, peak height, area under the curve (AUC), resolution factor and peak asymmetry. Precision was determined with a quantification of known amount of analyte and calculating the relative standard deviation for at least 6 samples. Sensitivity was expressed in terms of limit of detection (3:1 ratio between peak and chromatogram baseline noise) and limit of quantification (10:1 ratio between peak and baseline noise). Accuracy was determined after spiking the analyte to plasma, trachea and lungs from BALB/c mice and calculating the percentage of extracted drug. Linearity and range were established by plotting AUC ratio (analyte AUC divided by internal standard AUC) against analyte concentration. Regression line by the least mean squares method and correlation coefficient ($R^2$), y-intercept and slope were calculated.

Amphotericin B (AmB) levels in samples were determined by HPLC using a method validated by Puig-Sellart (2013). However, an ACE® C18 HPLC column (250 x 4.6 mm, 5 µm particle size) obtained from Hichrom Limited (Reading, UK) was used in this study instead of a Luna® C18 column (250 x 4.6 mm, 5 µm particle size). The column was attached to a guard column and it was kept at a constant temperature of 25°C through analysis. An injection volume of 20 µl and a flow rate of 1 ml/min were used on a 13 minute analysis run. Standards solutions were prepared from an initial AmB stock solution. This was prepared by dissolving AmB with DMSO (1 mg AmB/ml) followed by a dilution with methanol (to 0.1 mg AmB/ml). The reference samples, ranging from 0.01 to 25 µg/ml, were made by further serial dilutions of the stock solution with

appropriate volumes of methanol. The internal standard (IS) stock solution was prepared dissolving α-naphthol with methanol (300 µg IS/ml) and then spiked to each sample prior analysis (20 µg IS/ml, final concentration). The mobile phase was a gradient between acetonitrile and acetate buffer (10 mM, pH 4; Table 2.1). AmB and IS were detected at wavelengths of 407 nm and 294 nm respectively. To quantify the AmB present in AmB-NIVs formulations, the vesicles were disrupted with DMSO (0.3 ml formulation diluted to 5 ml with DMSO) followed with a dilution with methanol (1/5) prior analysis. AmB levels in tissues from *in vivo* experiments were determined using the same HPLC method. In that case, the AmB was extracted from tissues using an extraction solution composed by methanol and water in a 90 : 10 % v/v ratio with 20 µg IS/ml. Tissues were initially weighed and 0.6 ml of extraction solution was added per 100 mg of tissue. Then, samples were homogenised until total dispersion with a T10 basic ultra-turrax from IKA (Staufen, Germany) and centrifuged at 14,736 G for 15 minutes (ALC PK121R multispeed refrigerated centrifuge with A-M12 angle rotor, Thermo Life Sciences, Basingstoke, UK). The supernatant was analysed by HPLC in order to detect the amount of drug present in the sample. To evaluate the method ability in detecting AmB degradation, highly deteriorated AmB formulations were tested. AmB-CD and AmB-NIVs were kept at 70°C for 6 hours. Samples were analysed and chromatograms were recorded at different time points.

Cisplatin levels in samples were determined by HPLC-UV using a variation of a method validated by Alsaadi (2011). A Luna® C18 column (150 x 4.6 mm, 3 µm particle size) with an attached guard column (both from Phenomenex, Macclesfield, Cheshire, UK) was kept at 30°C. An injection volume of 10 µl, a flow rate of 1.5 ml/min and a wavelength of 254 nm were used on a 20 minutes analysis program. The cisplatin stock solution (1 mg/ml) was prepared by dissolving the compound powder with sodium chloride 0.9 % w/v (NaCl). Standard solutions, ranged from 0.12 to 30 µg/ml, were made by further serial dilutions of the stock solution with appropriate volumes of NaCl. Nickel chloride ($NiCl_2$, 300 µg/ml with NaCl) was used as an IS and sodium

diethyldithiocarbamate (DDTC, 100 mg/ml with 0.1 M NaOH) was used as a chelating agent. $NiCl_2$ (5µl) and DDTC (10 µl) were added to the analyte sample (85 µl) and left for 30 minutes at 37°C for the chelating reaction to occur. After that, chloroform (80 µl) was added to the mixture, blended in a vortex for 30 seconds and centrifuged at 14,736 G for 4 minutes at 4°C (ALC PK121R multispeed refrigerated centrifuge with A-M12 angle rotor, Thermo Life Sciences, Basingstoke, UK). The extracting chloroform layer (bottom) was injected to the HPLC system. The mobile phase was an isocratic gradient composed by acetate buffer (29 % v/v, 10 mM, pH 5), acetonitrile (31 % v/v) and methanol (40 % v/v). To quantify the cisplatin present in Cis-NIVs, the vesicles were disrupted with 0.1 M NaOH prior analyses (dilution 1/20).

Gemcitabine was quantified in samples by HPLC-UV using a variation of a method validated by Al-Gawhari (2013). A Sphereclone™ column ODS (150 x 4.6 nm, 5 µm particle size) with an attached guard column (both from Phenomenex, Macclesfield, Cheshire, UK) was kept at 25°C throughout the analysis. An injection volume of 20 µl, a flow rate of 0.7 ml/min and a wavelength of 269 nm were used on a 10 minutes analysis. The isocratic mobile phase was a mixture of acetonitrile and acetate buffer (10 mM, pH 5) at a ratio of 5:95 % v/v. Initial gemcitabine stock solution (1 mg/ml) was prepared by dissolving the drug powder with distilled water. Standard solutions, ranged from 0.10 to 100 µg/ml, were made by further serial dilutions of the stock solution with appropriate volumes of the mobile phase. A stock solution of the IS was prepared by dissolving 2'-deoxycytidine with distilled water (650 µg/ml) and spiked to each sample before analysis (25 µg/ml). To quantify the gemcitabine present in gemcitabine-NIVs, the vesicles were disrupted with isopropanol (50 % v/v) prior analyses.

To quantify the amount of surfactant (tetra-ethylene glycol mono-hexadecyl ether), cholesterol and dicetyl phosphate (DCP) in samples, an HPLC system was attached to an ELSD detector. A Gynkotek HPLC pump series P580 and an auto

sampler model GINA 50 (Macclesfield, UK) operated by Chromeleon software (version 6.30 SP3 Build 594, Dionex, Camberley, UK) were used. The HPLC detector was an Alltech ELSD model 500 (Carnforth, UK). The lipids present in NIVs formulations were assessed using a normal-phase HPLC coupled to an ELSD detector (Alsaadi *et al.*, 2013). The stationary phase was a YMC-PVA silica column (100 mm x 3.0 mm; 5 µm particle size) attached to a guard column (10 mm x 3.0 mm; 5 µm particle size) both from Hichrom (Reading, UK). The ELSD detector was operated at 80°C and a gas flow rate of 2.90 standard litre per minute, supplied by a compressor operated between 60 and 80 pound per square inch gauge. Lipid separation was achieved using a gradient elution at a flow rate of 1 ml/min with an injection volume of 20 µl (Table 2.2). The three channels were composed of iso-hexane (100 %), ethyl acetate (100 %) and a mixture of propan-2-ol (60 % v/v), acetonitrile (30 % v/v), methanol (10 % v/v), glacial acetic acid (1.42 µl/ml) and triethylamine (3.78 µl/ml). The stock solution of the three analytes of interest (1 mg/ml in chloroform, sonicated for 10 minutes) were mixed together and diluted with chloroform to prepare standards in the range of 3 to 250 µg/ml. The IS prednisolone (400 µl of 2 mg/ml in methanol) was added to each 10 ml of sample (standard, unknown sample or blank). From each sample, 100 µl was evaporated overnight and reconstituted in 100 µl of chloroform prior injection onto the column.

**Table 2.1** HPLC-UV mobile phase gradient used for the analysis of AmB samples. Solvent channel A with acetonitrile (100 %) and solvent channel B with acetate buffer (10 mM, pH 4; Puig-Sellart, 2013)

| Time (min) | Solvent channel A (%) | Solvent channel B (%) |
|---|---|---|
| 0 | 40 | 60 |
| 3 | 50 | 50 |
| 4 | 50 | 50 |
| 5 | 80 | 20 |
| 10 | 40 | 60 |
| 11 | 40 | 60 |

**Table 2.2** HPLC-ELSD mobile phase gradient used for the analysis of NIVs lipidic components: surfactant, cholesterol and DCP. Solvent channel A with isohexane (100 %), solvent channel B with ethyl acetate (100 %) and solvent channel C with a mixture of propan-2-ol (60 % v/v), acetonitrile (30 % v/v), methanol (10 % v/v), glacial acetic acid (142 µl/100 ml) and triethylamine (378 µl/100 ml; Alsaadi *et al.*, 2013).

| Time (minutes) | Solvent channel A (%) | Solvent channel B (%) | Solvent channel C (%) |
|---|---|---|---|
| 0 | 80 | 20 | - |
| 2 | 72 | 25 | 3 |
| 3 | 64 | 30 | 6 |
| 4 | 56 | 35 | 9 |
| 5 | 48 | 40 | 12 |
| 6 | 35 | 45 | 20 |
| 7 | 35 | 45 | 20 |
| 8 | 35 | 45 | 20 |
| 9 | 72 | 25 | 3 |
| 10 | 80 | 20 | - |
| 15 | 80 | 20 | - |

## 2.3. Determination of D-luciferin and luminescence levels in samples

The substrate D-luciferin (Luc) was quantified using a 96 well plate UV reader (SpectraMax M5) including a SoftMax Pro software version 5.2 (both from Molecular devices, Wokingham, UK). Luciferin samples were quantified at a wavelength of 328 nm. An initial luciferin stock standard solution (25 mg/ml) was prepared by dissolving luciferin powder in PBS pH 7.4. Solutions, range from 3 to 100 µg/ml, were made by further serial dilutions of the stock solution with appropriate volumes of PBS pH 7.4. To quantify luciferin present in Luc-NIVs, the vesicles were disrupted with Triton™ X-100 (1% w/v; dilution 1/2) prior to analysis.

The bioluminescence (BLI) produced by luciferase expressing cells in contact with luciferin was determined using the IVIS imaging system from Caliper Life Sciences (Runcorn, UK). The IVIS system was also used to quantify the chemiluminescence (CLI) associated to the oxidation reaction of luminol by the myeloperoxidase enzyme present in neutrophils. The IVIS camera exposure was set at 2 minutes and the luminescence values were reported as total flux of photons emitted per second (p/s). When luminescence was determined *in vivo*, animals were anesthetised with aerosol isoflurane prior and during the imaging (gas-anaesthesia system XGI-8). The luminescence, i.e. BLI or CLI, correspondent to the area of interest (Figure 2.1) was selected using the Living image software (version 4.3.1, all from Caliper Life Sciences, Runcorn, UK).

## 2.4. Production of NIVs formulations

To produce NIVs formulations, firstly a mixture of surfactant (tetra-ethylene glycol mono-hexadecyl ether), cholesterol and DCP in a 3:3:1 molar ratio were melted at 130°C to give a total lipid concentration of 150 mM (26.87 mg/ml of surfactant, 24.87 mg/ml cholesterol and 11.72 mg/ml DCP). The melted mixture was then cooled down to 70°C and hydrated with the appropriate solution i.e. water to produce empty-NIVs or AmB-CD to produce AmB-NIVs as described in detail below. The resulted suspensions were homogenised at 70°C using a Silverson mixer (Model L4R SU, Silverson Machines, Chesham, UK) fitted with a 5/8" tubular work head at 9,000 rpm for 30 minutes or for less time according to the final particle size (Mullen *et al.*, 1997; Carter *et al.*, 2009).

To produce AmB-NIVs, the drug was previously complexed with an aqueous solution of HPγCD in a ratio 1:100 w/w (AmB-CD; Rajagopalan *et al.*, 1986). The pH of AmB-CD was adjusted to pH 12 with 1 M sodium hydroxide and to pH 7.6 ± 0.1 with 2 M phosphoric acid. AmB-CD was added to the melted lipids to produce AmB-NIVs. The mixture was then homogenised for 5 minutes to produce larger particles (around 800 nm) or homogenised for 30 minutes to produce smaller particles (< 200 nm). The use of ultrafiltration to remove unentrapped drugs from AmB-NIVs was studied using a vivaflow 50-ultrafiltration kit of 50,000 MWCO PES from Sartorius Stedim Biotech (Epsom, UK). AmB-NIVs were diluted 10 times with distilled water and ultrafiltrated to its original volume with the vivaflow.

NIVs were freeze-dried using an Epsilon 2-4 LSC freeze dryer (Martin Christ Gefriertrocknungsanlagen GmbH, Osterode am Harz, Germany). Thermocouples were carefully placed inside the vials to monitor the temperature of the product during the process. Freeze dryer parameters such as vacuum pressure, shelf temperature and product temperature were recorded with the process documentation software LyoLog-32 (version 2.0.0.35, from Martin Christ

Gefriertrocknungsanlagen GmbH, Osterode am Harz, Germany). In early formulation studies, empty-NIVs and AmB-NIVs (with no lyoprotectant) were generally freeze-dried using a general method i.e. samples were placed in freeze-drying vials (2 ml/each) and added to the freeze drier. Then, samples were frozen at -70°C at a rate of 2°C/min (from 25°C to -70°C in 45 min) and kept at -70°C for 45 min. The main drying step was set at a shelf temperature of -20°C and a vacuum pressure of 0.140 mBar for 4 hours followed by a vacuum pressure of 0.055 mBar for 4 hours. Then the shelf temperature was raised to -10°C, 10°C and 20°C during 4 hours intervals at a vacuum pressure of 0.055 mBar. Freeze-dried empty-NIVs with or without lyoprotectants were rehydrated with a drug solution to produce NIVs by a variation of the dehydration-rehydration method (DRV; Kirby and Gregoriadis, 1984).

In order to optimise the vesicle freeze-drying method, lyoprotectants were added (sucrose, glucose, trehalose or hydroxypropyl-cyclodextrins). Mannitol was not considered a suitable lyoprotectant due to potential damage of the NIVs bilayer related to the crystal nature of the compound. Lyoprotectants were generally solubilised in the aqueous solution used to rehydrate the melted lipids (70°C) in order to be homogeneity distrusted along the bilayer. For instance, in AmB-NIVs, sucrose was incorporated to optimise the freeze-drying method of the vesicles. AmB-CD solution containing sucrose was used to hydrate the melted lipids (70°C) and produce AmB-NIVs with the lyoprotectant. Different concentrations of the disaccharide were investigated for its cryoprotectant effect: 0.10 g/ml and 0.17 g/ml corresponding to a sucrose to lipid concentration ratio of 1.5 and 2.7 times.

In the case of empty-NIVs, the cryoprotectants sucrose, glucose and trehalose, were incorporated at a concentration of 0.17 g/ml (2.7 times the lipid concentration). Different concentrations of sucrose were also incorporated into empty-NIVs at 0.20 g/ml, 0.34 g/ml and 0.50 g/ml corresponding to a concentration ratio of 3.1, 6 and 8 times the lipid concentration. Moreover,

different cyclodextrins were tested with various ring size being hydroxypropyl-α-cyclodextrin (HPαCD, 6 membered sugar ring molecule), hydroxypropyl-β-cyclodextrin (HPβCD, 7 membered sugar ring molecule) and hydroxypropyl-γ-cyclodextrin (HPγCD, 8 membered sugar molecule). The HP-CDs were tested as potential cryoprotectants at a concentration of 6 times lipid (0.34 mg/ml). HPγCD was also tested at 0.20 g/ml, 0.34 g/ml and 0.50 g/ml corresponding to 3.1, 6 and 8 times the lipid concentration of empty-NIVs. The effect of using different freezing conditions on vesicle characteristics was investigated for empty-NIVs. Samples were frozen at -20°C and -80°C for at least 12 hours or frozen quickly in liquid nitrogen (~ 250°C/min) before storing at -80°C. Annealing at -20°C followed by freezing at -80°C or with liquid nitrogen were other freezing conditions studied. The effect of using a more controllable system for freezing was also tested using the Christ freeze-drier (Epsilon 2-4 freeze dryer, Martin Christ Gefriertrocknungsanlagen GmbH, Osterode am Harz, Germany) where a freezing rate of 0.6°C/min was used. Vesicle structure after freeze thawing was assessed by vesicle size, polydispersity index and ζ-potential (Section 2.5).

During freeze-drying optimisation studies, empty-NIVs were lyophilised in a bottom-flat HPLC glass vial (0.2 ml/formulation) to reduce the amount of formulation used. Thermocouples were carefully placed inside the vials with formulation and inside an empty vial. The vials were pre-frozen at -80°C overnight before incorporating to the freeze dryer. Pre-frozen empty-NIVs with sucrose were added to the freeze drier and kept frozen at -80°C for 3 hours. The main drying step was set at a shelf temperature of -35°C and a vacuum pressure of 0.009 mBar for 50 hours. The final drying was performed at 15°C and a pressure of 0.009 mBar for 45 hours. Pre-frozen empty-NIVs with HP-CDs were added to the freeze drier and kept frozen at -80°C overnight. The main drying step was set at a shelf temperature of 30°C and a vacuum pressure of 0.009 mBar for 25 hours. The final drying was performed at 15°C and a pressure of 0.009 mBar for 25 hours. Larger batches of empty-NIVs with HPγCD were

aliquoted into bottom-flat freeze dryer vials (2 ml/vial*)*. Vials were pre-frozen at -80°C and then added to the freeze-drier where they were kept frozen at -80°C for 2h. The main drying step started at a shelf temperature of -80°C for 5 hours and a vacuum pressure was kept constant at 0.009 mBar for all the main drying and final drying. A shelf temperature ramp from -80°C to -35°C was performed during 2 hours, followed by a sustained main drying at -35°C for 23 hours. The final drying started with a shelf temperature ramp from -35°C to 10°C for 6 hours followed by a constant shelf temperature of 10°C for 15 hours. At the end of the method, the chamber atmosphere was bled with nitrogen gas and the vials were sealed under a pressure of 3.00 mBar.

Luciferin-NIVs (Luc-NIVs) were generally formulated by dehydration-rehydration (DRV) passive loading method, where freeze-dried empty-NIVs were rehydrated with a solution of luciferin (5 mg Luc/ml of PBS pH 7.4) to produce Luc-NIVs. For *in vivo* imaging purposes, freeze-dried empty-NIVs (1 ml formulation at 150 mM) were rehydrated with 1 ml of luciferin (25 mg/ml) and then diluted with 4 ml of PBS pH 7.4 to obtain a formulation with 5 mg/ml luciferin and 30 mM lipid. Active loading of Luc-NIVs was studied to assess the potential effect on luciferin entrapment efficiency into NIVs. The active loading methods consisted in using different buffered solution to create a pH gradient between the interior and the exterior of NIVs (Kheirolomoom *et al.*, 2010). Firstly, empty-NIVs were formulated with buffer 1 (Table 2.3). The external buffer 1 was interchanged with buffer 2 using a diafiltration technique four times with vivaflow 50-ultrafiltration kit 50,000 MWCO PES from Sartorius Stedim Biotech (Epsom, UK). Luciferin solution (5 mg/ml) was then added and left to interact with NIVs for 10 minutes or 24 hours. After that period, the unentrapped luciferin and the buffer 2 were removed from the exterior of the NIVs by 7 times diafiltration volumes and changed to the previous buffer 1. The buffered solutions investigated are described in Table 2.3. In the case of HEPES reverse buffer approach, NIVs were directly formulated with buffer 2, added luciferin and external buffer changed to HEPES buffer 1.

Cisplatin-NIVs were generally formulated using the passive DRV method, where freeze-dried empty-NIVs were rehydrated with cisplatin solution (1 mg cisplatin/ml of NaCl 0.9 % w/v).

NIVs incorporating both AmB and luciferin were formulated in order to provide treatment and imaging probe in the same drug administration. Freeze-dried AmB-NIVs (1 mg/ml AmB, 150 mM lipid) were rehydrated with luciferin solution (25 mg/ml Luc). Then diluted 5 times with PBS pH 7.4 to produce a formulation of 0.2 mg/ml AmB, 5 mg/ml luciferin and 20 mM lipid.

NIVs encapsulating minor groove binders (MGBs) were formulated by the passive DRV method. Firstly, MGBs were solubilised with DMSO and then diluted with PBS pH 7.4 (2 % v/v DMSO). The resulting mixture was used to hydrate freeze-dried empty-NIVs and obtain MGBs-NIVs formulations.

Larger batches of empty-NIVs and AmB-NIVs were attempted to transfer the manufacture method from a laboratory scale to a large scale manufacturing procedure. Empty-NIVs scale-up studies were carried out at Aptuit LLC (Glasgow, UK) in collaboration with Inhalosome C Ltd (Leeds, UK). Aptuit formulated three batches of 250 ml empty-NIVs. The three components (surfactant, cholesterol, DCP) were carefully weighed out and added to a 250 ml Duran® bottle. The lipids were melted at approximately 130°C and cooled to 70°C. The molten lipids were subsequently hydrated with warm water for injection (70°C) and constant agitation. Once hydrated, the lipid suspension was homogenised using UltraTurrax at 11,000 rpm for 20 minutes (IKA, Staufen, Germany). The suspension was further homogenised under high pressure (HPH; approximately 1500 bar) using a Panda Plus 2000 (GEA Mechanical Equipment, Oelde, Germany). The sample was passed through the HPH repeatedly to achieve a maximum particle size reduction. The particle size of the samples during production was determined using a dynamic light scattering (DLS)

Nanotrac 150 (Microtrac, Krefeld, Germany) and represented as a mean intensity diameter and standard deviation of the width of the distribution. However, particle size characteristics after formulation, were determined as described in Section 2.5.

Studies were also carried out in-house to scale up the production of AmB-NIVs (1 mg/ml AmB, 100 mg/ml HPγCD, 0.09 g/ml sucrose and 150 mM lipid). Two batches were produced of 250 ml (batch 1) and 100 ml (batch 2). The formulations were produced under sterile conditions. Vial stoppers and over seals were wrapped in autoclave pouches and sterilised by autoclaving at 121°C for 15 min. All glassware and the homogeniser head were double wrapped in tinfoil and sterilised for 2 hours at 160°C in an oven (European Pharmacopoeia, 2004). HPγCD was solubilised with sterile water for injection until complete dissolution. Sucrose was also dissolved with water prior incorporation to the cyclodextrin mixture. AmB was added to the solution and the pH was adjusted to 12 (with 1 M sodium hydroxide) and to 7.6 ± 0.1 (with 2 M phosphoric acid). The resulted suspension was made up to 250 ml or 100 ml with a volumetric flask and filtered to a sterile environment through a 0.22 μm syringe filter. The lipids (surfactant, cholesterol and DCP) were added to a sterile 500 ml (batch 1) or 250 ml (batch 2) Duran® bottle, mixed together and melted in an oil bath at 130°C. The temperature was dropped so that the composition was at 70°C then AmB-CD mixture (kept at 70°C) was added. The closed Duran® bottle was transferred to a water bath set at 70°C inside a class II safety cabinet. The lipid mixture was then homogenised at a speed of 10,200 1/min for 60 minutes at 70°C. In batch 1, the formulation was kept at 70°C before being filtered through a 0.45 μm syringe filter and aliquoted in freeze drier vials (2 ml/vials). In batch 2, the formulation was aliquoted directly to the freeze-drier vials without being kept at 70°C for filtration proposes. All the vial stoppers had to be partially removed before being added in the freeze drier, this step could not be done under aseptic conditions since the freeze drier used was not in a clean room. To test the sterility of the formulation, two different types of microorganism

cultures, fluid thioglycollate broth and tryptone soya broth, were spiked with the reconstituted AmB-NIVs formulation (Parveen *et al.*, 2011). Flasks were left to incubate for 2 weeks at 37°C and 25°C respectively. Negative and positive controls were cultured alongside samples. Sterile distilled water was spiked to the negative control. The positive control was inoculated with the contact of the broth with a hand and therefore placing naturally skin flora. The two AmB-NIVs large batches were freeze-dried using two different methods. Batch 1 was freeze-dried as described in Table 2.4 and Batch 2 was frozen at -80°C in a freezer for 12 hours and then dried in the freeze dryer as described in Table 2.5.

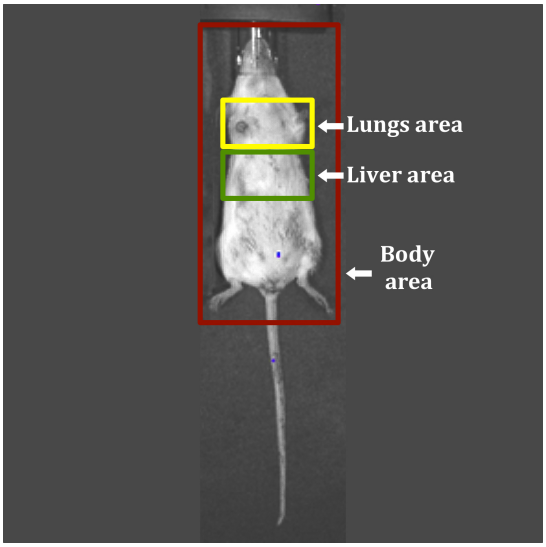


**Figure 2.1** Luminescence quantification of different regions of interest on mice image: body area (red), lung area (yellow) and liver area (green). Image of an uninfected BALB/c mouse.

**Table 2.3** Active loading approaches for Luc-NIVs production. Empty-NIVs were formulated with buffer 1 and the buffer from outside NIVs was exchanged to buffer 2 prior the addition of luciferin. Luciferin was left to react with the composition for 24 h and then the unentrapped luciferin and the buffer 2 from outside NIV were substituted for buffer 1 (Kheirolomoom *et al.*, 2010).

| Combination | Buffer 1 | Buffer 2 |
|---|---|---|
| HEPES buffer | 300 mM HEPES buffer (pH 8.0) | 20 mM citric acid with 150 mM NaCl (pH 5.0) |
| Tris buffer | 300 mM Tris buffer (pH 10.0) | 20 mM citric acid with 150 mM NaCl (pH 5.0) |
| Acetate gradient | 120 mM calcium acetate (pH 6.0) | 120 mM sodium acetate (pH 6.0) |

**Table 2.4** Freeze-drying program used to lyophilisate AmB-NIVs scale up batch 1 (n.a., not-applicable).

| Phase | Time (hours) | Shelf temperature (°C) | Vacuum (mBar) |
|---|---|---|---|
| **Load** | n.a. | +20 | n.a. |
| **Freeze** | 1 | -70 | n.a. |
| | 4 | -80 | n.a. |
| **Main drying** | 6 | -40 | 0.140 |
| | 6 | -20 | 0.055 |
| | 6 | -10 | 0.055 |
| | 6 | -5 | 0.055 |
| **Final drying** | 6 | +12 | 0.001 |
| | 6 | +18 | 0.001 |

**Table 2.5** Freeze-drying program used to lyophilisate AmB-NIVs scale up batch 2 (n.a., not-applicable).

| Phase | Time (hours) | Shelf temperature (°C) | Vacuum (mBar) |
|---|---|---|---|
| **Load** | n.a. | -80 | n.a. |
| **Main drying** | 40 | -80 | 0.003 |
| | 80 | -60 | 0.003 |
| | 3 | -50 | 0.003 |
| | 15 | -50 | 0.003 |
| | 3 | -45 | 0.003 |
| | 22 | -45 | 0.003 |
| **Final drying** | 5 | +10 | 0.003 |
| | 45 | +10 | 0.003 |

## 2.5. NIVs characterisation

NIVs formulations were characterised on the basis of vesicle size, polydispersity, ζ-potential, viscosity, entrapment efficiency and nanomechanical properties. Vesicle size (z-average number), polydispersity index (Pdi) and ζ-potential (ZP) of the vesicles were assessed with a Zetasizer Nano DLS using capillary ζ-potential cell (Malvern Instruments, Malvern, UK). Approximately 100 µl of the NIVs formulation was suspended in 2 ml of distilled water prior to analysis to avoid multi-scattering phenomena, unless otherwise stated. The resulting values were the mean of 3 samples each one measured 3 times. For particles larger than 1 µm, the Mastersizer laser diffraction particle size analyser was used (Malvern Instruments Ltd, Malvern, UK). The laser was not used unless laser intensity higher than 80 % was obtained. The settings were stabilised for general purpose, enhanced and spherical particles with a measurement time of 12 seconds and a stirring speed of 1800 rpm. The results presented were an average of 3 cycles.

Entrapment efficiency (EE %) of NIVs particles was calculated using the ultracentrifugation method. The drug entrapped within NIVs was separated from the un-entrapped drug by pelleting a NIVs suspension using a XL-90 ultracentrifuge (Beckman Coulter Life Sciences, High Wycombe, UK). The NIVs formulation (0.3 ml) was suspended in 2 ml of distilled water and ultracentrifuged at 310,801 g, 4°C for 1 hour using a 701Ti rotor (Beckman Coulter Life Sciences, High Wycombe, UK). The total amount of drug quantified in the pellet was compared to the total amount quantified in the whole formulation to obtain a percentage of entrapment efficiency (Equation 2.1).

$$\text{EE}\ (\%) = \frac{\text{Pellet}}{\text{Whole}}\ \text{x}\ 100 \qquad \text{Equation 2.1}$$

The total amount of drug in the supernatant was also quantified to quality control the determination method by percentage of recovery (Equation 2.2). Only analyses with recovery values of 100 ± 10 % were considered acceptable.

$$\text{Recovery (\%)} = \frac{(\text{Pellet} + \text{Supernatant})}{\text{Whole}} \text{ x } 100 \qquad \text{Equation 2.2}$$

Rheology measurements were undertaken using a HAAKE MARS III Rotational rheometer (Thermo Scientific, Warrington, UK). A 35 mm cone and plate geometry of 1° angle and made of titanium was used, with a gap of 0.053 mm. The HAAKE RheoWin measuring and evaluation software package was used for system control along with data gathering and analysis (version 4, Thermo Scientific, Warrington, UK). The temperature was kept constant at 25°C with a MARS III Temperature Module Controller (Thermo Scientific, Warrington, UK). Samples were spooned onto the plate to minimise further shearing. The cone was lowered at 1.25 cm/s to a fixed gap of 0.053 mm. Up and down hysteresis loop test data was generated with maximum shear rates of 1200 1/s and a sweep time of 60 seconds. The flow behaviour index and consistency index were derived from the power law equation (Equation 2.3) fitted by the RheoWin DataManager software (version 4, Thermo Scientific, Warrington, UK).

$$y = a\, x^{b} \qquad \text{Equation 2.3}$$

The power law equation related shear stress (y, Pa) with consistency index (a, Pa·s), shear rate (x, 1/s) and flow behaviour index (b, dimensionless). This model approximated the shearing behaviour of the formulation, with b=1 for Newtonian systems, b < 1 for shear thinning and b > 1 for shear thickening. The apparent viscosity taken was an average of the 10 apex values of the up flow curve (n=3). The area of hysteresis loop was also determined (Pa/s).

Atomic force microscopy (AFM) was used to image and obtain the nanomechanical properties of AmB formulations. The mapping AFM microscopy

was conducted in collaboration with Dr. Lamprou (University of Strathclyde, UK). AmB-CD and AmB-NIVs (5 µl) formulated as described in Section 2.4 were imaged. AmB-CD samples were deposited in freshly cleaved silicon wafer surface and AmB-NIVs onto mica surface (G250-2 Mica sheets 1" x 1" x 0.006", Agar Scientific Ltd, Essex, UK) and left to dry before imaging. The images were obtained by scanning the surface in air under ambient conditions using a MultiMode 8 Scanning Probe Microscope (Digital Instruments, Santa Barbara, CA, USA; Bruker Nanoscope analysis software Version 1.40). NIVs pictures were analysed on PeakForce quantitative nanomechanical property mapping mode using ScanAsyst-air probes, and the spring constant (0.5 N/m; Nominal 0.4 N/m) and deflection sensitivity was calibrated, but not the tip radius (nominal value of 2 nm). Mechanical properties of the particles such as height, diameter, surface roughness, force, deformation and dissipation were analysed using NanoScope analysis software version 1.40 (Digital Instruments, Santa Barbara, USA). AFM images were collected at random spot surface sampling (at least five areas).

The thermo-analytical technique of differential scanning calorimetry (DSC) was used to investigate thermal profile of NIVs formulations upon freezing in order to optimise the lyophilisation process. All experiments were carried out with a DSC 821$^{e}$ from Mettler-Toledo equipped with STARe software (version 8.0, Columbus, USA). Samples (10 µl) were placed inside a sealed aluminium pan and compared against a reference empty pan. Both the sample and the reference pan were frozen from 25°C to -65°C at a 10°C/min rate, and then the temperature was held at -65°C for 3 minutes. The heating rate, from -65°C to 25°C, was at 15°C/min (optimised ratio, with an acceptable heating speed *vs* number of points obtained) and the samples were held at 25°C for 3 minutes. Only the heating curve was used for thermal analysis since the cooling curve is biased due to the super cooling effect. The glass transition temperature of the maximally freeze-concentration fraction ($T_g'$) was calculated from the onset of the curve. The melting temperature (Tm) was determined from the peak point.

Water was analysed as a blank reference. Solutions of sucrose (0.50 g/ml), HPαCD (0.38 g/ml), HPβCD (0.38 g/ml), HPγCD (0.38 g/ml) and empty-NIVs with HPγCD (75 mM lipids, 0.38 g/ml cyclodextrin) were studied. Samples with very subtle $T_g$', such as AmB-NIVs, were added to the 40 µl pan in larger amounts (30 µl) and left to evaporate at room temperature until the weight was reduced by half, before analysing in the DSC. Since $T_g$' is independent of the solute concentration, this method was favourable to detect second order thermal transitions.

To assess the relative water content in freeze-dried samples, one gravimetric and one coulometric approach were used. The gravimetric approach was calculated using Equation 2.4.

$$\text{Water (\%)} = \frac{[W_t - W_0] - \left[ C \text{ x } \frac{(W_f - W_0)}{\rho} \right]}{(W_t - W_0)} \text{ x } 100 \qquad \text{Equation 2.4}$$

$W_t$ was the weight of the vial with the freeze-dried cake (g), $W_0$ was the weight of the vial empty (g), C was the concentration of all components (g/ml), $W_f$ was the weight for the vial with the liquid formulation before freeze-drying (g) and ρ was the formulation density (g/ml). A Karl Fisher Coulometer DL39 from Metter Toledo (Columbus, USA) was also used to determinate the trace amount of water in the lyophilised cake by coulometric titration. Cakes were solubilised with a mixture of chloroform and methanol (3:1 v/v). The weight of the lyophilised cake, weight of the solvent added to the cake and the difference in weight of the glass needle with the sample and after injection was recorded. The trace amount of water in the solvent mixture was firstly determined (n=3). The trace amount of water in the cake (C, % w/w) was calculated with Equation 2.5.

$$C = \frac{(C_1 W_1 - C_3 W_3)}{W_2} \qquad \text{Equation 2.5}$$

$C_1$ is the % w/w of water in the sample (given by the coulometer), $W_1$ is the weight of the sample (cake + solvent), $W_2$ is the weight of the lyophilised cake, $C_3$ is the % w/w of water in the solvent mixture (given by the coulometer) and $W_3$ is the weight of the solvent added to the sample.

### 2.6. Stability study of AmB-NIVs

Two stability studies were carried out to determine the chemical and physical stability of freeze-dried AmB-NIVs and its reconstituted vials.

Two batches of freeze-dried AmB-NIVs with sucrose as a lyoprotectant, produced and freeze-dried as stated in Section 2.4, were subjected to stability studies. Batch 1 was included in an accelerated stability study for 6 months (International Conference on Harmonisation, 2003). The freeze-dried vials were placed in an incubator at 40°C, in a fridge at 4°C and in a freezer at -80°C for 2 months, 4 months and 6 months. Batch 2 was subjected to a shorter stability study of 15 weeks. The vials were placed in an incubator at 40°C, in a fridge at 4°C and in a freezer at -80°C for 6 and 15 weeks. In both studies, 3 vials were reconstituted at each stability time point. The parameters studied were vesicle size, polydispersity index, ζ-potential, drug content and AmB entrapment efficiency (Section 2.5).

Freeze-dried AmB-NIVs vials from batch 1 were reconstituted to investigate the stability of the formulation once rehydrated. Several vials were rehydrated and placed at 25°C and 4°C constant temperature rooms. The time points of the study were: day 0, 24 h, 7 days, 14 days and 21 days. The structural parameters studied were vesicle size, polydispersity index, ζ-potential, AmB content and AmB entrapment efficiency (Section 2.5).

## 2.7. Aerosol properties of NIVs formulations

Three different vibrating-mesh nebulisers were used in the studies to determine the aerosol properties of nebulised NIVs: I-neb passive vibrating-mesh nebuliser and two active vibrating-mesh Aeroneb Go and Aeroneb Lab were used. The aerodynamic particle size of the aerosols was characterised using a multi-stage liquid impinger (MSLI) and a new generator impactor (NGI), both from Copley Scientific (Nottingham, UK). The geometric particle size of the aerosols was investigated with a laser diffraction method (Spraytec, Malvern Instruments, Malvern, UK) with the collaboration of Ms Sarah Byrne (Philips Respironics, Chichester, UK).

The MSLI was set up at a flow rate of 20 ± 1 L/min with 20 ml of the appropriate solvent in each stage (50:50 DMSO: methanol for AmB and PBS pH 7.4 for luciferin samples). When nebulisation was finished, the MSLI was turned carefully upside down to collect any drug on the wall of the stages. The filter of the last stage was soaked into the correspondent solution for 10 minutes in order to solubilise the drug impacted. Cisplatin formulations were not investigated with the MSLI to avoid safety issues involved with handling and cleaning procedures. The NGI was set up at a flow rate of 15 ± 1 L/min and a filter was placed at the end of the apparatus. When nebulisation was finished, each cup was soaked for 10 minutes, with the appropriate solvent for the drug being analysed. For example, for AmB samples, 5 ml/cup of DMSO:methanol (30:60 v/v) was used to extract the drug from the impactors, the induction port and the filter. Methanol (10 ml) was used for drug extraction of plastic components such as the nebuliser mouthpiece, adaptor and nebuliser mesh. After 10 minutes of incubation, the plastic components were removed from the solvent and extra DMSO was added to equilibrate with the DMSO:methanol proportion of the cup samples. Cisplatin solution samples were extracted with NaCl (0.9 % w/v) and Cis-NIVs were dissolved with 0.1 M NaOH. Empty-NIVs samples were extracted from the cups with 5 ml of chloroform:methanol (3:1)

and from the plastic components with 10 ml of 100 % methanol. The parameters studied with the NGI were mass median aerodynamic diameter (MMAD) and geometric standard deviation (GSD). And the parameter studied with MSLI was fine particle fraction (FPF < 5 μm, i.e. fraction of aerosol mass contained in particles with an aerodynamic diameter smaller than 5 μm and larger than 0.98 μm). All those calculated from the amount of drug detected by HPLC (Sections 2.2 and 2.3). A base ten logarithm of the cut-off diameter was plotted against drug cumulative percentage undersize to calculate MMAD, GSD and FPF < 5 μm. The particle size in the 50$^{th}$ mass percentile of cumulative percentage was the MMAD (Christopher *et al.*, 2013). The GSD was calculated according to Equation 2.6.

$$GSD = \left(\frac{d_{84.13}}{d_{15.87}}\right)^{\frac{1}{2}} \qquad \text{Equation 2.6}$$

Where $d_{84.13}$ was the diameter when the cumulative mass percentage was equal to 84.13 % and $d_{15.87}$ was the particle diameter when the cumulative mass was equal to 15.87 %. A GSD closer to the unit was indicative of mono-distributed particle size. The FPF < 5 μm was the percentage of particles between 0.98 and 5 μm and was calculated subtracting the percentage of drug with a size under 0.98 μm to percentage of droplets with a size under 5 μm.

Prior usages of the laser diffraction, the lenses were carefully cleaned in order to avoid any interference on the results. The output flow vacuum pump was set at 15 ± 1 L/min. Data was recorded until complete nebulisation of 0.5 ml of the tested formulation. Geometric diameters were automatically calculated and expressed like mass median diameter (MMD; Spraytec software, version 3.20, Malvern Instruments, Malvern, UK). The span value is a unit-less indication of polydispersity of the aerosol cloud, the closest to one the more mono-disperse (Equation 2.7). The Aeroneb Lab was not tested under the laser diffraction due

to the big dimensions of the nebuliser and the test being outside the University facilities.

$$\text{Span} = \frac{(90\ \% - 10\ \%)\ \text{undersize}}{\text{MMD}} \qquad \text{Equation 2.7}$$

A gravimetric approach was used to quantify how much volume of formulation was nebulised per minute (ml/min, Equation 2.8).

$$\text{Output (ml/min)} = \frac{(W_B - W_C)}{(\rho \text{ x } t)} \qquad \text{Equation 2.8}$$

The nebuliser was initially weighed empty ($W_A$), with the loaded formulation ($W_B$) and weighed again after nebulisation ($W_C$). The time necessary to complete nebulisation (Aeroneb Go and Aeroneb Lab) or up to acoustic signal (I-neb) was recorded (t). The percentage of drug delivered was calculated gravimetrically following Equation 2.9.

$$\text{Drug Delivered (\%)} = \frac{(W_B - W_C)}{(W_B - W_A)} \text{ x } 100 \qquad \text{Equation 2.9}$$

The effect of the mesh nebuliser on NIVs properties was investigated for the AmB-NIVs case. Changes on AmB-NIVs formulations upon nebulisation with I-neb, Aeroneb Go or Aeroneb Lab were analysed. The nebulisers were connected to a sealed container with 20 ml of distilled water and surrounded by ice to facilitate aerosol condensation (Figure 2.2). The nebulised AmB-NIVs impinged into the cold surface and then was collected to investigate whether the NIVs properties changed upon nebulisation. The parameters analysed were vesicle size (z-average), polydispersity index, ζ-potential and entrapment efficiency and those were compared to the same values before nebulisation (Equation 2.10).

$$\text{Recovery (\%)} = \frac{\text{Nebulised value}}{\text{Original value}} \text{ x } 100 \qquad \text{Equation 2.10}$$

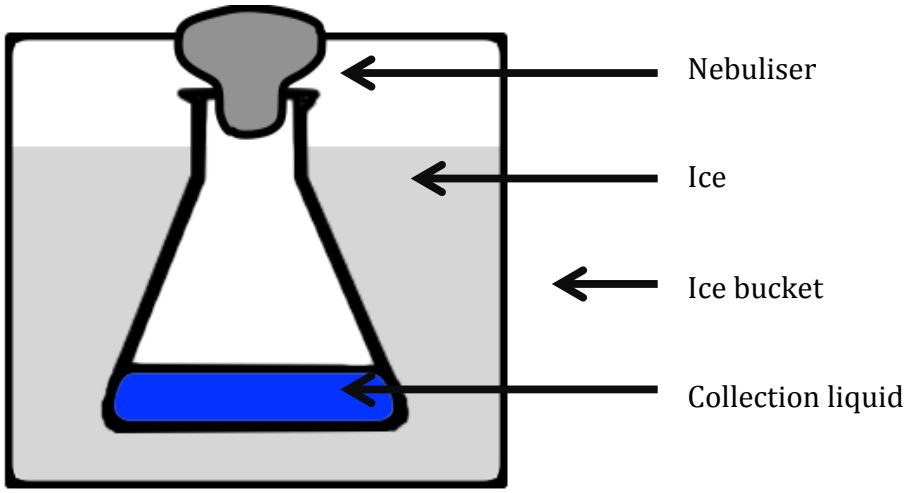


**Figure 2.2** Diagram representation of the set up used to study the effect of vibrating mesh nebulisation on NIVs properties. The nebuliser (I-neb, Aeroneb Go or Aeroneb Lab) was connected and sealed with paraffin film to a 250 ml flask with 20 ml of distilled water inside. The flask was surrounded by ice to facilitate condensation of the aerosol produced.

## 2.8. *In vitro* cell toxicity studies

B16-F10-luc cells were incubated at 37°C in a humidified atmosphere of 5 % $CO_2$. B16-F10-luc were seeded in complete Dulbecco's Modified Eagle Medium (DMEM) containing 4.5 g/L glucose, 5000 U/ml of penicillin, 5 mg/ml streptomycin, 200 mM L-glutamine and 10 % v/v foetal calf serum (all from Life Technologies, Runcorn, UK). B16-F10-luc cells were passaged every 24 or 48 hours, depending on confluence. B16-F10-luc produced BLI in contact with luciferin and this property was used to detect the cell growth inhibition related to the assessed drugs (as described in Section 2.3). The percentage of inhibition of cell growth was calculated as described in Equation 2.11.

$$\text{Suppression (\%)} = \frac{\text{Control} - \text{Treated}}{\text{Control}} \text{ x } 100 \qquad \text{Equation 2.11}$$

B16-F10-luc cells were used to assess the anticancer activity of new synthesised minor grove binders (MGBs supplied by Dr. Scott, Dr. Khalaf and Prof. Suckling, Strathclyde University, UK). MGBs nomenclature, chemical structure and molecular weight are described in the Appendix. All compounds were prepared at a concentration of 630 µg/ml diluted with DMSO. B16-F10-luc cells ($3.7x10^5$ cells/well, 200 µl) were added on a transparent 96 well plate spiked with 5 µl of MGB compounds (15.36 µg/ml, n=3), 5 µl of gemcitabine (15.36 µg/ml diluted with DMSO, n=3) and 5 µl of DMSO as a solvent control (n=6). After 24 hours of incubation, luciferin solution (20 µl of 150 µg/ml/well PBS pH 7.4) was added to each plate and the amount of BLI (Section 2.3) was used to determine percentage of suppression related to the solvent control (Equation 2.11). The lipophilicity distribution coefficient, log D at pH 7.4 (log $D_{7.4}$), of each compound was predicted using MarvinSketch (Equation 2.12; Version 15.2.2.0, from ChemAxon Ltd, Budapest, Hungary).

$$Log\ D_{oct/wat} = log\left(\frac{[solute]_{oct}^{ion} + [solute]_{oct}^{un-ion}}{[solute]_{wat}^{ion} + [solute]_{wat}^{un-ion}}\right) \qquad \text{Equation 2.12}$$

Log $D_{7.4}$ is the distribution coefficient related to the concentration of all forms, ionised (ion) or un-ionised (un-ion) in the water (wat) or octanol (oct) phase at pH 7.4 (Camenisch *et al.*, 1998).

MGBs compound with a significant percentage of suppression were considered candidates for the study of half maximal inhibitory concentration ($IC_{50}$). $IC_{50}$ were determined incubating B16-F10-luc ($1x10^5$ cells/well) cells with serial dilution of the compounds in media (n=3/treatment) on a 96 well plate for 24 hours. After 24 hours, luciferin solution (20 µl of 150 µg/ml/well PBS pH 7.4) was added before determine BLI by IVIS imaging (Section 2.3). The $IC_{50}$ of the formulation was calculated using GrapPad Prism version 6.0c (La Jolla, USA). Logarithmic of the compound concentration (µM) was plotted against % suppression and a nonlinear regression of *log(agonist) vs normalised response* was fitted. The $IC_{50}$ for DMSO was also calculated to ensure that the $IC_{50}$ of the compound was not due to the solvent vehicle concentration.

### 2.9. *In vivo* studies

All *in vivo* studies were carried out at the Strathclyde Biological Procedures Unit, which is a conventional multispecies unit located at the University of Strathclyde. The Unit undertakes periodical quarterly health screens and maintains core-breeding stock within Individual Ventilated Cages. All animals within the designated building were housed in at least the minimum conditions specified in the code of Practice housing guidelines (Home Office, 2014). The atmospheric conditions in the Unit were controlled with humidity between 45 – 65 % and a temperature between 19°C and 23°C. The light dark cycles were of 12 hours. The animals were kept over bedding composed of dust free sawdust and the nesting material was Sizzlenest®. Animals stayed within conventional

cages made of polypropylene or polysulfone (NKP cages, Coalville, UK) in a stocking density as per Home office code of Practice (Home Office, 2014). The husbandry type of food was a standard rodent breeder and grower made of wheat, wheat feed, barley, de-hulled extracted toasted soya, maize, macro minerals, soya oil, potato protein, hydrolysed wheat gluten, full fat soya, maize gluten meal, vitamins, micro minerals and amino acids (Special Diets Services, Essex, UK). Food and water were given *ad libitum* during the experimental period.

The effect of AmB-NIVs in the treatment of leishmaniasis was investigated in a *L. donovani* mice model. Age-matched in bred in-house female BALB/c were infected with *L. donovani* (strain LV82-luc; $1x10^7$ parasites/mice). Seven days post-infection the mice were randomized into 3 groups and treated with different formulations intravenously (1 or 0.05 mg AmB/kg). PBS pH 7.4 was administered to the control group; AmB-CD or AmB-NIVs were administered to the other two groups. The infection and treatment progression was monitored imaging the BLI of mice with the IVIS during the course of the study (Section 2.3). BLI values were obtained from images of the liver area (Figure 2.1). Luc-NIVs (50 mg/kg Luc and 0.30 mmol/kg lipid; intraperitoneal) were used as imaging enhancer to detect the LV82-luc parasite burdens. The imaging formulation was injected intravenously followed by IVIS imaging for 14 minutes maximum on day 8, 12 and 18 post-infection. The values obtained after 6 minutes post-luciferin administration were plotted to monitor the course of the infection over time. When the experiment was finalised, *ex vivo* spleen and liver were imaged under the IVIS. Smears of liver, spleen and bone marrow were also collected and parasite burdens counted (by Dr. Carter, University of Strathclyde, UK; Carter *et al.*, 1999).

The levels of neutrophils present in mice after drug treatment were determined as an indicator of drug-induced inflammatory response. The presence of neutrophils can be determined using the amount of CLI produced after injecting

luminol (Liu *et al.*, 1996). AmB formulations of different sizes, small (approximately 200 nm) or large (approximately 800 nm), were administered to healthy BALB/c intravenously and by inhalation (n=3/group). For inhalation studies, mice were placed inside a Volumatic Spacer (Allen & Hanburys, London, UK), with the open end sealed using paraffin film and the other end attached to the Aeroneb Lab nebuliser. Each formulation (0.5 ml; 1 mg AmB/kg) was nebulised until finalisation. Mice were imaged for 2 minutes under the IVIS to obtain a background reading. Then injected intra-peritoneal with luminol solution (0.2 ml, 100 mg/kg in PBS pH 7.4) and the amount of CLI over 30 minutes determined. Mice were then euthanised in a $CO_2$ chamber and lungs, spleen and liver were collected. Organs were imaged after being submerged in a solution of luminol (150 μg/ml). Lungs were analysed posteriorly for AmB content by HPLC (Section 2.2).

Two hamster models of visceral leishmaniasis were used to determine whether AmB-NIVs vesicle size influenced parasite burden decrease. An antimony susceptible parasite strain (LV82) and an antimony resistant parasite strain (LV200015) were used to infect a group of hamsters (females, 152 ± 13 g body weight) by tongue vein injection ($1x10^7$ amastigotes). Seven days after infection, hamsters were treated individually with AmB formulations (1 mg/kg AmB, 150 mmol/kg lipid). The control group was treated with distilled water. The other groups were treated with AmB-CD, AmB-NIVs of small (approximately 200 nm) or large (approximately 800 nm) particle size. NIVs were diluted ½ with distilled water prior nebulisation. Treatments were performed daily during day 7 and 11 post-infection from 9:00 to 13:00. Before treatment, hamsters were anesthetised with aerosolised isoflurane for 10 min. Each subject was individually treated with Aeroneb Lab, set up as shown in Figure 2.3.A. The treatment was performed until complete nebulisation of the formulation. If the subject awakened during treatment, extra 10 minutes of aerosolised isoflurane were added and the treatment resumed. At 14 days post-infections, hamsters were euthanised. Liver, spleen and bone marrow were obtained and smeared to

quantify parasite burdens (counted by Dr. Carter, University of Strathclyde, UK). Lungs and trachea were obtained and residual AmB-NIVs quantified by HPLC (Section 2.2).

To investigate whether the use of different types of vibrating-mesh nebulisers would be related to better lung delivery, two sets of experiments were conducted where nebuliser's performance was assessed *ex situ* or *in situ*. For the *ex situ* experiments, the lungs of the treated animals were obtained and the drug levels were quantified by HPLC (Section 2.2). Sprague Dawley in-bred male rats were used for the *ex situ* experiments (270 ± 22 g body weight, n=12). Rats were then anesthetised with 0.7 ml/kg of a mixture composed of 25 % v/v of Hypnorm (Fentanil citrate 0.315 mg/ml and fluanisone 10 mg/ml), 25 % v/v of Hypnovel (midazolam 15 mg/3ml) and 50 % water for injection. AmB-NIVs was formulated as described and diluted with distilled water before being nebulised. Rats were anesthetised and AmB-NIVs was individually administered by inhalation (1 mg/kg AmB, 150 mmol/kg lipid). Three different mesh nebulisers were used for the study, I-neb (continuous mode, power level 6), Aeroneb Go and Aeroneb Lab (n=4/nebuliser group). I-neb and Aeroneb Go mouthpiece were modified in order to match with the mouthpiece dimensions of the Aeroneb Lab (red arrow in Figure 2.3). Rats were euthanised 5 minutes after the nebulisation was finalised. Blood was taken from the heart and plasma obtained. Lungs, trachea, liver, brain, spleen and kidneys were collected from each individual and frozen at -80°C until day of analysis by HPLC. The percentage of drug detected in the organs compared to the amount delivered was also calculated. To investigate the use of two different vibrating-mesh nebulisers *in situ*, male BALB/c mice were nebulised Luc-NIVs and imaged with the IVIS (Section 2.3). A group of male BALB/c mice were injected with B16-F10-luc ($5x10^5$ cells/mice). Twenty days post-infection the mice were randomized into 2 groups (n=3/group) and imaged with Luc-NIVs aerosolised with the Aeroneb Go or I-neb. Luc-NIVs was also nebulised to a healthy group of mice with the Aeroneb Go to obtain background levels. Luc-NIVs was

formulated with a total luciferin concentration of 20.8 mg/l and lipidic concentration of 50 mM. Mice were placed inside a Volumatic Spacer (Allen & Hanburys, London, UK), with the open end sealed using paraffin film and the other end attached to the Aeroneb Go or I-neb nebuliser. I-neb was used with a power level 6 and each group was given 0.5 ml of the Luc-NIVs. After treatment, mice were subsequently imaged every 2 minutes. The BLI obtained 6 minutes after nebulisation was compared between groups. Mice were euthanised, lungs obtained and imaged *ex situ* before and after immersion with luciferin solution (150 µg/ml). The lungs were immersed in luciferin to obtain the maximum BLI value that they could emit. Therefore, the relation expressed in Equation 2.13 could be use as the percentage of BLI activated by the luciferin that reached the lungs.

$$\text{BLI activated } = \frac{\text{BLI lungs } ex\ vivo}{\text{BLI lungs } ex\ vivo \text{ immersed in Luc}}\ x100 \qquad \text{Equation 2.13}$$

A

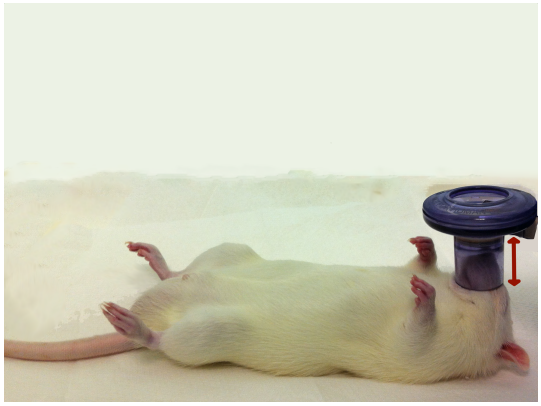

B

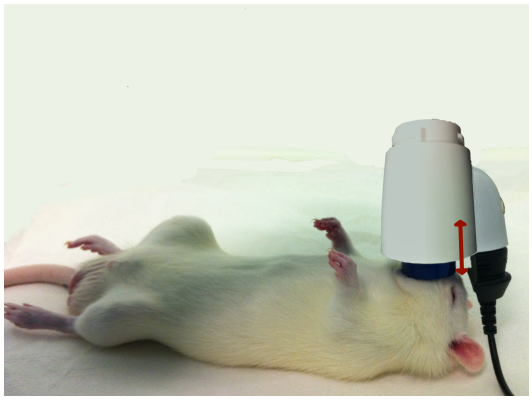

C

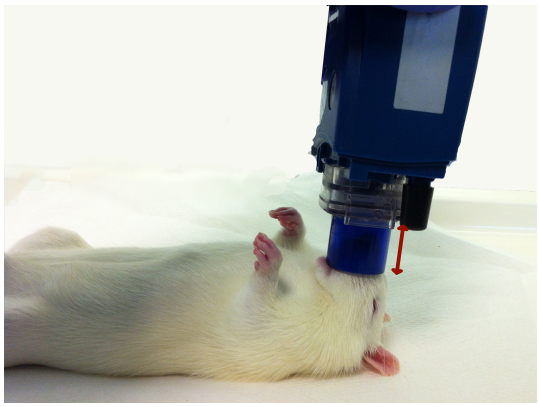

**Figure 2.3** Individual *in vivo* nebulisation set-up for (A) adapted Aeroneb Lab, (B) adapted Aeroneb Go, (C) I-neb power level 6. All nebulisers were unified for mouth-nose connector length and diameter (red arrow represents 22 mm).

The lead MGBs compounds assessed during *in vitro* studies in B16-F10-luc (Section 2.8) and *L. donovani* or *L. major* (Mr. Shaw, University of Strathclyde, unpublished data) were assessed *in vivo*. For the lung cancer model, BALB/c male mice were injected with $5x10^5$ B16-F10-luc cells and the amount of BLI emitted determined during the course of the experiment (days 4, 7, 11 and 14 post B16-F10-luc injection after being injected with 150 mg/kg of luciferin). In addition, mice were weighed at the start of the experiment and at the end, to determine if the compound had any adverse effect on mouse weight. Two similar experiments were performed with formulations administered by the intravenous route and the other one with the formulations administered directly to the lungs by inhalation. Mice were distributed in different groups: control, mice treated with empty-NIVs, mice treated with $MGB_{23}$ solution or mice treated with $MGB_{23}$-NIVs (n=5 mice/group). In the intravenous experiment, mice were injected with 0.2 ml/mice and in the inhalation experiment mice inhaled 0.1 ml/mice at the doses described in Table 2.6. Mice treated by inhalation were placed in volumetric chamber attached to the nebuliser Aeroneb Lab (n=5/treatment). As an exception, the mice group treated with $MGB_{23}$-NIVs by intravenously were administered the same dosage on day 3, day 9 and day 11 (10.5 mg/kg $MGB_{23}$, 0.30 mmol/kg lipid in PBS pH 7.4 containing 0.4 % v/v DMSO) due to limitations on formulation availability. On day 14, mice were euthanised. Lungs, liver and spleen (only for the intravenous route) were obtained and weighed. The amount of BLI emitted after lungs and liver had been immersed in luciferin solution (150 μg/ml PBS pH 7.4) was imaged.

The lead compound for *L. donovani* studies, $MGB_{58}$ was assessed for its *in vivo* efficacy against a murine model of visceral leishmaniasis. The efficacy of the $MGB_{58}$ against *L. donovani* was tested in BALB/c. Mice were infected with $1x10^7$ *L. donovani* LV82 amastigotes. Mice were treated by intravenous injection into the tail vain on day 7 at the doses described in Table 2.7. On day 14 mice were sacrificed and parasite burdens determined. The $MGB_{58}$ induced inflammation was tested with the luminol-CLC assay (Section 2.3). Healthy mice and mice

infected with *L. donovani* ($1x10^7$ LV82/mice, 7 days post-infection) were treated with PBS pH 7.4 containing 0.4 % v/v DMSO (control), empty-NIVs (0.30 mmol/kg lipid in PBS pH 7.4 containing 0.4 % v/v DMSO) and $MGB_{58}$-NIVs (10 mg/kg $MGB_{58}$, 0.30 mmol/kg lipid in PBS pH 7.4 containing 2 % v/v DMSO). Images of the mice whole body were obtained under the IVIS system and luminol was injected intraperitoneal (100 mg/kg) after two minutes of imaging.

### 2.10. Statistical analysis of data

Graph Pad Prism (version 6.0c) was used for statistical analysis of data. Data were tested for normality by D'Agostino-Pearson omnibus normality test or Kolmogorov-Smirnov test with Dallal-Wilkinson-Lilliefor p value if there were fewer data sets. Normally distributed data was analysed by student's 2 t-test or one way analysis of variance (ANOVA) combined with Turkey's one-way multiple comparison test. A two-way ANOVA was used when more than two factors were studied. Non-paramedic data (all *in vivo* results) were statistical analysed by Mann-Whitney test for two treatments or Kruskal-Wallis test followed by Dunn/Bonferroni post-hoc test for experiments with three or more groups. Results were considered significant at $p \leq 0.05$. All data was obtained at least in triplicate sets.

**Table 2.6** Treatment regimen of BALB/c with B16-F10-luc treated with different $MGB_{23}$ formulations. Mice were inoculated with B16-F10-luc cells on day 0 ($5x10^5$ cells/mouse). On day 3, 9 and 11 mice were treated by intravenous injection or by inhalation (n=5/treatment). # Refer only to inhaled administration; the $MGB_{23}$-NIVs group in the intravenous experiment was treated with the same dosage across the treatment (10.5 mg/kg $MGB_{23}$, 0.3 mmol/kg lipid). All formulations were diluted with PBS pH 7.4.

| Day | Treatment | Group (n=5 mice/treatment) | | | |
|---|---|---|---|---|---|
| | | **Control** | **Empty-NIVs** | **$MGB_{23}$ sol** | **$MGB_{23}$-NIVs #** |
| **3** | **MGB (mg/kg)** | - | - | 52.60 | 52.60 |
| | **NIVs (mmol/kg)** | - | 1.50 | - | 1.50 |
| | **DMSO (% v/v)** | 2.00 | 2.00 | 2.00 | 2.00 |
| **9** | **MGB (mg/kg)** | - | - | 26.25 | 26.25 |
| | **NIVs (mmol/kg)** | - | 0.75 | - | 0.75 |
| | **DMSO (% v/v)** | 1.00 | 1.00 | 1.00 | 1.00 |
| **11** | **MGB (mg/kg)** | - | - | 13.13 | 13.13 |
| | **NIVs (mmol/kg)** | - | 0.30 | - | 0.30 |
| | **DMSO (% v/v)** | 0.50 | 0.50 | 0.50 | 0.50 |

**Table 2.7** Treatment regimen of BALB/c with *L. donovani* treated with different $MGB_{58}$ formulations. Mice were infected with LV82 ($1x10^7$ parasites/mouse). On day 7, mice were treated by intravenous injection according to the dosage described (n=5/treatment). All the formulations were diluted with PBS pH 7.4 (H, indicates high dose and L, low dose).

| **Treatment** | **Group (n=5 mice for treatment)** | | | | |
|---|---|---|---|---|---|
| | **Control** | **Empty-NIVs** | **$MGB_{58}$ sol** | **$MGB_{58}$-NIVs (H)** | **$MGB_{58}$-NIVs (L)** |
| **$MGB_{58}$ (mg/kg)** | - | - | 50.00 | 50.00 | 10.00 |
| **NIVs (mmol/kg)** | - | 1.50 | - | 1.50 | 0.30 |
| **DMSO (% v/v)** | 2.00 | 2.00 | 2.00 | 2.00 | 0.40 |

# CHAPTER 3. AMPHOTERICIN B NON-IONIC SURFACTANT VESICLES FOR THE TREATMENT OF LEISHMANIASIS

## 3.1. Introduction

All the commercialised Amphotericin B (AmB) formulations (Fungizone®, AmBisome®, Amphotec® and Abelcet®) are limited to intravenous administration in order to treat visceral leishmaniasis. Therefore the development of a formulation that could be administered by a non-invasive route, such as inhalation, would be a large improvement (Mathias and Hussain, 2010). The use of NIVs carrier to encapsulate and deliver AmB has shown efficacy to treat visceral leishmaniasis in mice by the intravenous route (Mullen *et al.*, 1997). The same formulation had some efficacy to treat both fungal and leishmanial infections when administered by the pulmonary route (Alsaadi *et al.*, 2012). Moreover, critical preliminary AmB-NIVs characterisation were discussed in previous studies (Puig-Sellart, 2013) where drug toxicity and colloidal system stability were assessed. The AmB present in AmB-NIVs formulations was found in a multi-aggregated state, which is correlated with less mammalian toxicity than oligomer states found in other formulations such as Fungizone® (Espada *et al.*, 2008; Puig-Sellart, 2013). Furthermore, the NIVs components molar ratio of 3:3:1 (surfactant, cholesterol and DCP) was proven to be the most stable since glass-transition was abolished due to the high amounts of cholesterol present (Puig-Sellart, 2013).

Optimisation and validation of a drug quantification procedure is essential when a novel formulation is developed. High-performance liquid chromatography (HPLC) is a common approach for the analysis of pharmaceutical compounds (Gilpin, 2011). Briefly, the sample is injected in a high pressure pumped mobile phase and the analyte separation is based on its affinity for the sorbents of the stationary phase (Dong, 2006). After separation, the analyte content can be quantified by ultraviolet light (UV), mass spectrometry, charged aerosol, evaporative light scattering or a fluorescence detector. The Internal Conference of Harmonisation of Technical Requirements for Registration of Pharmaceuticals for Human Use, provide guidelines for

validation of HPLC methods (European Medicines Agency, 1995). Specificity, linearity, range, accuracy, precision, limit of detection and limits of quantification are some of the characteristics to evaluate in order to meet the requirements. The characteristics of the peak of interest should also be assessed. For example, a resolution of 2 points or greater between peaks and an asymmetry index less than 2 are desirable (Snyder *et al.*, 1997; Carstensen and Rhodes, 2000). A wide range of HPLC-UV methods have been validated to detect AmB in samples. The most common ones being a reverse phase HPLC-UV with a mixture of acetate or methanol with pH controlled buffer mobile phase and silica based stationary phase (Lambros *et al.*, 1997; Eldem and Arican-Cellat, 2001; Lue *et al.*, 2002; Italia *et al.*, 2009a; Chakrabarty and Pal, 2011).

In addition, the success of a vesicular delivery system as a drug carrier vehicle relies on its physicochemical characteristics, such as vesicle size, lamellarity, surface charge and encapsulation efficiency (Edwards and Baeumner, 2006). The vesicle size of NIVs formulations depends on several parameters i.e. lipidic components and method of preparation (Uchegbu and Vyas, 1998). The vesicle size and polydispersity index are generally determined with laser diffraction or dynamic light scattering (DLS) as the particle size is related to the rate at which the scattered light fluctuates. The vesicle diameter and bilayer characterisation can also be measured by microscopic techniques such as atomic force microscopy (AFM), transmission electron microscopy (TEM) and freeze fracture electron microscopy (FFEM; He *et al.*, 2008; Baalousha and Lead, 2012). Moreover, AFM can also be used to image the vesicle lamellarity and measure the mechanical properties of the samples (Bayindir and Yuksel, 2010; Lamprou *et al.*, 2013; Marianecci *et al.*, 2014). The surface charge of the vesicles is of high importance to measure the colloidal stability of the system. Vesicles that are charged have a reduction in particle aggregation and therefore increased stability (Lian and Ho, 2001). This was firstly postulated by Derjaguin, Landau, Verwey and Overbeek in the 1940s and is currently known as the DLVO theory. The DLVO theory suggests that when attractive forces are stronger than

repulsive energy, the particles tend to aggregate irreversibly. A vesicle formulation should have a ζ-potential of ± 30 mV to provide desirable colloidal stability (Duman and Tunç, 2009). The ζ-potential is normally quantified by the electrophoretic mobility of the particles once an electric filed is applied (Tandon *et al.*, 2008). Furthermore, the rheology of vesicle formulations is generally studied since the viscosity has an active paper in their characteristics (Gradzielski, 2011). For example, lipid concentration, vesicle size, ζ-potential and preparation method can affect the NIVs rheological properties (Uchegbu, 1999). The relationship between shear stress and shear rate and the influence of time on them are described in classical rheograms. When shear stress and shear rate are proportional, the fluid is considered Newtonian. However, most of the fluids are non-Newtonian, such as shear thinning or shear-thickening liquids, where the apparent viscosity decreases or increases respectively with the shear rate (Rao, 1999).

Freeze-drying or lyophilisation is a method to remove water or other solvents from a sample through sublimation (Figure 3.1). During sublimation, the solid solvent (normally water) is converted to gas without passing through the liquid phase. Hence protecting the thermal sensitivity of an active pharmaceutical ingredient. As a result, the final product can be stored for longer periods of time without the physical and chemical instabilities associated with aqueous dispersions (Ghanbarzadeh *et al.*, 2013). Freeze-drying is characterised with three different steps: freezing, primary drying and secondary drying (Franks, 2007; Rey and May, 2010). Freezing is critical in lyophilisation since the sample can be spoiled if not done properly. Moreover, it has a direct effect on the size of the ice crystals formed during nucleation. For example, quick freezing creates fine ice crystals which produce little damage to the sample but is associated with slower sublimation rates due to the small space in between molecules to let vapour escape. In the other hand, slow freezing induces the creation of bigger ice crystals, with a disordered structure and consequently higher sublimation rates. Freezing can also include an annealing step for further size

control of the ice crystals (Ayensu *et al.*, 2012). During freezing the product undergoes a freeze-concentration effect that varies depending on the behaviour of the formulation. For instance, crystalline components can freeze as a mixture of ice and solute crystals when their saturation solubility is reached (also called eutectic phase separation). Nonetheless, the majority of formulations have amorphous characteristics where the solute persists together with unfrozen water during freeze-concentration. Those amorphous samples exhibit a glass transition ($T_g'$) during freeze-concentration, where the supersaturated solution changes from being flexible to rigid, a process known as vitrification (Koster *et al.*, 2000). The next step after freezing is primary drying, where the pressure of the freeze-drier is lowered and heat is supplied to the formulation to induce sublimation. The vapour produced is quickly condensed in a cold condenser plate or chamber. Importantly, the sublimation speed is related to the partial pressure difference of water, at the sublimation front, and the condenser. Therefore, lower chamber pressure does not correlate to faster drying unless convection of heat from the shelf is transferred to the product. However, excess heat input may risk the ice structure. Therefore, the balance between those parameters is critical to create enough freeze-drying force whilst maintaining product temperature below crucial points (i.e. product temperature < $T_g'$). As a result, if primary drying is set above $T_g'$, the interstitial components are more flexible and the freeze-drying structure tends to collapse (Tang and Pikal, 2004). Therefore, primary drying must be set below $T_g'$ to maintain the interstitial structure and avoid sample collapse. This is normally controlled through setting the chamber pressure to 25 % of the optimal ice vapour pressure i.e. if $T_g'$ is -30°C (equivalent to 0.370 mBar ice vapour pressure), the chamber pressure should be set at 0.093 mBar (Figure 3.2). Although during primary drying most of the water is sublimated, the remaining unfrozen water can only be removed by desorption during secondary drying. In that last step, the shelf temperature is normally raised and the pressure is lowered to achieve a total amount of water less than 3 % w/w (Mohammed *et al.*, 2007). Lyophilisation generates various stresses that may affect the integrity of the

carrier membrane in liposomes or NIVs (Chen *et al.*, 2010). Formulation and process parameters should be optimised to overcome this problem. Furthermore, the inclusion of a lyoprotectant in the vesicular formulation could prevent damage (Ghanbarzadeh *et al.*, 2013) since they can stabilise the freeze-drying system by replacing water gaps (Crowe *et al.*, 1996) or by protecting vesicles from damage caused by ice crystals or fusion of vesicles (Stark *et al.*, 2010). Therefore, in order to obtain an acceptable freeze-dried product, the optimal lyoprotectants and technology parameters must be identified.

As the ICH Harmonised Tripartite Guideline (2003) stated, the main purpose of drug stability testing is to investigate on how the quality of a formulation varies with time and under a variety of environmental factors such as temperature, humidity and light. This to establish a shelf life and recommended storage conditions for the drug product. The guidelines described three types of studies, long term, intermediate and accelerated with storage conditions from 25 ± 2°C and 60 ± 5 % relative humidity to 40 ± 2°C and 75 ± 5 % relative humidity for 12 or 6 months respectively. Furthermore, the Food and Drug Administration (2015) proposed extra physiological stability parameters that should be investigated in liposome or vesicle formulations. These included maintenance of size uniformity, vesicle charge and entrapment efficiency upon storage at the tested conditions.

Several visceral leishmaniasis *in vivo* models have been used to test the efficacy of anti-leishmanial drugs. The laboratory strain LV82 has been widely used to infect mice and hamsters with visceral leishmaniasis (Mullen *et al.*, 1998; Carter *et al.*, 2001; Nieto *et al.*, 2003; Wasan *et al.*, 2010). To recreate antimonial resistance infections, clinical isolates have also been used (Carter *et al.*, 2001, 2005). More recently, the gene encoding for the luciferase enzyme has been incorporated to LV82 strain to produce LV82-luc parasites (Mißlitz *et al.*, 2000; Alsaadi *et al.*, 2012). These parasites express the luciferase protein, which produces bioluminescence (BLI) in contact with luciferin (Luc). The BLI values

of infected subjects is directly proportional to the number of parasites present in the region (de La Llave *et al.*, 2011). This property provides a highly sensitive method for non-invasive, real time detection of viable *Leishmania* parasites *in situ* (Shaw and Carter, 2014). Other luminescence methods can be used to characterise the *in vivo* effect of pharmaceutical formulations. For example, the administration of luminol produces chemiluminescence (CLI) in contact with the myeloperoxidase (MPO) generated by neutrophils. Gross *et al.*, (2009) firstly reported the use of luminol to assess the MPO activity *in vivo,* after administrating implants with external MPO and glucose oxidase. Therefore, the inflammatory response related to a drug treatment can be imaged by the luminol CLI reaction *in situ*.

The principal objective of this study section was to develop a suitable AmB-NIVs formulation for the inhaled treatment of visceral leishmaniasis. The aims to cover in the study were:

- Validate an HPLC-UV method to detect AmB from *in vivo* and *in vitro* samples.

- Characterise the process that affect drug encapsulation efficiency in AmB-NIVs.

- Optimise the freeze-drying methodology of AmB-NIVs.

- Measure the feasibility of AmB-NIVs scale-up production.

- Assess the stability of the final freeze-dried product and the rehydrated AmB-NIVs samples.

- Determine AmB-NIVs efficacy against a model of visceral leishmaniasis *in vivo.*

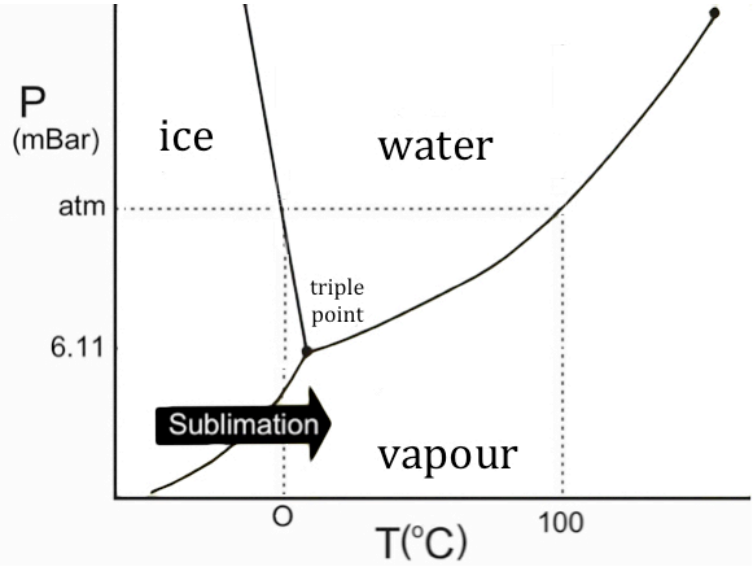


**Figure 3.1** Phase temperature diagram for water indicating the triple point between ice, water and vapour. Black arrow indicates the sublimation parameters required for freeze-drying. Atmosphere (atm) temperature is indicated at 1013.25 mBar.

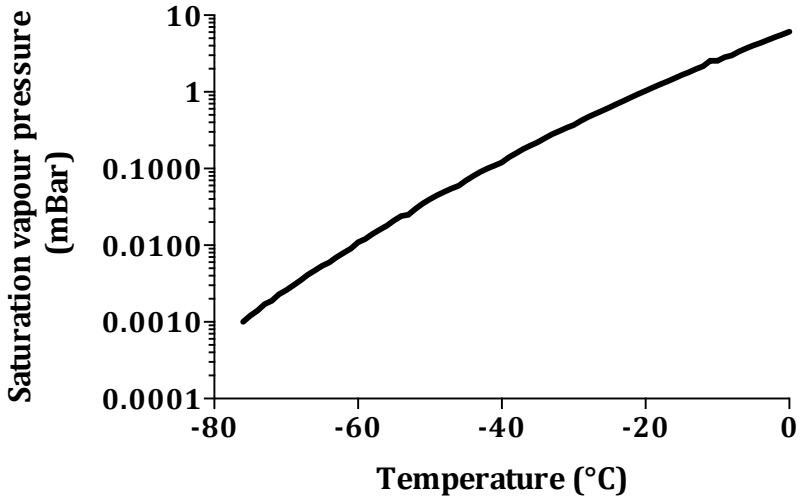


**Figure 3.2** Saturation vapour pressure over ice as a function of temperature. During primary drying the chamber pressure is normally set to 25 % of the ice vapour pressure corresponding to the critical $T_g'$ of the product (adapted from Wexler, 1977).

### 3.2. Sample quantification of AmB formulations by HPLC-UV

It was important to have a reliable method to determine drug entrapment and to quantify AmB levels within samples. Therefore, an HPLC-UV method used in previous studies to detect AmB with an IS, was adapted and validated. The two wavelengths used were separated enough to allow single quantification of each compound in different chromatograms i.e. 407 nm for AmB and 294 nm for IS. An example of the chromatograms used to quantify both compounds is represented in Figure 3.3. AmB peak eluted at 5.1 minutes and presented good asymmetry values (Table 3.1). An additional peak eluted before the main AmB peak, probably due to naturally present drug impurities (Figure 3.3). This additional peak was well separated from the main AmB peak, which had resolution values larger than 3. The IS eluted at 8.8 minutes and exhibited good asymmetry values. Standards were plotted as area under the curve (AUC) ratio between AmB and IS and showed good correlation to a linear relationship for the AmB concentration range of 0.1 to 100 μg/ml (correlation factor $R^2 > 0.99$; Figure 3.4). In addition, the AUC ratio for the standards had a small relative error (Table 3.1); which indicated that the method used to detect AmB had good precision. The limit of detection for the assay was 50 ng/ml and the limit of quantification was 100 ng/ml AmB (data not shown). Organs from uninfected BALB/c were spiked with AmB and the percentage of drug recovered quantified. High recovery values were obtained from plasma (96.1 ± 4.0 %), trachea (102.7 ± 5.7 %) and lungs (108.0 ± 1.8 %, n=3) indicating that the method could also be used to assess drug levels in tissues of treated subjects.

This HPLC method was also used to detect AmB degradation. To validate this approach, AmB dispersed in HPγCD (AmB-CD) and AmB-NIVs were kept at 70°C for up to 6 hours. Then, AmB levels at different time points of the incubation were quantified. High temperature did not affect AUC values for AmB-CD over time (Figure 3.5.A). However, comparison of AmB-CD chromatograms at time 0 and at 5.67 hour, showed that heating the formulation at 70°C affected the peak

of interest (chromatogram represented in Figure 3.5.E compared to chromatogram in Figure 3.5.G) resulting in a widening and a decrease in height for the AmB peak (peak height $p \leq 0.01$; Figure 3.5.C). The asymmetry values of AmB-CD peak changed from originally 1.23 ± 0.01 to 1.55 ± 0.01 at 70°C for 5.67 hours ($p \leq 0.01$). AmB-NIVs exposed to high temperature did not affect the amount of AmB detected by AUC (Figure 3.5.B). However, the chromatogram displayed variation in peak structure (Figure 3.5.F compared to Figure 3.5.H), which was apparent after heating the formulation at 70°C for 1 hour ($p \leq 0.001$; Figure 3.5.D). This indicated that the validated HPLC method was able to detect AmB degradation. Moreover, peak height values were demonstrated to be essential in identifying degradation of AmB within the described HPLC-UV method.

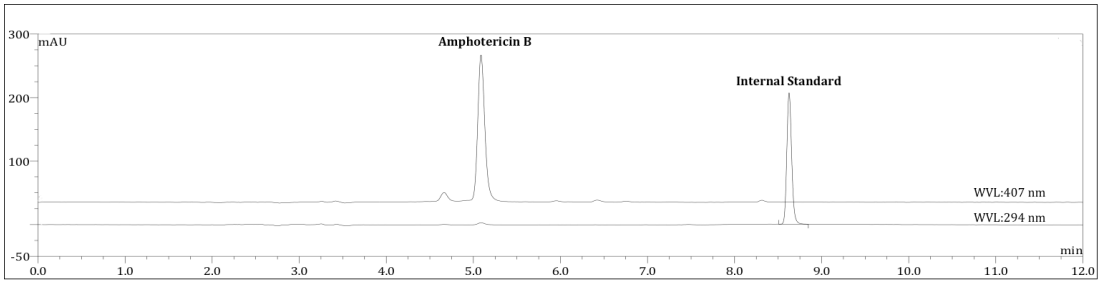


**Figure 3.3** Example of an HPLC-UV chromatogram for AmB solution (25 μg/ml AmB dissolved with methanol) spiked with the IS (α-naphthol, 20 μg/ml). AmB was detected at 407 nm and the IS at 294 nm (mAU, milli-absorbance unit; WVL, wavelength).

**Table 3.1** HPLC-UV peak characteristics for AmB solution (62.5 μg/ml AmB dissolved with methanol, WVL= 407 nm), IS (α-naphthol, 20 μg/ml, WVL=294 nm) and extra peak in the chromatogram (WVL=407 nm). Peak properties and intra-day relative standard deviation (SD) are represented. AmB resolution values were related to the extra peak eluted just before (AUC, area under the curve; AmB, amphotericin B; IS internal standard; WVL, wavelength)

| Peak | Characteristics | Mean ± SD (n=6) | Relative SD (%) |
|---|---|---|---|
| **Extra** | Resolution | 3.51 ± 0.49 | 13.99 |
| **AmB** | Retention time (min) | 5.13 ± 0.02 | 0.44 |
| | AUC (mV x min) | 67.23 ± 1.22 | 1.82 |
| | Peak asymmetry | 1.04 ± 0.00 | 0.39 |
| **IS** | Retention time (min) | 8.76 ± 0.01 | 0.06 |
| | AUC (mV x min) | 11.49 ± 0.28 | 2.42 |
| | Peak asymmetry | 1.10 ± 0.01 | 0.50 |
| | AUC ratio (AmB/IS) | 5.85 ± 0.04 | 0.67 |

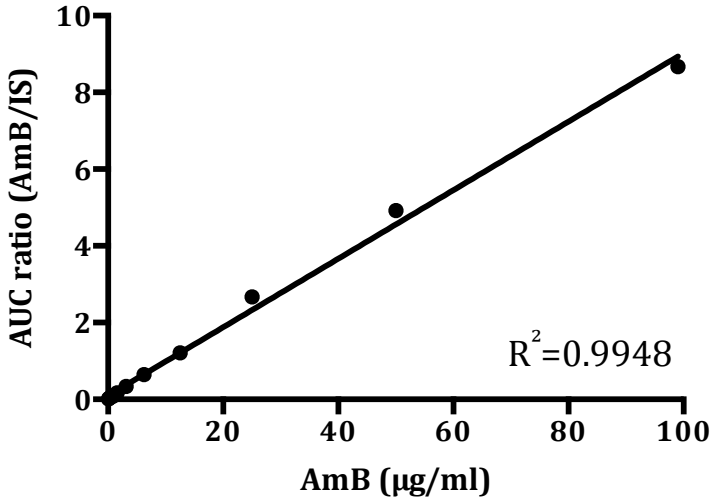


**Figure 3.4** Example of linear standard calibration of AmB and internal standard area under the curve (AUC, 0.1 to 100 µg/ml AmB with methanol). A standard curve was fitted to the data using a linear regression by the least mean squares method and the correlation coefficient, $R^2$, for the fitted line is shown (AmB, amphotericin B; IS, internal standard).

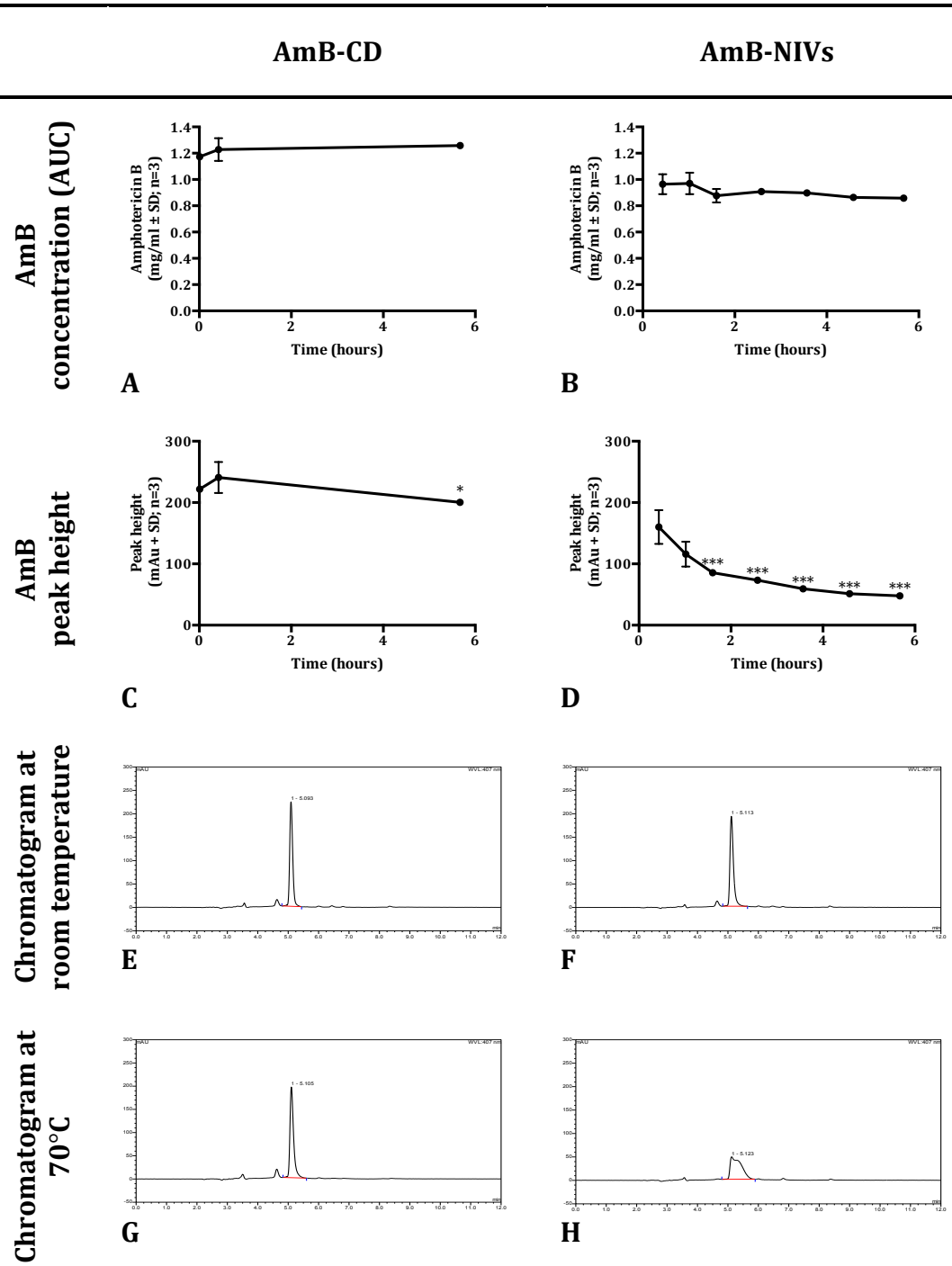


**Figure 3.5** Effect of heating in AmB-CD (1 mg/ml AmB, 100 mg/ml HPγCD, 1.4 g/ml sucrose) and AmB-NIVs formulations (1 mg/ml AmB, 100 mg/ml HPγCD, 1.4 g/ml sucrose, 150 mM lipid) at 70°C. The amount of AmB present, calculated from AUC, is represented in A (AmB-CD) and B (AmB-NIVs). AmB peak heights are plotted in C (AmB-CD) and D (AmB-NIVs). Figure E and F exemplify the chromatogram of AmB at time 0 (room temperature) and Figure G and H, the chromatogram at 70°C for 6 hours (* $p \leq 0.05$, *** $p \leq 0.001$ of different time points compared to time 0 i.e. room temperature).

### 3.3. AmB-NIVs characteristics:

#### 3.3.1. Atomic force microscope (AFM) studies

AFM studies were carried out to image the AmB formulations produced (Figure 3.6; Table 3.2). To formulate AmB-NIVs, AmB was previously complexed with HPγCD and then added to the melted lipids (surfactant, cholesterol and DCP) followed by a homogenisation step. Both the AmB-CD complexes and AmB-NIVs vesicles were detected under AFM (Figure 3.6). AmB-NIVs images presented two distinctive types of structures, ones more spherical than the others (Figure 3.6.A). The nature of the different type of structures was hypothesised once AmB-CD, without NIVs components, was imaged (Figure 3.6.B). The irregular compositions imaged in AmB-NIVs corresponded to residual lipids or the HPγCD complexes with AmB (signalled with a black arrow). While on the contrary, the more spherical entities were associated to the NIVs structure (highlighted in the images with a white arrow). The microscope images showed that the vesicles were multi-lamellar in nature since the different layers could be observed in some vesicles (Figure 3.6.A). Mechanical properties obtained from the AFM PeakForce QNM analysis indicated that AmB-NIVs were significantly higher ($p \leq 0.001$) and rougher ($p \leq 0.05$) than AmB-CD (Table 3.2). Force and dissipation values for AmB-CD were not obtained probably because the values were outside the limits of detection. Vesicle diameters of AmB-NIVs measured from the AFM images were consistent to the z-average value obtained using DLS detection (Table 3.2). However, the z-average of AmB-CD was significantly larger than the diameter value measured from the AFM images ($p \leq 0.001$). This is thought to be related to the higher polydispersity of AmB-CD complexes which interfered with the laser when DLS was used ($p \leq 0.001$ compared to AmB-NIVs polydispersity index; Table 3.2).

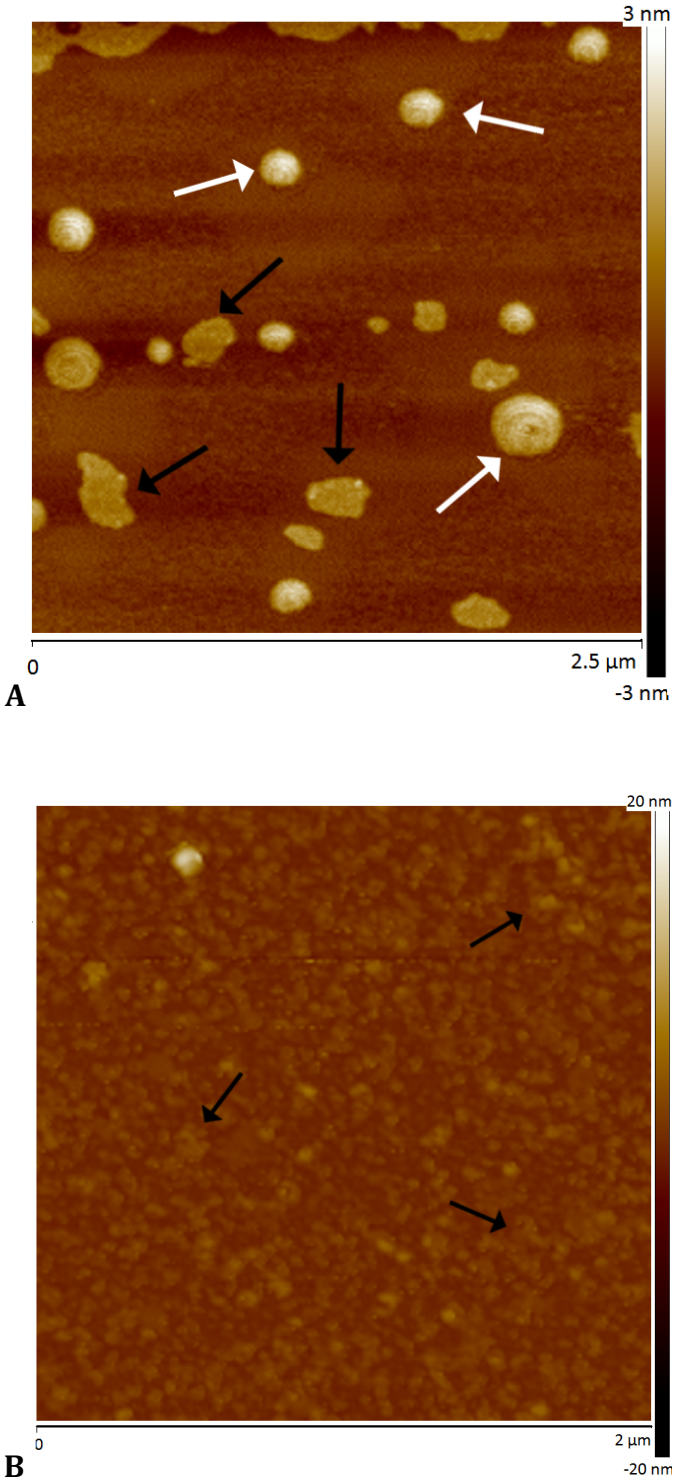


**Figure 3.6** Atomic force microscope images of (A) AmB-NIVs (1 mg/ml AmB; 100 mg/ml HPγCD; 150 mM lipids) with white arrows pointing at some AmB-NIVs vesicles and black arrows pointing at some irregular compositions. (B) AmB-CD complexes (B; 1 mg/ml AmB; 100 mg/ml HPγCD) with black arrows pointing at some AmB-CD complexes. X-axis defines width (µm) and y-axis represents depth (nm).

**Table 3.2** AmB-CD (1 mg/ml AmB, 100 mg/ml HPγCD) and AmB-NIVs (1 mg/ml AmB, 100 mg/ml HpγCD, 150 mM lipids) mechanical properties obtained from AFM and from DLS (AFM, atomic force microscope; DLS, dynamic light scattering; n.a., not-available; * $p \leq 0.05$, *** $p \leq 0.001$ between AmB-CD and AmB-NIVs properties; n=12 AFM and n=3 DLS).

| | Mechanical properties | AmB-CD | AmB-NIVs |
|---|---|---|---|
| AFM | Diameter (nm) | 180.22 ± 52.40 | 159.09 ± 46.54 |
| | Height (nm) | 1.67 ± 0.20 | 2.44 ± 0.30 *** |
| | Surface roughness (nm) | 0.36 ± 0.06 | 0.43 ± 0.09 * |
| | Force (nN) | n.a. | 104.63 ± 19.30 |
| | Deformation (nm) | 0.10 ± 0.26 | 1.20 ± 0.27 |
| | Dissipation (KeV) | n.a. | 68.98 ± 19.40 |
| DLS | Z-average (nm) | 504.72 ± 25.41 | 188.40 ± 5.51 *** |
| | Polydispersity index | 0.53 ± 0.04 | 0.13 ± 0.01 *** |

### 3.3.2. Vesicle size, vesicle charge, drug entrapment and rheology properties of AmB-NIVs

The homogenisation time of AmB-NIVs formulations was directly related to the size of the vesicles produced. Thus, homogenisation for 30 minutes produced AmB-NIVs with a smaller vesicle size compared to homogenisation for just 5 minutes ($p \leq 0.001$; Table 3.3). A decrease in the corresponding polydispersity index of the vesicles was also related to the homogenisation time ($p \leq 0.001$; Table 3.3). In general, AmB-NIVs had a negative vesicle charge larger than -60 mV. Moreover, the homogenisation time also influenced the vesicle charge of the particles, with a reduction in the negative charge occurring when samples were homogenised for a longer period ($p \leq 0.01$; Table 3.3). High amounts of AmB were entrapped inside the vesicles and this was independent of the vesicle size. In addition, dilution of the vesicle formulation 30 minutes before analysis, did not significantly affect the AmB drug entrapment efficiency (Table 3.3).

The rheological properties of AmB-NIVs fluid were shear-thinning (Table 3.3 and Figure 3.7). The power law model was fitted to AmB-NIVs rheograms and had an excellent fit, with a correlation coefficient higher than 0.999. The flow index values were smaller than the unit, demonstrating the shear-thinning property of the formulation (Table 3.3). AmB-NIVs had no-time dependent thixotropy confirmed by the area of the hysteresis loop, and by the unnoticeable separation between the up and down curves in the rheograms (Table 3.3 and Figure 3.7). The apparent viscosity of AmB-NIVs formulations with smaller vesicle size was significantly higher than the one for the AmB-NIVs formulations with larger sized vesicles ($p \leq 0.01$; Table 3.3). Contrary, the flow index, consistency index and hysteresis loop area obtained from the rheogram data were not influenced by the vesicle size of AmB-NIVs (Table 3.3).

**Table 3.3** Physicochemical properties of AmB-NIVs (1 mg/ml AmB, 100 mg/ml HPγCD, 150 mM lipids) of small or large vesicle size homogenised for 30 or 5 minutes respectively at 9,000 rpm. AmB-NIVs was also diluted 5 times with distilled water, 30 minutes prior entrapment efficiency determination (** $p \leq 0.01$, *** $p \leq 0.001$ small and large vesicle size compared; $R^2$, correlation coefficient).

| | Characteristics (mean ± SD; n=3) | Fresh AmB-NIVs | |
|---|---|---|---|
| | | 30 min homogenisation (small) | 5 min homogenisation (large) |
| Physicochemical properties | Z-average (nm) | 234.10 ± 4.43 | 838.21 ± 33.91 *** |
| | Polydispersity index | 0.33 ± 0.02 | 0.76 ± 0.03 *** |
| | ζ-potential (mV) | -63.71 ± 1.21 | -86.20 ± 5.03 ** |
| | Entrapment efficiency (%) | 80.82 ± 19.23 | 78.31 ± 5.90 |
| | Entrapment efficiency after dilution 5 times (%) | 74.87 ± 8.43 | 70.46 ± 4.30 |
| Rheological properties | Apparent viscosity (mPa·s) | 11.62 ± 1.06 | 8.54 ± 0.08 ** |
| | Flow index | 0.86 ± 0.04 | 0.92 ± 0.00 |
| | Consistency index (mPa·s) | 33.19 ± 13.45 | 14.54 ± 0.33 |
| | Hysteresis loop (Pa/s) | 410.10 ± 80.34 | 437.70 ± 119.05 |
| | $R^2$ | 1.00 ± 0.00 | 1.00 ± 0.00 |

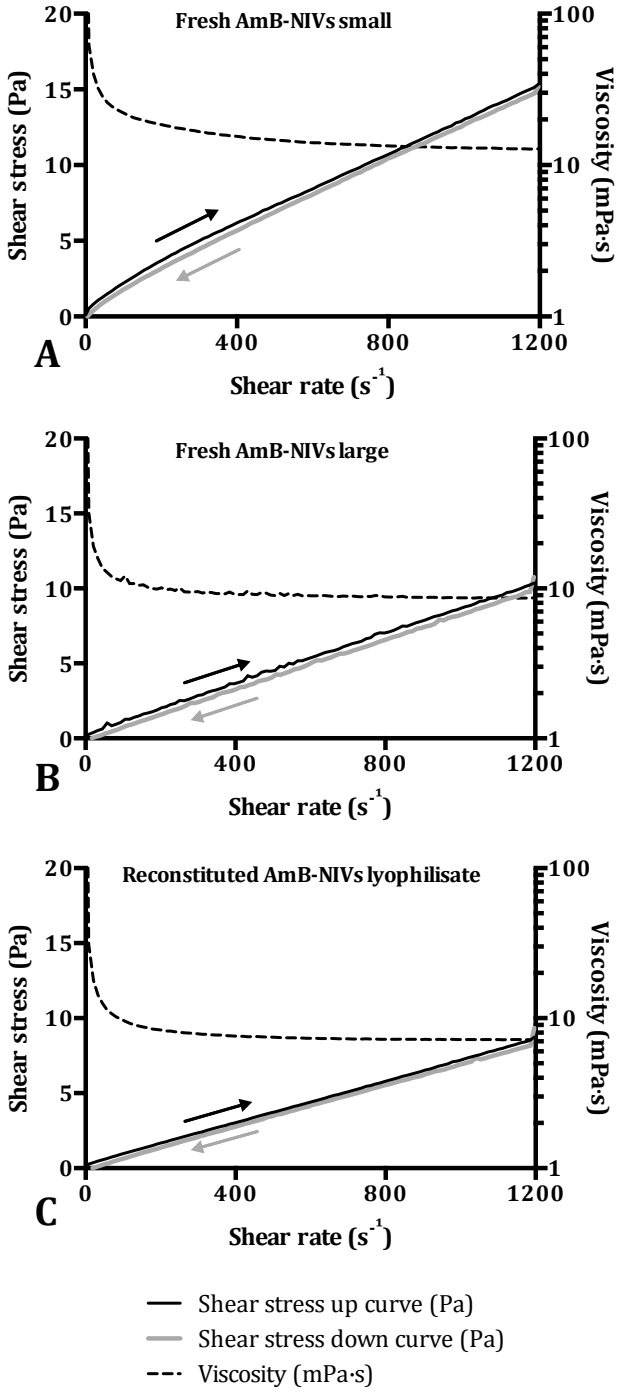


**Figure 3.7** Examples of rheograms of fresh AmB-NIVs (1 mg/ml AmB, 100 mg/ml HPγCD, 150 mM lipids) for formulations described in Table 3.3 i.e. AmB-NIVs with a small particle size (A, 234.10 ± 4.43 nm), larger vesicles size (B, 838.21 ± 33.91 nm) and AmB-NIVs after reconstitution of lyophilisate (C, formulation properties described in Figure 3.8 and Table 3.5). Shear rate varied from 0 to 1200 1/s and the shear stress curve was plotted, up (continuous black line) and down (continuous grey line). Viscosity values were plotted against shear with a black discontinuous line.

### 3.3.3. Processes influencing AmB-NIVs characteristics: ultrafiltration and freeze-drying

Ultrafiltration is a common technique used to remove unentrapped drug from vesicle formulations. The physicochemical characteristics of AmB-NIVs formulations before and after ultrafiltration were determined to see whether it had any adverse effects on the NIVs suspension. After ultrafiltration, the particle size increased slightly ($p \leq 0.05$; Table 3.4) but the polydispersity index and ζ-potential remained unaltered. In this case, the ultrafiltration of AmB-NIVs negatively impacted the drug entrapment efficiency since this decreased significantly compared to the fresh formulation ($p \leq 0.05$; Table 3.4).

In order to increase the long-term stability of AmB-NIVs, the production of lyophilised formulations was investigated. The freeze-dried AmB-NIVs cakes (with no lyoprotectant) were rehydrated with distilled water and their properties compared to the original formulation. The reconstituted AmB-NIVs had much larger vesicle size than the original formulation ($p \leq 0.05$) and the polydispersity values were also higher ($p \leq 0.01$; Table 3.4). However, despite the big increase in vesicle size the ζ-potential and entrapment efficiency for both populations were similar. Ultrafiltrated AmB-NIVs were also freeze-dried and the studies showed that the vesicle size also increased ($p \leq 0.05$; Table 3.4). The relative increase in size was greater in the ultrafiltrated formulation than that of the non-ultrafiltrated one ($p \leq 0.01$; 6.95 ± 24.27 fold). The lyophilisation process not only affected the size of the vesicles but it also imparted on the polydispersity index and the ζ-potential of the vesicles within reconstituted ultrafiltrated AmB-NIVs ($p \leq 0.01$; Table 3.4). However, AmB entrapment efficiency was similar to that of the original ultrafiltrated AmB-NIVs formulation. All these studies indicated that freeze-drying of AmB-NIVs significantly affected the physical properties of the vesicles, especially vesicle size. Therefore the addition of a cryoprotectant to protect against vesicle damage was investigated.

Sucrose was the excipient chosen since other AmB formulations in the market already used it as a cryoprotectant. Firstly, the effect of including sucrose in the formulation on initial vesicle characteristic was determined. Fresh AmB-NIVs containing sucrose had a significantly lower vesicle size ($p \leq 0.001$) and a lower polydispersity index compared to AmB-NIVs prepared without sucrose ($p \leq 0.01$; Table 3.5). In addition, a well-defined single size peak was observed during the z-average DLS detection for AmB-NIVs containing sucrose (data not shown). These indicated that the use of sucrose as an additive improved uniformity of the fresh AmB-NIVs. The apparent viscosity of AmB-NIVs containing sucrose was significantly higher than the apparent viscosity of the formulation without sucrose ($p \leq 0.01$; Table 3.5). Other parameters, such as ζ-potential and entrapment efficiency were similar for the two AmB-NIVs formulations, with or without sucrose.

AmB-NIVs containing sucrose (0.17 g/ml) were freeze-dried and reconstituted with distilled water previous analysis. The reconstituted AmB-NIVs with sucrose had vesicles with similar properties to the original sample i.e. vesicle size, polydispersity index, ζ-potential or entrapment efficiency (Figure 3.8). However, the freeze-dried cake had a broken appearance (Figure 3.9.A). Therefore, AmB-NIVs containing sucrose at a lower concentration of 0.09 g/ml i.e. ratio of 1.5 times the lipid concentration, were produced. The freeze-dried cake had better structural properties than that of the NIVs prepared using 0.17 g/ml sucrose (Figure 3.9.B) and it was easily reconstituted with distilled water. Rehydration of AmB-NIVs containing 0.09 g sucrose/ml had vesicle with the same z-average, polydispersity index and entrapment efficiency as the original formulation. The apparent viscosity of the reconstituted formulation was significantly lower than that of the original formulation ($p \leq 0.001$; Table 3.6; Figure 3.7.C). In addition, the consistency index of the fitted power law equation was also significantly smaller than the pre-lyophilised samples ($p \leq 0.001$; Table 3.6). As a further possible improvement, the effect of dilution the formulation

before freeze-drying was determined since increasing the interstitial space between vesicles in the freeze-dried scaffolding could have a faster rehydration effect. The freeze-dried cake was easier to rehydrate than the non-diluted formulation due to larger pores created (Figure 3.9.C). Although, the mean vesicle size, ζ-potential and polydispersity index of the reconstituted AmB-NIVs were similar to the original formulation, the entrapment efficiency was significantly lower ($p \leq 0.05$; Figure 3.8.D). Therefore, these studies indicated that optimum formulation for AmB-NIVs was the inclusion of sucrose at 0.09 g/ml and that the formulation should not be diluted before freeze-drying.

### 3.3.4. AmB-NIVs containing luciferin (AmB-luc-NIVs)

Freeze-dried AmB-NIVs were reconstituted with luciferin in order to obtain NIVs with both AmB and luciferin for use in treatment and imaging. A comparison between NIVs particles, containing both drug and substrate, and AmB-NIVs containing only drug, is described in Table 3.7. Physical properties such as z-average, polydispersity index and ζ-potential of AmB-luc-NIV were similar to AmB-NIVs. AmB concentration and entrapment efficiency were independent of NIVs containing luciferin or not. Around 50 % of the luciferin included in the AmB-luc-NIVs particles was incorporated in the interior of the vesicles (Table 3.7). Therefore, luciferin can be entrapped to the AmB-NIVs formulation without affecting the original physicochemical properties and consequently, the formulation can be used for both treatment and imaging proposes.

**Table 3.4** Physicochemical properties of non-ultrafiltrated and ultrafiltrated AmB-NIVs (1 mg/ml AmB, 100 mg/ml HPγCD and 150 mM lipids), fresh or after reconstitution of the freeze-dried cake with water (* $p \leq 0.05$, ** $p \leq 0.01$ comparing fresh formulation to rehydrated lyophilisate; $^{+}$ $p \leq 0.05$, $^{++}$ $p \leq 0.01$ comparing fresh non-ultrafiltrated with fresh ultrafiltrated AmB-NIVs; Pdi, polydispersity index).

| Properties (mean ± SD; n=3) | AmB-NIVs non-ultrafiltrated | | AmB-NIVs ultrafiltrated | |
|---|---|---|---|---|
| | Fresh | Rehydrated lyophilisate | Fresh | Rehydrated lyophilisate |
| **Z-average (nm)** | 238.50 ± 3.56 | 361.20 ± 11.62 ** | 248.00 ± 1.42 + | 1100.80 ± 197.04 * |
| **Pdi** | 0.27 ± 0.02 | 0.39 ± 0.01 ** | 0.26 ± 0.01 | 0.67 ± 0.07 ** |
| **ζ-potential (mV)** | -65.40 ± 0.92 | -72.40 ± 0.85 | -81.73 ± 1.21 | -68.87 ± 2.67 ** |
| **Entrapment efficiency (%)** | 90.45 ± 8.34 | 85.35 ± 15.62 | 72.37 ± 6.54 ++ | 74.69 ± 1.61 |

**Table 3.5** Physicochemical properties of fresh AmB-NIVs (1 mg/ml AmB, 100 mg/ml HPγCD and 150 mM lipids) formulated without sucrose or containing sucrose as a lyoprotectant additive (0.09 g/ml sucrose; ** $p \leq 0.01$, *** $p \leq 0.001$ between fresh AmB-NIVs and AmB-NIVs with sucrose).

| Physicochemical properties (mean ± SD; n=3) | Fresh AmB-NIVs | |
|---|---|---|
| | AmB-NIVs | AmB-NIVs with sucrose (0.09 g/ml) |
| **Z-average (nm)** | 238.50 ± 3.56 | 193.44 ± 3.03 *** |
| **Polydispersity index** | 0.27 ± 0.02 | 0.16 ± 0.02 ** |
| **ζ-potential (mV)** | -65.40 ± 0.92 | -69.30 ± 1.23 |
| **Entrapment efficiency (%)** | 90.45 ± 8.34 | 88.76 ± 7.06 |
| **Apparent viscosity (mPa·s)** | 11.62 ± 1.06 | 14.51 ± 0.16 ** |

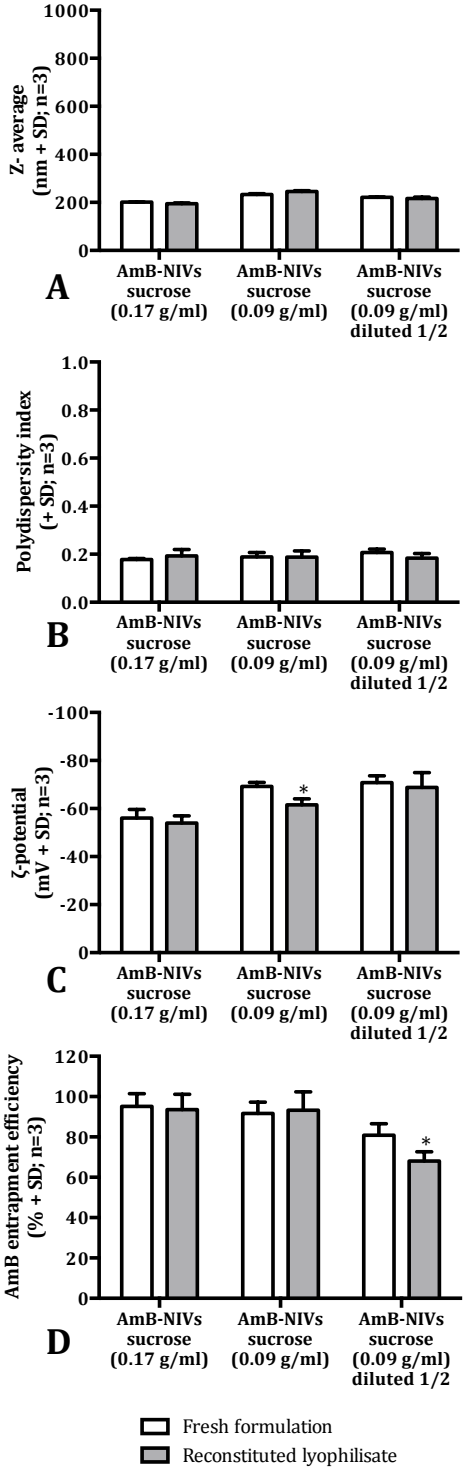


**Figure 3.8** Physicochemical properties of reconstituted AmB-NIVs lyophilisates (1 mg/ml AmB, 100 mg/ml HPγCD and 150 mM lipids) incorporating sucrose as a lyoprotectant and compared to the fresh formulation. The formulations contained sucrose at a concentration of 0.17 g/ml (2.7x lipid), 0.09 g/ml (1.5x lipid) and 0.09 g/ml diluted 1/2 before freeze-drying. Z-average (A), polydispersity index (B), ζ-potential (C) and AmB entrapment efficiency (D) were represented (* $p \leq 0.05$ between fresh formulation and reconstituted lyophilisate).

**Table 3.6** Rheological properties of fresh AmB-NIVs and reconstituted AmB-NIVs lyophilisate (1 mg/ml AmB, 100 mg/ml HPγCD, 0.09 g/ml sucrose and 150 mM lipids). An example of reconstituted lyophilisate rheogram is shown in Figure 3.7.C (*** $p \leq 0.001$ fresh formulation compared to the reconstituted lyophilisate AmB-NIVs).

| Rheological properties (mean ± SD; n=3) | AmB-NIVs with sucrose | |
|---|---|---|
| | Fresh formulation | Rehydrated lyophilisate |
| **Apparent viscosity (mPa·s)** | 14.51 ± 0.16 | 7.18 ± 0.04 *** |
| **Flow index** | 0.91 ± 0.01 | 0.95 ± 0.01 |
| **Consistency index (mPa·s)** | 26.68 ± 2.45 | 10.20 ± 0.89 *** |
| **Hysteresis loop (Pa/s)** | 129.33 ± 232.90 | 316.50 ± 24.27 |
| **$R^2$** | 1.00 ± 0.00 | 1.00 ± 0.00 |

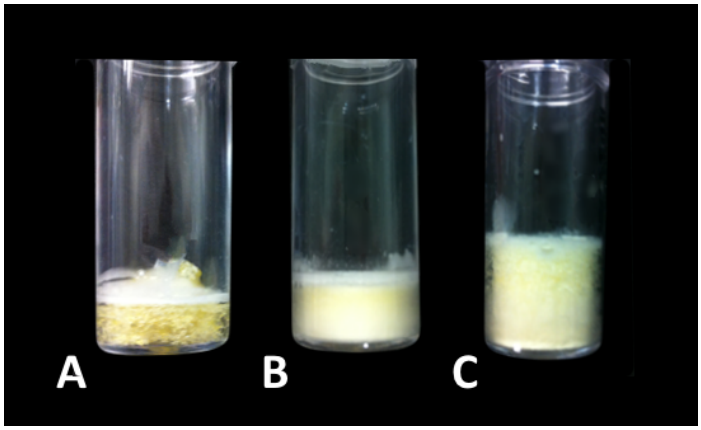


**Figure 3.9** Appearance of AmB-NIVs freeze-dried cakes (1 mg/ml AmB, 100 mg/ml HPγCD, 150 mM lipids and different concentrations of sucrose). AmB-NIVs with 0.17 g/ml sucrose (A), AmB-NIVs with 0.09 g/ml sucrose (B) and AmB-NIVs with 0.09 g/ml sucrose and diluted 1/2 with water before freeze-drying (C).

**Table 3.7** Physicochemical characteristics of NIVs containing AmB (0.2 mg/ml) and luciferin (5 mg/ml) formulated when freeze-dried AmB-NIVs were rehydrated with luciferin solution. Comparison with NIVs that only contained AmB (formulated when freeze-dried AmB-NIVs were rehydrated with distilled water). Not applicable (n.a.).

| **Physicochemical properties (mean ± SD; n=3)** | **Rehydrated freeze-dried AmB-NIVs vials with:** | |
|---|---|---|
| | **Distilled water** | **Luciferin solution** |
| **Z-average (nm)** | 338.02 ± 20.59 | 385.03 ± 31.32 |
| **Polydispersity index** | 0.52 ± 0.07 | 0.57 ± 0.07 |
| **ζ-potential (mV)** | -78.43 ± 0.60 | -75.30 ± 2.77 |
| **AmB (mg/ml)** | 0.16 ± 0.00 | 0.17 ± 0.00 |
| **AmB entrapment efficiency (%)** | 85.62 ± 5.83 | 88.12 ± 4.91 |
| **Luciferin (mg/ml)** | n.a. | 8.55 ± 0.43 |
| **Luciferin entrapment efficiency (%)** | n.a. | 44.76 ± 0.72 |

### 3.3.5. Study of scale-up formulation of AmB-NIVs

In most preliminary characterisation studies AmB-NIVs were formulated in small batches of 10 ml. However, it is important to determine how this method would be adapted for larger-scale manufacture. In this study, two larger batches of AmB-NIVs were prepared, batch 1 (250 ml) and batch 2 (100 ml). In addition, the samples prepared from these batches were used in stability studies to help determine the shelf life of AmB-NIVs product (Section 3.3.6.).

Firstly, AmB-CD (1 mg/ml AmB, 100 mg/ml HPγCD, 0.09 g/ml sucrose) were easily sterilised by passing through a 0.22 μm filter. The amount of AmB-CD was measured before and after filtration and showed that there was no drug loss on filtration (Table 3.8). AmB-CD complexes were more uniform after being passed through a 0.22 μm filter as the polydispersity index reflected uniformity and the particle size significantly decreased ($p \leq 0.001$, Table 3.8). The filtrated AmB-CD was used to rehydrate the melted lipids (150 mM lipid) and the formulations were homogenized for 1 hour to achieve a vesicle size of 225.8 ± 5.8 nm (batch 1) and 190.52 ± 1.62 nm (batch 2).

Following, AmB-NIVs (batch 1) were filtered before being freeze-dried. However, passing the formulation through a 0.22 μm filter was difficult and to alleviate this problem, the formulation was kept at 70°C and filters with larger pore size (0.45 μm) were used instead. Filtering the AmB-NIVs formulation resulted in a reduction in mean z-average compared to the unfiltered formulation ($p \leq 0.01$; Table 3.8) but the polydispersity index, ζ-potential and amount of AmB were unaffected. During the freeze-drying process, a thermometric probe was placed in one vial to assess the temperature of the product during the different steps of the process. The temperature in the sample during the freezing step reached -70°C, 10°C above the set shelf temperature (Figure 3.10 and Table 2.4). The peak obtained at 6 hours for the product and shelf temperature was probably related to when the vacuum pump

started. The shelf and product temperature reached equilibrium at the end of the secondary drying (18°C and 15°C respectively; Figure 3.10), which was considered as a good estimation of freeze-drying finalization. After lyophilisation, the characteristics of the reconstituted formulation in batch 1 were compared to the original fresh filtered formulation. There was a significant increase in vesicle size when freeze-dried vesicles were reconstituted with water compared to the original formulation but the size was still under 240 nm ($p \leq 0.05$; Table 3.9). Freeze-drying the formulation had no significant effect on the polydispersity index and ζ-potential but there was a significant decrease in the amount of drug within the formulation ($p \leq 0.01$; Table 3.9). Despite the concentration of AmB being reduced; the entrapment efficiency was kept stable. The apparent viscosity and the consistency index of the rehydrated AmB-NIVs were significantly lower than that of the original filter-sterilised AmB-NIVs formulation ($p \leq 0.05$ and $p \leq 0.01$; Table 3.9). The freeze-dried formulation maintained the shear-thinning and non-time thixotropy flow characteristics of the original formulation. The sterility of batch 1 was determined through spiking fluid thioglycolate broth, which grows both aerobic and aerobic microorganism, and tryptone soya broth, which only grows aerobic bacteria. The fluid thioglycolate broth had bacterial colonies present in one out of three flask spiked with AmB-NIVs at two weeks after inoculation. The colonies were present in the top half of the flask, which indicated that they were facultative anaerobes. The tryptone soya broth culture had no sign of bacterial contamination up to week 4 of incubation.

There were variations in cake appearances for different samples from batch 1 when they were removed from the freeze drier (Figure 3.13). Vials located in the centre of the freeze drier had higher levels of abnormalities, including collapse and melt back. Whereas vials positioned to the periphery of the freeze drier had a uniform distribution of constituents. From a total of 94 freeze-dried vials, 4 were discarded due to pressure release when recapped, 15 were discarded because they were showing signs of collapse or melt back, 36 were

kept but presented structural imperfections to some extent, and 39 vials had good cake structure. Vials that had good cake structure or slight imperfections were kept and used in stability studies. The percentage of water left in the cake of vials with good cake structure, determined by Karl Fisher, was 2.45 ± 1.65 % w/w.

The second scaled-up batch of AmB-NIVs (100 ml) was not filter-sterilised before freeze-drying and the lyophilisation method was modified in order to avoid the structural abnormalities obtained in batch 1. Those structural irregularities in freeze-dried cakes were probably due to the high pressure in the chamber as this is related to the product temperature during main drying (i.e. 0.0140 mBar corresponds to -39°C; Figure 3.2). Following batch 1 production, the glass phase transition ($T_g'$) of sucrose and AmB-NIVs containing sucrose was determined at -33.05 ± 0.48°C and -27.51 ± 0.88°C respectively (mean ± SD, n=3). Examples of the calorimetrograms obtained with the DSC are shown in Figure 3.12. As a consequence, during the freeze-drying of batch 2, the freeze drier chamber was set at lower pressure (0.003 mBar, -69°C). This resulted in maintenance of AmB-NIVs temperature below -27.51°C for at least 100 hours (Figure 3.13). Moreover in this case, all the AmB-NIVs cakes had good appearance and there was no evidence of cracking, melt back or collapse (Figure 3.14). The residual water content of the cakes was lower than batch 1, at 0.06 ± 0.03 % (determined by Karl Fisher coulometry).

The physicochemical characteristics of freeze thawed and reconstituted freeze-dried AmB-NIVs (batch 2) were compared to that of the original suspension. The particle size and polydispersity index was unchanged after the freeze-thawing cycle but significantly increased after freeze-drying ($p \leq 0.001$ for z-average and $p \leq 0.05$ for polydispersity; Table 3.10.). The freeze-drying process also affected the vesicle charge by decreasing the negative potential ($p \leq 0.01$; Table 3.10.). However, the vesicles still had a z-average size that was less than 240 nm and a lower than 0.20 polydispersity index. The vesicle charge was also

higher than -30 mV, indicating that the vesicles would not clump in suspension. The concentration of AmB in the reconstituted vials was lower than that of the original formulation ($p \leq 0.01$) but the entrapment efficiency was similar (Table 3.10). The sterility of batch 2 was tested in a similar way to batch 1. In this case, there was no evidence of microbial growth in fluid thioglycolate broth or tryptone soya broth spiked with the formulation at 4 weeks post-inoculation.

**Table 3.8** Physicochemical characteristics after filter-sterilisation of AmB-CD (0.22 µm filter) and AmB-NIVs (0.45 µm filter; scaled-up formulation from batch 1: 250 ml of 1 mg/ml AmB, 100 mg/ml HPγCD, 0.09 g/ml sucrose, 150 mM lipids; ** $p \leq 0.01$, *** $p \leq 0.001$ comparing before and after filtration).

| | Physicochemical properties (mean ± SD; n=3) | Scaled-up batch 1 fresh AmB-NIVs | |
|---|---|---|---|
| | | Before filtration | After filtration |
| AmB-CD (0.22 µm filter) | Z-average (nm) | 1,822.22 ± 122.54 | 345.46 ± 2.30 *** |
| | Polydispersity index | 0.91 ± 0.08 | 0.34 ± 0.02 *** |
| | AmB (mg/ml) | 1.16 ± 0.09 | 0.92 ± 0.14 |
| AmB-NIVs (0.44 µm filter) | Z-average (nm) | 225.85 ± 5.81 | 203.53 ± 3.16 ** |
| | Polydispersity index | 0.22 ± 0.01 | 0.20 ± 0.05 |
| | ζ-potential (mV) | -46.07 ± 0.99 | -48.00 ± 1.84 |
| | AmB (mg/ml) | 0.45 ± 0.01 | 0.44 ± 0.01 |

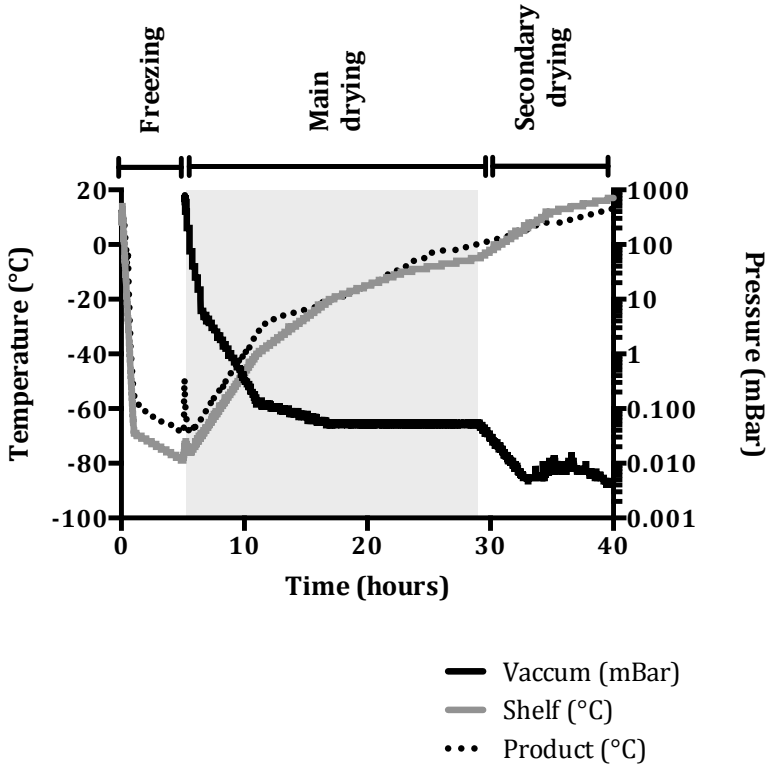


**Figure 3.10** Freeze drier program used to lyophilise AmB-NIVs from batch 1 (250 ml of 1 mg/ml AmB, 100 mg/ml HPγCD, 0.09 g/ml sucrose, 150 mM lipids). Shelf temperature and vacuum pressure set as described in Table 2.4. The product temperature was recorded with an intra-cake thermometric probe.

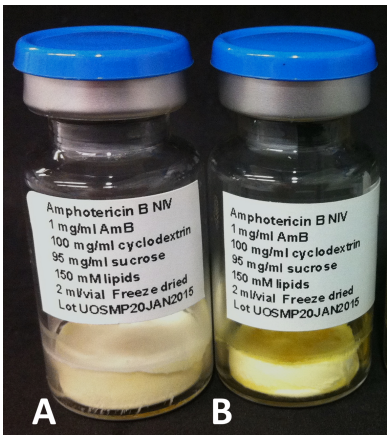


**Figure 3.11** Examples of different appearances of AmB-NIVs freeze-dried cakes from scaled-up batch 1 (250 ml of 1 mg/ml AmB, 100 mg/ml HPγCD, 0.09 g/ml sucrose and 150 mM lipid). Example of a good cake with uniform distribution of constituents (A) and example of cake with signs of collapse and melt back (B).

**Table 3.9** Physicochemical and rheological properties of freeze-dried AmB-NIVs from scaled-up batch 1 (250 ml of 1 mg/ml AmB, 100 mg/ml HPγCD, 0.09 g/ml sucrose and 150 mM lipid). Freeze-dried samples as described in Table 2.4 and Figure 3.10 (* $p \leq 0.05$, ** $p \leq 0.01$ between pre-lyophilisation and rehydrated lyophilisate).

| | Characteristics (mean ± SD; n=3) | Scaled-up batch 1 AmB-NIVs | |
|---|---|---|---|
| | | Liquid pre-lyophilisation | Rehydrated lyophilisate |
| Physicochemical properties | Z-average (nm) | 203.51 ± 3.16 | 211.21 ± 1.25 * |
| | Polydispersity index | 0.20 ± 0.05 | 0.17 ± 0.01 |
| | ζ-potential (mV) | -48.00 ± 1.84 | -47.00 ± 1.21 |
| | AmB (mg/ml) | 0.44 ± 0.07 | 0.36 ± 0.03 ** |
| | Entrapment efficiency (%) | 85.18 ± 8.90 | 81.55 ± 4.98 |
| Rheological properties | Apparent viscosity (mPa·s) | 13.27 ± 0.34 | 12.21 ± 0.23 * |
| | Flow index | 0.84 ± 0.01 | 0.89 ± 0.02 |
| | Consistency index (mPa·s) | 40.70 ± 3.00 | 25.96 ± 3.85 ** |
| | Hysteresis loop (Pa/s) | 612.17 ± 134.81 | 313.20 ± 103.00 |
| | $R^2$ | 1.00 ± 0.00 | 1.00 ± 0.00 |

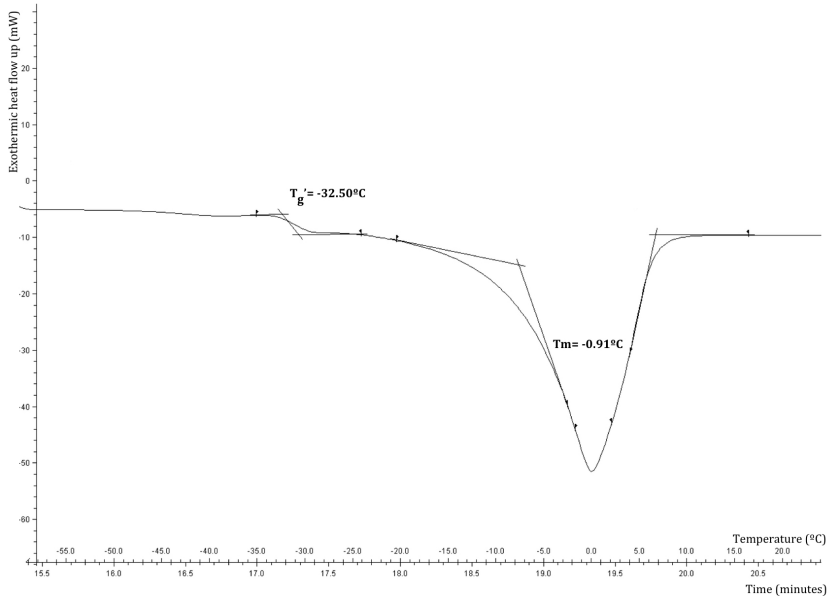


**A-** Sucrose solution

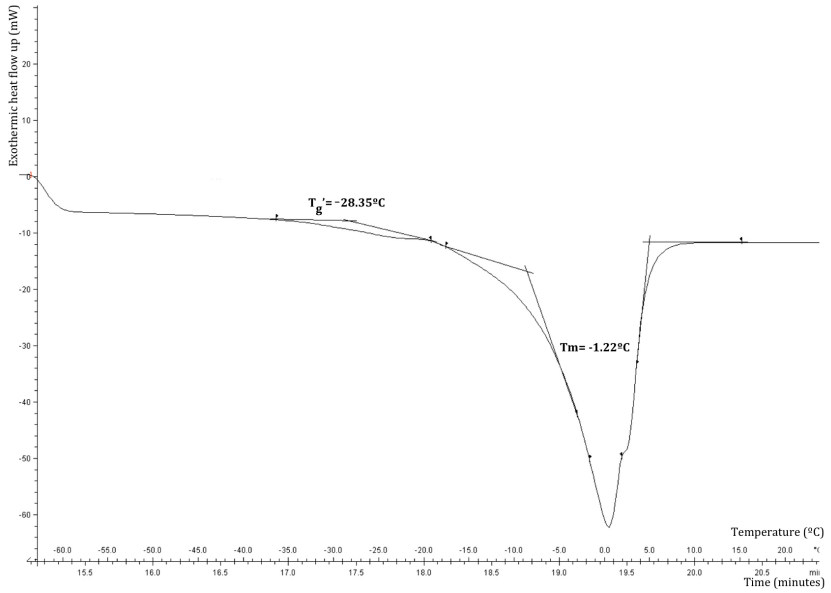


**B-** AmB-NIVs with sucrose

**Figure 3.12** Examples of DSC calorimetrograms of sucrose solution (A; 0.50 g/ml; 10.83 mg sample) and AmB-NIVs (B; 1 mg/ml AmB, 100 mg/ml HPγCD, 0.09 g/ml sucose, 150 mM; 14.50 mg sample). Onset of the curve was established as the $T_g$' and curve peak was established as Tm (°C; Tm, melting temperature).

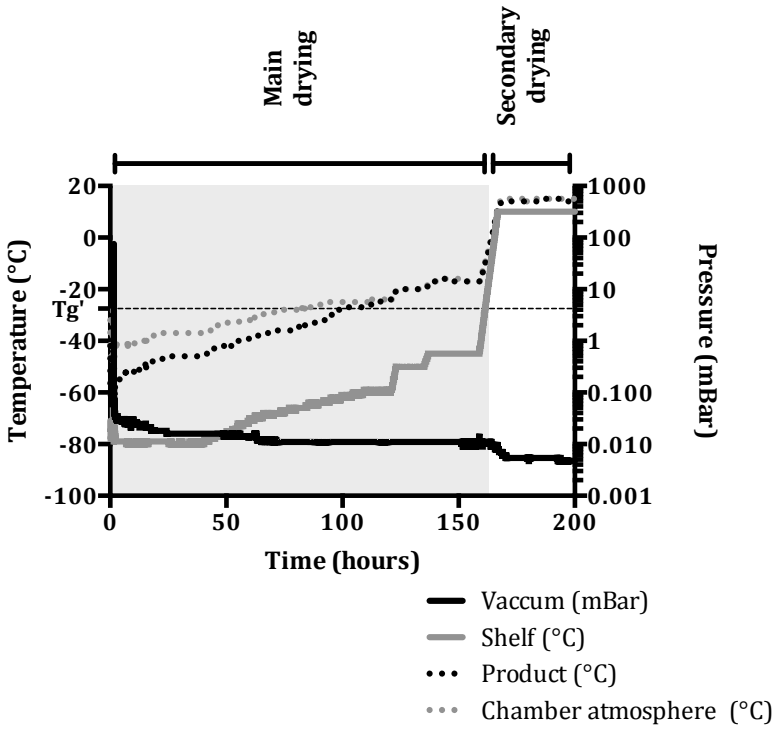


**Figure 3.13** Freeze drier program used to lyophilise AmB-NIVs from batch 2 (100 ml of 1 mg/ml AmB, 100 mg/ml HPγCD, 0.09 g/ml sucrose, 150 mM lipids). Shelf temperature and vacuum pressure set as described in Table 2.5. The product temperature and the chamber atmosphere temperature were recorded with an intra-cake thermometric probe. Phase transition temperature for AmB-NIVs with sucrose marked in the left y-axis ($T_g'$ = -27.51°C).


**Figure 3.14** Examples of AmB-NIVs freeze-dried cakes appearance from scale-up batch 2 (100 ml of 1 mg/ml AmB, 100 mg/ml HPγCD, 0.09 g/ml sucrose and 150 mM lipid). Example of good cakes with uniform distribution of constituents and with no signs of collapse or melt back (front and bottom section).

**Table 3.10** Physicochemical properties of fresh, frozen and freeze-dried AmB-NIVs scaled-up batch 2 (100 ml of 1 mg/ml AmB, 100 mg/ml HPγCD, 0.09 g/ml sucrose, 150 mM lipids). Freeze-thaw samples were frozen at -80°C and thaw at room temperature. Rehydrated lyophilisate was freeze-dried as described in Table 2.5 and Figure 3.13 (* $p \leq 0.05$, ** $p \leq 0.01$ and *** $p \leq 0.001$ compared to the liquid pre-lyophilisation value).

| **Physicochemical properties (mean ± SD, n=3)** | **Scaled-up batch 2 AmB-NIVs** | | |
|---|---|---|---|
| | **Liquid pre-lyophilisation** | **Freeze- thaw cycle** | **Rehydrated lyophilisate** |
| **Z-average (nm)** | 190.71 ± 1.62 | 196.26 ± 2.74 | 235.68 ±3.83 *** |
| **Polydispersity index** | 0.16 ± 0.01 | 0.12 ± 0.01 | 0.18 ± 0.01 * |
| **ζ-potential (mV)** | -74.33 ± 1.61 | -61.98 ± 1.40 | -55.66 ± 7.77 ** |
| **AmB (mg/ml)** | 0.97 ± 0.07 | 0.86 ± 0.02 | 0.73 ± 0.03 ** |
| **Entrapment efficiency (%)** | 86.19 ± 5.83 | 98.64 ± 11.66 | 90.93 ± 4.91 |

### 3.3.6. Stability studies of freeze-dried AmB-NIVs

Several freeze-dried vials from AmB-NIVs batch 1 (1 mg/ml AmB, 100 mg/ml HPγCD, 0.09 g/ml sucrose, 150 mM lipids) were stored at 40°C, 4°C or -80°C as part of an accelerated long-term stability study. The characteristics of the formulations were analysed at 2, 4 and 6 months after formulation. Changes in the appearance of the cake occurred in the majority vials stored at 40°C after 2 months. Some of the freeze-dried cakes collapsed and could not be rehydrated and consequently, analysis was not possible for the whole study at 40°C. In contrast, vials stored at 4°C and -80°C maintained their appearance during the whole study. The particle size and polydispersity index of reconstituted AmB-NIVs from vials stored at -80°C maintained within a ± 10 % variation from the properties at day 0 up to 6 months (Figure 3.15.A). The samples stored at 4°C had a vesicle size and polydispersity index increase outside the ± 10 % range (but less ± 15 %; Figure 3.15.A-B). The vesicle size of particles stored at 40°C increased significantly to 426.52 ± 13.70 nm at the second month time point ($p \leq 0.05$; Figure 3.15.A). On the other hand, storage at different temperatures had no negative effect on the ζ-potential of vesicles as this only varied to more negative values over the course of the study (+ 10 %; Figure 3.15.C). Storage at 40°C for two months, resulted in a significant decrease in the drug concentration within vials compared to the original formulation ($p \leq 0.01$; Figure 3.15.D). The amount of AmB in samples stored at 4°C or -80°C was similar to the original sample up to 6 months of storage ($p \leq 0.05$; Figure 3.15.D). AmB entrapment efficiency was stable through the whole stability study, independent of storage temperature (Figure 3.15.E). The AmB peak height value from the HPLC chromatograms decreased for vials stored at 40°C (Figure 3.15.F) up to 30 % from the original value ($p \leq 0.01$). Vials stored at 4°C or -80°C had stable peak height up to 6 months of the study.

In addition, AmB-NIVs samples from batch 2 were subjected to a shorter stability study of 15 weeks. Samples were stored at 40°C, 4°C or -80°C and the

properties analysed at 6 and 15 weeks post-formulations. The freeze-dried cake within all of the vials, maintained its good appearance up to 15 weeks of the study and there were no signs of visual collapse or melt-back in any samples. The vesicle size of AmB-NIVs was stable for vials stored at 4°C or -80°C. However, samples stored at 40°C had vesicles that were significantly larger than those in the original reconstitution ($p \leq 0.001$; Figure 3.16.A). A similar increase in the polydispersity index was obtained, with vesicle size remaining homogeneous for vials stored at 4°C or -80°C whereas samples stored at 40°C had significantly larger values (Figure 3.16.B). The ζ-potential was unaffected by storage temperature as the charge of all the samples did not vary more than + 10 % over the course of the study compared to original suspension (Figure 3.16.C). In addition, the AmB content of the samples was unaffected since the AmB concentration within vials did not vary more than ± 10 % compared to the original formulation (Figure 3.16.D). Only samples stored at 4°C varied significantly after 6 weeks (+ 10 %) but returned back to original levels at the 15 weeks time point. The entrapment efficiency of AmB-NIVs was also similar over the period of the study for all storage conditions (Figure 3.16.E). Consistent with drug stability, the peak height for AmB did not significantly alter for samples stored at each for the three temperatures (Figure 3.16.F).

The results of these stabilities studies indicated that freeze-dried AmB-NIVs have a shelf life up to 4 months if stored at 4°C or -80°C and less than 6 weeks if stored at 40°C.

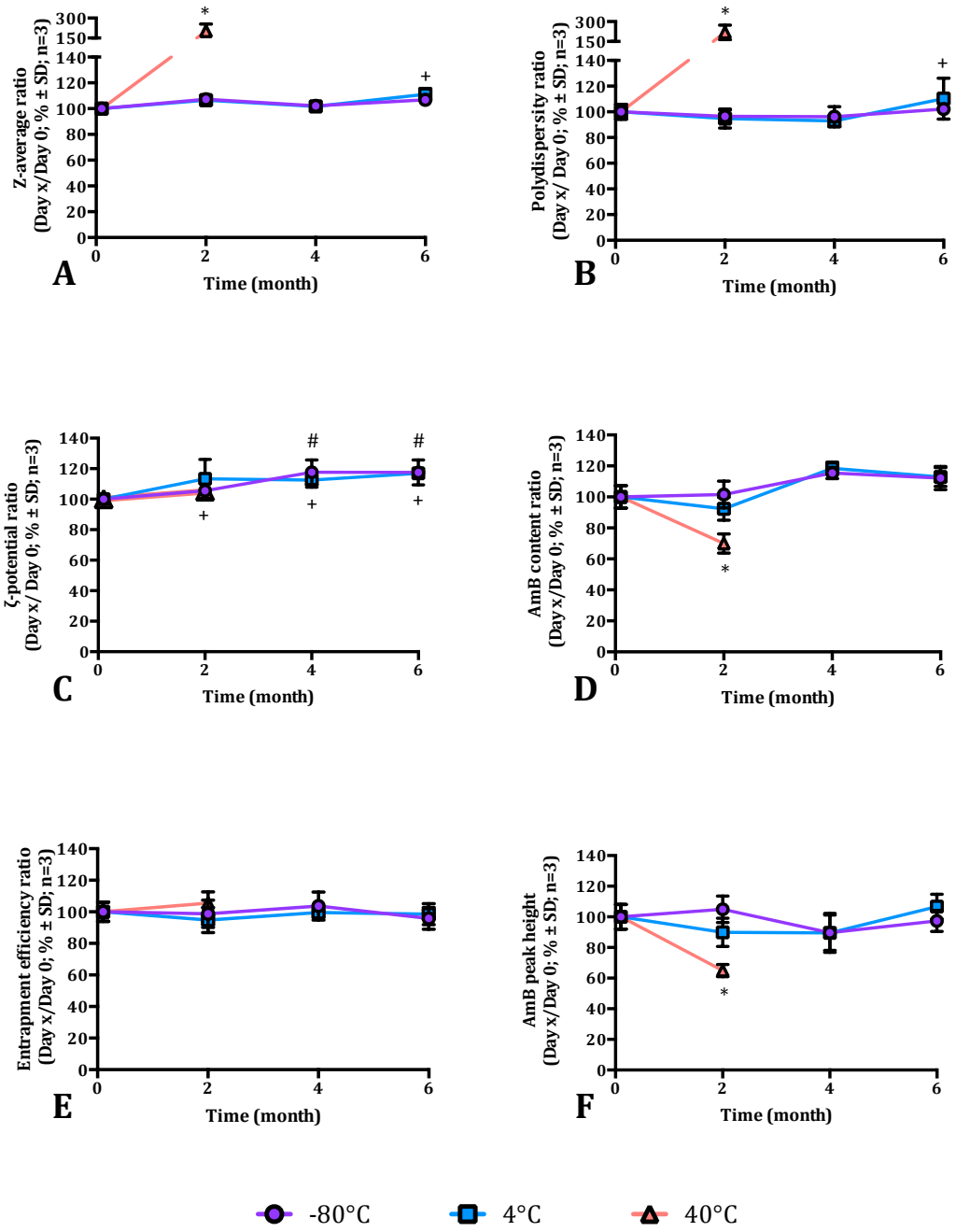


**Figure 3.15** Stability study of AmB-NIVs freeze-dried vials from scaled-up batch 1 (250 ml of 1 mg/ml AmB, 100 mg/ml HPγCD, 0.09 g/ml sucrose, 150 mM lipids). Samples were stored at 40°C, 4°C or -80°C over a period of 6 months. The physicochemical properties analysed at time 0, 2, 4, 6 months post-formulation were z-average (A), polydispersity index (B), ζ-potential (C), AmB concentration (D), AmB entrapment efficiency (E) and AmB HPLC peak height (F). The values were plotted as ratio between the day of analysis and the values on day 0. Values outside the ± 10 % range were marked as * for samples stored at 40°C, ⁺ for samples stored at 4°C and # for samples stored at -80°C.

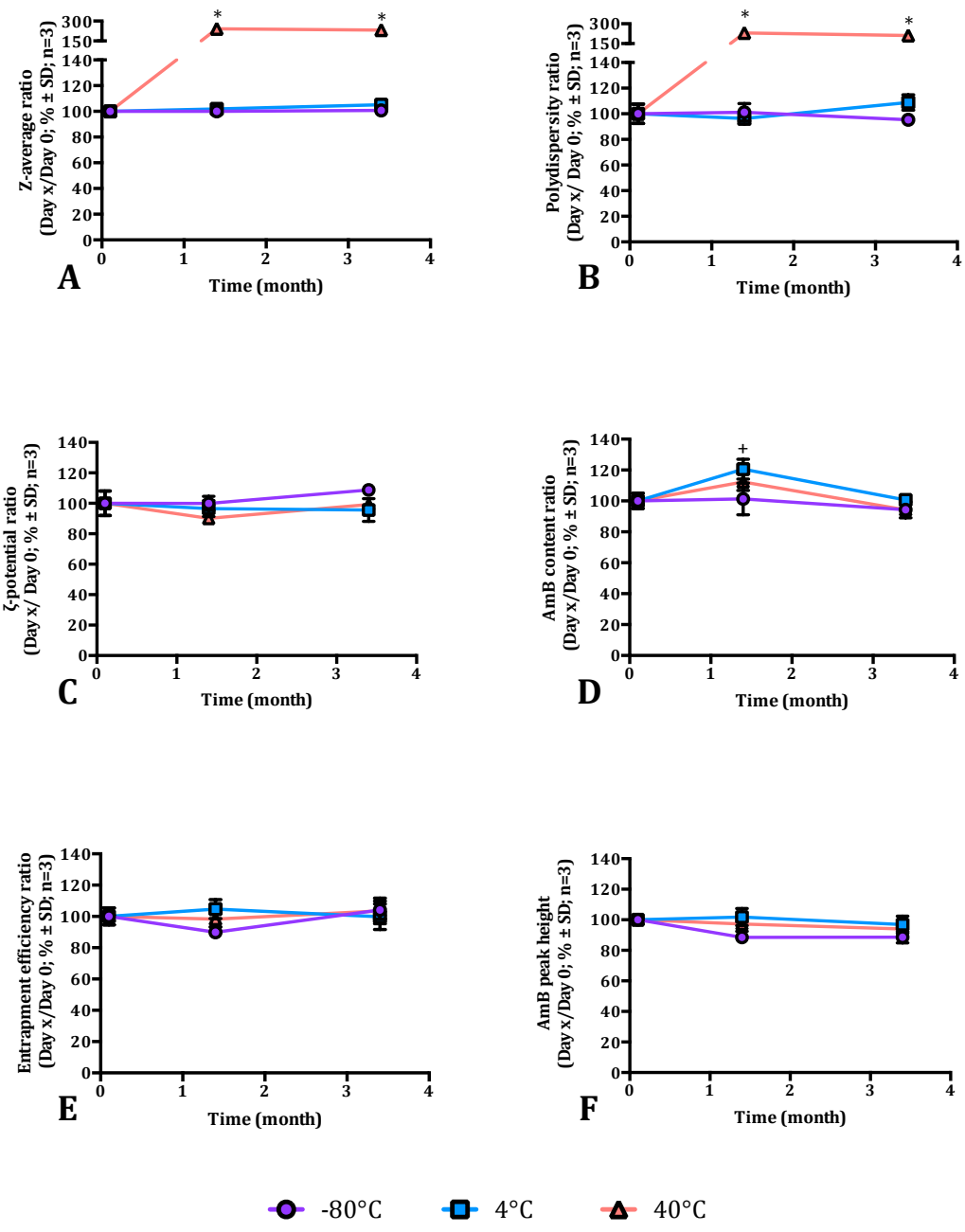


**Figure 3.16** Stability study of AmB-NIVs freeze-dried vials from scaled-up batch 2 (1 mg/ml AmB, 100 mg/ml HPγCD, 0.09 g/ml sucrose, 150 mM lipids). Samples were stored at 40°C, 4°C or -80°C over a period of 15 weeks. The physicochemical properties analysed at time 0, 6 and 15 weeks post-formulation were z-average (A), polydispersity index (B), ζ-potential (C), AmB concentration (D), AmB entrapment efficiency (E) and AmB HPLC peak height (F). The values were plotted as ratio between the day of analysis and the values on day 0. Values outside the ± 10 % range were marked as * for samples stored at 40°C and ⁺ for samples stored at 4°C.

### 3.3.7. Stability of reconstituted AmB-NIVs vials

It is important to know the stability of the reconstituted AmB-NIVs in order to show how long the formulation is usable after rehydration. Therefore, several freeze-dried vials from batch 1 AmB-NIVs (1 mg/ml AmB, 100 mg/ml HPγCD, 0.09 g/ml sucrose, 150 mM lipids) were reconstituted and stored for up to 21 days at 25°C or 4°C. The size of the AmB-NIVs particles over the 21-day period was similar to that at reconstitution and remained into the 211.22 nm ± 10 % size range when the formulation was stored after rehydration at 4°C or 25°C (Figure 3.17.A). The polydispersity index varied over time but the tendency was towards homogeneity rather than more dispersity, especially after storage at 25°C (Figure 3.17.B). The ζ-potential of the reconstituted AmB-NIVs stored at 4°C was stable over the 21 days of the study. Some of the vials stored at 25°C slightly increased the negative charge more than -47.00 mV + 10 % limit compared to day 0 (Figure 3.17.C). The amount of AmB present in the reconstituted vials remained stable at 4°C over the 21 days after rehydration of the cakes. The AmB content within vials stored at 25°C significantly decreased by day 14 (Figure 3.17.D). The amount of AmB entrapped within vesicles was significantly lower than the day 0 value for both storage temperatures on day 7 after rehydration (below 81.55 ± 10 % entrapment efficiency) but returned to similar original values on days 14 and 21. Indicating that the day 7 results may not have been reliable (Figure 3.17.E). The AmB peak height for reconstituted samples stored at 4°C and 25°C did not change over the 21 days of the study (Figure 3.17.F).

The results of these studies indicate that reconstituted freeze-dried AmB-NIVs have a shelf life of 7 days if stored at 25°C and up to 21 days if stored at 4°C.

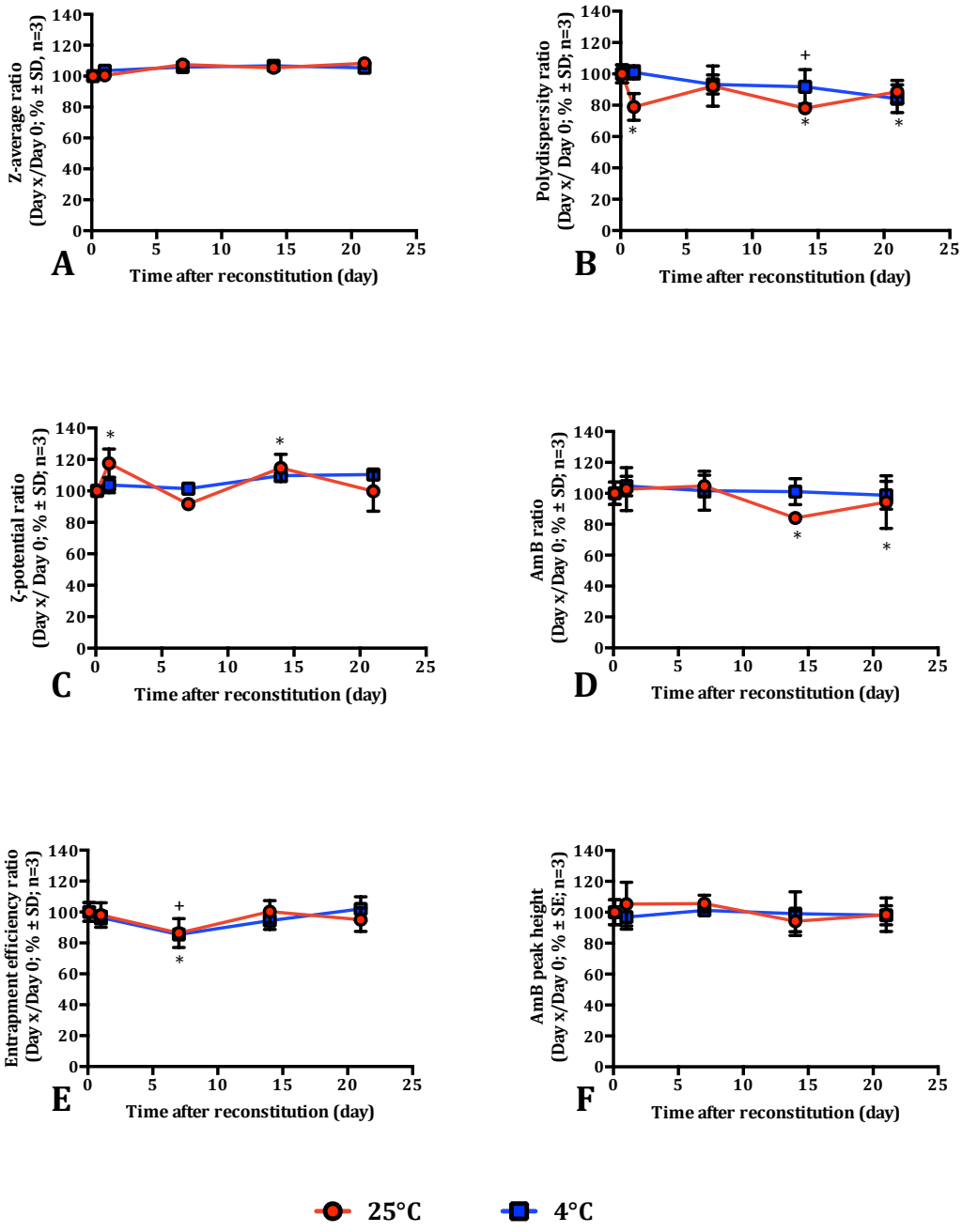


**Figure 3.17** Stability study of reconstituted AmB-NIVs (1 mg/ml AmB, 100 mg/ml HPγCD, 0.09 g/ml sucrose, 150 mM lipids, freeze-dried from batch 1). Samples were stored at 4°C and 25°C over a period of 21 days. The physicochemical properties analysed were z-average (A), polydispersity index (B), ζ-potential (C), AmB concentration (D), AmB entrapment efficiency (E) and AmB HPLC peak height (F). The values were plotted as ratio between the day of analysis and the values of just-reconstituted vials on day 0. Values outside the ± 10 % range were marked as * for samples stored at 25°C and + for samples stored at 4°C.

### 3.4. *In vivo* efficacy of AmB-NIVs to treat visceral leishmaniasis:

#### 3.4.1. Efficacy of AmB-NIVs administered intravenously in a mice model of LV82-luc

The *in vivo* efficacy of AmB-NIVs was determined using a murine model of *L. donovani,* where mice were infected with luciferase-expressing promastigotes (LV82-luc). Imaging studies showed that most of the BLI produced by the parasites was localised in the liver area of the mice (Figure 3.18.A). The values of BLI for the control group were constant for all the course of the study (Figure 3.19). Treatment on day 7 with AmB-CD or AmB-NIVs (1 mg AmB/kg) by the intravenous route showed that either AmB formulations resulted in a similar significant reduction in BLI from day 8 post-infection ($p \leq 0.01$; Figure 3.19). On day 18, mice were sacrificed and parasites burdens in the spleen and the liver were assessed determining the amount of BLI emitted *ex vivo* by these organs (Table 3.11). Spleens and livers from mice treated with AmB-CD or AmB-NIVs emitted significantly lower amounts of BLI than the same organs from control mice ($p \leq 0.05$ for spleen and $p \leq 0.01$ for liver; Table 3.11). Parasite burdens within the spleen, liver and bone marrow were counted by direct examination of Giemsa stained samples for each mouse. Parasites were not detected in the spleen but were present within the livers of infected mice. Treatment with both AmB formulations resulted in a significant decrease in liver parasite burdens compared to control ($p \leq 0.01$ for AmB-CD and $p \leq 0.05$ for AmB-NIVs; Table 3.12). The relationship between the BLI of *ex vivo* liver and the parasite burdens counted at the end of the study, presented a good correlation factor despite the few time points available (Figure 3.20). This correlation confirmed the reliability of using BLI values to quantify luciferase-expressing parasites.

A second similar experiment was performed in order to investigate the anti-leishmania effect of lower AmB concentration in the formulations (0.5 mg AmB/kg). Moreover, the efficacy of AmB-NIVs containing sucrose was

compared to the formulation without the additive. The LV82-luc parasite infection was localised in the livers as observed for the control group in Figure 3.21.A. Treatment on day 7 post-infection with AmB-CD (0.05 mg AmB/kg) by the intravenous route showed no difference from the BLI present in control group (Figure 3.21.B and Figure 3.22). However, AmB-NIVs formulations with and without sucrose (0.05 mg AmB/kg) resulted in significant reduction in BLI compared to control or AmB-CD groups ($p \leq 0.05$; Figure 3.22; Figure 3.21.C-D). After the mice were sacrificed, the burdens in spleen and liver were assessed through detecting the amount of BLI emitted (Table 3.13). Only spleens and liver BLI from mice treated with AmB-NIVs with sucrose were significantly lower than the control group ($p \leq 0.01$ for spleen and $p \leq 0.05$ for liver; Table 3.13).

Infection with *L. donovani* is associated with hepatosplenomegaly; therefore spleen and liver weights were determined. Surprisingly spleens of mice treated with AmB-NIVs weighed significantly more than spleens from control mice ($p \leq 0.01$; control, 0.19 ± 0.01 g; AmB-CD, 0.20 ± 0.01 g; AmB-NIVs, 0.26 ± 0.01 g; mean ± SE; 1 mg AmB/kg; n=4). This increase in spleen weight could be associated with an inflammatory reaction within the organ. Therefore, the effect of AmB-NIVs treatment on neutrophil recruitment, which occurs during an inflammation response, was determined by monitoring chemiluminescence levels (CLI) after injection of luminol (Section 3.4.2.).

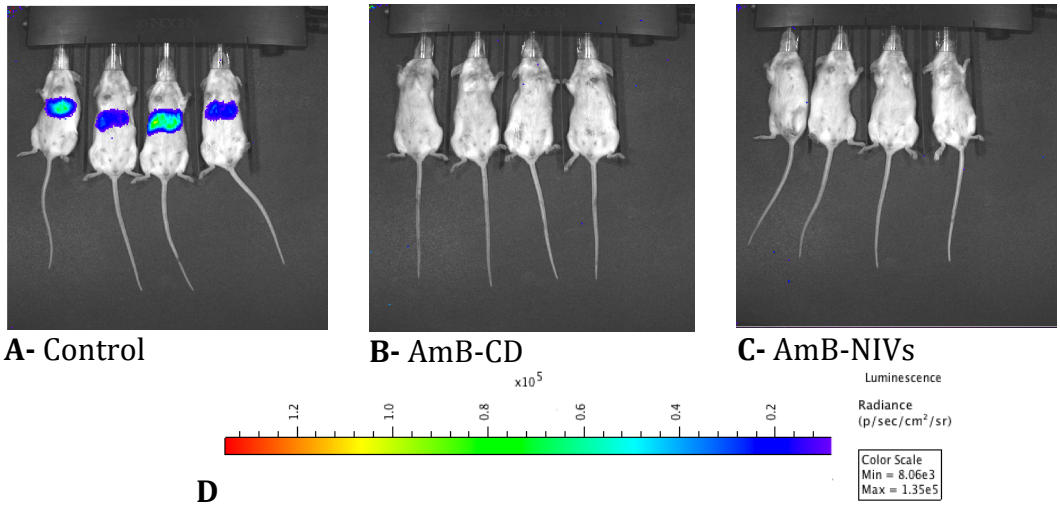


**Figure 3.18** IVIS examples of BLI images obtained from BALB/c infected with LV82-luc and treated on day 7 post-infection with PBS pH 7.4 (A; control), AmB-CD (B; 1 mg/ml AmB, 100 mg/ml HPγCD) or AmB-NIVs (C; 1 mg/ml AmB, 100 mg/ml HPγCD, 150 mM lipids) at a concentration of 1 mg AmB/ kg. The image corresponds to day 12 post-infection. The color gradient from red to blue indicated the decrease of parasite bioluminescence for all the pictures (D).

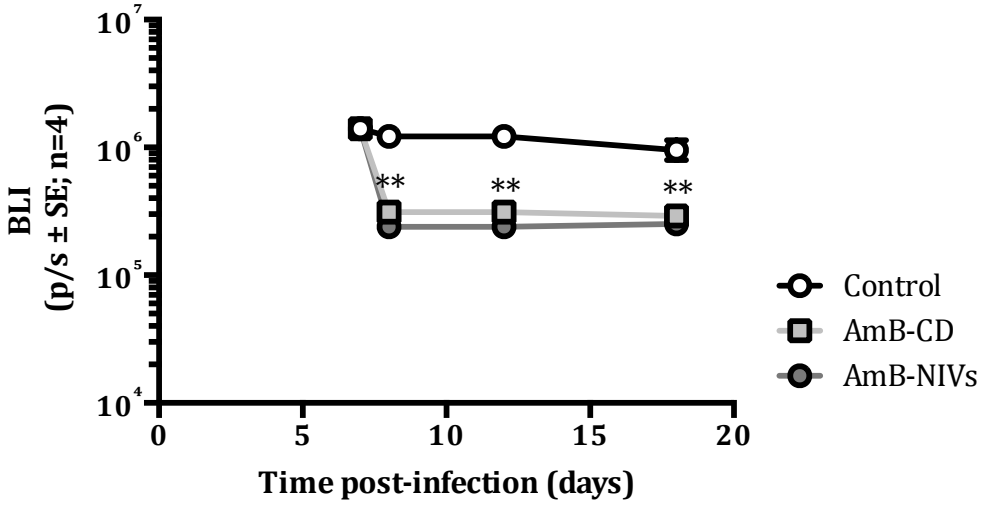


**Figure 3.19** BLI values of BALB/c infected with LV82-luc and treated on day 7 post-infection with PBS pH 7.4 (control), AmB-CD (1 mg/ml AmB, 100 mg/ml HPγCD) or AmB-NIVs (1 mg/ml AmB, 100 mg/ml HPγCD, 150 mM lipids) at a concentration of 1 mg AmB/ kg. The BLI values were obtained from liver area only (** $p \leq 0.01$ between control group and AmB-CD and AmB-NIVs groups; n=4/group).

**Table 3.11** The effect of treatment with different AmB formulations on LV82-luc parasite BLI in the spleen and liver *ex vivo*. Mice were infected with LV82-luc and treated by intravenous injection on day 7 with PBS pH 7.4 (control), AmB-CD (1 mg/ml AmB, 100 mg/ml HPγCD) or AmB-NIVs (1 mg/ml AmB, 100 mg/ml HPγCD, 150 mM lipids) at a concentration of 1 mg AmB/kg. BLI was obtained using the IVIS after immersing the organs with luciferin solution (150 µg/ml) on day 18 post-infection. The mean suppression percentage in BLI numbers compared to control values is shown in parenthesis (* $p \leq 0.05$, ** $p \leq 0.01$ compared to control values; n=4/group).

| Treatment | *Ex vivo* BLI (x$10^3$, p/s ± SE) (suppression % ± SE) | |
|---|---|---|
| | **Spleen** | **Liver** |
| **Control** | 12.62 ± 1.34 | 121.01 ± 31.32 |
| **AmB-CD** | 5.03 ± 0.31 * (60.15 ± 2.44) | 14.24 ± 1.38 ** (88.23 ± 1.14) |
| **AmB-NIVs** | 6.04 ± 0.28 * (64.15 ± 12.08) | 6.17 ± 0.16 ** (96.17±1.28) |

**Table 3.12** The effect of treatment with different AmB formulations on LV82-luc parasite burdens in the spleen, liver and bone marrow. Mice were infected with LV82-luc and treated by intravenous injection on day 7 with PBS pH 7.4 (control), AmB-CD (1 mg/ml AmB, 100 mg/ml HPγCD) or AmB-NIVs (1 mg/ml AmB, 100 mg/ml HPγCD, 150 mM lipids) at 1 mg AmB/kg. Parasite burdens were counted on day 18 post-infection. The mean suppression in parasite numbers compared to control values is shown in parenthesis (* $p \leq 0.05$, ** $p \leq 0.01$ compared to control values; n.d, non-detectable; n=4/group).

| Treatment | Parasite burden ± SE (Suppression % ± SE) | | |
|---|---|---|---|
| | **Spleen** | **Liver** | **Bone marrow** |
| **Control** | 1.19 ± 0.82 | 39.57 ± 7.58 | n.d. |
| **AmB-CD** | n.d. | 6.53 ± 0.50 ** (83.51 ± 1.28) | n.d. |
| **AmB-NIVs** | n.d. | 10.80 ± 5.07 * (72.71 ± 9.06) | n.d. |

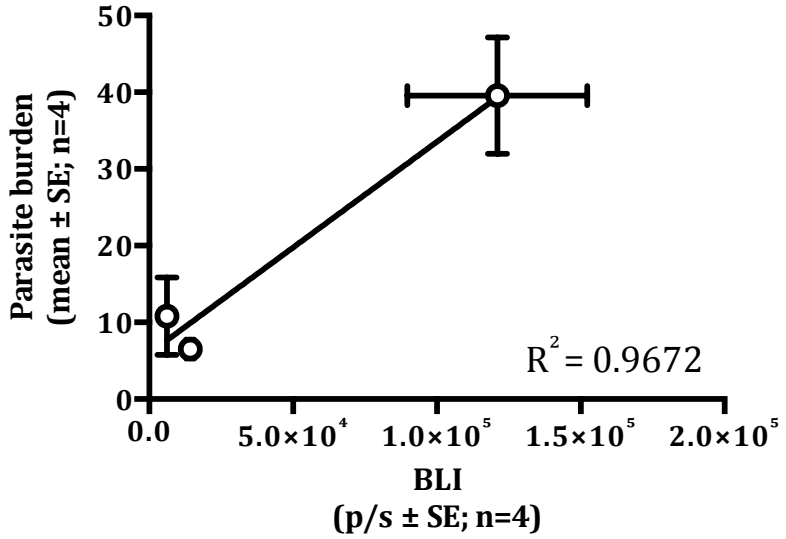


**Figure 3.20** Relationship between BLI of liver *ex vivo* (Table 3.11) and parasite burdens numbers (Table 3.12) of mice infected with LV82-luc after 18 days post-infection ($R^2$, correlation coefficient; n=4).

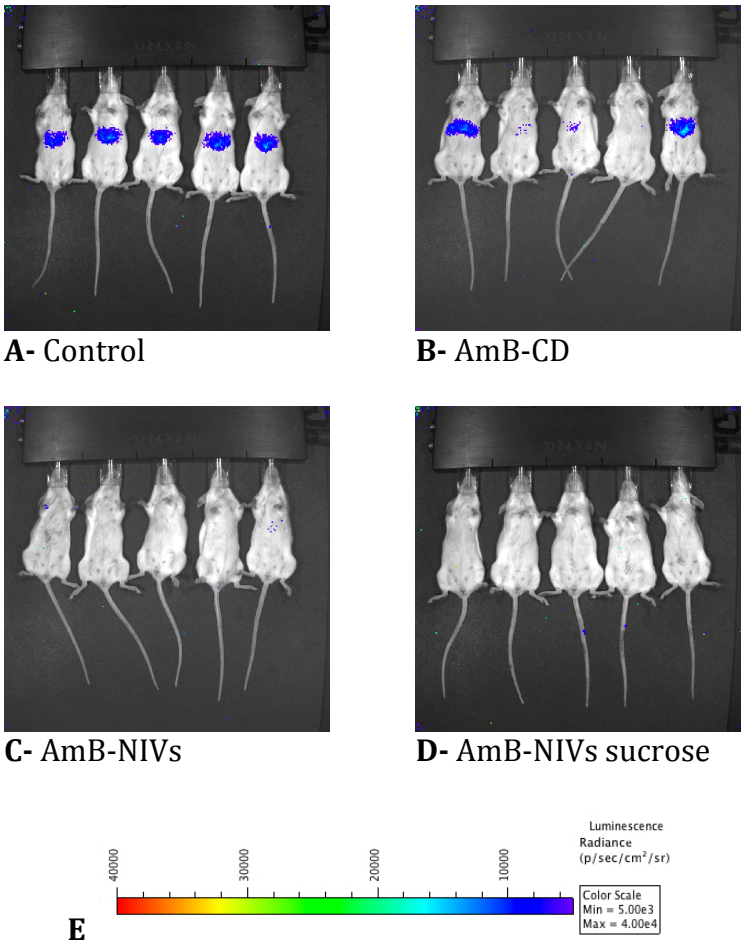


**Figure 3.21** IVIS examples of BLI image obtained from BALB/c infected with LV82-luc and treated on day 7 post-infection with PBS pH 7.4 as control (A), AmB-CD (B; 0.05 mg/ml AmB, 5 mg/ml HPγCD), AmB-NIVs (C; 0.05 mg/ml AmB, 5 mg/ml HPγCD, 7.5 mM lipids) or AmB-NIVs with sucrose (D; 0.05 mg/ml AmB, 5 mg/ml HPγCD, 4.5 mg/ml sucrose, 7.5 mM lipids) at a concentration of 0.05 mg AmB/kg. The image corresponds to day 9 post-infection. The gradient from colour red to blue indicated the decrease of parasite bioluminescence for all the pictures (E).

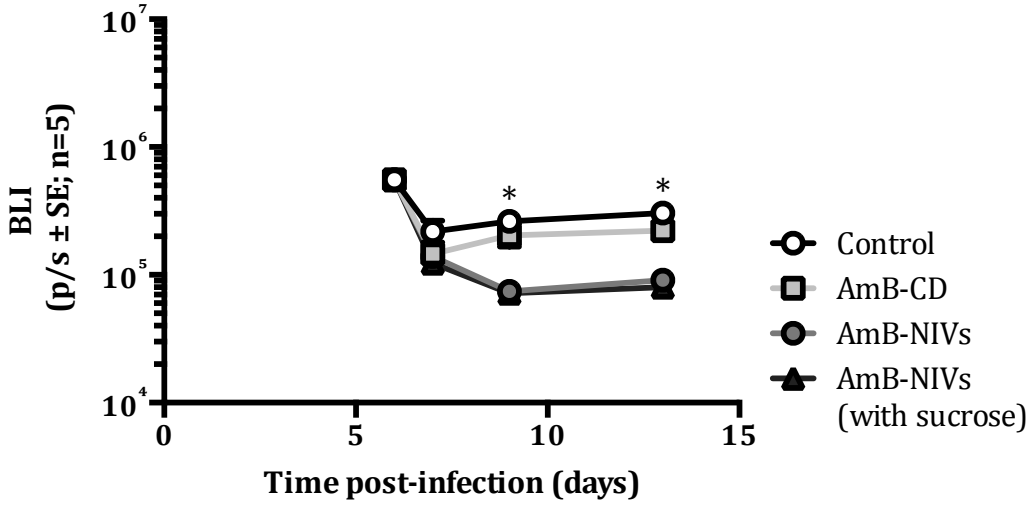


**Figure 3.22** BLI values of BALB/c infected with LV82-luc and treated on day 7 post-infection with PBS pH 7.4 as control, AmB-CD (0.05 mg/ml AmB, 5 mg/ml HPγCD), AmB-NIVs (0.05 mg/ml AmB, 5 mg/ml HPγCD, 7.5 mM lipids) or AmB-NIVs with sucrose (0.05 mg/ml AmB, 5 mg/ml HPγCD, 4.5 mg/ml sucrose, 7.5 mM lipids) at a concentration of 0.05 mg AmB/kg. The BLI values were obtained from liver area only (* $p \leq 0.05$ significant difference between control and AmB-CD compared to AmB-NIVs and AmB-NIVs with sucrose groups).

**Table 3.13** The effect of treatment with different AmB formulations on LV82-luc parasite BLI in the spleen and liver *ex vivo*. Mice were infected with LV82-luc and treated by intravenous injection on day 7 with PBS pH 7.4 as control, AmB-CD (0.05 mg/ml AmB, 5 mg/ml HPγCD), AmB-NIVs (0.05 mg/ml AmB, 5 mg/ml HPγCD, 7.5 mM lipids) or AmB-NIVs with sucrose (0.05 mg/ml AmB, 5 mg/ml HPγCD, 4.5 mg/ml sucrose, 7.5 mM lipids) at a concentration of 0.05 mg AmB/kg. BLI was obtained imaging the organs *ex vivo* on day 14 post-infection. The mean suppression in BLI percentage numbers compared to control values is shown in parenthesis only for significant values (* $p \leq 0.05$, ** $p \leq 0.01$ compared to control values).

| **Treatment** | ***Ex vivo* BLI (x $10^3$, p/s ± SE) (suppression % ± SE)** | |
|---|---|---|
| | **Spleen** | **Liver** |
| **Control** | 27.90 ± 8.70 | 43.00 ± 5.43 |
| **AmB-CD** | 12.37 ± 3.79 | 37.66 ± 3.83 |
| **AmB-NIVs** | 10.74 ± 1.08 | 23.86 ± 2.55 |
| **AmB-NIVs with sucrose** | 7.43 ± 1.15 ** (73.38 ± 4.61) | 21.90 ± 1.96 * (49.07 ± 5.10) |

### 3.4.2. Inflammatory response associated with treatment of AmB-NIVs of different vesicle size by intravenous or inhalation route of administration

Intravenous treatment with large AmB-NIVs (828.0 ± 77.2 nm) resulted in significantly higher levels of CLI from uninfected mice compared to controls ($p \leq 0.05$ between 2 and 12 minutes after luminol injection; Figure 3.23.A). On the contrary, intravenous administration of small AmB-NIVs (200.4 ± 3.4 nm) did not present a significant increase on neutrophil recruitment compared to the control group. The route of administration influenced results as treatment with the same AmB formulations by inhalation (small and large AmB-NIVs) did not influence neutrophil recruitment and similar amount of CLI were emitted by control and drug treated groups (Figure 3.23.B). To further study this effect, the levels of neutrophils present in the *ex vivo* spleen, liver and lungs of the treated mice by inhalation were assessed placing the relevant organ in luminol solution prior imaging. There was no significant difference in the amount of CLI emitted by organs from control and drug treated mice (Table 3.14). Indicating that treatment with AmB-NIVs by inhalation did not cause neutrophil recruitment above the control levels. The amounts of AmB present in the lungs of the treated mice were also assessed. There was no difference in the amount of AmB present in the lungs of mice treated with small or large AmB-NIVs, indicating that vesicle size did not influence drug delivery (Table 3.14).

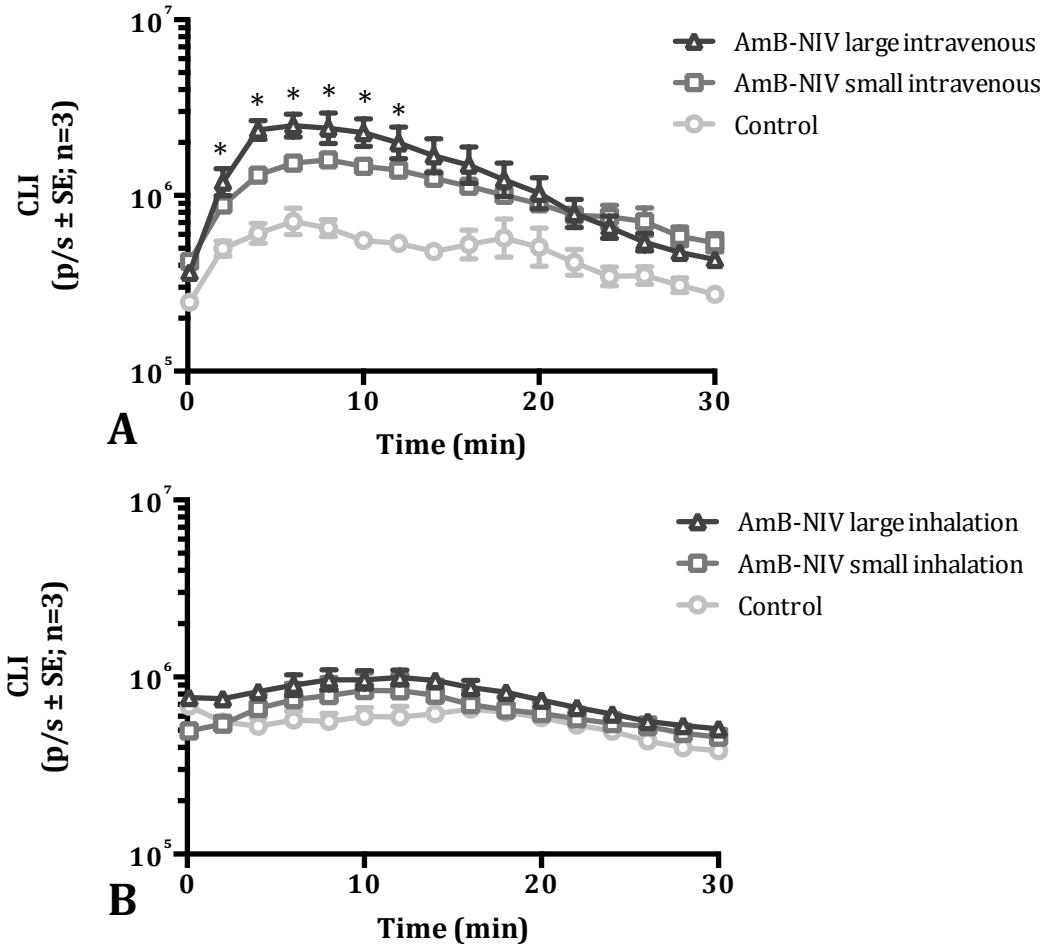


**Figure 3.23** Luminol CLI produced by neutrophils related to inflammatory response to treatment. Healthy mice were administered small (200.4 ± 3.4 nm) or large (828.0 ± 77.2 nm) AmB-NIVs (1 mg/ml AmB, 100 g/ml HPγCD, 150 mM lipids) at a concentration of 1 mg AmB/kg by intravenous administration (A) and by inhalation using Aeroneb Lab vibrating-mesh nebuliser (B). Whole body images were obtained under the IVIS system, luminol (ip, 0.2 ml, 100 mg/kg) was injected after 2 minutes and imaging continued up to 30 minutes. PBS was used as a control in the intravenous administration and distilled water was the control for the inhaled treatment (* $p \leq 0.05$ for AmB-NIVs large compared to control).

**Table 3.14** Luminol CLI produced by neutrophils related to inflammatory response to inhaled treatment of small (200.4 ± 3.4 nm) or large (828.0 ± 77.2 nm) AmB-NIVs (1 mg/ml AmB, 100 g/ml HPγCD, 150 mM lipids) at a concentration of 1 mg AmB/kg. Obtained spleen, liver and lungs were immerged in luminol solution and imaged to detect the maximum *ex vivo* CLI. AmB levels in lungs were quantified by HPLC (n.a., not applicable; n=3).

| **Inhaled treatment** | ***Ex vivo* luminol CLI (x $10^3$, p/s ± SE)** | | | **AmB levels** |
|---|---|---|---|---|
| | **Spleen** | **Liver** | **Lungs** | **Lungs (ng/mg tissue ± SE)** |
| **Control** | 7.08 ± 0.83 | 15.59 ± 1.29 | 12.24 ± 3.47 | n.a. |
| **AmB-NIVs small** | 4.52 ± 1.10 | 14.62 ± 2.64 | 10.68 ± 3.80 | 0.59 ± 0.08 |
| **AmB-NIVs large** | 8.34 ± 1.95 | 16.47 ± 7.58 | 10.00 ± 9.32 | 0.42 ± 0.10 |

### 3.4.3. Efficacy of inhaled AmB-NIVs of different vesicle size against two strains of *L. donovani* parasites

Studies using luciferase-expressing parasites (LV82-luc) gave low parasite burdens in control mice (Table 3.12). Therefore, the efficacy of AmB-NIVs formulation against *L. donovani* was determined using a more infective hamster visceral leishmaniasis model. The formulations were administered by inhalation following a five-dose day regimen. The subjects were infected with wild type amastigotes, harvested from previously infected hamsters. Two strains of *L. donovani* were used in the studies: LV82, which is susceptible to antimony treatment and 200015, which is resistant.

Infection with wild type LV82 parasites gave high parasite burdens in the liver, spleen and bone marrow on day 14 post-infection (Table 3.15). The high parasite levels were not associated with any adverse effect on the hamster animal weight over the course of the study. Individual subject's weight did not decrease more than 10 % for any of the treatment groups (data not shown). Treatment by the pulmonary route with AmB-CD did not present any significant reduction of the parasite burdens in the spleen, liver or bone marrow of the treated mice (Table 3.15). Treatment with AmB-NIVs formulations containing small vesicle significantly reduced parasite burdens in the bone marrow ($p \leq 0.05$; Table 3.15), but had no affect on spleen or liver compared to control values. Treatment by inhalation with AmB-NIVs formulation containing larger vesicles caused a significant inhibition in parasite burdens in the spleen ($p \leq 0.01$), liver ($p \leq 0.05$) and bone marrow ($p \leq 0.01$; Table 3.15). At sacrifice, the lungs, tracheas and plasma were collected from each hamster and AmB levels present determined (Table 3.16). Similar amounts of AmB were present in the tracheas and the lungs of hamsters given either AmB-CD or either AmB-NIVs formulations (small or large). No AmB was detected in any of the plasma samples from drug treated hamsters (Table 3.16).

Control hamsters infected with *L. donovani* strain 200015 had high parasite burdens on day 14 post-infection (Table 3.17). Treatment by the pulmonary route with AmB-CD significantly reduced spleen ($p \leq 0.05$) but not liver or bone marrow parasite burdens compared to control values. Hamster treated with AmB-NIVs containing smaller vesicles had spleen, liver and bone marrow burdens that were similar to control values. Treatment by inhalation with AmB-NIVs containing larger vesicles resulted in significant decrease in spleen ($p \leq 0.05$) and liver ($p \leq 0.05$; Table 3.17) parasite numbers compared to control values but not in the bone marrow.

**Table 3.15** The effect of inhaled AmB formulations on LV82 parasite burdens in the spleen, liver and bone marrow. Hamsters were infected with LV82 and treated daily by inhalation from day 7 to day 12 post-infection with distilled water (control), AmB-CD (1 mg/ml AmB, 100 mg/ml HPγCD), small AmB-NIVs (222.51 ± 1.15 nm; 1 mg/ml AmB, 100 mg/ml HPγCD, 150 mM lipids) or large AmB-NIVs (889.35 ± 5.78 nm; 1 mg/ml AmB, 100 mg/ml HPγCD, 150 mM lipids) at a dose of 1 mg AmB/ kg. Parasite burdens were counted on day 14 post-infection. The mean suppression percentage in parasite numbers compared to control values is shown in parenthesis (only for significant values; * $p \leq 0.05$, ** $p \leq 0.01$ compared to control values).

| Treatment | LV82 parasite burden ± SE; n=4 (Suppression % ± SE; n=4) | | |
|---|---|---|---|
| | Spleen | Liver | Bone marrow |
| **Control** | 56.87 ± 17.87 | 2102.43 ± 692.18 | 238.33 ± 72.30 |
| **AmB-CD** | 8.79 ± 1.85 | 176.08 ± 37.64 | 73.50 ± 28.94 |
| **AmB-NIVs small** | 10.46 ± 4.82 | 352.99 ± 83.25 | 16.00 ± 7.43 * (93.29 ± 3.12) |
| **AmB-NIVs large** | 3.59 ± 2.61 ** (93.68 ± 4.59) | 70.64 ± 38.99 * (96.64 ± 1.85) | 5.33 ± 4.62 ** (97.76 ± 1.94) |

**Table 3.16** Levels of AmB present in trachea, lungs and plasma of hamsters treated with inhaled AmB-CD (1 mg/ml AmB, 100 mg/ml HPγCD), small AmB-NIVs (222.51 ± 1.15 nm; 1 mg/ml AmB, 100 mg/ml HPγCD, 150 mM lipids) or large AmB-NIVs (889.35 ± 5.78 nm; 1 mg/ml AmB, 100 mg/ml HPγCD, 150 mM lipids) at a dose of 1 mg AmB/ kg. Hamsters were infected with LV82 and treated daily by inhalation from day 7 to day 12 post-infection. On day 14, organs were obtained and drug levels analysed by HPLC (n.d., non-detectable).

| Treatment | AmB levels (ng/mg tissue ± SE; n=4) | | |
|---|---|---|---|
| | Trachea | Lungs | Serum |
| **AmB-CD** | 2.75 ± 0.82 | 6.79 ± 2.61 | n.d. |
| **AmB-NIVs small** | 1.28 ± 0.13 | 3.39 ± 0.18 | n.d. |
| **AmB-NIVs large** | 1.23 ± 0.13 | 2.62 ± 0.14 | n.d. |

**Table 3.17** The effect of inhaled AmB formulations on 200015 parasite burdens in the spleen, liver and bone marrow. Hamsters were treated by inhalation daily from day 7 to 12 post-infection with distilled water (control), AmB-CD (1 mg/ml AmB, 100 mg/ml HPγCD), small AmB-NIVs (371.52 ± 16.22 nm; 1 mg/ml AmB, 100 mg/ml HPγCD, 150 mM lipids) or large AmB-NIVs (802.04 ± 40.85 nm; 1 mg/ml AmB, 100 mg/ml HPγCD, 150 mM lipids) at a dose of 1 mg AmB/ kg. Parasite burdens were counted on day 14 post-infection. The mean suppression in parasite numbers compared to control values is shown in parenthesis (only for significant values; * $p \leq 0.05$ compared to control values).

| Treatment | 200015 parasite burden ± SE; n=5 (Suppression % ± SE; n=5) | | |
|---|---|---|---|
| | Spleen | Liver | Bone marrow |
| **Control** | 231.67 ± 70.77 | 5362.01 ± 1028.41 | 1272.75 ± 167.25 |
| **AmB-CD** | 43.70 ± 22.79 * (81.14 ± 9.84) | 2771.10 ± 1413.25 | 465.20 ± 268.82 |
| **AmB-NIVs small** | 130.94 ± 10.50 | 3689.55 ± 809.72 | 1387.80 ± 122.79 |
| **AmB-NIVs large** | 39.74 ± 16.23 * (82.84 ± 7.00) | 889.33 ± 491.68 * (83.41 ± 9.17) | 286.25 ± 116.24 |

## 3.5. Discussion

The overall aim of these studies was to produce an AmB-NIVs formulation, which was stable on storage, effective against *L. donovani* and could be given by inhalation. For formulation, stability and quantification purposes, a method to detect AmB was validated to suit the study requirements. HPLC is the most prevalent procedure of choice for the analysis of pharmaceutical active compounds and since AmB possesses several chromophore groups, the incorporation of an ultraviolet detector to the HPLC is the most common approach (HPLC-UV, Gilpin, 2011). The HPLC-UV method used in this studies was adapted from Puig-Sellart (2013) with the only difference being the manufacturer of the column used. The method was reassessed and revalidated for this condition and reliable precision data was obtained with low relative standard deviation for the analytes, in accordance to regulatory bodies (European Medicines Agency, 1995). A combination of low limit of detection, favourable precision and sensitivity with high recovery percentage from spiked organs, made the described method suitable to detect AmB levels in organs from *in vivo* experiments. An addition peak, eluting just before the main AmB, was also detected in this method. Puig-Sellart (2013) adapted the gradient percentage of the mobile phase from Italia *et al.*, (2009) to separate the additional peak and to obtain suitable resolution values. The resolution factor for the presented method was up to 10 times bigger than earlier studies, indicating superior AmB separation from previous eluted peaks.

Studies showed that despite AUC analysis did not detect AmB degradation, the peak height was a robust parameter to recognise drug deterioration. For instance, no new peaks related to AmB breakdown products were observed in highly degraded samples, but it was possible that degradation products co-eluted at the same time in the HPLC assay using the adopted chromatographic conditions, hence similar AUC values. This results correlated with Fittler *et al.* (2007), which demonstrated that their spectrophotometry assay did not detect

the degradation of AmB observed using bioassays. Moreover in this current study, the elution time span of previously heated AmB was slightly larger and parameters such as peak height or asymmetry values were affected. Therefore, the peak height value as well as AUC, were monitored as methods of detecting possible drug degradation. From the results obtained, it was apparent that AmB degradation occurred after 1 hour at 70°C. Consequently, it was important that AmB was only heated at 70°C for a minimal time required for NIVs production.

AmB was complexed with HPγCD before being incorporated to the melted lipidic fraction to produce AmB-NIVs. HPγCD was dissolved in water (10 % w/v) and AmB (1 mg/ml) was added followed by a pH change to 12 and to 7.6 (as described for γCD in Rajagopalan *et al.*, 1986). This methodology produced a yellow solution clear to the naked eye, in contrast to the aggregates observed with AFM imaging (He *et al.*, 2008). This correlated to studies by Jansook *et al.*, (2010) which described that cyclodextrin concentrations higher than 5 % dissolved the drug-cyclodextrin complexes in the form of aggregates. The AmB-CD aggregates imaged using AFM had a stucture that were similar to those described by Mahalingam *et al.*, (2004) for β-cyclodextrin. NIVs vesicles appeared multi-lamellar in structure since the different bilayer sheets were observed in close-up AFM images. In previous studies, the multi-lamellarity of the NIVs formulations was determined using freeze fracture electron microscopy (FFEM, Alsaadi, 2011). However, the sample preparation procedures used in FFEM, such as fracturing at -110°C, could directly affect the vesicle characteristics. Therefore, using AFM cantilever, which directly imaged liquid samples, was less likely to impact on results. The application of modern AFM PeakForce QNM microscopy tools also allowed the mechanical properties of the AFM images to be determined. The diameter of AmB-CD aggregates were below 100 nm which was in agreement with previous studies (Jansook *et al.*, 2010). The diameter of particles present in AmB-CD was 5 times higher when z-average of DLS was used instead of AFM. This was associated with a high value for the polydispersity index, which directly influenced the z-average diameter of

DLS (Baalousha and Lead, 2012). On the other hand, the ratio of z-average and the particle diameter by AFM for AmB-NIVs approached one indicating that AmB-NIVs samples were clearly monodisperse. As a conclusion, the z-average results obtained by DLS were only similar to the diameters observed under the AFM when the particles were highly monodisperse.

The homogenisation time was directly related to the vesicle size of AmB-NIVs, lengths of 5 or 30 minutes produced particle size around 800 nm or 200 nm respectively. Similar observations were reported for gemcitabine-NIVs formulations (Al-Gawhari, 2013) and others (Uchegbu and Vyas, 1998). Gemcitabine-NIVs vesicle size reduced from 450 to 200 nm from 5 to 30 minutes homogenisation (Al-Gawhari, 2013). AmB-NIVs vesicle charges were generally lower than -60 mV, which conferred colloidal stability by vesicle repulsion and, collision or flocculation avoidance. Furthermore, the vesicle size influenced vesicle charge with smaller particles having less charge than larger particles. But in all cases, the charge never exceeded the - 30 mV dividing line for stability on colloids (Duman and Tunç, 2009). Similar differences in ζ-potential were also reported for small and large gemcitabine-NIVs (Al-Gawhari, 2013). The entrapment efficiency value, i.e. the amount of drug incorporated in the vesicles, is a crucial factor in the formulation of any vesicle-like drug delivery system. In this case, the loading efficiency of AmB into the NIVs was higher than 70 % and was independent of vesicle size in the range of 200 to 800 nm. The high encapsulation efficiency values of AmB-NIVs could be related to the lipophilicity nature of the drug (Noormandi *et al.*, 2012) and the value obtained was similar to other AmB non-ionic surfactant colloids (Tan *et al.*, 2010).

The amount of drug outside the vesicles is generally removed by centrifugation, gel filtration or dialysis (Uchegbu, 1999). In some studies, gel filtration columns are used to remove un-encapsulated AmB (Van Etten *et al.*, 1995; Osaka *et al.*, 1997) but those systems are expensive if not reused, require dilution of the

formulation and are unfeasible for scale-up production (Uchegbu, 1999). Alsaadi (2011) investigated the use of ultrafiltration methods to remove un-encapsulated cisplatin from cisplatin-NIVs formulations. Using the same ultrafiltration process for AmB-NIVs resulted in vesicle swelling and had a detrimental effect upon entrapment efficiency, which contrast with results of previous researchers for other drugs (Darwis and Kellaway, 2001; Lestner *et al.*, 2010; Alsaadi, 2011). The entrapment efficiency of ultrafiltrated AmB-NIVs decreased by approximately 20 % compared to the fresh formulation. This could have been due to the hydrophobic drug being adsorbed on the membrane support as mentioned by Morand *et al.*, (2007) or related to the dilution of the formulation required prior to ultrafiltration. Therefore, the decision was made to not ultrafiltrate AmB-NIVs. Moreover, the use of encapsulated and free AmB may benefit of a biphasic distribution profile and increase samples stability (Marianecci *et al.*, 2014).

Only small batches of drug formulation were produced in initial studies as this reduced research cost and allowed changes to the formulation to be made easily. However, once AmB-NIVs formulation was optimised and validated, a larger batch production was studied to identify a large-scale manufacture method. In the presented case, AmB-NIVs was formulated without the incorporation of a solvent phase to facilitate scale-up process and the homogenisation mixture of lipids with AmB was successfully used. Homogenisation of AmB-NIVs at 70°C for 60 minutes favourably produced AmB-NIVs with high entrapment efficiency percentages. However, the terminal filtration step used in batch 1 to ensure sterility was challenging and adversely affected the drug stability. The reason for that is that the formulation was maintained at 70°C to facilitate filtration of the suspension through a 0.45 μm filter. Longer exposures of AmB to high temperature were believed to affect the stability. Therefore, the terminal filtration step was not used in the second scale-up batch so the stability of AmB was not jeopardised. Moreover, the freeze-drying process could not be carried out in a GLP laboratory, hence, when

the vial caps were removed prior freeze-drying; the formulation was exposed to external contaminants.

Freeze-drying AmB have previously demonstrated to ameliorate the drug storage stability (Rajagopalan *et al.*, 1986; Puig-Sellart, 2013). AmB-NIVs (with no cryoprotectant) were successfully freeze-dried but the vesicle size increased by up to 5 times when the formulation was rehydrated with water. Ice crystal formation during freezing could have damaged the bilayer and caused the increase in vesicle size (Stark *et al.*, 2010; Ghanbarzadeh *et al.*, 2013). Structural collapse during freezing or main drying could have also jeopardized the AmB-NIVs bilayer (Chen *et al.*, 2010; Koudelka *et al.*, 2010). The incorporation of the cryoprotectant sucrose into the formulation, successfully maintained the physicochemical characteristics of reconstituted freeze-dried AmB-NIVs. Two theories have been suggested to explain the lyoprotectant properties of saccharides such as sucrose. The water replacement theory suggested that the lyoprotectant gradually replaces the water molecules in the bilayer, this maintaining the head group spacing of the surfactant in the dry state and therefore preserving its structure when rehydrated (Crowe *et al.*, 1996). The other published theory postulated a vitrification model. The lyoprotectant become a stable glass matrix during freezing and prevents the bilayer fusion or aggregation (Koster *et al.*, 2000). Sucrose was tested as a lyoprotectant for AmB-NIVs since it has already been used in other lyophilised liposomal formulations (Abra and Szoka, 1988). In this case, 9 % w/v sucrose provided enough cryoprotectant effect to maintain the structural properties whereas higher concentrations jeopardised the structural characteristics of the freeze-dried cake. Dilution of the formulation prior to freeze-drying resulted in good reconstituted characteristics but the entrapment efficiency of the drug was compromised. This was probably due to leakage of the drug to compensate for the osmotic difference between the intra-vesicle and inter-vesicle solution. Therefore, sucrose was incorporated to the AmB-NIVs formulation at an optimised concentration of 9 % w/v or 1.5 times the lipid concentration. Scale-

up formulations of AmB-NIVs with 9 % sucrose were lyophilised in two batches. The first batch presented a series of cake abnormalities after lyophilisation, especially for vials located in the centre of the freeze dryer chamber (Gan *et al.*, 2005). This included melt-back and collapse of the cakes. DSC studies suggested that the temperature within the AmB-NIVs formulation exceeded the critical glass $T_g$' of the system during primary drying compromising the stable glass matrix (Chen *et al.*, 2010). To evade the structural abnormalities obtained in batch 1, the freeze-drying method used in batch 2 was modified and the product temperature was kept below $T_g$'. This concluded in freeze-dried cakes with good structural properties and no sign of melt-back. AmB-NIVs had a very low residual water content, in line with the regulatory authorities that suggest less than 3 % w/w water content (Mohammed *et al.*, 2007). The amount of total AmB detected on the reconstituted lyophilisate was less than the original sample in both scaled-up batches. Although this could be related to drug degradation during freeze-drying other hypothesis should be considered. For example, manual error associated to vial dosage and rehydration or sample processing (Tang and Pikal, 2004; Gan *et al.*, 2005).

The hydration of lyophilised AmB-NIVs with D-luciferin successfully produced NIVs encapsulating both components. Moreover, the AmB-NIVs properties when rehydrated with distilled water or luciferin did not vary. This suggested the possibility of using AmB-luc-NIVs formulation both as treatment and imaging probe for luciferase parasites, such as LV82-luc.

Determination of rheology characterisation of liquid pharmaceutics is important as it allows to understand formulation processes and drug delivery administration such as nebulisation (Uchegbu, 1999). AmB-NIVs formulations had a clear shear-thinning behaviour and a non-time thixotropy flow at the shearing forces applied. A power law model was fitted to the rheograms and the calculated flow index of less than 1 confirmed the pseudoplastic shear-thinning properties observed in the rheograms. For instance, shearing processes would

cause changes in the colloidal structure of AmB-NIVs but the structure would be regained when the stress is withdrawn. This is a desired property in pharmaceutical formulations as this means that a formulation would recover after being exposed to shear forces (Pestana *et al.*, 2008). Longer homogenisation processes, which were used to produce smaller sized vesicles, resulted in more viscous AmB-NIVs formulations than short homogenisation times. Therefore, the rheology behaviour of AmB-NIVs may be based on the shear history of the formulation (Gradzielski, 2011). Furthermore, the addition of sucrose as a cryoprotectant increased the apparent viscosity of AmB-NIVs (Wang and Guo, 2008). In addition, the lyophilisation process of AmB-NIVs had a detrimental effect on the apparent viscosity of AmB-NIVs since reconstituted freeze-dried vesicles had smaller viscosity profiles than their fresh precursor (Doherty *et al.*, 1994; Moreno *et al.*, 2001).

The stability of the freeze-dried AmB-NIVs formulation was tested over a period of 6 months using different storage temperatures (40°C, 4°C or -80°C) and two different scaled-up batches (batch 1 and batch 2; following ICH Harmonised Tripartite Guideline, 2003). In both stability studies the AmB-NIVs vesicles maintained the physicochemical properties i.e. vesicle size, polydispersity index and ζ-potential when AmB-NIVs samples were stored at -80°C. However, storage at the higher temperature of 40°C resulted in a significant increase in vesicle size and polydispersity index after 42 days. The vesicle size was constant for formulations stored at 4°C for up to 4 months. AmB-NIVs from batch 1 stored at 40°C showed significant cake abnormalities after 2 months of storage but this was not observed in AmB-NIVs from batch 2 stored at 40°C. This probably reflected the difference in total water content between both batches, since batch 1 contained higher amounts of residual water than batch 2. The total amount of AmB present in vials from batch 1 was stable for up to 6 months if they were stored at 4°C or -80°C. Samples stored at 40°C had significantly lower amounts of AmB present in the formulation. The entrapment efficiency was maintained constant for the 6 months stability study at 4°C or -80°C. Another

stability study was performed to investigate the integrity of reconstituted AmB-NIVs vials. Rehydrated vials maintained acceptable NIVs physical properties up to day 21 if stored at 4°C or 25°C. The entrapment efficiency values were stable during the course of the study. However, the total amount of AmB within vials was significantly lower by day 14 when stored at room temperature (25°C) but not when stored at 4°C. In conclusion, freeze-dried AmB-NIVs vials can be stored for up to 4 months at 4°C and can be used up to day 21 when reconstituted with water and kept at 4°C.

Despite the *in vitro* release profile of various formulations containing AmB has been published, in this present study this experiment was deliberately omitted. The reason for that is related to the low solubility of the drug. To solve this issue others have adapted the release medium (Zhang *et al.*, 2009; Kim *et al.*, 2010). The addition of surfactants such as sodium dodecyl sulphate (Tiyaboonchai *et al.*, 2001; Jain and Kumar, 2010) or organic solvents such as DMSO or methanol (Esposito *et al.*, 2003; Jee *et al.*, 2012) in the release medium is a common practice. However, those release mediums differ considerably from *in vivo* conditions and experimental results derived from such systems and their applicability to *in vivo* performance was highly questionable. Therefore, in this current study, pre-clinical *in vivo* studies were directly performed to assess the efficacy of AmB-NIVs.

The *in vivo* efficacy of AmB-NIVs was investigated in rodent models of visceral leishmaniasis. Studies using mice infected with LV82-luc showed that using NIVs directed more the AmB dose to the parasite locations within the liver compared to similar treatment with AmB-CD or control. High concentration doses of AmB (1 mg/kg) in AmB-CD or AmB-NIVs treatments resulted in similar reductions in parasite burdens for both formulations compared to the control. A reduced AmB dose (0.05 mg/kg), presented a significant difference between treatments. The treatment with AmB-NIVs was superior to treatment with AmB-CD and control. Moreover, there was a strong correlation between

parasite burdens and BLI at the end of the study. Although this study contains only three data points, the relation matches with De La Llave *et al.*, (2011), who demonstrated similar correlations between BLI values and parasite numbers determined by polymerase chain reaction.

Mice treated with AmB-NIVs had higher spleen weights compared to controls and this could have been related to an induced inflammatory response. Studies to determine neutrophil levels in mice using luminol-induced CLI showed that higher levels of light were emitted from mice treated intravenously with large AmB-NIVs (800 nm) but not small AmB-NIVs (200 nm). Since MPO levels are concentrated in mononuclear phagocytic systems (Deimann, 1984), the high luminol CLI could be associated to larger NIVs recruitment by those cells. Larger vesicles have previously been associated with increased rates of phagocytosis by the mononuclear phagocytic system (Abra and Szoka, 1988; Nagayasu *et al.*, 1999). Nonetheless, AmB-NIVs treatment of the same formulations by inhalation did not induce neutrophil recruitment, which could be related to the low systemic absorption following inhalation therapy.

Lower infectivity rates associated to LV82-luc parasites led to further efficacy studies with the *Leishmania* strains LV82 or 200015. AmB-NIVs formulations were administered by inhalation and their efficacy tested in a hamster model of the different parasite strains. LV82 is a laboratory strain susceptible to antimonial treatment and the clinically isolated strain 200015 is an antimony resistant strain (Carter *et al.*, 2001). The use of two different strains to corroborate the efficacy of AmB-NIVs increased the robustness of the results. The parasites were injected to the hamsters by the sublingual vein since this technique was related to less tissue destruction and fewer severity episodes than open-heart surgery (Heimann *et al.*, 2009). However, in some cases this technique resulted in higher variation in parasite burden and sometimes resulted in poor infection rates. This questioned the use of sublingual vein puncture as a reliable method for parasite infection into hamsters. Despite these

drawbacks, the parasite burden levels for LV82 and 200015 were acceptable in the described experiments. In both infections, AmB-NIVs of larger vesicle size successfully supressed the parasite burdens in spleen and liver. AmB-NIVs of small vesicle size only inhibited LV82 in the bone marrow but no effect was observed against 200015 in the spleen, liver or bone marrow. AmB-NIVs with large particle size were superior in liver parasite inhibition than smaller vesicles (Abra and Hunt, 1981; Abra *et al.*, 1984). Furthermore, in this case, larger inhaled AmB-NIVs vesicles also exhibited a superior effect in the spleen compared to smaller particles. Due to these facts, AmB-NIVs vesicles are believed to be retained by the mononuclear phagocyte system, where they might interact with the *Leishmania* parasites and exhibit their toxicity action.

In conclusion, a suitable AmB-NIVs formulation for the treatment of visceral leishmaniasis was developed:

- An HPLC-UV method was validated and used to determine AmB content in samples.

- AmB-NIVs were successfully formulated and characterised. Small and large AmB-NIVs vesicle size were synthesised.

- The addition of sucrose as lyoprotectant stabilised the vesicle size on rehydration of the freeze-dried product.

- The formulation procedure was able to undergo scale-up processes.

- Freeze-dried AmB-NIVs vials were stable up to 4 months and up to 21 days when reconstituted with water, all kept at 4°C.

- AmB-NIVs was able to supress the progress of visceral leishmaniasis when administered both by intravenous route or inhalation.

Intravenously administration of AmB-NIVs was associated to larger inflammatory response than inhaled administration and AmB-NIVs with larger vesicle size were superior on treating the infection compared to smaller sizes.

# CHAPTER 4. DEVELOPMENT OF LYOPHILISED NON-IONIC SURFACTANT VESICLES FOR DIFFERENT APPLICATIONS

## 4.1. Introduction

Nano-carriers such as NIVs, have been extensively used to enhance drug efficacy (Barratt and Bretagne, 2007; Azarmi *et al.*, 2008; Paranjpe and Müller-Goymann, 2014; Rigon *et al.*, 2015) with some of the advantages of using a vesicle-based delivery system being: increased bioavailability (Wauthoz and Amighi, 2014), elongated controlled drug release (Cook *et al.*, 2005), selective target (Hossann *et al.*, 2010) and minimal toxic side effects (Brime *et al.*, 2002). Nevertheless, a major concern when developing a vesicle drug delivery system is formulation stability, both on manufacture and on long-term storage (Rigon *et al.*, 2015). For example, during fabrication conditions, the active pharmaceutical ingredient could lose its efficacy when exposed to organic solvents, heat sonication or high temperatures (Mufamadi *et al.*, 2011). In addition, maintaining drug encapsulation is a major challenge for vesicular formulations since drug might leak from the carrier (Clerc and Barenholz, 1995; Alsaadi, 2011), the vesicles might aggregate (Verwey, 1947) or the drug - carrier might undergo decomposition (Fresta *et al.*, 1993; Wasan *et al.*, 2009; Abdelkader *et al.*, 2012). In order to improve the physicochemical stability of these systems, water is generally removed by freeze-drying. However, this process generates various stresses that may affect the integrity of the carrier membrane (Chen *et al.*, 2010). Therefore formulation and process parameters should be optimised to overcome this problem. Moreover, other stability issues can persist after freeze-drying. For example, those related with drug leakage from the delivery carrier (Alsaadi, 2011). Consequently, an ideal system to overcome these problems would be a stable generic delivery carrier system, which could encapsulate different drugs.

Kirby and Gregoriadis (1984) investigated a dehydration and rehydration vesicle (DRV) method to successfully encapsulate drugs into liposomes. That DRV method involved the removal of the solvent surrounding the empty vesicles followed by a rehydration with a drug solution to produce drug-loaded

liposomes. A variation of the DRV method was investigated in this study to formulate NIVs. Here, the aqueous solvent around empty-NIVs was removed by freeze-drying and the resulting lyophilised cake was rehydrated with the drug solution. Empty-NIVs have already demonstrated to be stable upon storage (Alsaadi *et al.*, 2013) and with the DRV encapsulation method, unstable drugs could be formulation *in situ,* as needed.

The principal goal of this study was to develop a lyophilisate NIVs platform able to encapsulate different drugs and thus could be used for different applications. Therefore the aims to cover in the study were:

- Validate the detection methods required for particle and drug analysis.

- Characterise the scaled-up production of empty-NIVs and study the formulation suitability for sterilisation by filtration.

- Identify a freezing protocol to maintain empty-NIVs characteristics upon freeze thawing and assess suitable lyoprotectants that maintain the original properties.

- Characterise the incorporation of different drugs into the NIVs using the passive DRV method.

- Investigate whether DRV active loading would improve the substrate entrapment efficiency in NIVs, in particular for luciferin.

- Assess the delivery and efficacy of luciferin loaded NIVs using BLI imaging.

## 4.2. Sample quantification of cisplatin, gemcitabine, D-luciferin or NIVs lipid components

To successfully study the development of lyophilised NIVs for different applications, it was important to determine the amount of drug present in the different samples. Therefore, published methods to quantify cisplatin, gemcitabine, D-luciferin or NIVs lipidic components were adapted as required and validated.

Cisplatin was detected using an HPLC-UV method after the compound was derivatised with sodium diethyldithiocarbamate (DDTC). Nickel chloride was spiked in all samples and used as an IS. Both nickel chloride and cisplatin complexed with DDTC were detected at 254 nm (Figure 4.1). Excess DDTC, which did not chelate with the compounds, appeared in the chromatogram at a retention time of 5 minutes. The complex between cisplatin and DDTC ($Pt(DDTC)_2$) eluted at 6 minutes, with adequate peak asymmetry values and resolution (Table 4.1). The IS complex with DDTC ($Ni(DDTC)_2$) eluted after the cisplatin peak, at 8 minutes, with asymmetry values around unity. Cisplatin standards were prepared from 0.12 to 30.00 μg/ml serial dilution with NaCl 0.9 % w/v or NaOH 0.1 M as diluents (Figure 4.2). Both calibrations curves were similar and presented a linear relationship with correlation factors higher than 0.999.

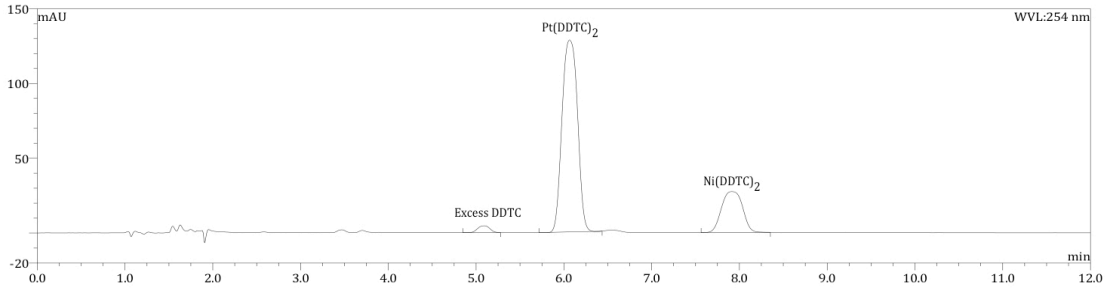


**Figure 4.1** Example of a chromatogram illustrating the separation and elution of $Pt(DDTC)_2$ at 6 minutes (30 µg/ml) and $Ni(DDTC)_2$ at 8 minutes. Excess of DDTC eluted at 5 minutes. ($Pt(DDTC)_2$, complex between cisplatin and diethyldithiocarbamate; $Ni(DDTC)_2$, complex between nickel chloride and diethyldithiocarbamate; mAU, milli absorbance unit; WVL, wavelength; min, minutes).

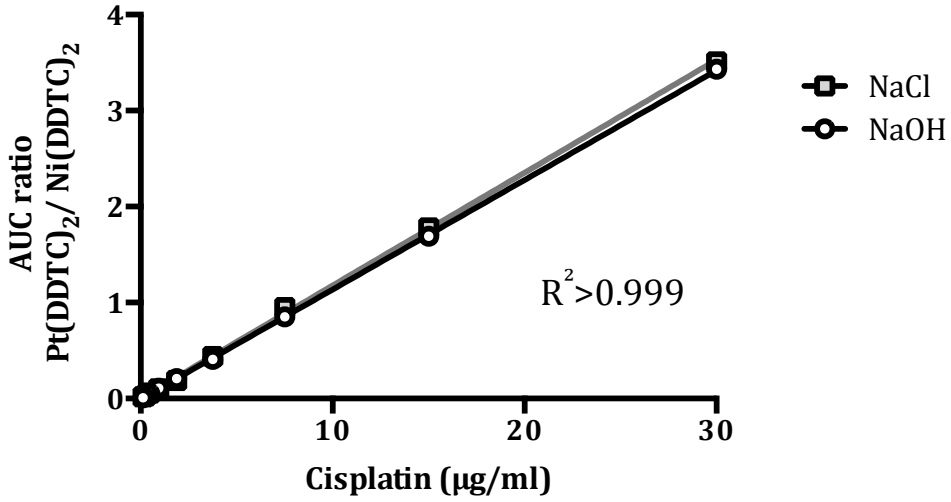


**Figure 4.2** Example of linear standard calibrations for $Pt(DDTC)_2$ and IS $Ni(DDTC)_2$ (0.12 to 30.00 µg/ml cisplatin). Serial dilutions with NaCl 0.9 % w/v or NaOH 0.1 M were analysed. Standard curves were fitted to the data using linear regression by the least mean squares method and the correlation coefficient for the fitted lines is shown (AUC, area under the curve; $Pt(DDTC)_2$, complex between cisplatin and diethyldithiocarbamate; $Ni(DDTC)_2$, complex between nickel chloride and diethyldithiocarbamate; $R^2$, correlation coefficient).

**Table 4.1** HPLC-UV peak characteristics and their relative standard deviation for cisplatin complex $Pt(DDTC)_2$ at 10 µg/ml and IS, $Ni(DDTC)_2$. Inter-day resolution values were related to the peak that eluted after (AUC, area under the curve; $Pt(DDTC)_2$, complex between cisplatin and diethyldithiocarbamate; $Ni(DDTC)_2$, complex between nickel chloride and diethyldithiocarbamate).

| Peak | Characteristics | Mean ± SD (n=6) | Relative SD (%) |
|---|---|---|---|
| **Excess DDTC** | Resolution | 3.45 ± 0.55 | 16.04 |
| **$Pt(DDTC)_2$** | Retention time (min) | 6.16 ± 0.53 | 8.53 |
| | AUC (mV x min) | 11.75 ± 1.10 | 9.35 |
| | Peak asymmetry | 1.03 ± 0.09 | 8.79 |
| | Resolution | 5.02 ± 0.58 | 11.56 |
| **$Ni(DDTC)_2$** | Retention time (min) | 7.96 ± 0.76 | 10.28 |
| | AUC (mV x min) | 7.36 ± 0.76 | 10.28 |
| | Peak asymmetry | 1.03 ± 0.12 | 11.31 |
| | AUC ratio ($Pt(DDTC)_2$/$Ni(DDTC)_2$) | 1.58 ± 0.11 | 7.08 |

The HPLC-UV method described in Al-Gawhari (2013) to detect and quantify gemcitabine was modified. Deoxycytidine was spiked in all the samples and used as IS. In this case, both gemcitabine and IS were detected at a wavelength of 269 nm (Figure 4.3). The first compound to elute was the IS at 3 minutes followed by gemcitabine at 4 minutes. Gemcitabine standards presented a linear relationship between 0.10 to 100.00 µg/ml and the correlation factor was higher than 0.999 (Figure 4.4). The resolution factor between both peaks was higher than 3 (Table 4.2).

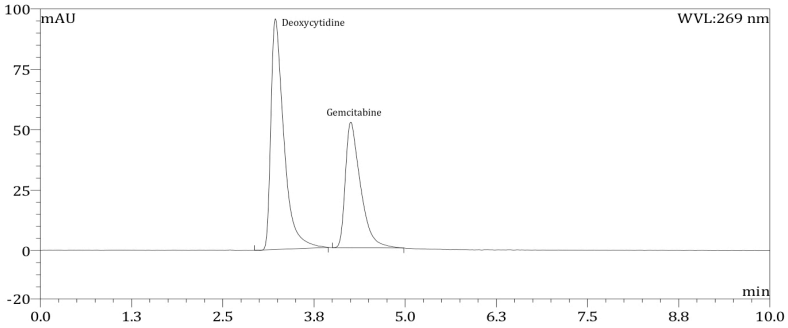


**Figure 4.3** Example of an HPLC-UV chromatogram illustrating the separation and elution of gemcitabine (25 µg/ml) at minute 4 and IS deoxycytidine at minute 3, both detected at 269 nm (mAU, milli absorbance unit; WVL, wavelength; min, minutes).

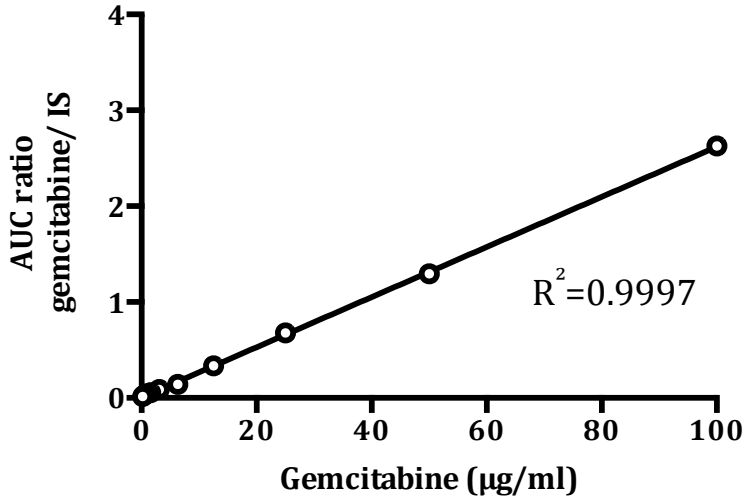


**Figure 4.4** Example of linear standard calibration curve for gemcitabine and 2'-deoxycytidine (IS; 0.2 to 100.0 µg/ml gemcitabine). Standard curve was fitted to the data using linear regression by the least mean squares method and the correlation coefficient for the fitted line is shown (AUC, area under the curve; $R^2$, correlation coefficient).

**Table 4.2** HPLC-UV peak characteristics and intra-day relative standard deviation for gemcitabine (25 µg/ml) and IS 2'-deoxycytidine. IS resolution values related to the gemcitabine peak that eluted after (AUC, Area under the curve; Gem, gemcitabine).

| Peak | Characteristics | Mean ± SD (n=6) | Relative SD (%) |
|---|---|---|---|
| Gemcitabine | Retention time (min) | 4.36 ± 0.00 | 0.10 |
| | AUC (mV x min) | 11.62 ± 2.14 | 18.38 |
| | Peak asymmetry | 1.72 ± 0.09 | 5.09 |
| IS | Retention time (min) | 3.22 ± 0.00 | 0.11 |
| | AUC (mV x min) | 17.73 ± 3.02 | 17.01 |
| | Peak asymmetry | 1.92 ± 0.08 | 3.97 |
| | Resolution | 3.10 ± 0.03 | 0.83 |
| | Peak asymmetry | 1.92 ± 0.08 | 3.97 |
| | AUC ratio (Gem/IS) | 0.65 ± 0.02 | 2.98 |

D-luciferin (Luc) samples were directly quantified using an UV detector. The maximum wavelength of absorption was found at 328 nm (Figure 4.5.A). Serial dilutions of luciferin in PBS pH 7.4 presented linearity between the range of 3 and 100 µg/ml (Figure 4.5.B). The correlation factor fitted to the standard curve was higher than 0.99.

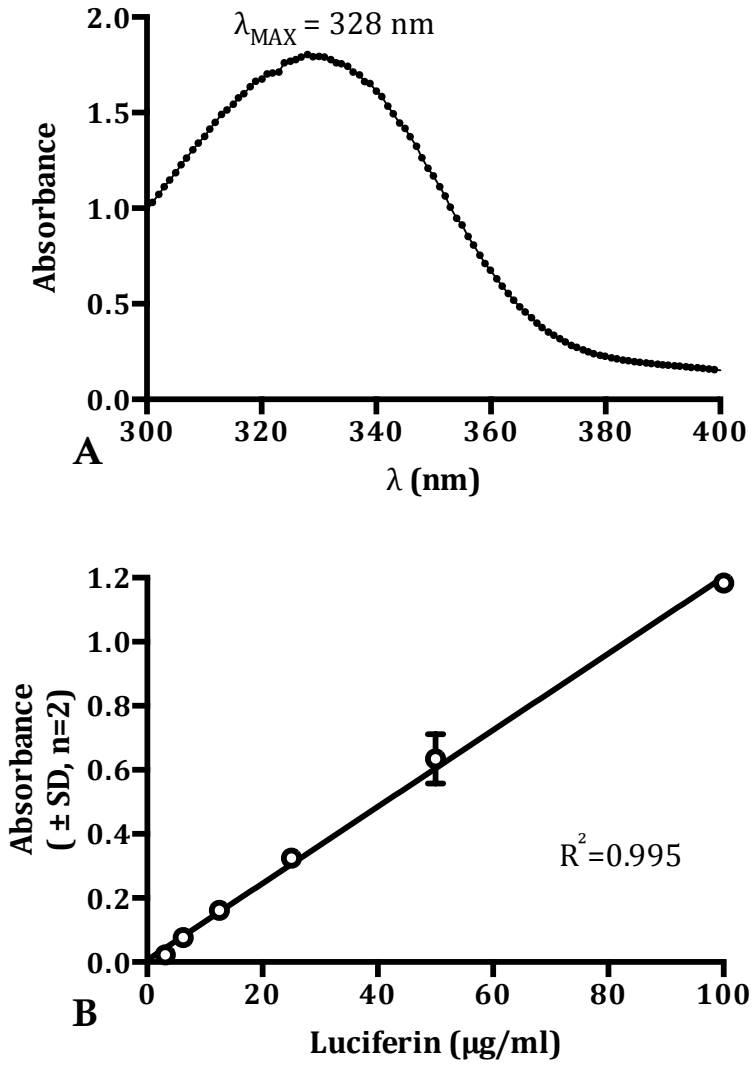


**Figure 4.5** Absorbance spectra associated to D-luciferin with maximum wavelength absorption of λ=328 nm (A). Example of linear standard calibration curve for luciferin (3.13 to 100.00 µg/ml luciferin). Points fitted with a regression line by the least mean squares method and correlation coefficient was represented by $R^2$ (B).

The three lipidic components in empty-NIVs: tetra-ethylene glycol mono hexadecyl ether (surfactant), cholesterol and dicetyl phosphate (DCP) were analysed with an HPLC attached to an ELSD detector. This method was identified by Alsaadi *et al.* (2013) and validated by Puig-Sellart (2013). The IS, prednisolone, was spiked to all samples prior to analysis. Four peaks were detected in the chromatogram, which corresponded to the elution of cholesterol at 2 minutes, surfactant at 5 minutes, IS at 8 minutes and dicetyl phosphate at 12 minutes (Figure 4.6). Each component's AUC value was reported against the area of the IS. The ratio between both areas displayed a linear relationship between 25 to 250 µg/ml for cholesterol and surfactant and from 25 to 150 µg/ml for DCP. All correlation factors were greater than 0.9 (Figure 4.7).

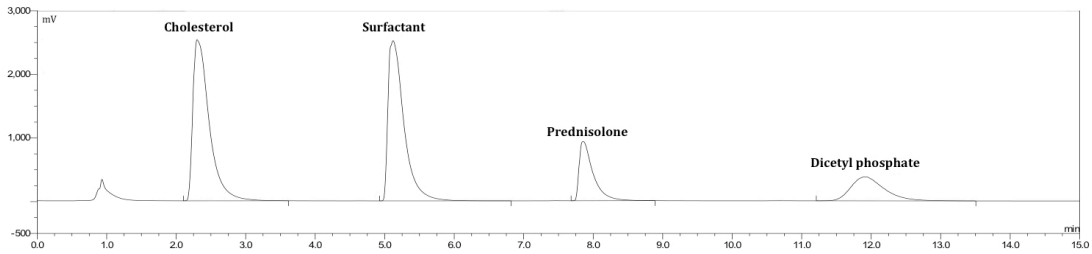


**Figure 4.6** HPLC-ELSD chromatogram illustrating the separation and elution of cholesterol, surfactant, prednisolone (IS) and dicetyl phosphate at 2.3, 5.1, 7.9 and 11.7 minutes respectively. Each lipid was analysed at a concentration of 200 µg/ml (mV, millivolts; min, minutes).

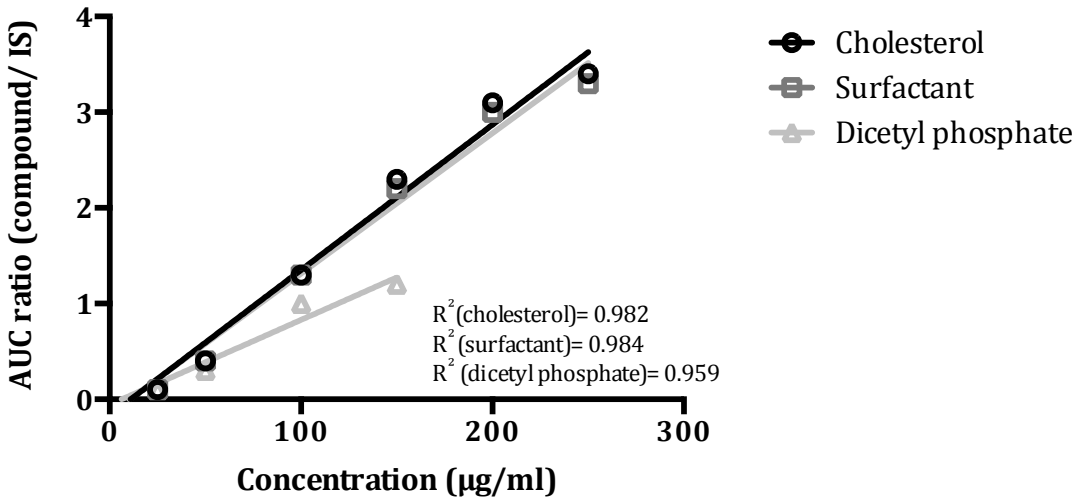


**Figure 4.7** Example of linear standard calibration curves for cholesterol, surfactant and dicetyl phosphate related to the IS prednisolone (25 to 250 µg/ml cholesterol and surfactant, 25 to 150 µg/ml dicetyl phosphate). Standard curves were fitted to the data using linear regression by the least mean squares method and the correlation coefficient for the fitted lines is shown (AUC, area under the curve; $R^2$, correlation coefficient)

.

### 4.3. Empty-NIVs characteristics and scaled-up production

Empty-NIVs were prepared by melting the lipidic components followed by hot water hydration and homogenisation. Empty-NIVs formulated at a laboratory scale (10 ml, 150 mM lipids) had a vesicle size smaller than 200 nm (Table 4.3). The samples were white in colour, opaque and extremely viscous (Figure 4.8.A and Table 4.4). When empty-NIVs were lyophilised and rehydrated with distilled water, the particle size enlarged significantly ($p \leq 0.001$) and the vesicle charge decreased ($p \leq 0.01$; Table 4.3). Freshly prepared empty-NIVs behaved as a shear-thinning fluid (Table 4.4, Figure 4.8.A). Furthermore, the power law model, fitted to the rheograms, had an excellent correlation and the flow index values were smaller than the unit corroborating the shear-thinning property. In addition, empty-NIVs had no-time dependent thixotropy demonstrated by the area of the hysteresis loop, and indistinguishable up and down curves in the rheograms. In the case of the freeze-dried and rehydrated empty-NIVs, a smaller consistency index than the original formulation was found ($p \leq 0.001$) but the formulation maintained similar apparent viscosity (Table 4.4; Figure 4.8.B).

The feasibility of scale-up the production of empty-NIVs was carried out at Aptuit (Glasgow, UK) in collaboration with Inhalosome C Ltd (Leeds, UK). Three scale-up batches of 250 ml empty-NIVs were produced using the previously described method supplemented with a high-pressure homogenisation (HPH) step. The HPH procedure was incorporated to reduce the vesicle size so that the there could be a terminal sterile filtration step (0.22 μm). The first scale-up batch of empty-NIVs was prepared at 150 mM lipidic concentration. On the first pass through the HPH, an air block was formed and some sample was lost. The HPLC-ELSD analysis confirmed that the remaining sample contained the following percentages of the starting material after the incident: 54.0 % cholesterol, 54.3 % surfactant and 58.3 % DCP. To regain the original sample volume, the remaining suspension was made back up to 250 ml with distilled

water. After 85 passes through the HPH the vesicles within the empty-NIVs suspension had a minimum mean intensity diameter of 400 nm (determined with DLC Nanotrac), which was not suitable for sterile filtration. On the other hand, empty-NIVs batch 2 was prepared as batch 1 (150 mM lipid) but the hot lipid mixture was immediately transferred, after homogenisation, to the HPH to mitigate the blockage problems. After 140 passes through the HPH device, a maximum reduction in size of 870 nm was achieved. Additional distilled water (50 ml) was incorporated to the formulation in order to dilute the suspension. This followed by 80 more passes through the HPH so as to produce NIVs particles of 220 nm. The vesicles within the empty-NIVs suspension easily passed through a 0.22 μm syringe filter. The scaled-up batch 3 was produced at a lipid concentration of 124 mM and passed through the HPH 120 times. The mean intensity diameter obtained was 440 nm and only further dilution of the formulation to 107 mM and extra 140 HPH passes achieved particle size of 200 nm. The final empty-NIVs formulation was assessed for suitability of sterile filtration using a 0.22 μm syringe filter and it was found to pass with ease. Empty-NIVs total lipid concentrations were assessed after going through the HPH to determine whether any loss occurred during the process. None of the components decreased in concentration more than 20 % when empty-NIVs passed through the HPH 30, 70 or 140 times (Table 4.5). Filter sterilised empty-NIVs were tested to determine whether any lipid component was adsorbed through the 0.22 μm membrane. There was some loss of the vesicle components after filtration, but they were low (95.11 % cholesterol, 94.49 % surfactant and 96.75 % dicetyl phosphate; concentration post-filtration compared to pre-filtration). This indicated that sterile filtration was a successful sterilisation method for scaled-up empty-NIVs produced through HPH.

Laboratory scale empty-NIVs were compared to the scaled-up formulations in terms of physical properties (Table 4.3). Scale-up formulations had a smaller vesicle size than the laboratory scale formulations ($p \leq 0.001$; Table 4.3). However, the polydispersity index and ζ-potential were similar in both types of

formulations. Laboratory scale and scaled-up empty-NIVs formulations were lyophilised and rehydrated with water prior to analysis. In both cases, vesicle size significantly increased after rehydration of the lyophilisate ($p \leq 0.001$; Table 4.3). In addition, the polydispersity of the vesicles enlarged ($p \leq 0.05$) and the vesicle charge decreased ($p \leq 0.01$; except for batch 3). In terms of rheology behaviour, the flow index values for scaled-up formulations were smaller than the unit, which was similar to the shear-thinning property of laboratory scale production (Figure 4.8.C). Furthermore, the hydration of scaled-up lyophilisates resulted in a suspension with higher apparent viscosity and consistency index than its fresh predecessor ($p \leq 0.001$; Table 4.4).

**Table 4.3** Physical properties of freshly formulated and rehydrated freeze-dried empty-NIVs produced in a laboratory scale batch (10 ml) compared to three scaled-up batches (250 ml). Empty-NIVs laboratory scale, were produced at 150 mM lipid concentration. Scaled-up empty-NIVs batch 1 were formulated at 124 mM, batch 2 at 134 mM and batch 3 at 107 mM (Section 2.4). Physical properties were analysed with the DLS Zetasizer Nano. Crosses signify significant difference between laboratory and scaled-up formulations ($^{+}$ $p \leq 0.05$, $^{++}$ $p \leq 0.01$ and $^{+++}$ $p \leq 0.001$). Stars indicate significant difference between fresh and rehydrated freeze-dried properties (* $p \leq 0.05$, ** $p \leq 0.01$ and *** $p \leq 0.001$).

| Physical properties (mean ± SD; n=3) | | Empty-NIVs laboratory scale | Empty-NIVs scaled-up | | |
|---|---|---|---|---|---|
| | | | Batch 1 | Batch 2 | Batch 3 |
| Fresh formulation | Z-average (nm) | 190.50 ± 2.09 | 116.70 ± 0.78 $^{+++}$ | 153.17 ± 1.68 $^{+++}$ | 108.97 ± 0.76 $^{+++}$ |
| | Pdi | 0.36 ± 0.05 | 0.28 ± 0.01 | 0.36 ± 0.05 | 0.27 ± 0.02 |
| | ζ-potential (mV) | -56.80 ± 4.35 | -58.67 ± 2.49 | -56.73 ± 1.72 | -57.77 ± 1.80 |
| Rehydrated lyophilisate | Z-average (nm) | 820.73 ± 39.11 $^{***}$ | 680.93 ± 0.55 $^{***}$ | 876.60 ± 0.58 $^{***}$ | >1000 $^{***}$ |
| | Pdi | 0.50 ±0.05 $^{*}$ | 0.55 ± 0.07 $^{**}$ | 0.58 ± 0.08 $^{*}$ | 1.00 $^{***}$ |
| | ζ-potential (mV) | -44.83 ± 0.12 $^{**}$ | -43.47 ± 2.07 $^{**}$ | -43.47 ± 2.07 $^{**}$ | -59.25 ± 1.91 |

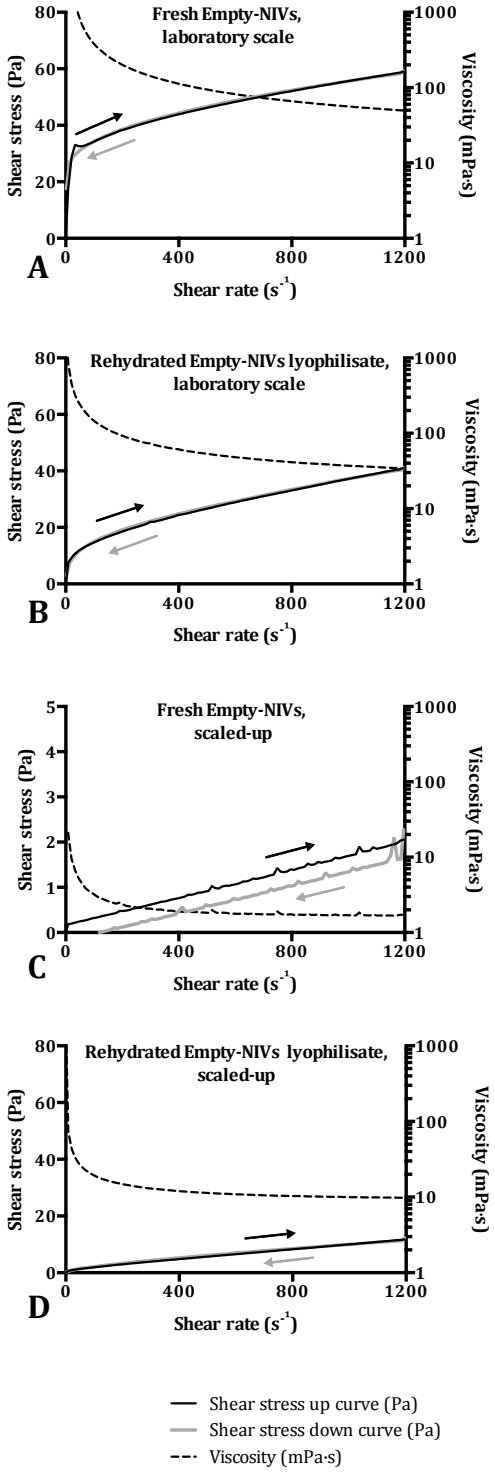


**Figure 4.8** Examples of flow rheograms for laboratory scale empty-NIVs freshly prepared with 150 mM lipid (A) and rehydrated lyophilisate (B). Rheograms for scaled-up empty-NIVs (only for batch 3 with 107 mM lipid) freshly prepared (C) and rehydrated lyophilisate (D). Formulation properties are described in Table 4.3 and Table 4.4. Shear rate varied from 0 to 1200 1/s and the shear stress curve was plotted, up (continuous black line) and down (continuous grey line). Viscosity values were plotted against shear with a black discontinuous line .

**Table 4.4** Rheological flow properties of fresh and freeze-dried empty-NIVs formulated in a laboratory scale compared to three scaled-up batches. Empty-NIVs laboratory scale produced at 150 mM lipid concentration. Scaled-up empty-NIVs batch 1 formulated at 124 mM, batch 2 at 134 mM and batch 3 at 107 mM (Section 2.4). Crosses signify significant difference between laboratory and scaled-ups formulations ($^{+}$ $p \leq 0.05$, $^{++}$ $p \leq 0.01$ and $^{+++}$ $p \leq 0.001$). Stars signify significant difference between fresh and freeze-dried properties (* $p \leq 0.05$, ** $p \leq 0.01$ and *** $p \leq 0.001$).

| | Rheological properties (mean ± SD; n=3) | Empty-NIVs laboratory scale | Scaled-up empty-NIVs | | |
|---|---|---|---|---|---|
| | | | Batch 1 | Batch 2 | Batch 3 |
| Fresh formulation | Viscosity (mPa·s) | 54.18 ± 3.81 | 2.19 ± 0.20 $^{+++}$ | 1.96 ± 0.07 $^{+++}$ | 1.73 ± 0.04 $^{+++}$ |
| | Flow index | 0.17 ± 0.05 | 0.85 ± 0.01 $^{+++}$ | 0.86 ± 0.00 $^{+++}$ | 0.85 ± 0.01 $^{+++}$ |
| | Consistency index (mPa·s) | 14,570.00 ± 1,442.50 | 6.23 ± 0.05 $^{+++}$ | 5.18 ± 0.21 $^{+++}$ | 4.91 ± 0.19 $^{+++}$ |
| | Hysteresis (Pa/s) | 364.24 ± 42.89 | 447.87 ± 12.75 | 386.27 ± 5.95 | 420.83 ± 13.45 |
| | $R^2$ | 0.97 ± 0.01 | 1.00 ± 0.00 | 1.00 ± 0.00 | 0.99 ± 0.00 |
| Rehydrated lyophilisate | Viscosity (mPa·s) | 42.85 ± 11.49 | 3.32 ± 0.08 *** | 8.45 ± 0.19 *** | 9.58 ± 0.25 *** |
| | Flow index | 0.44 ± 0.02 ** | 0.80 ± 0.00 ** | 0.79 ± 0.01 ** | 0.77 ± 0.02 ** |
| | Consistency index (mPa·s) | 2,141.00 ± 262.39 *** | 13.12 ± 0.12 *** | 35.41 ± 2.05 *** | 46.11 ± 6.13 *** |
| | Hysteresis (Pa/s) | -186.90 ± 121.34 | 549.33 ± 7.26 *** | 52.05 ± 73.61 ** | -22.95 ± 51.69 *** |
| | $R^2$ | 1.00 ± 0.00 | 1.00 ± 0.00 | 1.00 ± 0.00 | 1.00 ± 0.00 |

**Table 4.5** Lipid mixture composition of empty-NIVs scaled-up batch after homogenisation in a high-pressure homogeniser (HPH). Samples at point 0 were obtained after normal homogenisation at 11,000 rpm for 20 min. Then empty-NIVs were passed through a HPH 30, 70 and 140 times. The concentration of each lipidic component (cholesterol, surfactant and dicetyl phosphate) was represented as a relation with each theoretical concentration.

| Passes through high-pressure homogeniser | Compound concentration (% of theoretical; n=1) | | |
|---|---|---|---|
| | Cholesterol | Surfactant | Dicetyl phosphate |
| **0** | 89.4 | 89.7 | 89.2 |
| **30** | 89.3 | 89.3 | 89.9 |
| **70** | 82.5 | 82.0 | 82.9 |
| **140** | 83.5 | 83.1 | 83.9 |

## 4.4. Lyophilisation optimisation of empty-NIVs

The lyophilisation and subsequent rehydration of empty-NIVs (without lyoprotectant) resulted in the production of NIVs with a mean vesicle size that was much larger than that of the original formulation (Table 4.3). Therefore the effect of incorporating different lyoprotectants and different freeze-drying conditions was studied. Firstly, empty-NIVs were prepared with and without different cryoprotectants and their fresh properties were described in Table 4.6. The physical characteristics of NIVs containing glucose were similar to empty-NIVs without the additive. In contrast, NIVs containing sucrose were more polydisperse than empty-NIVs without the lyoprotectant ($p \leq 0.01$). NIVs with trehalose were slightly larger ($p \leq 0.05$), with a higher polydispersity index and lower vesicle charge ($p \leq 0.01$; Table 4.6). The physical properties of NIVs containing different types of HP-CDs (HPαCD, HPβCD or HPγCD) were similar to empty-NIVs without the additives. Only HPβCD-NIVs were less charged than empty-NIVs without HP-CDs ($p \leq 0.01$). The data in Table 4.6 demonstrated that empty-NIVs formulated with most of the lyoprotectants tested maintained the physical characteristics of original empty-NIVs formulations.

The freezing step in lyophilisation is critical in the whole freeze-drying procedure. In this study, empty-NIVs were formulated with different cryoprotectants (glucose, sucrose and trehalose) and their characteristics (i.e. vesicle size, polydispersity and ζ-potential) determined before and after being frozen using different freezing methods (Figure 4.9). The different freezing methods included freezing at -18°C and -80°C, freezing at different rates (flash cooling with liquid nitrogen and slow at 0.6°C/min) or annealing at -18°C (before dropping the temperature with liquid nitrogen or with a -80°C freezer). Empty-NIVs without cryoprotectant were highly susceptible to disruption when freeze thawed. Freezing at -18°C or -80°C produced an increase in particle size of 6.2 fold compared to the fresh formulation ($p \leq 0.001$; Figure 4.9). Fast freezing with liquid nitrogen caused the least disruption, even though vesicles

doubled in size compared to the original formulation. Slow freezing did not present any advantage as particles enlarged 5.7 times their original size ($p \leq 0.001$). Annealing at -18°C before storage at -80°C increased particle size by 5.6 times ($p \leq 0.001$). Annealing at -18°C followed by a fast freezing of empty-NIVs with liquid nitrogen resulted in an increase of particle size of 2.2 fold compared to the original formulation ($p \leq 0.01$). The majority of freezing methods used for empty-NIVs without a cryoprotectant, resulted in larger particles and a significantly higher polydispersity index ($p \leq 0.01$). Vesicle charge was generally not affected by the different freezing techniques. Only freezing at -80°C caused a significant decrease in ζ-potential for empty-NIVs without cryoprotectant, compared to the fresh sample ($p \leq 0.01$).

NIVs containing glucose as an additive maintained their particle size when frozen at -80°C or using liquid nitrogen. The ratio between the freeze-thawed size and original size was 1.1 in both cases. Freezing glucose-NIVs at -18°C significantly enlarged the vesicle size 4.7 times ($p \leq 0.001$, Figure 4.9). Annealing at -18°C followed by freezing at -80°C or followed with liquid nitrogen immersion also affected the z-average resulting in a significant vesicle size increase ($p \leq 0.001$). Slow freezing glucose-NIVs at 0.6°C/min was not advantageous since it increased the particle size (1.9 times, $p \leq 0.001$). Including glucose in the empty-NIVs formulation prevented an increase in polydispersity, however the vesicle charge decreased when freezing with all the studied methods ($p \leq 0.01$), apart from freezing at -80°C.

NIVs prepared with sucrose as cryoprotectant had a stable vesicle size when frozen at -80°C or in liquid nitrogen. The ratio of vesicle size between fresh and thawed formulation was 1.2 and 1.1 respectively. The annealing approach was not advantageous since the particles were enlarged by up to 3.7 size fold ($p \leq 0.001$, Figure 4.9). Slow freezing rates of 0.6°C/min also resulted in larger vesicles, which were 1.9 fold larger than those in the original suspension ($p \leq 0.001$). The polydispersity index of the vesicles containing sucrose was not

affected by any of the freezing protocols but all the different approaches significantly affected the surface charge of the vesicles ($p \leq 0.01$; except using a slow freezing rate of 0.6˚C/min).

NIVs containing trehalose as a cryoprotectant were highly affected by freezing procedures. Freezing at -18°C and -80°C increased the vesicle size 5.5 and 2.2 times the original size ($p \leq 0.001$ and $p \leq 0.01$ respectively, Figure 4.9). Using fast freezing with liquid nitrogen was the only technique that did not increase the particle size significantly (ratio freeze thawed *versus* initial size of 1.5). The annealing approach increased the size of the particles up to 4.6 times their initial value ($p \leq 0.001$). Freezing at a slow rate enlarged the particles 3.3 times when thawed ($p \leq 0.001$). The polydispersity index of trehalose-NIVs, was only affected when samples where fast frozen in liquid nitrogen after an annealing step ($p \leq 0.05$). The ζ-potential was significantly reduced with all the approaches ($p \leq 0.05$; Figure 4.9) but did not vary when samples with trehalose were frozen at -18°C and with liquid nitrogen.

Overall, these studies showed that the freezing procedure of NIVs significantly affected the particle size characteristics. Freezing at -80°C or with liquid nitrogen were the best approaches to freeze NIVs with a cryoprotectant. Both glucose and sucrose were the best cryoprotectant for NIVs as they prevented changes in the surface size of NIVs after freeze thawing.

**Table 4.6** Physical characteristics of freshly formulated empty-NIVs and NIVs with glucose, sucrose, trehalose, HPαCD, HPβCD and HPγCD additives. Glucose, sucrose and trehalose contained 0.17 g/ml additive or 2.7 time lipid concentration and HPαCD, HPβCD and HPγCD incorporated 0.34 g/ml of additive or 6 times lipid concentration (HPαCD, hydroxypropyl-α-cyclodextrin; HPβCD, hydroxypropyl-β-cyclodextrin; HPγCD, hydroxypropyl-γ-cyclodextrin; * $p \leq 0.05$, ** $p \leq 0.01$ compared to empty-NIVs, n=3).

| Fresh formulations | Z-average (nm ± SD) | Polydispersity index (± SD) | ζ-potential (mV ± SD) |
|---|---|---|---|
| **Empty-NIVs** | 221.25 ± 15.49 | 0.35 ± 0.09 | -49.10 ± 0.72 |
| **Glucose-NIVs** | 227.01 ± 9.30 | 0.49 ± 0.03 | -50.60 ± 0.31 |
| **Sucrose-NIVs** | 227.42 ± 10.89 | 0.54 ± 0.02 ** | -53.38 ± 1.59 |
| **Trehalose-NIVs** | 257.30 ± 13.36 * | 0.57 ± 0.06 ** | -43.01 ± 0.80 ** |
| **HPαCD-NIVs** | 205.94 ± 1.10 | 0.28 ± 0.02 | -52.54 ± 1.15 |
| **HPβCD-NIVs** | 247.33 ± 4.42 | 0.27 ± 0.00 | -41.8 3± 1.51 ** |
| **HPγCD-NIVs** | 185.95 ± 1.04 | 0.23 ± 0.01 | -53.14 ± 0.23 |

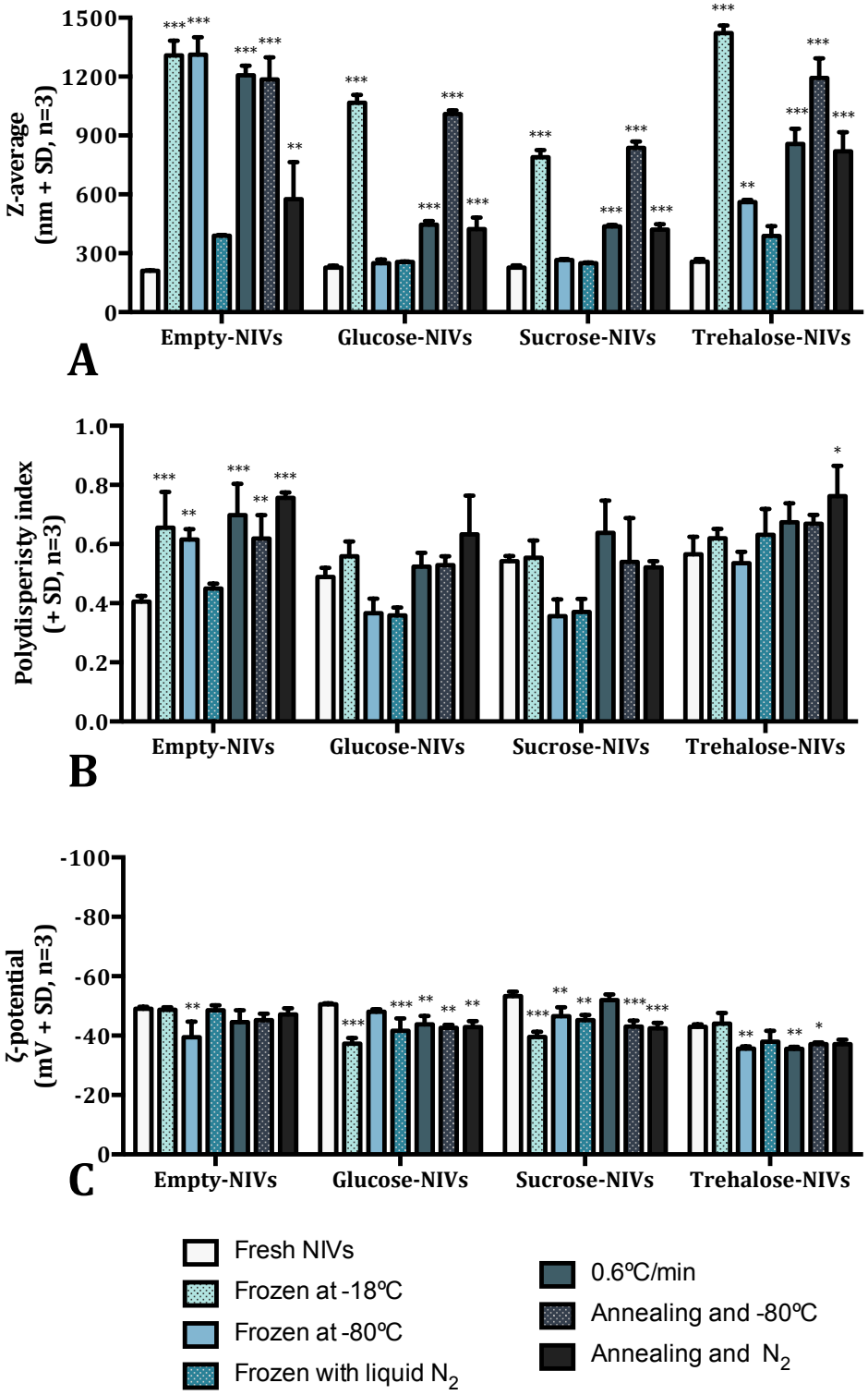


**Figure 4.9** The effect of incorporating different cryoprotectants on the physical characteristics of empty-NIVs after freeze-thawing. Empty-NIVs were prepared with and without glucose, sucrose or trehalose (0.17 g/ml cryoprotectant or 2.7 times lipid concentration). Vesicles were frozen at -18°C, -80°C, fast frozen with liquid nitrogen, slowly freezing at 0.6°C/min or annealed at -18°C. Vesicle size (A), polydispersity index (B) and ζ-potential (C) of the freeze-thawed formulations were compared to the fresh sample (* $p \leq 0.05$, ** $p \leq 0.01$ and *** $p \leq 0.001$).

Ideally a lyoprotectant should prevent the structure of NIVs vesicles to collapse during freeze-drying. To do so, the amorphous lyoprotectant should be kept in a glass state during main freezing (product temperature < $T_g'$). If the lyoprotectant is at a more molten or rubber-like state (> $T_g'$) the freeze-drying cake structure could collapse and this could result in vesicle damage. To determine the suitable protocol for lyophilisation, all the phase transitions temperatures between -65°C to 25°C for the NIVs formulations and lyoprotectants were recorded. Examples of the thermograms obtained in each sample are shown in Figure 4.10. Three replicates were used to determine the mean $T_g'$ and Tm (Table 4.7). Studies of the lyoprotectant solutions indicated that HPα/β/γCD $T_g'$ were significantly higher than the sucrose one ($p \leq 0.001$; Table 4.7). Empty-NIVs without a lyoprotectant did not displayed a $T_g'$. However, inclusion of sucrose or HPγCD into the empty-NIVs formulations incorporated a $T_g'$ for the NIVs, with HPγCD giving the highest value ($p \leq 0.001$; Table 4.7). Empty-NIVs without and with lyoprotectants were frozen at -80°C and then lyophilisated. Freeze-drying of empty-NIVs without lyoprotectant significantly affected the vesicle characteristics on rehydrating with distilled water (Table 4.3, Figure 4.11). Those vesicles were larger, presented higher polydispersity and decreased in ζ-potential ($p \leq 0.001$; Figure 4.11). All indicating that lyophilisation produced a vesicle formulation that was not uniform. Incorporating sucrose into the empty-NIVs resulted in a dose-dependent decrease in particle size of empty-NIVs when freeze-dried (Figure 4.11). However, even vesicles formulated with the higher sucrose concentration (0.50 g/ml) were still significantly larger than those of the original suspension ($p \leq 0.001$; Figure 4.11). The presence of sucrose did not prevent the significant increase in polydispersity index or the decrease in ζ-potential observed after rehydration with water ($p \leq 0.001$). Freeze-dried empty-NIVs without a lyoprotectant had 1.6 ± 0.8 % final gravimetric water content whereas empty-NIVs with sucrose had no gravimetrically detectable water content. In conclusion, the incapacity of sucrose to prevent the damage of NIVs vesicles upon freeze-drying led to the investigation of other additives such as HP-CDs.

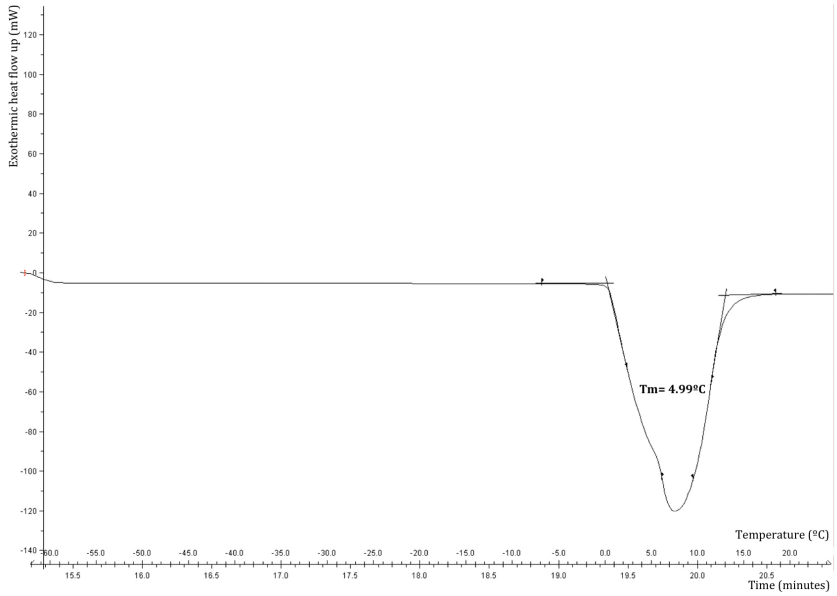


**A –** Empty-NIVs

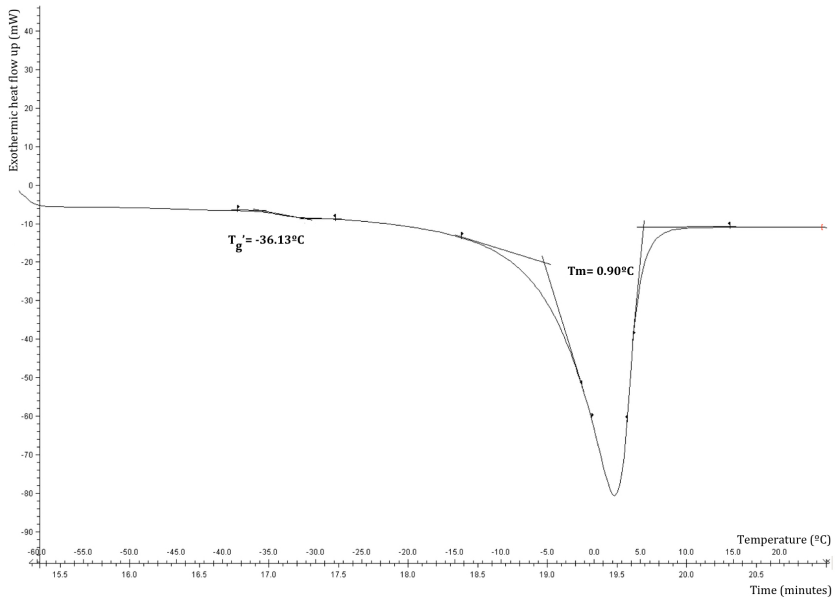


**B –** Sucrose-NIVs

**Figure 4.10** Examples of differential scanning calorimetry thermograms of empty-NIVs (A, 75 mM lipids; 9.41 mg), sucrose-NIVs (B, 0.50 g/ml sucrose, 75 mM lipids; 11.84 mg). Figure continues on the next pages.

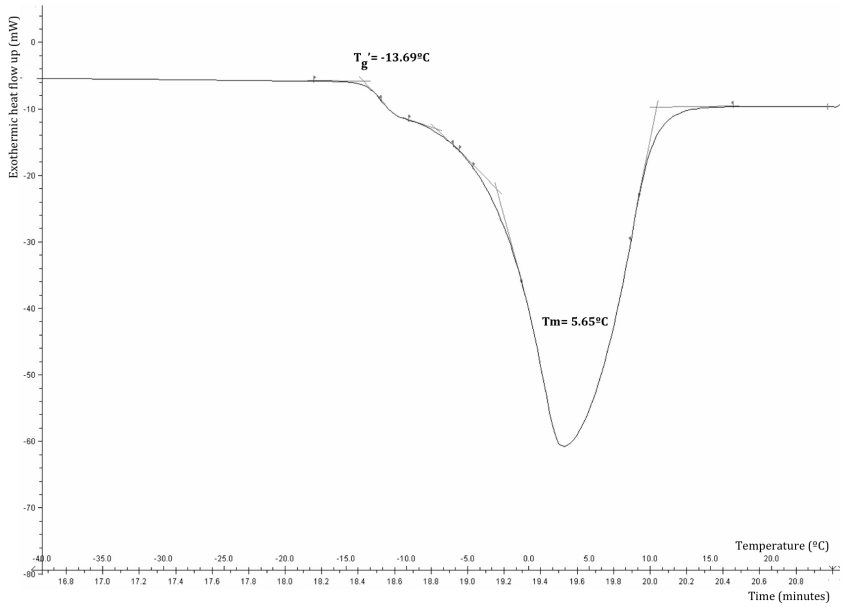


**C –** HPαCD

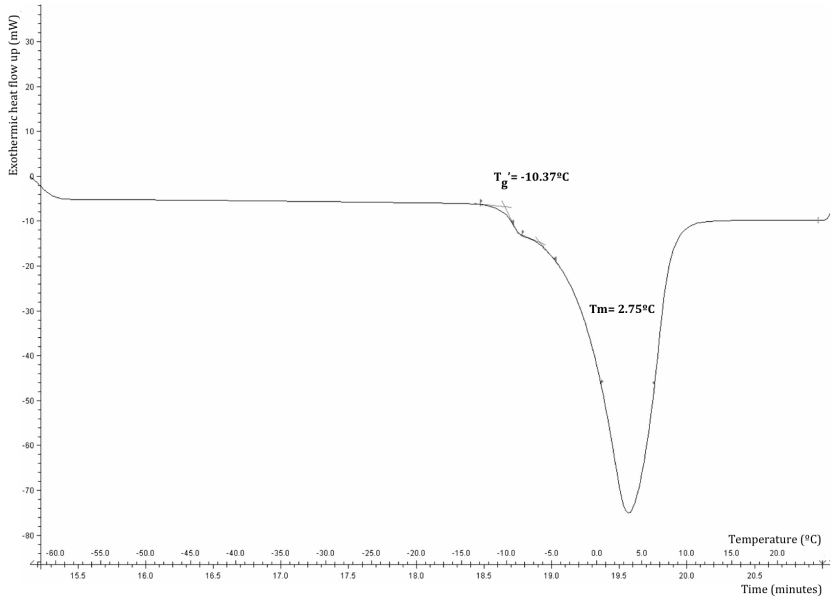


**D –** HPβCD

**Figure 4.10 (continuation)** Examples of differential scanning calorimetry thermograms of HPαCD solution (C, 0.50 g/ml; 10.49 mg) and HPβCD solution (D, 0.50 g/ml; 10.09 mg). Figure continues on the next page.

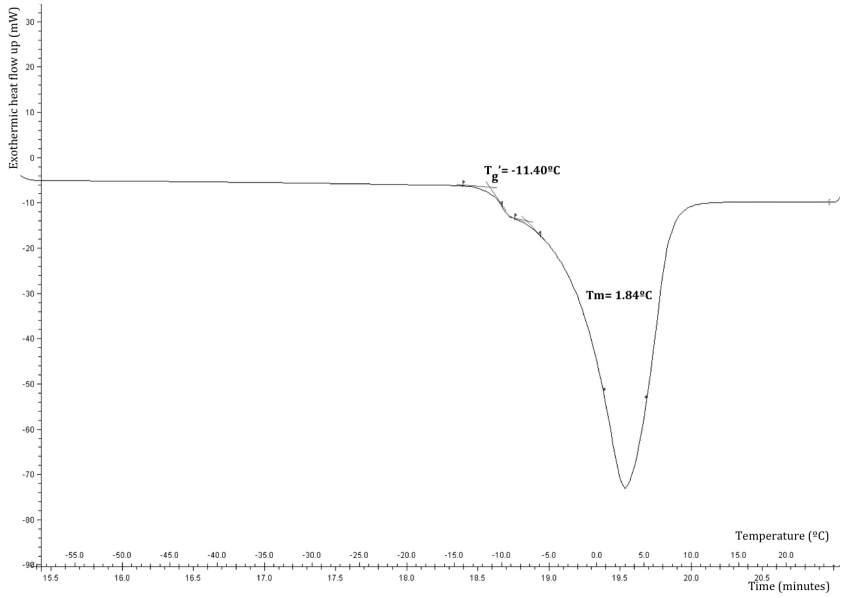


**G –** HPγCD

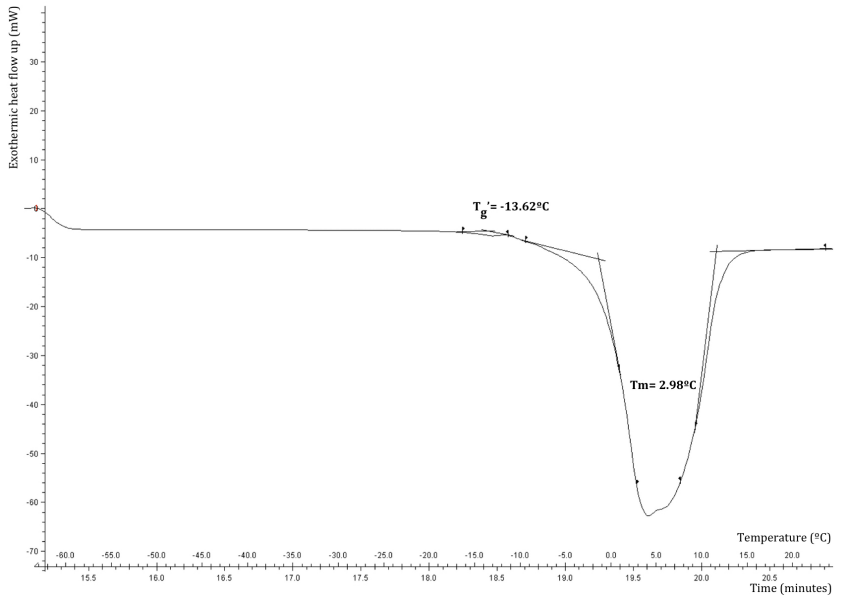


**H –** HPγCD-NIVs

**Figure 4.10 (continuation)** Examples of differential scanning calorimetry thermograms of HPγCD solution (G, 0.50 g/ml; 10.46 mg), HPγCD-NIVs (H, 0.38 g/ml HPγCD, 75 mM lipids; 8.56 mg).

**Table 4.7** Calorimetric values for different samples analysed. Glass transition temperature ($T_g'$) and melting temperature (Tm) of distilled water, empty-NIVs (150 mM), sucrose solution (0.50 g/ml), sucrose-NIVs (0.50 g/ml sucrose, 75 mM lipids), HPαCD solution (0.38 g/ml), HPβCD solution (0.38 g/ml), HPγCD solution (0.38 g/ml) and HPγCD–NIVs (0.38 g/ml HPγCD, 75 mM lipids). N.p. indicated thermal not present in the thermograms.

| Sample | Glass phase transition ($T_g'$; ˚C ± SD; n=3) | Melting temperature (Tm; ˚C ± SD; n=3) |
|---|---|---|
| Distilled water | n.p. | 3.96 ± 1.40 |
| Empty-NIVs | n.p. | 5.04 ± 0.29 |
| Sucrose solution | -33.05 ± 0.48 | -0.92 ± 0.12 |
| Sucrose-NIVs | -36.28 ± 0.23 | 0.69 ± 0.21 |
| HPαCD | -13.70 ± 0.19 | 3.85 ± 1.56 |
| HPβCD | -10.51 ± 0.13 | 2.34 ± 0.47 |
| HPγCD | -11.55 ± 0.14 | 1.94 ± 0.08 |
| HPγCD-NIVs | -14.34 ± 1.01 | 3.08 ± 0.14 |

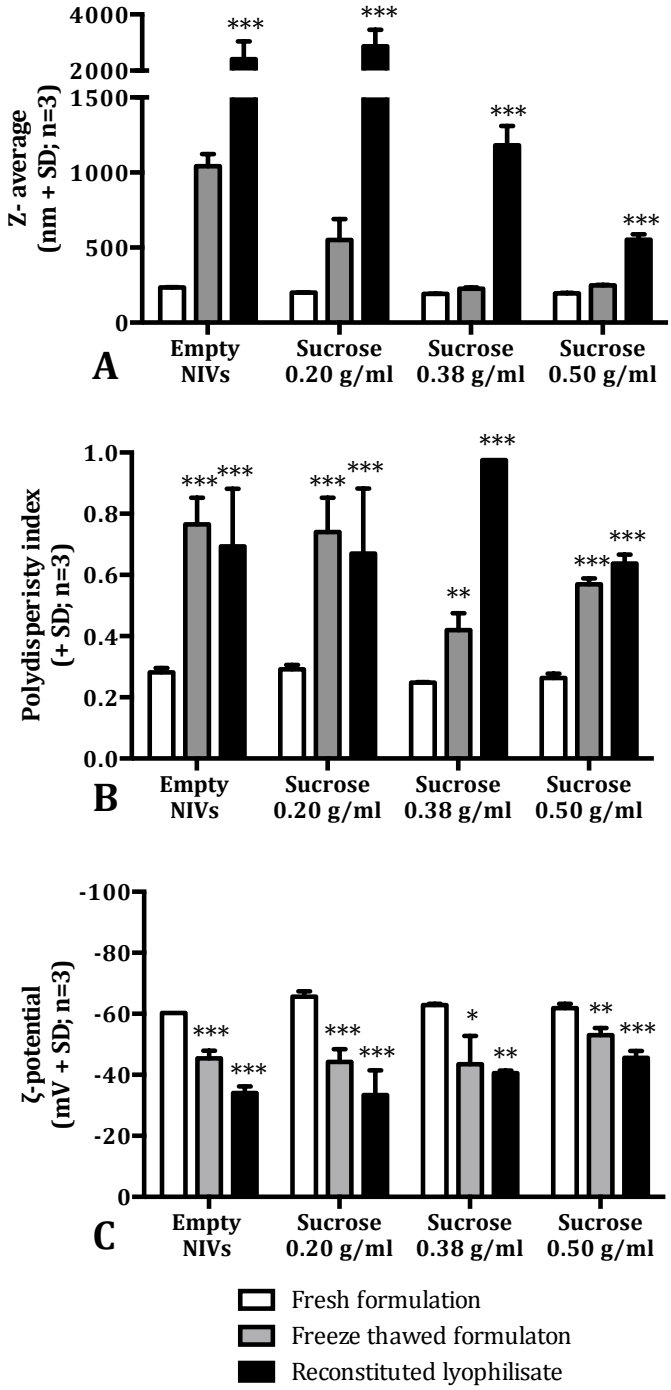


**Figure 4.11** Cryoprotectant and lyoprotectant effect of sucrose on empty-NIVs. NIVs were formulated without (empty-NIVs) and with sucrose (0.20, 0.38 and 0.50 g/ml equivalent to 3.1, 6.0 and 8.0 times the lipidic concentration of NIVs). Samples were frozen at -80°C overnight and then thawed or freeze-dried. Frozen samples were thawed at room temperature and freeze-dried samples were reconstituted with distilled water prior analysis of vesicle size (A), polydispersity index (B) and vesicle charge (C). Comparisons with the original fresh formulations were statistically different when marked with a star (* $p \leq 0.05$, ** $p \leq 0.01$, *** $p \leq 0.001$).

Empty-NIVs were formulated with different HP-CDs presenting different number of sugars in their ring structure i.e. HPαCD with 6 sugars, HPβCD with 7 sugars and HPγCD with 8 sugars. The additive ability to maintain vesicle integrity after freeze thawing and freeze-drying was determined (Figure 4.12). Firstly, to investigate the cryoprotectant ability of different HP-CD, NIVs containing the additives were frozen overnight at -80°C and thawed at room temperature before analysing the physical characteristics of the vesicles present within the formulations. The vesicle size and polydispersity index of NIVs containing HPαCD increased significantly compared to the fresh formulation ($p \leq 0.001$; Figure 4.12). In contrast, empty-NIVs prepared using HPβCD or HPγCD maintained their physical characteristics after freeze thawing. Following freezing, empty-NIVs containing the different sized HP-CD were freeze-dried and the lyoprotectant ability of the additives investigated (Figure 4.12). Empty-NIVs including HPαCD enlarged in size and polydispersity ($p \leq 0.001$) and the vesicle charge decreased ($p \leq 0.01$). Rehydrated HPβCD empty-NIVs also contained larger vesicles with a higher polydispersity index ($p \leq 0.001$) compared to the original formulation although vesicle charge was not affected. In contrast, NIVs containing the 8-membered ring in HPγCD-NIVs maintained their original vesicle size, polydispersity index and their ζ-potential was significant lower compared to the original formulation ($p \leq 0.01$; Figure 4.12). The water contents for the lyophilised cake of empty-NIVs prepared using the different HP-CDs were similar (data not shown). Therefore differences in water content were not responsible for the divergences within HP-CDs. Overall, these results indicated that HPγCD was the best lyoprotectant for NIVs, and optimisation of the concentration used was then determined.

The lowest concentration of HPγCD tested was 0.20 g/ml. This concentration failed to act as a cryoprotectant of NIVs as vesicle size increased significantly ($p \leq 0.001$; Figure 4.13). When HPγCD-NIVs (0.20 g/ml) were freeze-dried, vesicle enlarged even more, plus polydispersity index and surface charge significantly varied ($p \leq 0.01$). The addition of higher amounts of HPγCD, 0.38 or 0.50 g/ml,

protected the integrity of NIVs against freeze thawing and freeze-drying. A significant decrease in the ζ-potential of the NIVs compared to the original formation was still present ($p \leq 0.01$). Nonetheless, the incorporation of HPγCD resulted in a dose-dependent decrease in particle size when empty-NIVs were freeze-dried (Figure 4.14). HPγCD concentration equal or higher than 0.38 g/ml (6 times lipid concentration) already achieved the unity ratio between vesicle size of rehydrated cake and original formulation. The dose-dependent lyoprotectant effect of HPγCD was significantly superior to the one for sucrose (Figure 4.14). These results indicated that HPγCD was the best lyoprotectant for empty-NIVs and that at least 0.38 g/ml additive was required. Following, the effect of using different drug solution to rehydrate a larger batch of empty-NIVs (0.38 g/ml HPγCD) was investigated.

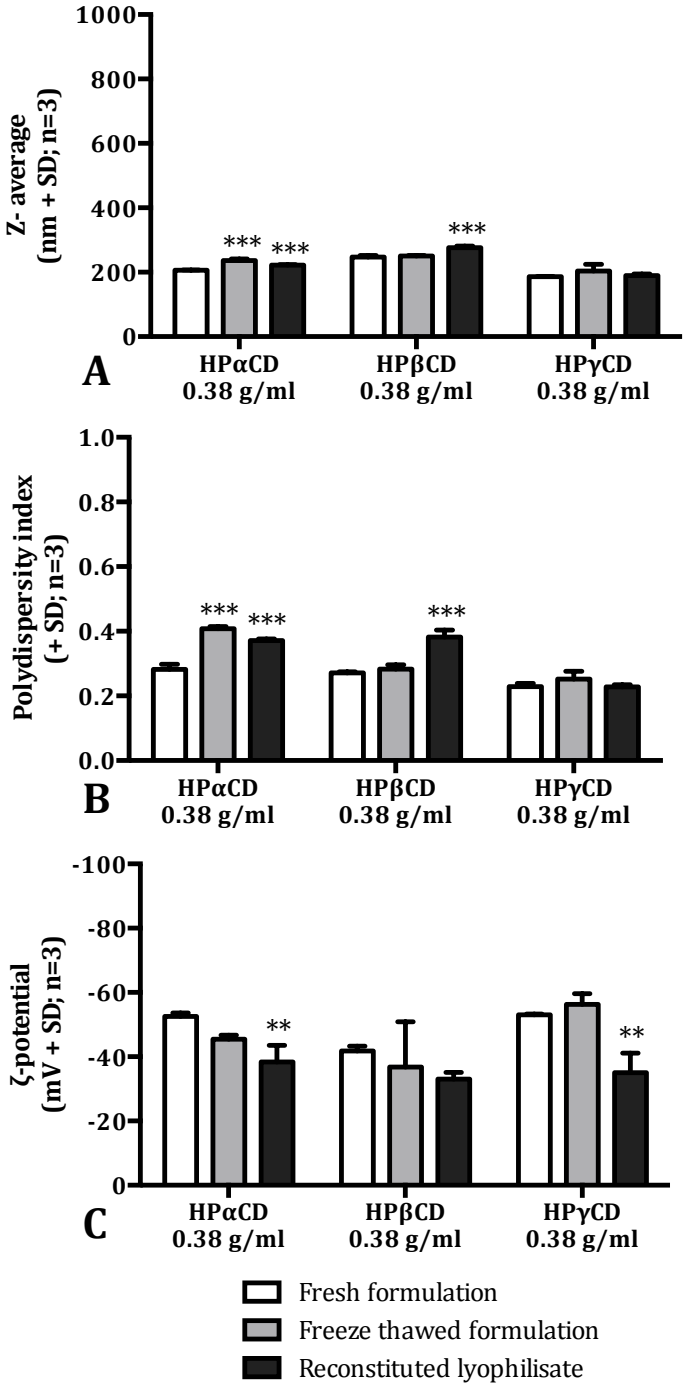


**Figure 4.12** Cryoprotectant and lyoprotectant effect of different ring-sized HP-CD (0.38 g/ml or 6 times lipidic NIVs concentrations). Freeze-thawed and freeze-dried samples were compared to the fresh formulations in terms of vesicle size (A), polydispersity index (B) and ζ-potential (C). The cyclodextrins used were HPαCD, HPβCD and HPγCD. Physicochemical properties were compared to the original fresh formulations (** $p \leq 0.01$, *** $p \leq 0.001$).

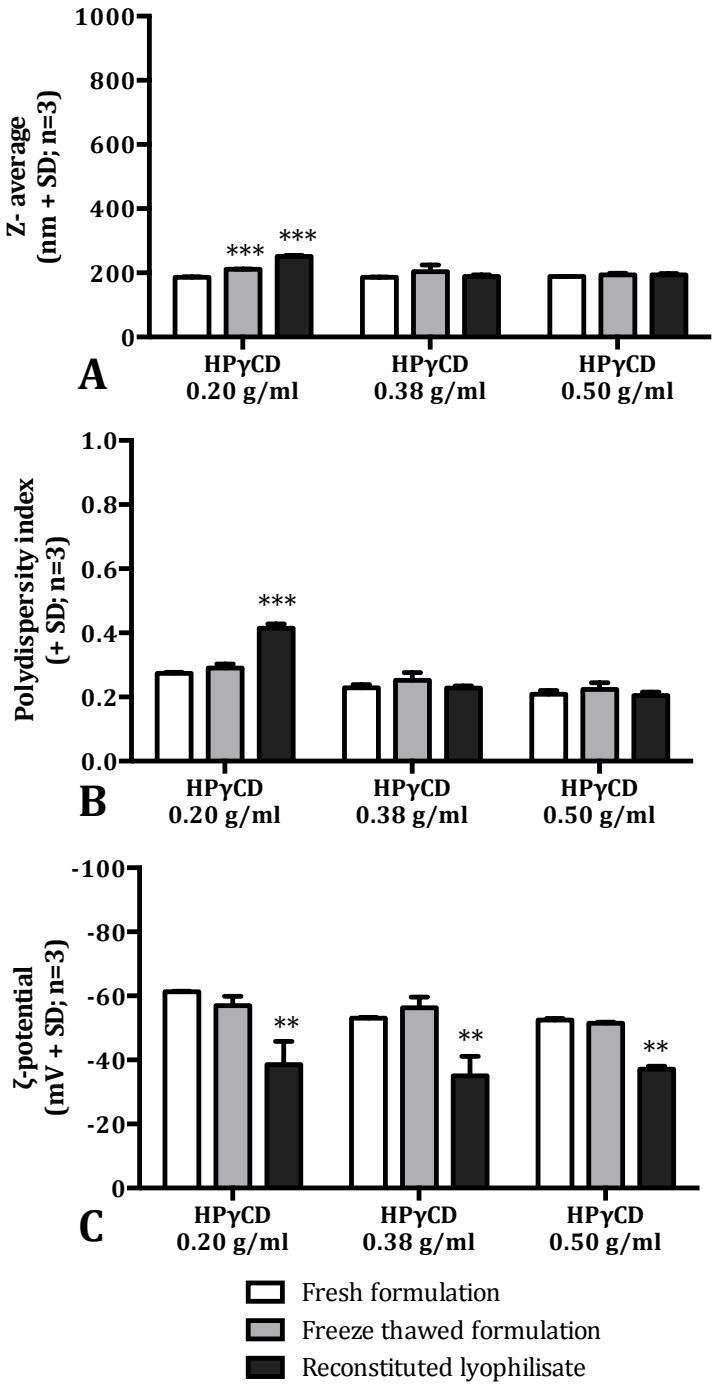


**Figure 4.13** Cryoprotectant and lyoprotectant effect of different concentrations of HPγCD (0.20, 0.38, 0.50 g/ml corresponding to 3.1, 6.0 and 8.0 times lipidic NIVs concentration). Freeze-thawed and freeze-dried samples were compared to their fresh formulations in terms of vesicle size (A), polydispersity index (B) and vesicle size (C; ** $p \leq 0.01$, *** $p \leq 0.001$).

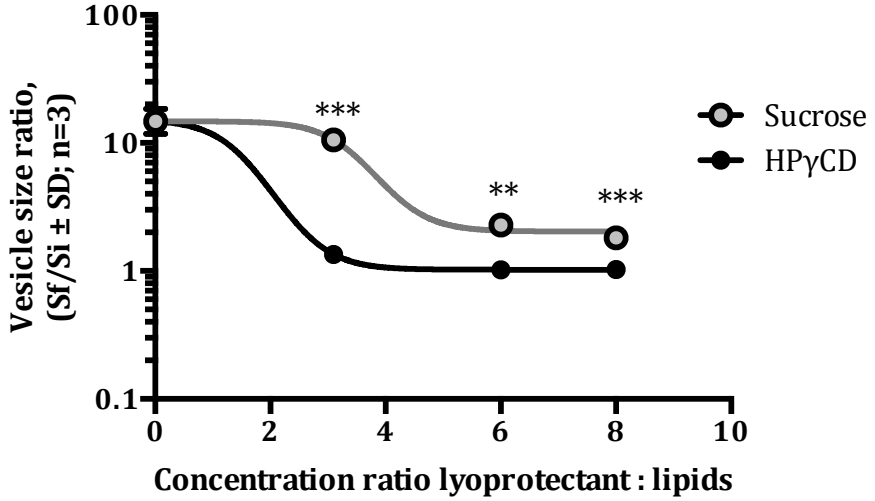


**Figure 4.14** Relation between amount of lyoprotectant (sucrose or HPγCD) and vesicle size after freeze-drying. Sf/Si corresponds to the vesicle size of the fresh formulation (Si) related to the vesicle size of the rehydrated lyophilisate (Sf). A Sf/Si value closer to 1 indicate successful lyoprotectant effect of the additive. The concentration ratio between lyoprotectant and NIVs lipids was 3.1, 6 and 8 times (corresponding to 0.20, 0.38 and 0.50 g/ml additive). The mean from 3 measurements is shown and p values compared between additives (** $p \leq 0.01$ and *** $p \leq 0.001$).

The influence of the solution used to rehydrate freeze-dried HPγCD empty-NIVs was studied. A larger batch of empty-NIVs with HPγCD (0.38 g/ml) additive was prepared and freeze-dried into aliquots. After freeze-drying the percentage of water left in the lyophilisate was 0.004 ± 0.014 % w/w (detected by Karl Fischer coulometric titration). Freeze-dried cakes were rehydrated with distilled water, sodium chloride (0.9 % w/v), PBS pH 7.4, cisplatin solution (1 mg/ml cisplatin with NaCl 0.9% w/v), luciferin solution (5 mg/ml Luc with PBS), gemcitabine solution (1 mg/ml gemcitabine with distilled water) or AmB (1 mg/ml AmB with 100 mg/ml HPγCD). Although there was a significant increase in vesicle size in some of the rehydrated samples compared to the original (Figure 4.15.A) the vesicle size never increased over 310 nm. There was a significant increase in NIVs vesicle size when the lyophilized cake was rehydrated with distilled water, NaCl, cisplatin or gemcitabine ($p \leq 0.05$). Nonetheless, the drug solution did not influence vesicle size of the rehydrate since the particle size of the drug and its solute were similar (i.e. NaCl and cisplatin, water and gemcitabine, PBS and Luc). All the rehydrated samples had a significant greater polydispersity than the original formulation ($p \leq 0.05$; Figure 4.15.B) with Gemcitabine-NIVs and AmB-NIVs having the smallest values. The surface charge of NIVs was only significantly different from that of the original formulation for PBS-NIVs ($p \leq 0.001$; Figure 4.15.C).

The entrapment efficiencies of freeze-dried empty-NIVs rehydrated with different drugs solution are shown in Figure 4.16. AmB had the highest entrapment and cisplatin the lowest. The entrapment efficiencies obtained with empty-NIVs with HPγCD were lower than that produced when NIVs suspensions were incorporated to empty-NIVs without cryoprotectant. For example, the entrapment efficiency for Luc-NIVs was usually around 50 % when empty-NIVs without lyoprotectant were rehydrated; whereas a value of 24 % was obtained using empty-NIVs with HPγCD.

The use of a lyoprotectants in the NIVs formulation increased the final osmotic pressure of the formulation compared to the NIVs without cryoprotectant. Empty-NIVs without cryoprotectant, formulated with 150 mM of lipid components, presented a theoretical osmotic pressure of 150 mOsM. The addition of HPγCD (0.38 g/ml) to empty-NIVs increased the osmotic pressure to 364.54 mOsM (theoretical calculation). To maintain a physiological osmotic pressure (285 -295 mOsM) in empty-NIVs with HPγCD and 150 mM lipids, 1 ml of freeze-dried formulation had to be rehydrated with 1.27 ml of water. As a result, the formulation would have an osmotic pressure of 290 mOsM and a final concentration of lipids of 119.2 mM. Another example is Gemcitabine-NIVs, which had to be diluted 1.27 times with distilled water to become an isotonic formulation (0.78 mg/ml gemcitabine, 119.2 mM lipids). In the case of cisplatin, the drug is only stable in a sodium chloride solution, which already has tonicity. Therefore when 1 mg/ml of cisplatin solution with NaCl was used to rehydrate 150 mM empty-NIVs with HPγCD, a dilution of 2.33 with distilled water had to be applied to obtain an isotonic formulation (0.43 mg/ml cisplatin, 64.4 mM lipids). Similar method had to be applied when 5 mg/ml luciferin solution with PBS was used to rehydrate empty-NIVs (2.15 mg/ml Luc, 64.4 mM lipids). AmB-NIVs formulated with the DRV method, presented a final osmotic pressure of 422.4 mOsM. Water dilution of the final AmB formulation with a 1.46 fold decreased the osmotic pressure to 290 mOsM (0.68 mg/ml AmB, 103 mM lipids).

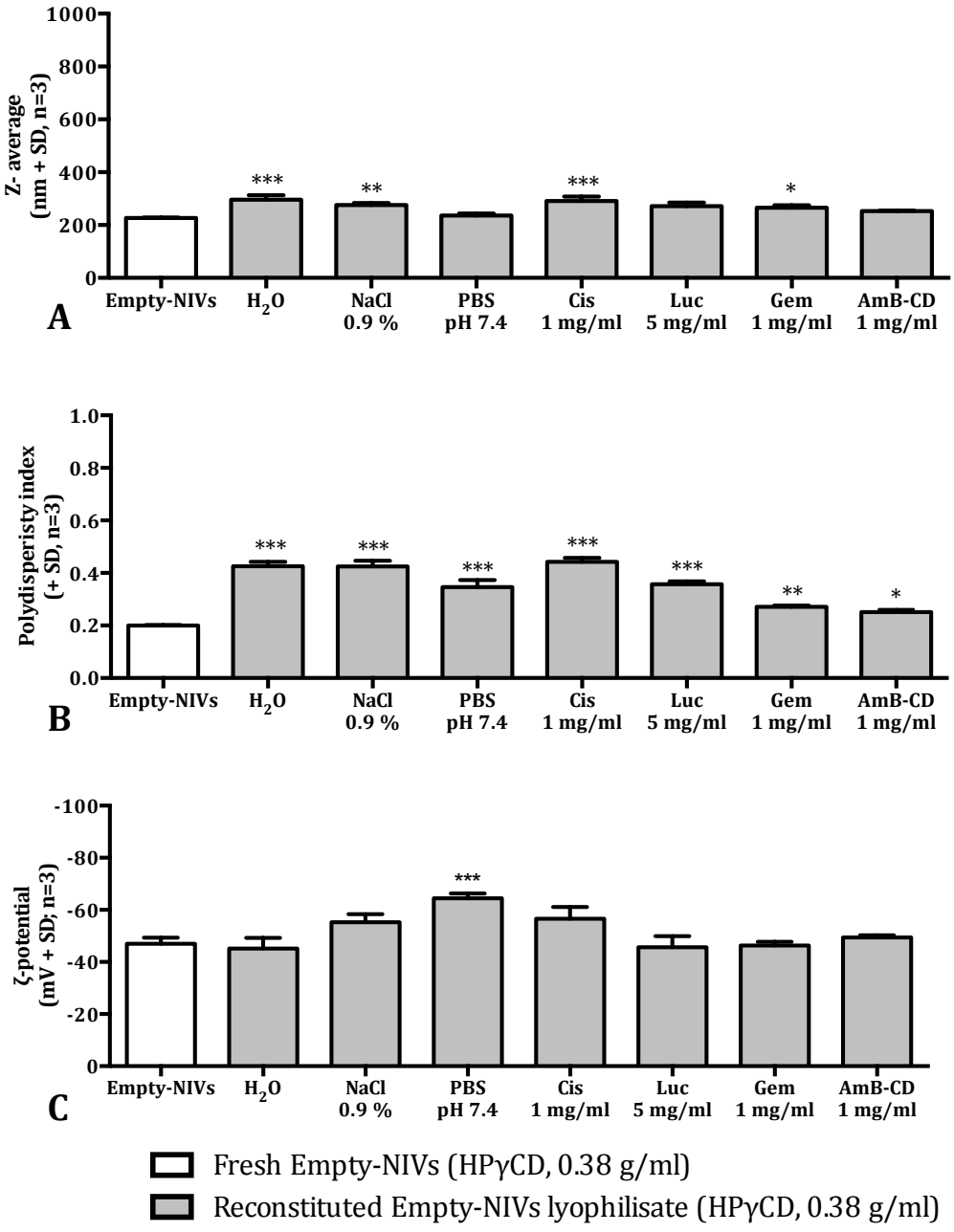


**Figure 4.15** Effect of rehydrating lyophilised empty-NIVs containing HPγCD (0.38 g/ml, 150 mM lipid) with different solutions: distilled water ($H_2O$), sodium chloride (NaCl, 0.9 % v/v), phosphate buffered saline (PBS, pH 7.4) cisplatin solution (cis, dissolved in NaCl 0.9 % v/v, 1 mg/ml), luciferin solution (dissolved in PBS at 5 mg/ml), gemcitabine solution (Gem, 1 mg/ml with distilled water) and AmB (AmB-CD, 1 mg/ml AmB dissolved in 100 mg/ml HPγCD). Vesicle size (A), polydispersity index (B) and ζ-potential (C) of the fresh formulation compared to the reconstituted empty-NIV lyophilisates (* $p \leq 0.05$, ** $p \leq 0.01$, *** $p \leq 0.001$).

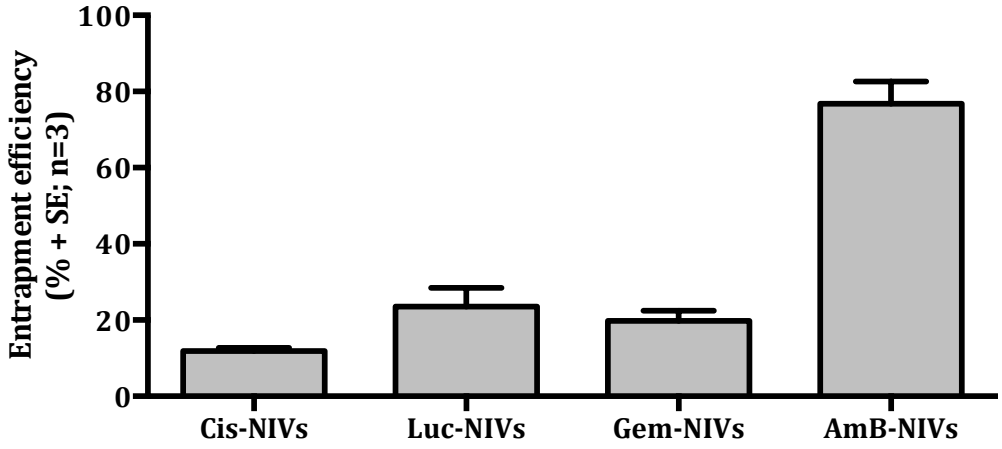


**Figure 4.16** Entrapment efficiency of different drugs solutions used to rehydrate freeze-dried empty-NIVs containing HPγCD (0.38 g/ml additive, 150 mM lipid). The drug solutions used were: cisplatin (Cis-NIVs, dissolved in NaCl 0.9 % v/v, 1 mg/ml cisplatin), luciferin (Luc-NIVs, dissolved in PBS at 5 mg/ml luciferin), gemcitabine (Gem-NIVs, 1 mg/ml gemcitabine with distilled water) and AmB (AmB-NIVs, 1 mg/ml AmB dissolved in 100 mg/ml HPγCD).

### 4.5. Luciferin-NIVs characteristics

Luciferin (Luc) is highly unstable at elevated temperatures therefore incorporation of the compound in a mixture of melted lipids for homogenisation would not be advisable. Hence, Luc-NIVs were formulated with the DRV method where luciferin solution was used to rehydrate lyophilised empty-NIVs to produce Luc-NIVs. The luciferin entrapment efficiency for this passive loading methodology was 40.30 ± 4.42 % (Figure 4.17.A). Luciferin was left to interact with the empty-NIVs for 10 minutes and for 24 hours prior to analysis resulting in an entrapment efficiency of luciferin independent of the incubation time. Alternative, active loading was investigated by forming a transmembrane pH or salt gradient in order to increase the encapsulation efficiency of luciferin (Table 2.3). Empty-NIVs formulated using the acetate method were over 1,000 nm in diameter with a neutral ζ-potential resulting in an unstable colloidal suspension (Figure 4.18). As a consequence, further studies with the acetate gradient methodology were not performed. In contrast, NIVs formulated with HEPES buffer pH 8.0 or Tris buffer pH 10.0 had a z-average size between 200 and 250 nm and a vesicle charge around -75 mM, which suggested colloidal stability. Once the empty-NIVs vesicles were formulated, the extra vesicular buffer was changed and luciferin incorporated before changing back to original buffer. Both HEPES and Tris buffer methodologies maintained NIVs physical properties along the active loading procedure. Only ζ-potential of the HEPES approach was reduced when external buffer was changed ($p \leq 0.001$; Figure 4.18.C) but returned to original values when HEPES buffer was reincorporated. Luciferin entrapment efficiency of NIVs formulated with either HEPES or Tris method was not higher than the passive method (Figure 4.17.A). Samples formulated with the reverse HEPES approach were directly formulated with buffer 2 (20 mM citric acid and 150 mM NaCl, pH 5.0). The vesicle size was considerably larger than the empty-NIVs formulated with HEPES or Tris buffer and presented several variations during the process of adding luciferin and changing the external buffer to HEPES (Figure 4.18). The reverse HEPES approach increased

the luciferin entrapment efficiency compared to the passive loading ($p \leq 0.05$; Figure 4.17.A). However, even though reverse HEPES presented a slight increase in luciferin entrapment efficiency, the total amount of luciferin decreased significantly from the original loading concentration ($p \leq 0.001$; Figure 4.17.B). The decline was probably associated to losses during diafiltration. As a result, DRV passive loading was the methodology of choice to formulate Luc-NIVs.

Mice infected with *L. donovani*, LV82-luc were imaged on day 7 post-infection with luciferin solution (PBS, pH 7.4; Figure 4.19.A). No BLI was observed in the IVIS images when luciferin solution was used. Mice were also imaged with Luc-NIVs, formulated by the DRV passive loading approach. In this case, mice presented intense and located BLI in the liver area, which was significantly different from the luciferin solution group ($p \leq 0.001$; Figure 4.19.B).

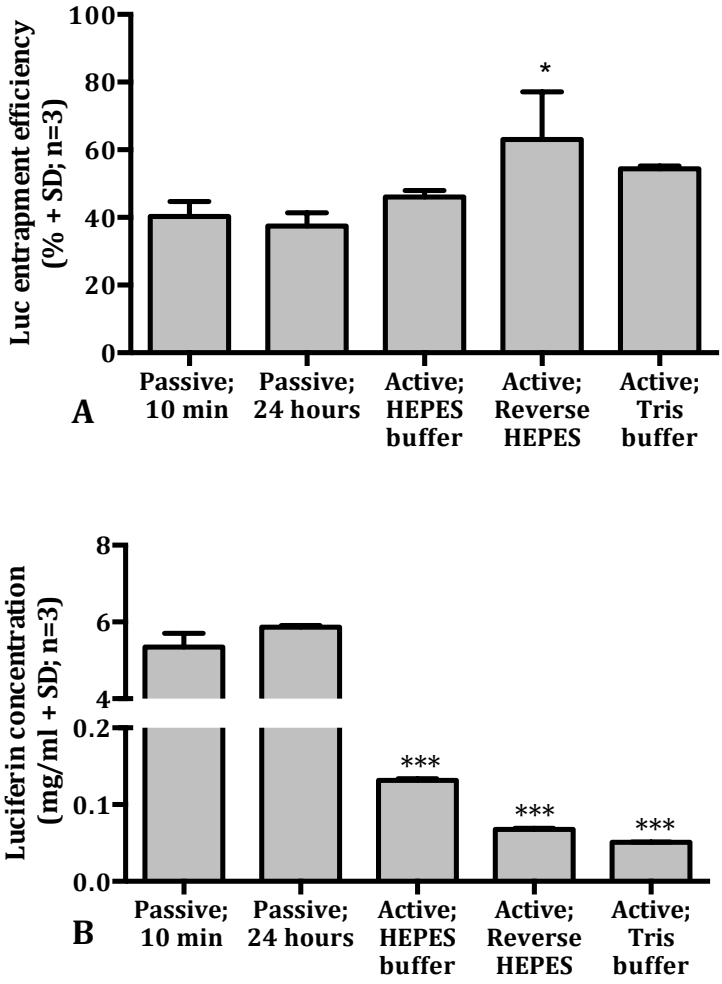


**Figure 4.17** Luciferin entrapment efficiency (A) and luciferin total concentration (B) of Luc-NIVs prepared with different DRV techniques. Luc-NIVs prepared by passive loading were formulated by rehydrating empty-NIVs with 5 mg/ml of luciferin in PBS pH 7.4 for 10 minutes or 24 hours before analysis (30 mM lipidic concentration). Active loading of luciferin was investigated by pH gradient with HEPES or Tris buffer (5 mg/ml of Luc in PBS pH 7.4; 30 mM lipids; Table 2.3). Statistics compared active to passive DRV loading techniques (* $p \leq 0.05$, *** $p \leq 0.001$).

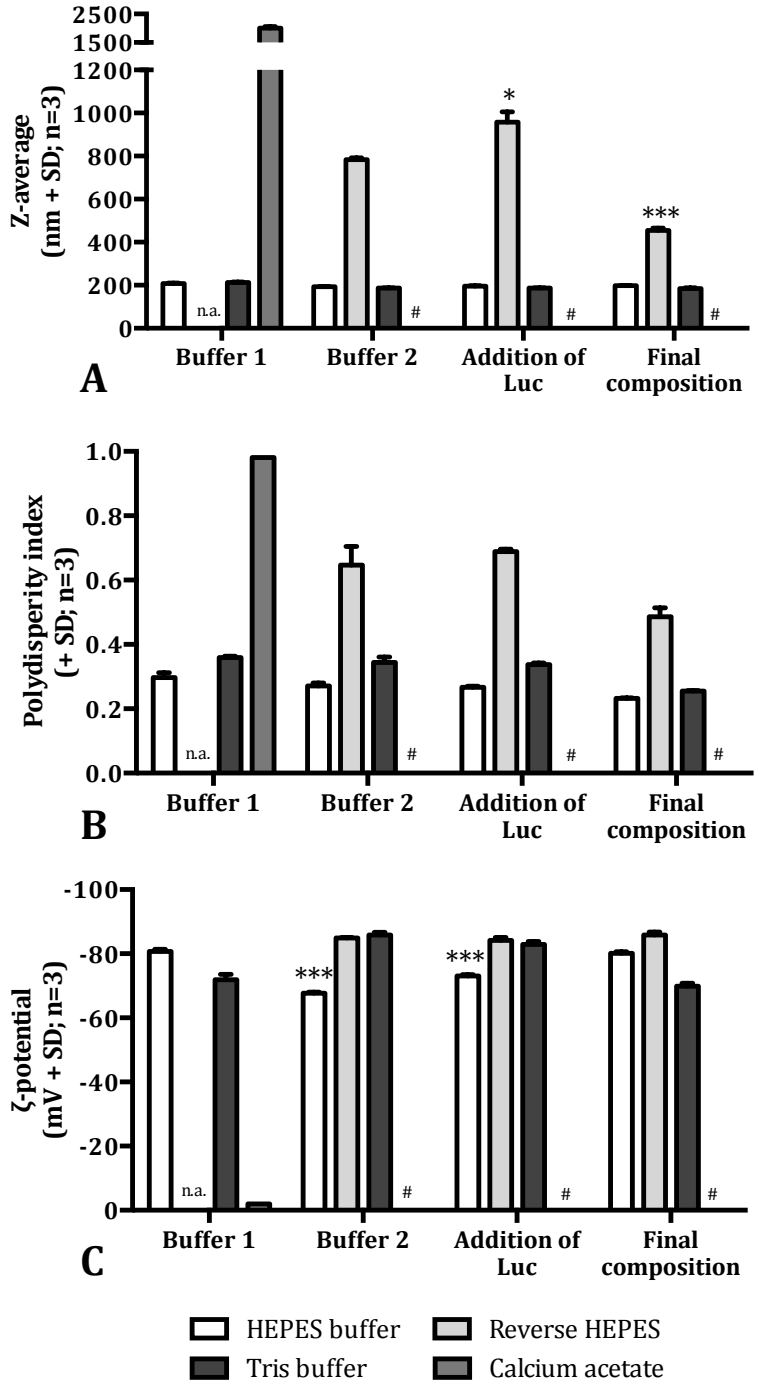


**Figure 4.18** Physical characteristics of NIVs during luciferin DRV active loading steps. Vesicle size (A), polydispersity index (B) and ζ-potential (C) were detected in different steps of the process. The active loading methods investigated were HEPES buffer, reverse HEPES, Tris buffer, and calcium acetate. The buffers corresponding to each step are described in Table 2.3 (n.a., not applicable; #, data was not obtained since stability issues were encountered in earlier stages of the formulation; * $p \leq 0.05$, *** $p \leq 0.001$ compared to initial formulation).

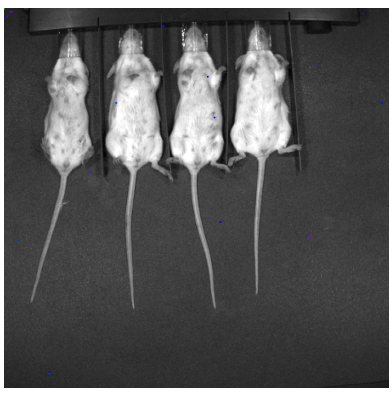

**A-** Luc-sol; 3.62 ± 0.33 p/s

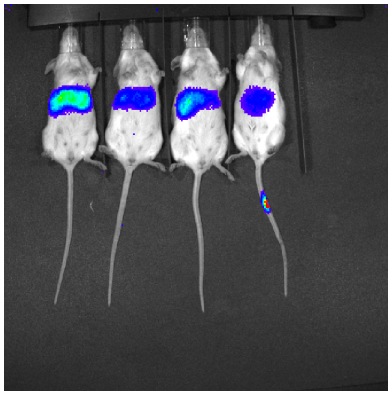

**B-** Luc-NIVs; 15.24 ± 2.94 p/s ***

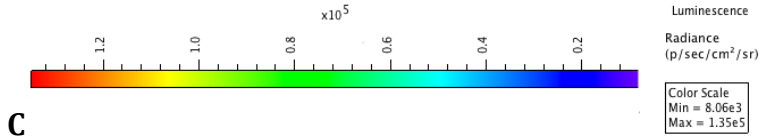


**C**

**Figure 4.19** IVIS examples of BLI images obtained from BALB/c infected with LV82-luc and imaged on day 7 post-infection with luciferin solution (A) and Luc-NIVs (B). Mice image was taken 10 minutes post-intraperitoneal injection of the tested formulation. Minimum of photons/sec was $8.06 \times 10^3$ and maximum of $1.35 \times 10^5$ (C). Values of BLI for the liver area are noted below each image ($\times 10^5$ ± SE; *** $p \leq 0.001$ compared to luciferin sol group). Uninfected control mouse imaged presented a BLI liver background of $0.75 \times 10^5$ p/s for luciferin solution and $0.68 \times 10^5$ p/s for Luc-NIVs imaging.

## 4.6. Discussion

The overall aim of these studies was to produce a lyophilised NIVs formulation with stable properties, able to encapsulate a variety of drugs, and with the potential to be used for multiple applications. The drugs tested in these studies were the anticancer drugs cisplatin and gemcitabine, AmB and the imaging-prove luciferin.

For formulation and analytical purposes, the methods used to detect cisplatin, gemcitabine, luciferin and the three lipidic components of the NIVs, were successfully validated to suit the study requirements. To quantify cisplatin, the compound was derivatised with DDTC in order to enhance its UV signal (Lopez-Flores *et al.*, 2005). The HPLC-UV assay was adapted from method III described in Alsaadi's thesis (2011). However, the method presented several variations from its original. In this case, the flow rate was decreased to 1.5 ml/min since 1.7 ml/min resulted in excessive pressure for the HPLC system. Another noticeable change was the mobile phase used. In this study, an acetate buffer was used instead of distilled water to provide a pH buffering into the system. The cisplatin standard curves were diluted either with NaCl or NaOH with both types showing similar levels of linearity. Therefore, whether cisplatin solution was dissolved with NaCl or with NaOH (used for disrupting Cis-NIVs vesicles and quantify the platinum encapsulated) did not affect the outcome of the HPLC analysis. The high relative standard deviation of the method was representative of low precision; this was also reported by Alsaadi (2011). The use of the IS nickel chloride was key to compensate for any errors and allowed for the correction of the matrix effects (Lopez-Flores *et al.*, 2005). However, the pre-column derivatisation reaction between cisplatin or nickel chloride with DDTC was probably the cause of the high variation in the analytical method.

A method to successfully quantify gemcitabine by HPLC-UV was also validated (adapted from Parshina *et al.*, 2008 and Al-Gawhari, 2013). The intra-day

precession for the described method was superior than others (Al-Gawhari, 2013). The IS (2'-deoxycytidine) and gemcitabine eluted with favourable peak characteristics and the standard curve presented excellent linear regression. Contrary to Parshina *et al.* (2008), the maximum wavelength of UV absorption related to gemcitabine was observed at 269 nm, same as deoxycytidine. As a consequence, both analytes were detected in the same wavelength chromatogram, rather than a different wavelength for each component.

The substrate luciferin was used to image luciferase expressing cells, such as LV82-luc or B16-F10-luc and a method to quantify the amount of luciferin was required. Firstly, the development of an HPLC-UV method to quantify luciferin was attempted (Hadj-Mohammadi and Chaichi, 1996). However, the standard peak obtained was not symmetric and extra small peaks appeared along the chromatogram. Those probably related to the low stability of luciferin in contact with solvents such as methanol. Moreover, due to the nature of D-luciferin, samples were easily transformed to its optical isomer L-luciferin and other degradation products. The use of a UV detector, without the prior chromatographic separation and the necessary solvents, resulted in a successful method to quantify luciferin. Similar approaches have been previously used (Kheirolomoom *et al.*, 2010). In addition, the luciferin maximum wavelength of absorption was significantly different from the AmB one. Therefore, in the case of samples containing both AmB and luciferin, the analytes were successfully characterised with HPLC-UV (λ=407 nm) for AmB and with UV (λ=328 nm) for luciferin.

A normal phase HPLC method with an ELSD detector was used to quantify the three components of NIVs (surfactant, cholesterol and DCP; Alsaadi *et al.*, 2013). Previous studies validated the method (Puig-Sellart, 2013) and the three analytes plus an IS were successfully quantified in the same chromatogram.

Empty-NIVs were successfully formulated in a laboratory scale. The mean vesicle size of empty-NIVs was smaller than 200 nm but its extreme high viscosity made sterile filtration difficult. The rheology flow of empty-NIVs had similar characteristics to that of AmB-NIVs (Chapter 3), both were shear thinning to a certain extend and non-time thixotropic. Scaled-up production of empty-NIVs included a HPH procedure, which decreased the particle size and viscosity of empty-NIV and those were sterile filtered with ease (0.22 μm). Lower viscosity values could be associated to the extra HPH step (Masson *et al.*, 2011) or lower final lipid concentrations. HPH was also proved to be benignant to the NIVs, since the lipid composition was not jeopardised after this step. The dilution of empty-NIVs scaled-up batches to smaller lipidic concentration was required in order to obtain a suitable particle size for sterile-filtration. Indicating that the lipidic concentration was a critical factor in achieving a reduction of particle size by HPH. At the full lipid concentration, 150 mM, which was used for batch 1 and 2 the formulation either, blocked the high-pressure homogeniser or the particle size could not be reduced enough for filtration. The dilution of the formulation to 107 mM lipid concentration, as with batch 3, enabled a further reduction of particle size and the formulation was successfully filtered sterilised. Overall, scale-up production of empty-NIVs with smaller particle size to allow sterile filtration can be obtained. It should be noted that the concentration of the lipid mixture itself (≤ 107 mM) was critical to this being achieved.

The lyophilisation and rehydration of empty-NIVs formulation (both laboratory or scale-up production methods) resulted in the production of NIVs with much larger vesicle size than that of the original formulation. In those cases, the vesicle bilayer was damaged during freeze-drying, probably associated with ice crystals formed during freezing or as a consequence of vesicle aggregation following dehydration. Therefore, the optimisation of the lyophilised protocol for empty-NIVs, in conjunction with formulation and technological parameters, was required. The addition of a lyoprotectant appeared to play a key role during

NIVs lyophilisation, presumably due to the water replacement and/or vitrification protection mechanisms (Koster *et al.*, 2000). The freezing step was fundamental in the lyophilisation of empty-NIVs since most of the damaged vesicles were associated to the cooling step. The best approaches in freezing NIVs were fast cooling to low freezing temperature, such as -80°C or liquid nitrogen. Contrary, slow freezing (0.6°C/min) or freezing at lower temperatures (-18°C) affected the NIVs structure with an increase of vesicle size. Therefore, a quick-freezing approach was thought to diminish the freeze-concentration effect and resulted in a favourable NIVs vesicle protection. In contrast, other authors demonstrated that slow freezing was beneficial for certain liposome particles (Siow *et al.*, 2007). Similar to what happen in nature, very slow freezing rates allow the water molecules to reach equilibrium on both sides of the bilayer, as water is removed to the external side due to freeze-concentration (Poncet and Lebel, 2003). These could result in a reduction of internal ice crystals which is beneficial for bilayer structures (Siow *et al.*, 2008). In the case of slowly freezing of NIVs, a cooling rate of 0.6°C/min was not slow enough to protect against the formation of internal ice crystals. In conclusion, even though submerging the samples in liquid nitrogen also resulted in successful freezing outcomes, freezing at -80°C became the method of choice due to easier availability of equipment.

The incorporation of a lyoprotectant into the NIVs bilayer was required to protect against impairment effects produced by freeze-drying. All the lyoprotectants studied were incorporated in the melted lipid mixture, prior homogenisation of NIVs. This ensured homogeneous distribution of the additives alongside of the bilayer. The carbohydrates glucose, sucrose and trehalose were the first lyoprotectants to study. Previous published studies had demonstrated their efficacy in maintaining vesicle-like structures upon freeze-drying (Abra and Szoka, 1988; Miyajima, 1997; Stark *et al.*, 2010; Kundu *et al.*, 2012; Yang *et al.*, 2013). The additives were firstly screened for cryoprotectant abilities at a concentration ratio of 2.7 times the lipid concentration (as used by

Gilead Sciences Limited, 2012). Glucose and sucrose demonstrated successful cryoprotectant abilities when NIVs were quickly frozen whereas NIVs containing trehalose increased in vesicle size upon freeze thawing. The following freeze-drying NIVs experiments were only focused on the disaccharide sucrose. Due to the fact that glucose is associated to a much lower $T_g'$ (~40°C, Koster *et al.*, 2000), the monosaccharide is thought to exhibit less protective effect upon lyophilisation (Chen *et al.*, 2010). Moreover, sucrose has been proven to be effective in protecting other liposomes membrane integrity (Elhissi *et al.*, 2006; Yang *et al.*, 2007, 2013). Therefore, increasing sucrose concentrations in empty-NIVs were tested as lyoprotectant. However, not even the highest amount of sucrose (0.50 g/ml) was able to protect against the detrimental freeze-drying effects. Nevertheless, a sigmoidal dose-response relation was observed, showing that increasing amounts of sucrose reduced the size variation difference from its original. This relation suggested that theoretically higher mass ratio of sucrose: lipid in the NIVs dry state (i.e. 10:1) were needed to achieve successful lyophilisation protection. Others have also observed an amelioration or even a plateau when more carbohydrate was added (Miyajima, 1997). However, special attention should be paid to the osmotic pressure when high amounts of sucrose are used. As a result, sucrose was concluded to be an unsuccessful candidate for lyoprotection of empty-NIVs.

The rationale of investigating HP-CDs, as lyoprotectants, arose from studying the lyophilisation of AmB-NIVs (Chapter 3). It was noted that freeze-dried AmB-NIVs without any lyoprotectant did not experiment such a large vesicle size increase as empty-NIVs. It was then demonstrated that this effect was related to the HPγCD used to solubilise AmB rather than the presence of the drug itself. Cyclodextrins are cyclic oligosaccharides formed by units of glucose with the ability to form inclusion complexes (Loftsson and Duchêne, 2007). Many other oligosaccharides have been investigated as lyoprotectants, including fructans, malto-oligosaccharides or manno-oligosaccharides (Hincha *et al.*, 2008). However, to our knowledge, the use of cyclodextrins as lyoprotectants for NIVs

has not been reported yet. Firstly, empty-NIVs were formulated with the presence of different HP-CD. CD without hydroxyl group modifications were not tested in the study due to their high cytotoxicity to respiratory epithelial cell (Salem *et al.*, 2009). Only HPγCD, the eight units derivate, was successful in avoiding modification of the NIVs vesicles upon lyophilisation. Empty-NIVs with HPγCD maintained their original size during the freezing step and ultimately during the freeze-drying and rehydration process. HPβCD was a good cryoprotectant but did not exhibit lyoprotectant activity in empty-NIVs. The smallest ring HPαCD failed in protecting the particles already in the freezing step. The optimal HPγCD concentration was demonstrated to be 0.38 g/ml (corresponding to 6.0 times the lipidic concentration).

The use of HPγCD as lyoprotectant in NIVs presented several advantages over the use of sucrose. Firstly, HPγCD was the only additive able to maintain the NIVs physical characteristics both when freeze-thawed and lyophilised-rehydrated. The lyoprotectant effect of HPγCD was achieved at much lower concentrations than it would have been required for sucrose. A beneficial mechanism that could be associated to HP-CDs is the improved water replacement protection due to the vast amount of hydrogen donors and acceptors in those molecules (van den Hoven *et al.*, 2012). Moreover, one of the most important advantages of using HP-CDs over other saccharides was their high phase transition temperature ($T_g'$). The $T_g'$ associated to HP-CDs were approximately three times higher than the sucrose. A higher $T_g'$ of the additive allowed a bigger difference in vapour pressure between the sample, at the sublimation front, and the temperature at the condenser. This resulted in a faster sublimation process and improved vitrification effect. Previous publications reported that a $T_g'$ temperature increase of 1°C results in 13% reduction in primary drying time (Pikal and Shah, 1990). Consequently, the cost associated to the freeze-drying of the formulation with HPγCD as a lyoprotectant, would significantly decrease.

Freeze-dried empty-NIVs with HPγCD were successfully formulated in a scaled-up batch. Although significant enlargement in vesicles size was observed, NIVs were proven to remain below 310 nm upon rehydration with different solutions. The rehydration of empty-NIVs lyophilisates with different compounds (cisplatin, luciferin, gemcitabine or amphotericin B) and their correspondent solvents (NaCl 0.9 %, PBS pH 7.4 or distilled water) confirmed that the obtained vesicle size was independent of the drug used. The entrapment efficiency of those compounds in the rehydrated NIVs varied depending on the drug tested. In the case of cisplatin, the drug was incorporated to the lyophilised NIVs at a concentration of 1 mg/ml dissolved with NaCl 0.9 %. Higher cisplatin concentration of cisplatin could only be achieved by heating up the samples (maximum of 10 mg/ml at 70°C; Woo *et al.*, 2008) which was associated to a high risk of crystallisation when temperature restored (Alsaadi, 2011). The entrapment efficiency values obtained by rehydrating freeze-dried NIVs (with HPγCD) with 1 mg/ml cisplatin were similar to the ones obtained by Alsaadi (2011), when 6 mg/ml cisplatin was incorporated to the melted lipids prior homogenisation. Cis-NIVs studied by Alsaadi at a 1 mg/ml did not pellet during ultracentrifugation, therefore a value for entrapment efficiency could not be obtained. In the present case, 1 mg/ml Cis-NIVs were succesfully pelleted; and entrapment fraction obtained. The reason for that was thought to be related to the HPγCD additive, as this could have provided the structural strength necessary for the NIVs vesicles to pellet upon ultracentrifugation. As for luciferin, the entrapment efficiency obtained by rehydrating Empty-NIVs with HPγCD was 10 to 15% lower than the entrapment efficiency obtained by loading of empty-NIVs without cryoprotectant. The difference in vesicle size between both formulations could explain this variation. As previously described, empty-NIVs freeze-dried without cryoprotectant can largely expand when rehydrated, which would reciprocate with higher luciferin entrapment efficiency values (Fresta *et al.*, 1993; Arunothayanun *et al.*, 2000; Jahn *et al.*, 2007). Another possibility could be that the lyoprotectant obstructed, to a certain extend, the incorporation of luciferin within the NIVs. A similar case was

observed when gemcitabine solution was used to rehydrate empty-NIVs with HPγCD as a lyoprotectant. The entrapment of those formulations was 40 % inferior to the one reported by Al-Gawhari (2013) where freeze-dried empty-NIVs without lyoprotectant were rehydrated. However, the particle size of Al-Gawhari's formulations was 7 times larger than empty-NIVs freeze-dried with HPγCD. As for AmB, AmB-CD was also used to rehydrate lyophilised empty-NIVs with HPγCD. The high amounts of CDs incorporated to this formulation were inadequate for further drug development studies. However the experiment was used as additional proof of concept of the passive DRV method to produce NIVs *in situ*. The encapsulation values obtained with the DRV method were inferior to the ones obtained when AmB-NIVs were produced by the homogenisation technique. Yet, remarkably higher entrapment efficiency values of AmB were achieved compared to rehydration with cisplatin, gemcitabine or Luc. This could be related to the nature of AmB or the cyclodextrin inclusion complexes.

Special attention was paid to the final tonicity of the formulations used for inhaled administration. Hypertonic solutions decrease the ciliary beat frequency and disrupt epithelial cells on nebulisation (Min *et al.*, 2001). This ciliostasis could results in slight bronchoconstriction and coughing after inhalation (Hirsh, 2002). The addition of lyoprotectants to a formulation contributes to its osmotic pressure and this should be assessed with precaution. An ideal formulation tonicity should be around the physiological 285 – 295 mOsM. Empty-NIVs with HPγCD resulted in a theoretical hypertonic formulation (365 mOsM), however a dilution with distilled water or use of 119 mM lipidic concentration instead of 150 mM, would reach isotonic values. Further dilutions values were necessary for Cis-NIVs since the anticancer could only be solubilised in 0.9 % NaCl. Cisplatin is not stable with distilled water as it isomerises quickly to the cis-trans form. Therefore, to obtain isotonic Cis-NIVs, the rehydrated formulation required further dilution with distilled water.

When the substrate luciferin was incorporated to the NIVs vesicles by passive loading, the concentration of entrapped sample within NIVs never exceeded its amount outside the vesicles, i.e. 50 % entrapment efficiency. Others investigated the use of active loading techniques for amphipathic compounds, based in a formation of a trans membrane gradient, such a pH (Zhigaltsev *et al.*, 2005) or acetate gradient (Clerc and Barenholz, 1995). Luciferin, as a small amphipathic molecule, was an ideal candidate to test the active loading techniques in NIVs. The protocols used were a variation of Kheirolomoom *et al.* (2010); using a diafiltration technique to exchange buffers rather than a Sephadex column. NIVs formulated with calcium acetate resulted in critical unstable characteristics probably related to the ionic strength of the buffer. Contrary, NIVs with HEPES or Tris buffer were successfully formulated. Only NIVs formulated by the reverse HEPES method encapsulated more luciferin than the samples obtained by passive loading. Nevertheless, the diafiltration of the buffers resulted in losses of luciferin compared to the amount initially incorporated. Results published by Kheirolomoom *et al.* (2010) could not be reproduced in Luc-NIVs formulations and the formulation of Luc-NIVs was maintained with the passive DRV methodology.

The infection rate of mice containing LV82-luc could only be quantified with Luc-NIVs. Luciferin solution alone did not exhibit BLI in the subjects. This support the advantage of using NIVs over the solution alone (as mentioned in Chapter 3; Carter *et al.*, 2001; Alsaadi *et al.*, 2012; Shaw and Carter, 2014). *Leishmania* parasites are located in macrophages, which were difficult to target with luciferin solution. *In vivo* BLI imaging with luciferin solution could lead to false conclusions of null rates of infection i.e. no BLI observed even though LV82-luc present. However, imaging with Luc-NIVs improved the detection of the parasites and BLI values correlated the rate of infection.

In conclusion, a lyophilisate NIVs able to encapsulate different drugs to be used for different applications were obtained:

- Analytical methods to determine cisplatin, gemcitabine, luciferin and the lipid components were successfully validated to fit the purpose of the study.

- Empty-NIVs were scaled-up with success and the concentration of lipid components was proven to be detrimental for particle reduction during high-pressure homogenisation.

- Empty-NIVs were successfully freeze-dried with the incorporation of HPγCD as a lyoprotectant and the maintenance of the formulation characteristics upon lyophilisation/rehydration was achieved.

- Freeze-dried empty-NIVs with HPγCD were able to encapsulate different drugs by the DRV method, such as cisplatin and gemcitabine. Therefore avoiding any undesirable storage stability issues as the formulation can be created as needed.

- Passive DRV loading of luciferin into NIVs was more advantageous than active loading.

- *In vivo* Luc-NIVs, produced with the passive DRV loading technique, were noticeable superior than luciferin solution alone when *in vivo* imaging of luciferase expressing LV82-luc parasites.

# CHAPTER 5. THE EFFECT OF USING VIBRATING-MESH NEBULISATION ON NON-IONIC SURFACTANT VESICLES

## 5.1. Introduction

The development of inhaled pharmaceuticals requires preliminary aerosol characterisation in order to ensure successful drug deposition within the lungs. As previously discussed, a key characteristic to take into account is the droplet size of the aerosol produced, since this is strongly related to the particle deposition along the airways (Section 1.2). Large particles impact in the upper conducting region of the lungs whereas smaller particles deposit in the distal regions of the lungs (Figure 1.1; Byron, 1986). Two types of *in vitro* techniques are mainly used to measure the aerosol size of an inhaled formulation. One depends on inertial impaction and the other on laser diffraction.

Inertial impaction techniques are described in the pharmacopoeias to control, predict and assess inhaled drug performance (European Pharmacopoeia, 2008). The inertial impaction of particles is based on the movement of the aerosol cloud in an air stream and depends on aerodynamic diameter ($D_{aer}$). This can be derived from the Stroke's law and it is the diameter of a hypothetical sphere (of 1 g/cm$^3$ of density) that has the same setting velocity as the particle (Equation 5.1; Colombo *et al.*, 2012).

$$D_{aer} = \sqrt{\frac{\rho_p}{\rho_1}}\, D_g \qquad \text{Equation 5.1}$$

Where $\rho_p$ is the mass density of the particle, $\rho_1$ is the unit density and $D_g$ corresponds to the geometric diameter. Impactors separate aerosol clouds into different size ranges following the model of particle deposition in human airways. Larger aerosols carrying big momentum cannot follow the airflow of the apparatus and thus deposit into earlier chambers of the impactor. Whereas, smaller aerosols follow the airflow stream and deposit in compartments further down the impactor. Aerosol particles collide upon a solvent in impinger devices or hit the flat surface in impactor apparatus. Apart from lung deposition prediction, impactors are also used for quality control of drug formulations. The

European Pharmacopoeia describes one twin and three multistage apparatus (European Pharmacopoeia, 2008). The twin impinger was the first reported apparatus (Figure 5.1.A). It is a glass instrument where particles impinge on the liquid loaded into the device. It operates at a flow rate of 60 L/min and has a cut-off diameter of 6.4 μm. This means that particles found in the second stage correspond to the respirable portion (< 6.4 μm). On the other hand, the multi-stage liquid impinger (MSLI) has a mouthpiece attached to the aerosol device and 4 stages. The walls are made of glass, each stage contains solvent and the fifth compartment is a filter paper, which collects any remaining particles (Figure 5.1.B). The apparatus can be used at different airflows with variant cut-off diameters that depend on the airflow (Equation 5.2; Asking and Olsson, 1997).

$$D_Q = D_{Q_{ref}} \left(\frac{Q_{ref}}{Q}\right)^{1/2} \qquad \text{Equation 5.2}$$

Where $D_Q$ is the cut-off diameter to be calculated at the new flow rate (Q) and $D_{ref}$ is the cut-off diameter of reference, e.g. 60 L/min. The advantage of the MSLI over other impactors is the presence of solvent in each collection stage. This is important, as it avoids the re-entrainment phenomena where aerosol droplets are reincorporated into the airflow, particularly with DPIs. Similar to the MSLI, another apparatus named Andersen cascade is able to operate with different airflows (Equation 5.2; Figure 5.1.C). Aerosol particles with sufficient inertia impact into their specific size collector plate in the cascade and the rest follow alongside the airflow to the next stage. However, the newest impactor described in the pharmacopoeia is the next generation impactor (NGI), which is the only impactor that works horizontally and collects the aerosol droplets on cups of different cut-off diameter (Figure 5.1.D). It has seven stages and a micro orifice collector. The NGI was created in 1997 after a group of industrial researchers came together to design an apparatus that met the requirements of the pharmaceutical industry.

The data obtained using any of the multi-stage impingers or impactors can be used to calculate the aerodynamic aerosol size distribution of an aerosolised formulation. The mass median aerodynamic diameter (MMAD) of an active ingredient can also be determined. The MMAD is the diameter at which 50 % of the particles have a mass bigger than the other 50 % (European Pharmacopeia, 2005). The MMAD is determined from the log-normal distribution of the mass-weighed data calculated by plotting a log cut-off diameter against cumulative percentage undersize (United States Pharmacopoeia, 2008). However, some data may not be log-normally distributed (Lewis and Copley, 2013) but it is possible to correct for this by determining the cumulative distribution points either side and nearest to the $50^{th}$ mass percentile (Christopher *et al.*, 2013). The distribution of the particles in the apparatus is generally described by the geometric standard deviation (GSD; Equation 2.6). A GSD closer to one indicates a mono-distributed aerosol size. Fine particle fraction (FPF < 5 μm) is the fraction of the aerosol mass contained in particles with an aerodynamic diameter smaller than 5 μm and larger than 0.98 μm. On the whole, achieving a low MMAD and a GSD close to one is used to indicate a fine aerosol size and a tight size distribution. However, the aerodynamic aerosol size distribution calculated with impactor techniques can only be classified into a small number of size ranges, and the ranges depend on the number of stages within the apparatus. For example, the twin impactor possesses one cut-off diameter whereas the NGI has seven. Electrostatic charge, fine particle adhesion on the walls and losses between stages may also disturb particle collection. Moreover, impactor analysis is time consuming and is not automated.

Laser diffraction instruments have the potential to solve most of the limitations encountered in impactor analysis. They are easy-to-use and can analyse particles over a broad size range. In addition, the measurement is fast, non-flow dependent and has the facility for automatic data recording. A unique characteristic of laser diffraction methods is being able to carry out time measurements of the cloud distribution (Boer *et al.*, 2002) and analyse multi-

modal aerosol distribution (Triballier *et al.*, 2003). However, low particle concentration may lead to subtle laser obstruction so the aerosol cloud may not be able to be measured. Laser diffraction does not detect aerodynamic diameter. Instead, it measures geometric diameter in terms of mass median diameter (MMD). This value does not consider particle density and assumes that particles are spherical. Therefore, if particles are not spherical or do not have unit density, the $D_g$ value is expected to be higher than the $D_{aer}$ (Equation 5.1). Nonetheless Pilcer *et al.*, (2008) demonstrated that the data obtained with the impactors (MSLI and NGI) can be compared to the data obtained with laser diffraction techniques by a correlation factor.

Animal models have been extensible used to investigate the effect of inhaled drug therapies (Cheng *et al.*, 2008; Oller and Oberdörster, 2010). However, human airways have features that are not present in other species such as relative symmetry (Miller *et al.*, 1993). Moreover, the breathing pattern and obligate nose breathing in rodents are also distinct from humans (Sakagami, 2006; Cryan *et al.*, 2007; Nahar *et al.*, 2013). Despite those differences, Schlesinger (1985) demonstrated that the relationship between aerosol size and lung deposition in humans and animals such as dogs, rats, guinea pigs, hamsters and mice, was comparable. However, alveolar distal impaction reached a peak between 2 and 4 μm in humans whereas in the experimental animals this value was lower, at around 1 μm. Animal models provide valuable data on pharmacokinetics, therapeutic effect and toxicology for novel drug formulations. However, the differences between animals and human airways should always be taken into account, so that researchers understand that these are just preliminary screening models. Others have used mathematical models to study aerosol distribution in the airways as an alternative to *in vivo* models (Patel *et al.*, 2012). However, these methods have a high degree of complexity and sometimes are only remotely related to the physiological human lung deposition. The use of imaging techniques during *in vivo* studies improved the accurate detection of the particle deposition within the lungs. For example,

radiolabelled inhaled drugs can be detected by scintigraphy studies (Newman, 1993), positron emission tomography imaging (Pérez-Campaña *et al.*, 2014), magnetic resonance imaging (Thompson and Finlay, 2012) or fluorescent imaging (Yi *et al.*, 2012).

The principal objective of this study was to characterise what effect vibrating-mesh nebulisation would have on the pulmonary delivery of NIVs. Therefore experiments were carried out with the following aims:

- Study the effect of using vibrating-mesh nebulisers on the physicochemical properties of AmB-NIVs, using two active vibrating-mesh nebulisers (Aeroneb Go and Aeroneb Lab) and one passive vibrating-mesh nebuliser (I-neb).

- Calculate the apparent viscosity of different AmB-NIVs formulations and its effect on vibrating-mesh nebuliser performance.

- Assess the aerosol size and droplets polydispersity produced by the different nebulisers for AmB-NIVs, Cis-NIVs, Luc-NIVs and empty-NIVs.

- Determine what effect using the different vibrating-mesh nebulisers had on *in vivo* drug deposition of AmB-NIVs.

- Characterise the *in vivo* deposition of inhaled Luc-NIVs in the site of action (B16-F10-luc tumours).

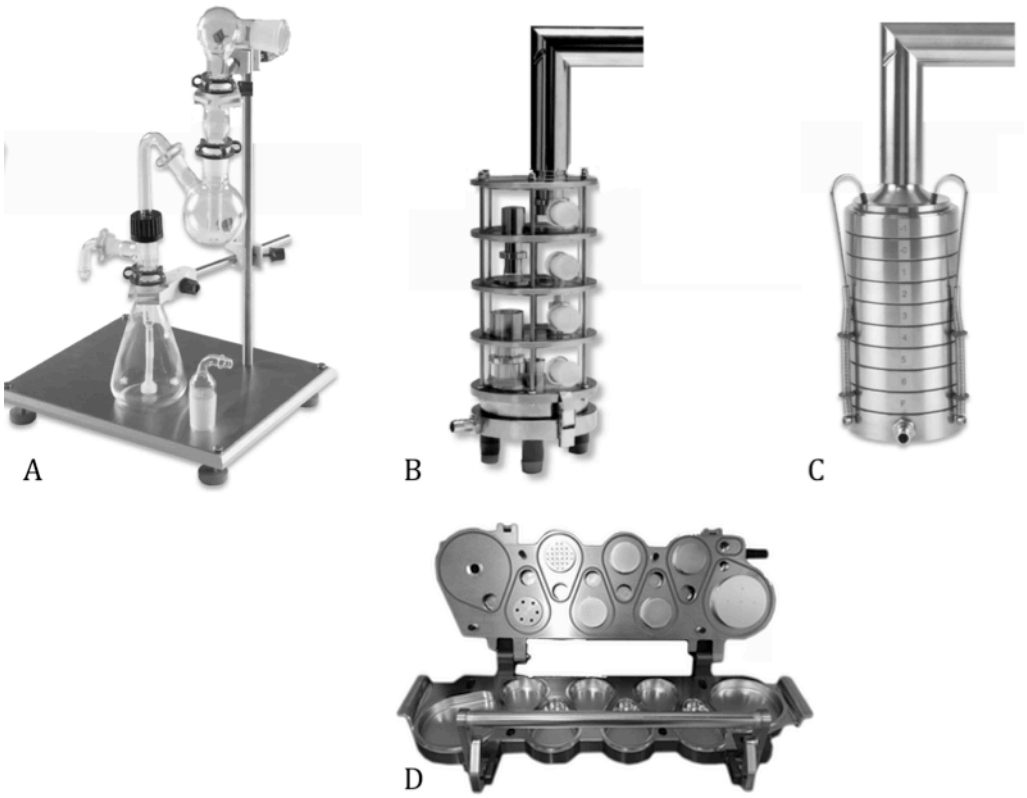


**Figure 5.1** Representations of a glass twin impinger (A), a multi-stage liquid impinger (B), an Andersen cascade impactor (C) and a next generation impactor (D). All described in detail in European-Pharmacopeia (2008; not to scale).

## 5.2. Physicochemical characteristics of NIVs upon vibrating-mesh nebulisation

The effect of vibrating-mesh nebulisation on NIVs physicochemical characteristics was studied using freshly prepared AmB-NIVs. The formulation was nebulised using two active vibrating-mesh nebulisers (Aeroneb Go and Aeroneb Lab) and one passive vibrating-mesh nebuliser (I-neb). AmB-NIVs characteristics before and after aerosolisation were compared i.e. z-average, polydispersity index, ζ-potential and entrapment efficiency (Figure 5.2).

AmB-NIVs particle size decreased significantly after nebulisation for all three vibrating-mesh nebulisers ($p \leq 0.01$; Figure 5.2.A). AmB-NIVs particles were originally 209.40 ± 2.70 nm but after nebulisation their size decreased to 169.17 ± 5.68 nm, 185.73 ± 1.50 nm or 185.47 ± 3.58 nm when nebulised with I-neb, Aeroneb Go or Aeroneb Lab respectively (mean ± SD, n=3). However, polydispersity index, vesicle charge and drug entrapment, were unaffected by nebulisation (Figure 5.2).

As discussed in Chapter 3, sucrose was added to the AmB-NIVs formulation to increase the colloidal stability of the formulations upon freeze-drying. The suspension was aerosolised with Aeroneb Go and its properties compared to the formulations without sucrose to assess whether the presence of the disaccharide affected the formulation upon nebulisation (Table 5.1). The vesicle size of AmB-NIVs with sucrose significantly lowered from 193.4 ± 3.03 nm to 170.9 ± 2.94 nm after nebulisation ($p \leq 0.01$; mean ± SD; n=3;). However, the nebulised z-average difference with AmB-NIVs containing sucrose was less pronounced than the one for AmB-NIVs without sucrose ($p \leq 0.001$; Table 5.1). Other formulation properties such as polydispersity index, ζ-potential or entrapment efficiency were similar for both AmB-NIVs formulations.

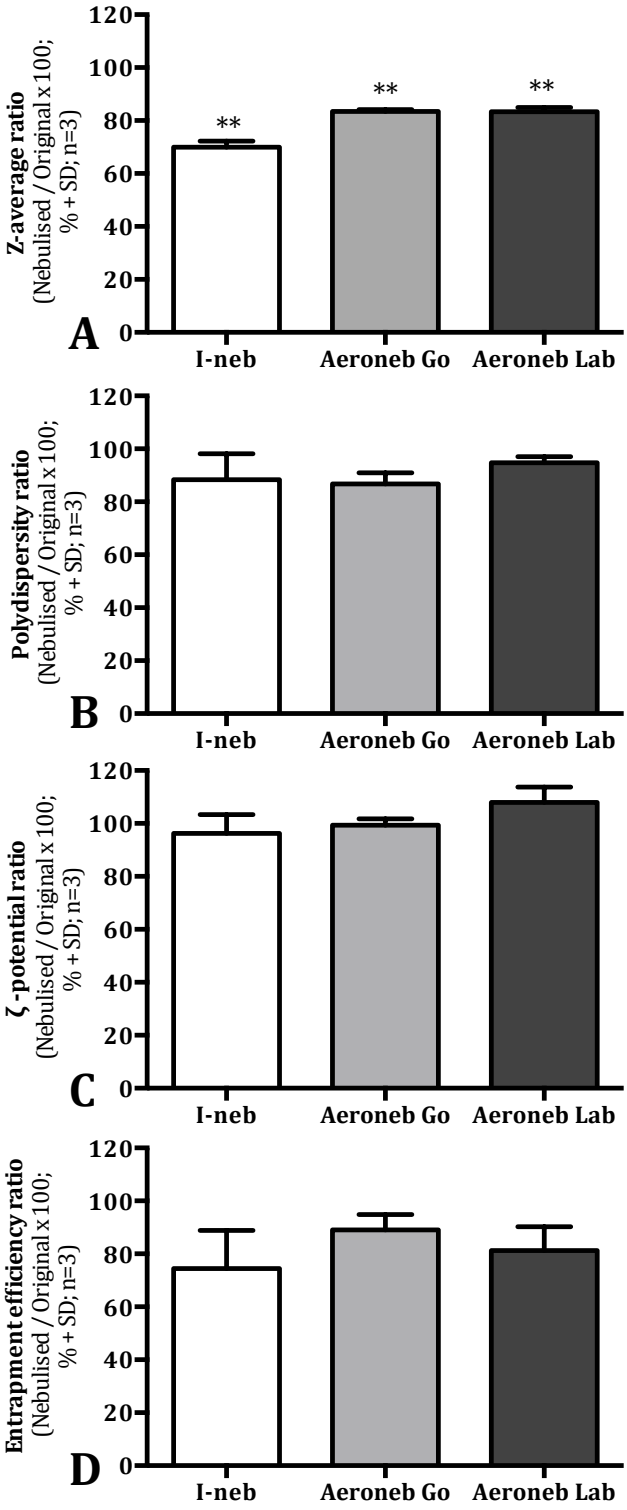


**Figure 5.2** Physicochemical changes in AmB-NIVs (0.5 mg/ml AmB, 50 mg/ml HPγCD, 75 mM lipid) upon nebulisation with I-neb (continuous mode, PL10), Aeroneb Go or Aeroneb Lab. Formulation properties before and after nebulisation were determined and are shown as a percentage of the pre-nebulisation values for z-average (A), polydispersity index (B), ζ-potential (C) and AmB entrapment efficiency (D; ** $p \leq 0.01$ compared to pre-nebulisation values).

**Table 5.1** Physiochemical properties of aerosolised AmB-NIVs (0.5 mg/ml AmB, 50 mg/ml HPγCD, 75 mM lipid) prepared with or without sucrose as a lyoprotectant (45 mg/ml sucrose). The active vibrating-mesh nebuliser Aeroneb Go was used to nebulised the formulations. Properties after nebulisation are shown as a percentage of the pre-nebulisation values for z-average, polydispersity index, ζ-potential and AmB entrapment efficiency (*** $p \leq 0.001$ compared to the formulation without sucrose).

| **Properties after nebulisation (nebulised/original x 100; % ± SD; n=3)** | **AmB-NIVs formulation** | |
|---|---|---|
| | **Without sucrose** | **With sucrose** |
| **Z-average** | 83.48 ± 0.67 | 91.46 ± 1.52*** |
| **Polydispersity index** | 86.80 ± 4.11 | 94.13 ± 5.32 |
| **ζ-potential** | 99.34 ± 2.40 | 100.35 ± 2.35 |
| **Entrapment efficiency** | 89.02 ± 5.81 | 91.83 ± 6.20 |

## 5.3. The effect of NIVs viscosity on the performance of vibrating-mesh nebulisers

During previous studies, AmB-NIVs formulation had to be diluted before it could be nebulised using the vibrating-mesh nebulisers. This suggested a strong correlation between formulation viscosity and nebuliser performance. To study this relation, AmB-NIVs were prepared at different lipid concentrations and their rheological properties studied (Table 5.2). The lipid concentration was plotted against the corresponding apparent viscosity, where distilled water was used as a blank. The results suggested that there was a strong correlation between formulation apparent viscosity and AmB-NIVs lipid concentration ($R^2$>0.99; Figure 5.3). However, other rheological properties did not vary for different lipid concentrations. There was no linear correlation between lipid concentration and flow index, consistency index or hysteresis loop ($R^2$<0.80). Therefore, AmB-NIVs were an ideal formulation to test the effect of apparent viscosity on the performance of vibrating-mesh nebulisers.

I-neb, Aeroneb Go and Aeroneb Lab were used to nebulise AmB-NIVs with different apparent viscosity profiles. The aerosol output (Equation 2.8) and percentage of drug delivered (Equation 2.9) were quantified gravimetrically. In general, the aerosol output of the three vibrating-mesh nebulisers decreased as the apparent viscosity of the formulation increased (Figure 5.4.A). AmB-NIVs formulations with an apparent viscosity greater than 2.13 mPa·s were difficult to aerosolise with aerosol outputs smaller than 0.05 ml/min for both I-neb and Aeroneb Lab nebulisers. Aeroneb Go was significantly superior at nebulising viscous samples (up to 3.25 mPa·s; $p \leq 0.01$). However, AmB-NIVs formulations with a viscosity higher than 3.25 mPa·s were nebulised with difficulty with the Aeroneb Go as well as the other nebulisers. The aerosol output for distilled water was similar for all the studied nebulisers (Figure 5.4.A).

The percentage of drug delivered for all three nebulisers, increased with the viscosity up to 2.13 mPa·s (Figure 5.4.B). More viscous samples were delivered with difficulty, especially by the I-neb. Aeroneb Lab delivered a significantly higher percentage of drug formulations with an apparent viscosity of up to 2.13 mPa·s ($p \leq 0.05$, Figure 5.4.B). The results for drug delivered using very viscous formulations (≥ 3.25 mPa·s) were not reliable since very little aerosol was produced.

**Table 5.2** Rheology flow characteristics of different AmB-NIVs formulations. A stock suspension of AmB-NIVs (1 mg/ml AmB, 100 mg/ml HPγCD, 150 mM lipid) was diluted with water to obtain the different samples. Distilled water was used to calculate null lipid concentration values (n=3).

| Lipid concentration (mM) | Apparent viscosity (mPa·s ± SD) | Flow index (± SD) | Consistency index, K (mPa·s ± SD) | Hysteresis loop (Pa/s ± SD) |
|---|---|---|---|---|
| **150** | 8.92 ± 0.11 | 0.91 ± 0.00 | 16.79 ± 6.88 | 279.25 ± 51.55 |
| **100** | 4.53 ± 0.09 | 0.94 ± 0.01 | 6.88 ± 0.36 | 313.25 ± 51.27 |
| **75** | 3.25 ± 0.17 | 0.93 ± 0.01 | 5.40 ± 0.14 | 367.20 ± 18.81 |
| **50** | 2.13 ± 0.17 | 0.88 ± 0.00 | 4.65 ± 0.05 | 398.50 ± 9.05 |
| **30** | 1.54 ± 0.01 | 0.83 ± 0.01 | 5.07 ± 0.30 | 415.25 ± 0.92 |
| **0** | 0.93 ± 0.00 | 0.72 ± 0.02 | 6.14 ± 0.26 | 448.60 ± 1.56 |

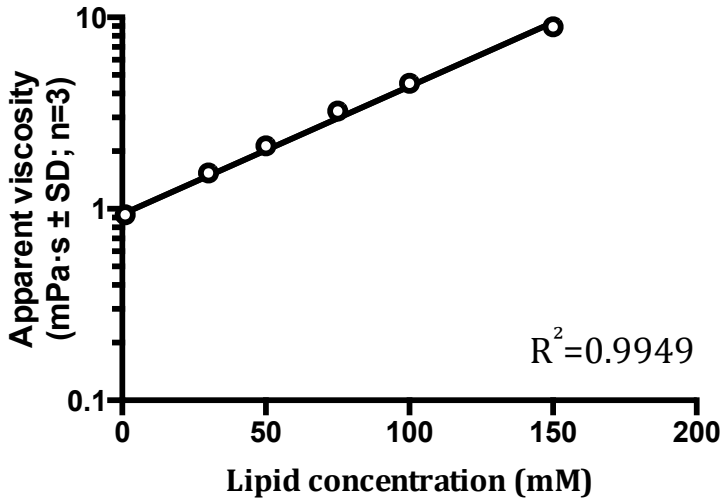


**Figure 5.3** Relation between AmB-NIVs lipid concentration and apparent viscosity. A stock suspension of AmB-NIVs (1 mg/ml AmB, 100 mg/ml HPγCD, 150 mM lipid) was diluted with water to obtain the different samples. Distilled water was used as control solution. The apparent viscosity was calculated from the apex curve of the formulation rheogram. Data was fitted using a linear regression by the least mean squares method and the correlation coefficient $R^2$, for the fitted line is shown.

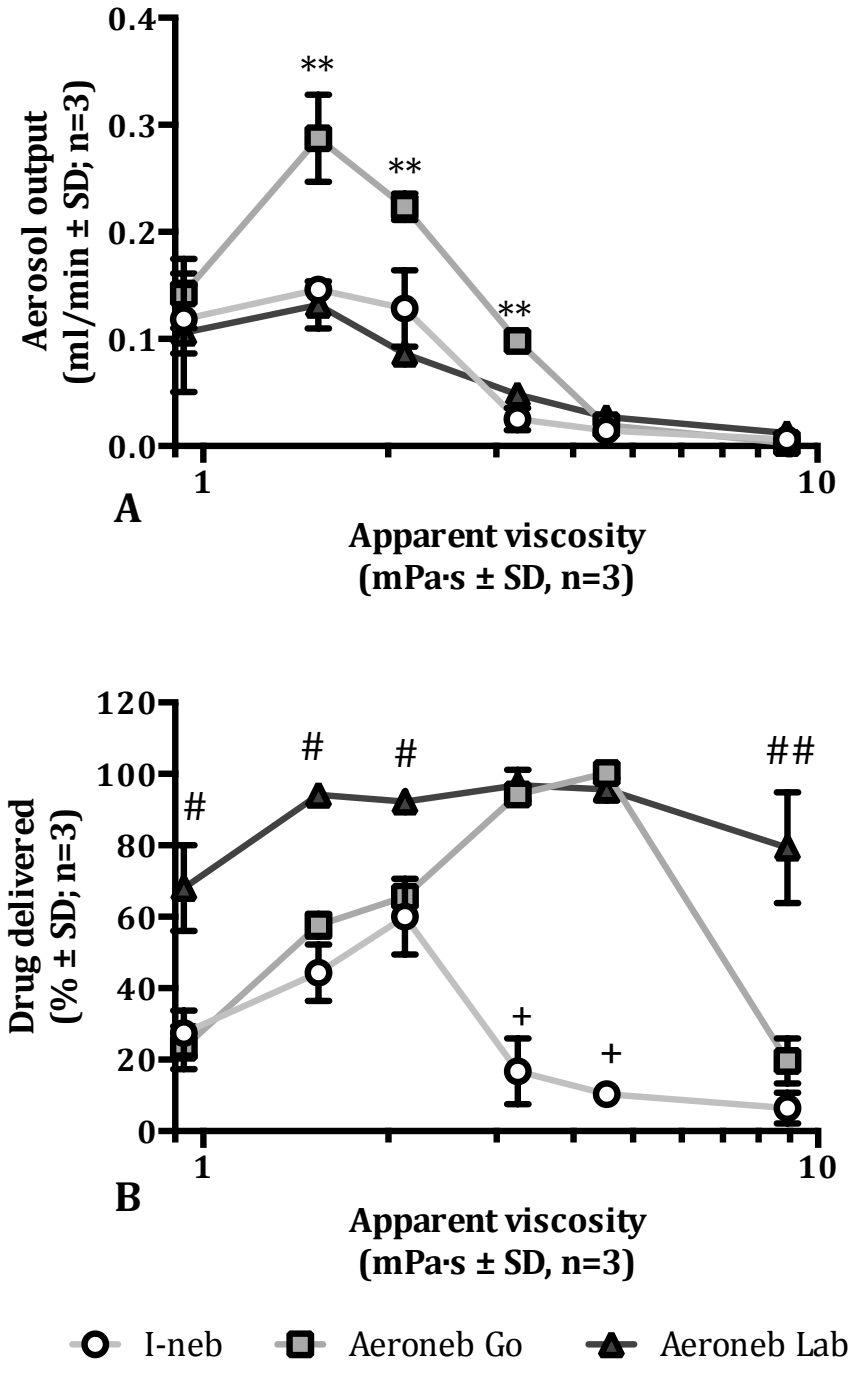


**Figure 5.4** Aerosol output (A) and percentage of drug delivered (B) associated to different vibrating-mesh nebulisers (I-neb continuous mode PL10, Aeroneb Go or Aeroneb Lab) affected by apparent viscosity. AmB-NIVs formulations described in Table 5.2 and Figure 5.3 were nebulised, including distilled water as blank. The performances of the three vibrating-mesh nebulisers were compared between them ($^{\#}$ $p \leq 0.05$, $^{\#\#}$ $p \leq 0.01$ for Lab; ** $p \leq 0.01$ for Aeroneb Go and $^{+}$ $p \leq 0.05$ for I-neb).

## 5.4. NIVs aerosol size analysis

Examples of the aerosol cumulative distribution and calculation of MMAD, FPF < 5 μm and GSD with NGI or MSLI are shown in Figure 5.5. Accurate calculation of MMAD and GSD using the MSLI apparatus was sometimes infeasible as none of the percentage undersize passed near to the 50 or 15.87 mass percentile (Figure 5.5.B). Therefore, the values obtained from the MSLI analysis were centred on FPF < 5 μm. The aerosol diameter of nebulised AmB, cisplatin, luciferin and empty-NIVs formulations were measured when aerosolised with active or passive vibrating-mesh nebulisers.

For AmB formulations, the aerosol size diameter was calculated using a NGI (MMAD, Figure 5.6) a laser diffraction instrument (MMD; Figure 5.7) and a MSLI (FPF < 5 μm; Table 5.3). When AmB-CD was nebulised in a NGI, the MMAD for the I-neb nebuliser was higher than that of the active vibrating-mesh nebulisers ($p \leq 0.001$; Figure 5.6.A); i.e. Aeroneb Go and Aeroneb Lab produced smaller AmB-CD aerosol particles than the I-neb. Similarly, AmB-NIVs had a smaller MMAD when nebulised with the active vibrating-mesh nebulisers compared to the I-neb ($p \leq 0.001$; Figure 5.6.A). The GSD polydispersity indexes of AmB formulations (AmB-CD and AmB-NIVs) were similar for the three nebulisers (Figure 5.6.B). On the other hand, results obtained using laser diffraction device also showed that the Aeroneb Go produced AmB-CD aerosol particles that were significantly smaller with those produced using the I-neb (MMD; $p \leq 0.05$; Figure 5.7.A). However, no difference in MMD values was observed for AmB-NIVs nebulised with both types of nebuliser. Noticeably, higher span polydispersity values were related to Aeroneb Go nebulising both AmB-CD and AmB-NIVs compared to the I-neb ($p \leq 0.01$ for AmB-CD and $p \leq 0.01$ for AmB-NIVs; Figure 5.7.B). The polydispersity values for Aeroneb Go aerosols in the laser diffraction distribution graphs had a double peak, suggesting dual size dispersion (data not shown). AmB formulations were also aerosolised into a MSLI so that the FPF < 5 μm for different vibrating-mesh nebulisers could be

compared. Based on the FPF < 5 μm obtained, the Aeroneb Go was superior at nebulising both AmB-CD and AmB-NIVs ($p \leq 0.01$ and $p \leq 0.05$ respectively, Table 5.3). Overall, no difference between aerosol properties was observed when AmB was nebulised in the CD complex form or encapsulated within the NIVs carrier i.e. MMAD, MMD and FPF < 5 μm were similar for both AmB-CD and AmB-NIVs.

The speed at which the aerosol was produced could be modified with the I-neb vibrating-mesh nebuliser as the device had various disks with different power levels (PL). The aerosol generated per minute was significant higher if a PL of 10 rather than a PL6 was used ($p \leq 0.05$; Table 5.4). Nonetheless the aerosol output did not influence the aerodynamic properties of AmB-NIVs and the MMAD and GSD values were similar using either PL setting (Table 5.4).

The influence of AMB-NIVs vesicles size on aerosol size was also investigated. It is important to note that AmB-NIVs particle size (in the nanometre range) is a different concept from the aerosol diameter (in the micrometre range). AmB-NIVs with a vesicle size of 200 nm or 700 nm were nebulised using the I-neb and the characteristics of the aerosol determined using a NGI or a laser diffraction instrument. Both methods showed that the two formulations had similar aerodynamic (MMAD) or geometric (MMD) aerosol diameters (Figure 5.8.A). The only difference observed was in the aerosol polydispersity sizes, where the larger vesicles had significantly higher aerosol cloud dispersity, both for GSD or span values ($p \leq 0.05$ for GSD, $p \leq 0.001$ for span; Figure 5.8.B).

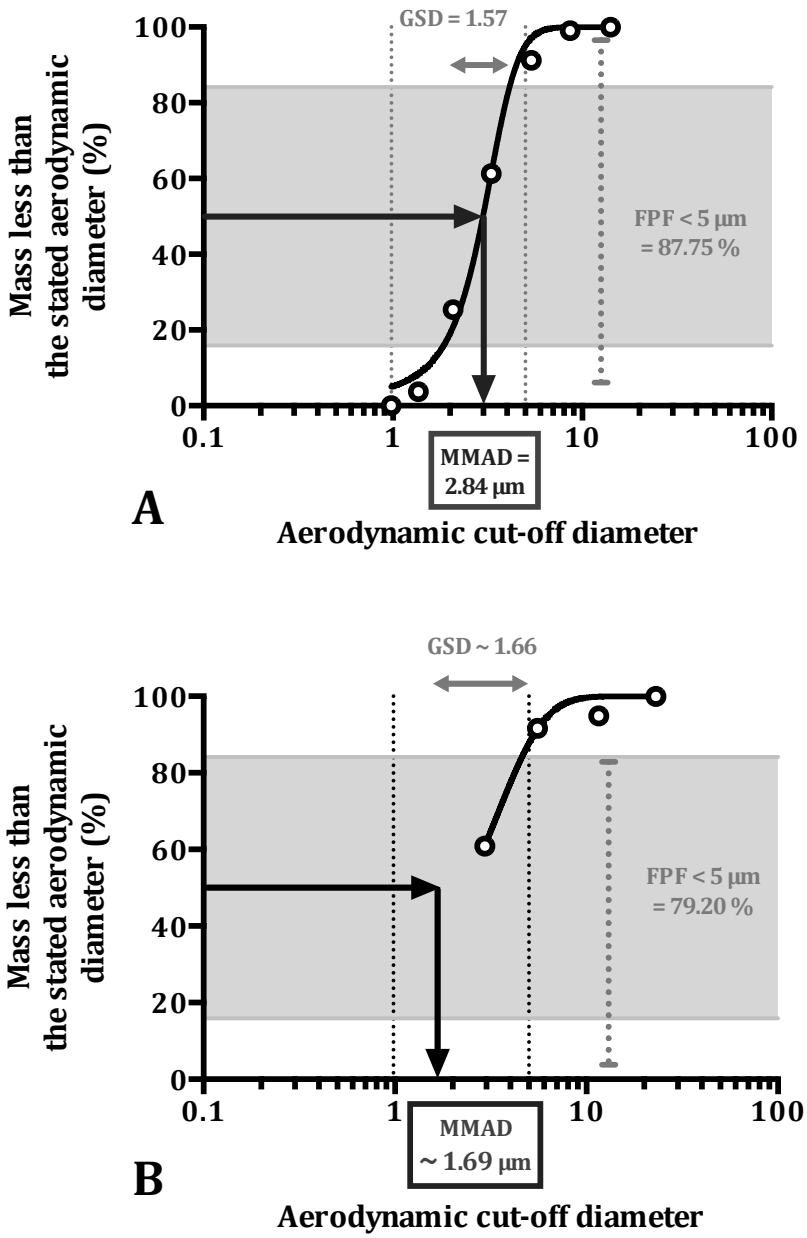


**Figure 5.5** Examples of aerosol cumulative distribution related to the aerodynamic diameter for AmB-NIVs nebulised with Aeroneb Go to a NGI (A) or to a MSLI (B). The mass median aerodynamic diameter (MMAD) was calculated by plotting a base ten-logarithm cut-off diameter against cumulative percentage undersize and determined the interpolation of the 50$^{th}$ mass percentile. The calculation of MMAD is represented in the graphs with a black continuous arrow. The geometric standard distribution (GSD) is calculated using Equation 2.6 and stated in the graph in a grey coloured area and arrow. Fine particle fraction (FPF < 5 µm) is the fraction of the aerosol mass contained in particles with an aerodynamic diameter smaller than 5 µm and bigger than 0.98 µm, represented in the graph with a dotted line. MMAD and GSD for MSLI (B) are calculated by approximation as no percentage undersize passes near to the 50 or 15.87 mass percentile (n=1).

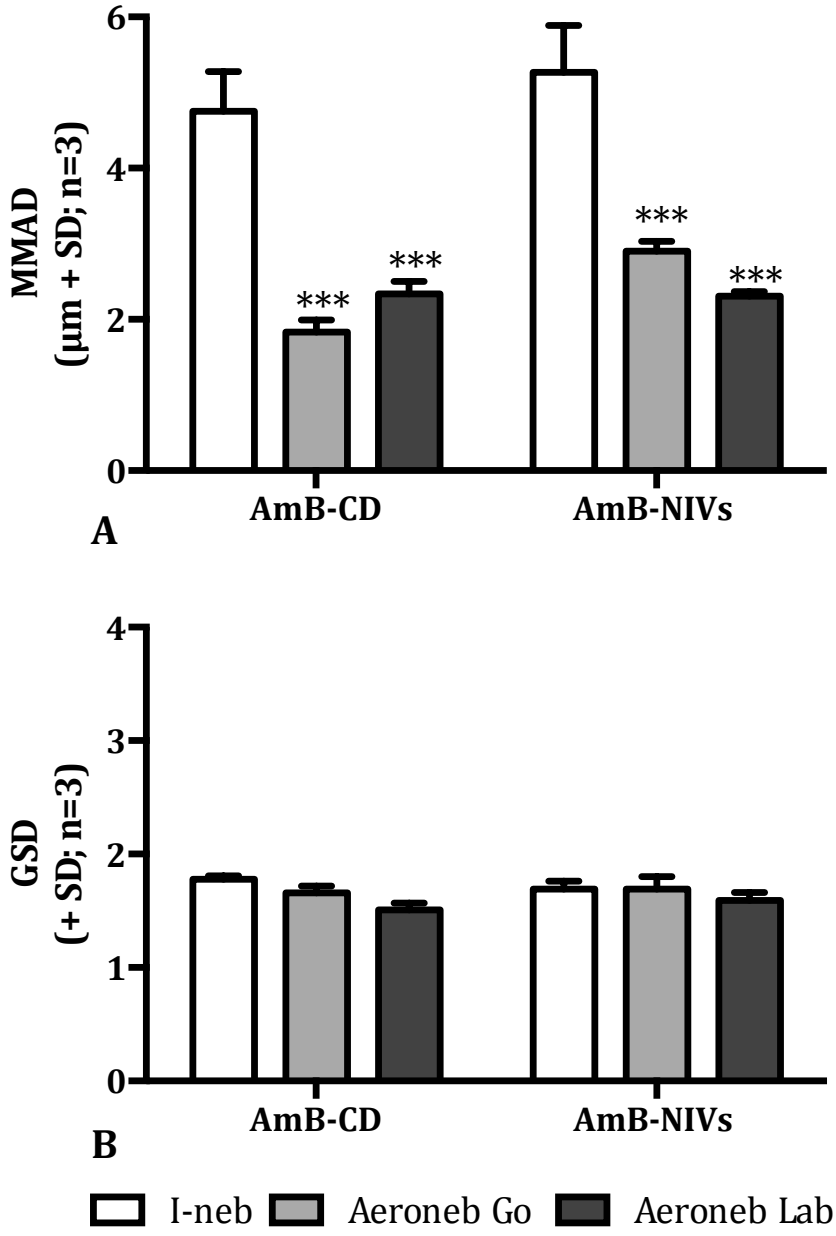


**Figure 5.6** NGI aerodynamic aerosol size analysis for AmB formulations. AmB-CD (0.5 mg/ml AmB, 50 mg/ml HPγCD) and AmB-NIVs (0.5 mg/ml AmB, 50 mg/ml HPγCD, 75 mM lipid) were nebulised with I-neb (continuous mode, PL10), Aeroneb Go and Aeroneb Lab. MMAD (A) and GSD (B) calculated after sample nebulisation in a NGI set up at a flow rate of 15 L/min (MMAD, mass median aerodynamic diameter; GSD, geometric standard deviation; NGI, new generator impactor; *** $p \leq 0.001$ compared to I-neb).

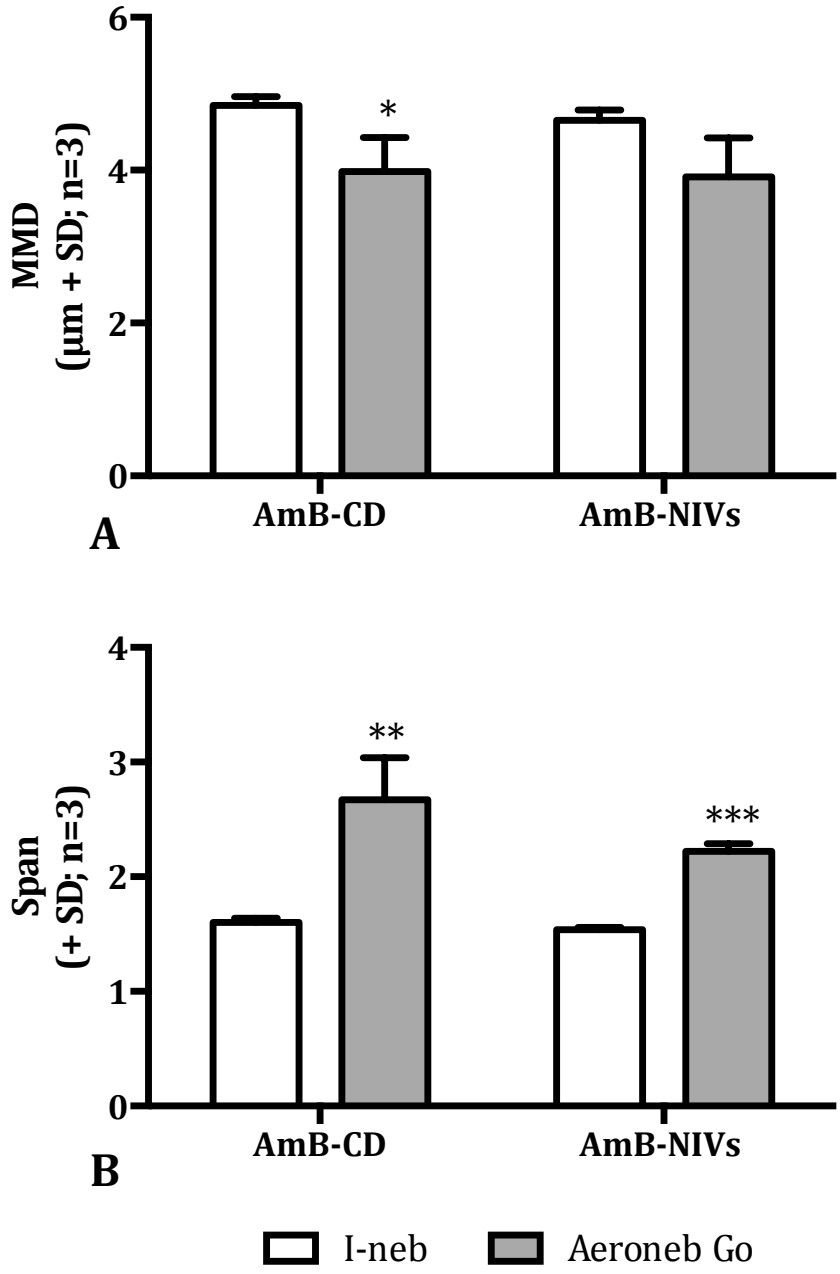


**Figure 5.7** Geometric aerosol size of AmB formulations. AmB-CD (0.5 mg/ml AmB, 50 mg/ml HPγCD) and AmB-NIVs (0.5 mg/ml AmB, 50 mg/ml HPγCD, 75 mM lipid) were nebulised with I-neb (continuous mode, PL10) and Aeroneb Go. MMD (A) and span (B) calculated after sample nebulisation to a laser diffraction instrument with an output flow vacuum of 15 L/min (MMD, mass median diameter; * $p \leq 0.05$, ** $p \leq 0.01$, *** $p \leq 0.001$ compared to I-neb).

**Table 5.3** MSLI aerodynamic aerosol size analysis of AmB formulations. AmB-CD (0.5 mg/ml AmB, 50 mg/ml HPγCD) and AmB-NIVs (0.5 mg/ml AmB, 50 mg/ml HPγCD, 75 mM lipid) were nebulised with I-neb (continuous mode, PL10), Aeroneb Go and Aeroneb Lab. FPF < 5 µm calculated after sample nebulisation in a MSLI set up at a flow rate of 20 L/min (MSLI, multi-stage liquid impinger; FPF < 5 µm, fine particle fraction; * $p \leq 0.05$, ** $p \leq 0.01$ compared to I-neb).

| Vibrating-mesh nebulisers | FPF < 5 µm (% ± SD; n=3) | |
|---|---|---|
| | AmB-CD | AmB-NIVs |
| **I-neb** | 62.83 ± 6.61 | 65.23 ± 4.30 |
| **Aeroneb Go** | 86.48 ± 3.27 ** | 82.87 ± 4.58 * |
| **Aeroneb Lab** | 64.33 ± 7.11 | 66.73 ± 3.85 |

**Table 5.4** AmB-NIVs aerodynamic properties of the formulation nebulised with different speed outputs. AmB-NIVs (0.5 mg/ml AmB, 50 mg/ml HPγCD, 75 mM lipid) was nebulised into a NGI with an I-neb vibrating-mesh nebuliser with a PL10 and a PL6 disk. Aerosol output, MMAD and GSD were calculated after sample nebulisation in a NGI set up at a flow rate of 15 L/min (MMAD, mass median aerodynamic diameter; GSD, geometric standard deviation; NGI, new generator impactor; PL, power level; * $p \leq 0.05$ compared to PL10 nebulisation; n=3).

| AmB-NIVs aerodynamic properties | I-neb nebulisation speed | |
|---|---|---|
| | Faster (PL10) | Slower (PL6) |
| **Aerosol output (ml/min ± SD)** | 0.17 ± 0.03 | 0.10 ± 0.01 * |
| **MMAD (µm ± SD)** | 5.27 ± 0.62 | 5.33 ± 0.15 |
| **GSD (± SD)** | 1.69 ± 0.07 | 1.69 ± 0.03 |

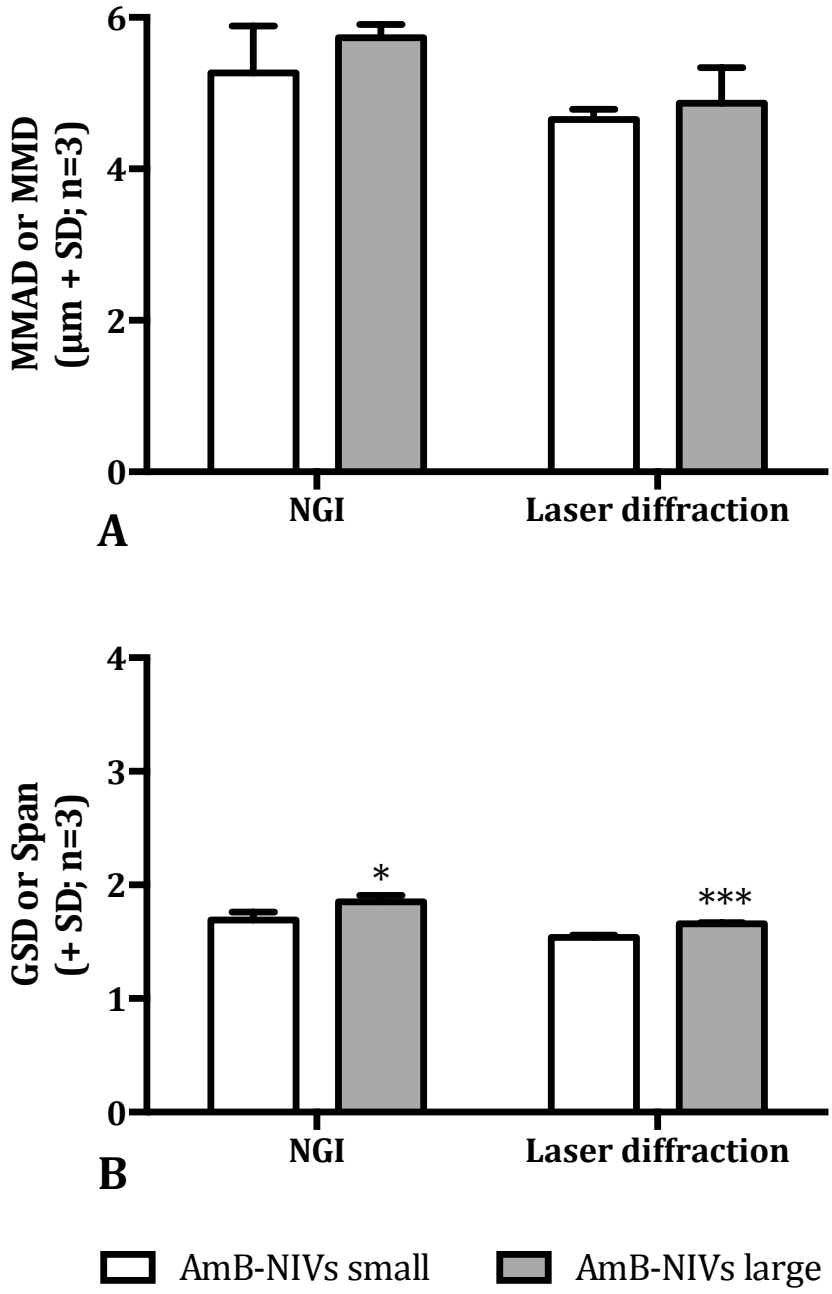


**Figure 5.8** Aerosol diameter of different AmB-NIVs formulations with different vesicle size. Small AmB-NIVs (0.5 mg/ml AmB, 50 mg/ml HPγCD, 75 mM lipid; 205.1 ± 1.4 nm) and large AmB-NIVs (0.5 mg/ml AmB, 50 mg/ml HPγCD, 75 mM lipid; 655.8 ± 40.9 nm) were nebulised into a NGI and a laser diffraction instrument with an I-neb (continuous mode, PL10). The correspondent MMAD (for the NGI) and MMD (for the laser diffraction) are represented (A). The aerosol polydispersity GSD (for the NGI) and span (for the laser diffraction) are stated (B; MMAD, mass median aerodynamic diameter; MMD, mass median diameter; GSD, geometric standard deviation; NGI, new generation impactor; * $p \leq 0.01$, *** $p \leq 0.001$ small compared to large).

The aerosol properties of nebulised cisplatin formulations were assessed with a NGI (Figure 5.9) and a laser diffraction instrument (Figure 5.10). The NGI aerodynamic size for cisplatin solution was significantly smaller when Aeroneb Lab was used to produce the aerosol compared to the I-neb or Aeroneb Go ($p \leq 0.01$; Figure 5.9.A). Both Aeroneb Go and Aeroneb Lab produced Cis-NIVs aerosols with a significantly smaller aerodynamic size than I-neb ($p \leq 0.01$ for the Aeroneb Go; $p \leq 0.01$ for the Aeroneb Lab; Figure 5.9.A). Aeroneb Go produced Cis-sol and Cis-NIVs aerosols that had a significantly higher GSD polydispersity compared to that of I-neb or Aeroneb Lab ($p \leq 0.05$; Figure 5.9.B). When the geometric aerosol size of cisplatin solution for the different nebulisers was determined, I-neb produced a smaller geometric aerosol size compared to Aeroneb Go ($p \leq 0.001$; Figure 5.10.A). However, the geometric MMD for Cis-NIVs was similar for both vibrating-mesh nebulisers (Figure 5.10.A). The span polydispersity index for Cis-NIVs nebulised with Aeroneb Go, was significantly higher than the value obtained for the I-neb ($p \leq 0.05$; Figure 5.10.B). No span differences were observed between Aeroneb Go and I-neb when Cis-sol was nebulised. In contrast with the results for AmB formulations, cisplatin formulations had a different aerosol size for cisplatin solution and Cis-NIVs, especially when aerosolised with Aeroneb Go, i.e. Aeroneb Go produced smaller aerosol particles for Cis-NIVs than for Cis-sol ($p \leq 0.05$; both aerodynamic and geometric sizes).

The aerosol cloud size for luciferin formulations was measured using the MSLI. The FPF < 5 μm for luciferin solution aerosols was similar regardless of the nebuliser used. However, the FPF < 5 μm obtained for Luc-NIVs was higher for the I-neb compared to Aeroneb Go or Aeroneb Lab ($p \leq 0.01$; Table 5.5).

The MMAD associated for each individual component of the NIVs formulation (cholesterol, surfactant and DCP) was determined by nebulising empty-NIVs and measuring the amount of each constituent in the compartments of the NGI (Figure 5.11). The aerosol size associated with empty-NIVs was higher than the

desired 5 μm cut off. However, the aerodynamic aerosol size calculated for each individual constituent of the NIVs formulations had a similar MMAD (Figure 5.11.A). The type of nebuliser used did not impact on results, as a similar aerodynamic aerosol size was observed using I-neb or Aeroneb Go. However, the Aeroneb Go gave an aerosol with a significantly higher GSD polydispersity values than the I-neb for the three constituents ($p \leq 0.001$ for cholesterol; $p \leq 0.01$ for surfactant; $p \leq 0.05$ for DCP; Figure 5.11.B). In addition, the geometric aerosol size of empty-NIVs nebulised using an I-neb into a laser diffraction instrument was 6.47 ± 0.34 μm (MMD ± SD) and the formulation had a span of 1.14 ± 0.08.

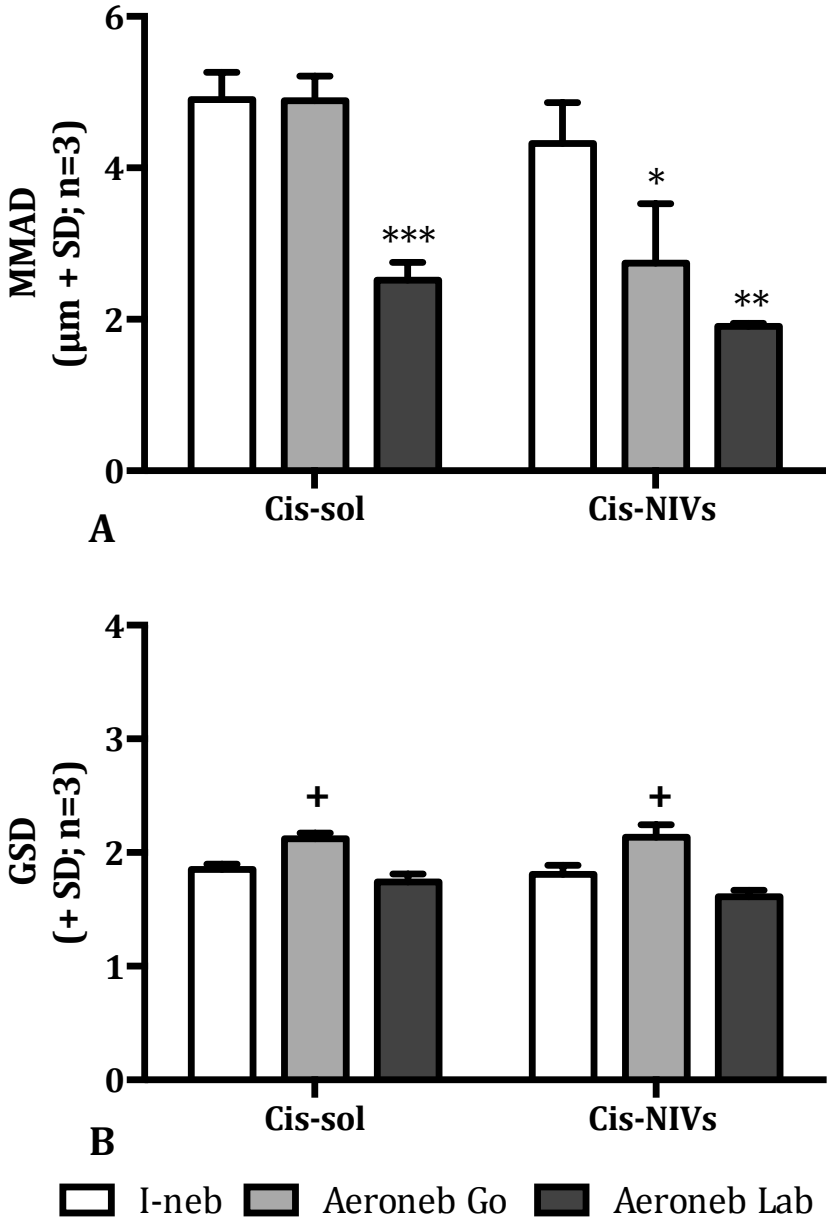


**Figure 5.9** NGI aerodynamic size analysis of cisplatin formulations. Cis-sol (0.5 mg/ml cisplatin in 0.9 % w/v NaCl) and Cis-NIVs (freeze-dried empty-NIVs, 62 mM lipid, rehydrated with 0.5 mg/ml cisplatin in 0.9 % w/v NaCl) were nebulised with I-neb (continuous mode, PL10), Aeroneb Go and Aeroneb Lab. MMAD (A) and GSD (B) calculated after sample nebulisation in a NGI set up at a flow rate of 15 L/min (MMAD, mass median aerodynamic diameter; GSD, geometric standard deviation; NGI, new generator impactor; * $p \leq 0.05$, ** $p \leq 0.01$ and *** $p \leq 0.001$ compared to I-neb, $^{+}$ $p \leq 0.05$ compared to I-neb and Aeroneb Lab).

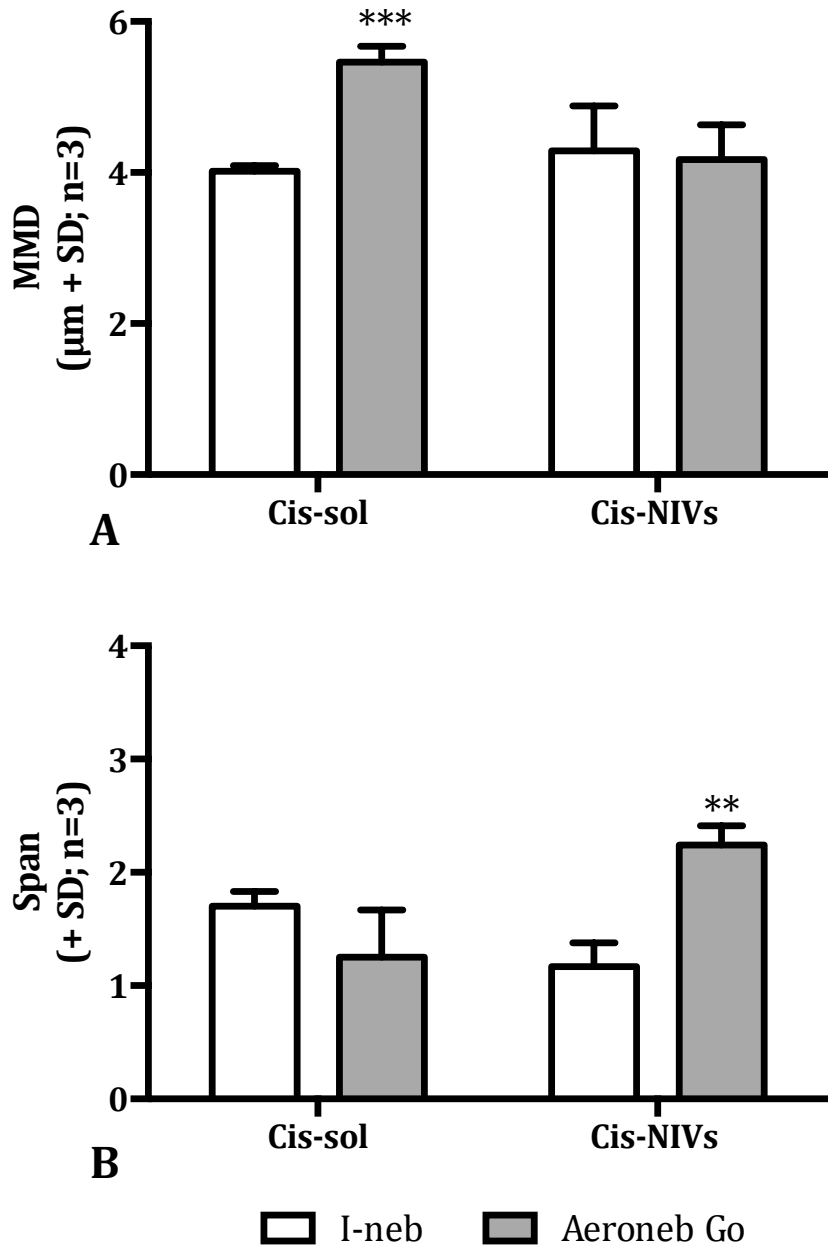


**Figure 5.10** Geometric aerosol size of cisplatin formulations. Cis-sol (0.5 mg/ml cisplatin in 0.9 % w/v NaCl) and Cis-NIVs (freeze-dried empty-NIVs, 62 mM lipid, rehydrated with 0.5 mg/ml cisplatin in 0.9 % w/v NaCl) were nebulised with I-neb (continuous mode, PL10) and Aeroneb Go. MMD (A) and span (B) calculated after sample nebulisation to a laser detection method with an output flow vacuum of 15 L/min (MMD, mass median diameter; ** $p \leq 0.01$, *** $p \leq 0.001$ compared to I-neb).

**Table 5.5** MSLI aerodynamic particle analysis for luciferin formulations. Luc-sol (4.35 mg/ml Luc dissolved with PBS pH 7.4) and Luc-NIVs (freeze-dried empty-NIVs, 75 mM lipid, rehydrated with 4.35 mg/ml Luc dissolved with PBS pH 7.4) were nebulised with I-neb (continuous mode, PL10), Aeroneb Go and Aeroneb Lab. FPF < 5 µm calculated after sample nebulisation in a MSLI set up at a flow rate of 20 L/min (MSLI, multi-stage liquid impinger; FPF, fine particle fraction < 5 µm; ** $p \leq 0.01$ compared to I-neb).

| **Vibrating-mesh nebulisers** | **FPF < 5 µm (% ± SD; n=3)** | |
|---|---|---|
| | **Luc-sol** | **Luc-NIVs** |
| **I-neb** | 51.00 ± 1.73 | 83.33 ± 0.27 |
| **Aeroneb Go** | 31.33 ± 17.95 | 59.07 ± 4.65 ** |
| **Aeroneb Lab** | 50.40 ± 6.50 | 63.87 ± 6.85 ** |

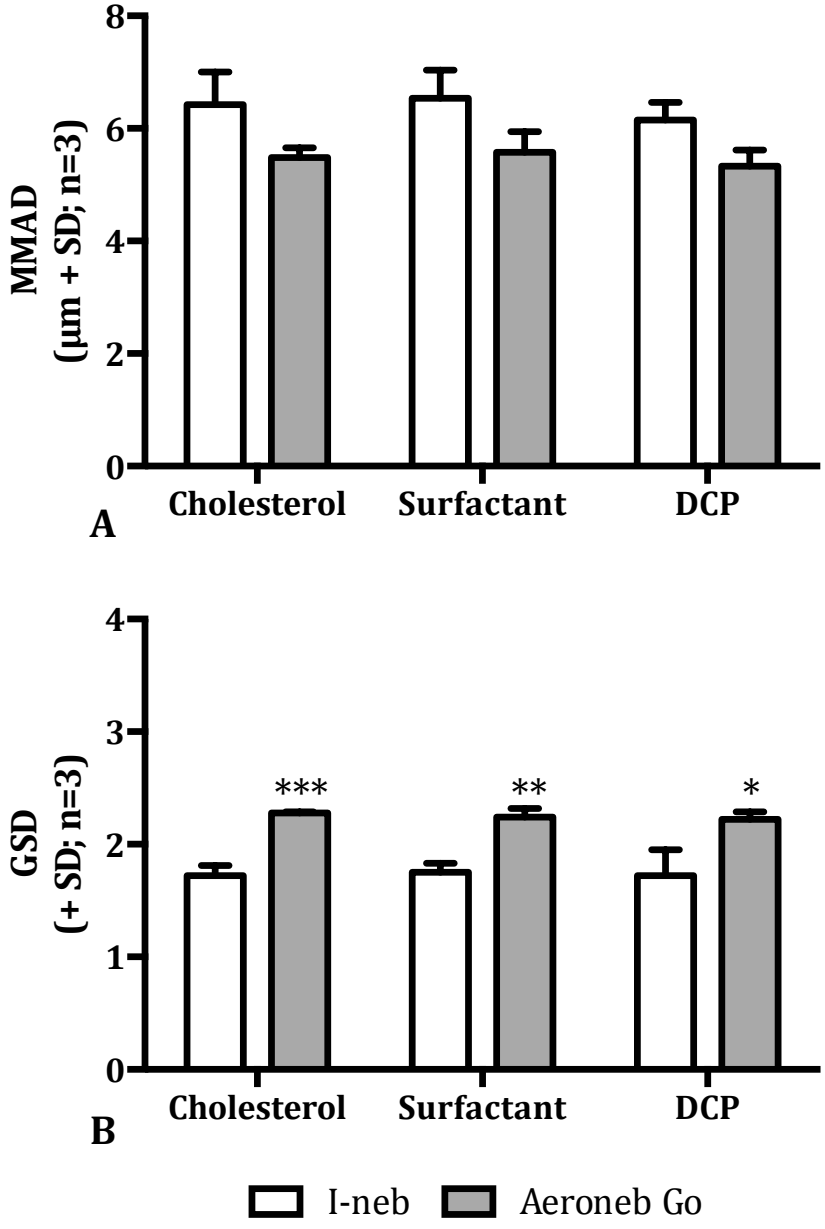


**Figure 5.11** NGI aerodynamic size analysis of empty-NIVs components: cholesterol, tetra-ethylene glycol mono hexadecyl ether (surfactant) and dicetyl phosphate (DCP). Freeze-dried empty-NIVs (62 mM lipids) were rehydrated with distilled water and nebulised with I-neb (continuous mode, PL10) or Aeroneb Go to a NGI set up at a flow rate of 15 L/min. Recovered samples were analysed with HPLC-ELSD method (MMAD, mass median aerodynamic diameter; GSD, geometric standard deviation; NGI, new generator impactor; * $p \leq 0.05$, ** $p \leq 0.01$ and *** $p \leq 0.001$ compared to I-neb).

## 5.5. *In vivo* delivery of NIVs using different vibrating-mesh nebulisers

The *in vivo* inhalation performance of I-neb, Aeroneb Go and Aeroneb Lab were investigated *ex situ* nebulising AmB-NIVs into healthy rats followed by HPLC analysis of organs. In that study, no detectable AmB levels were observed in the liver, brain, spleen, kidney or plasma of the treated subjects (data not shown). However, AmB was detected in the trachea and the lungs (Table 5.6). Rats treated with AmB formulations using the I-neb, Aeroneb Go and Aeroneb Lab had no different amounts of AmB in their trachea. However, rats treated using the I-neb had significantly higher amounts of AmB in their lungs compared to rats treated by inhalation using the Aeroneb Go ($p \leq 0.05$; Table 5.6). The amount of AmB detected in the organs was compared to the quantity of drug nebulised. Less than 1 % of the AmB nebulised was detected in the lungs and trachea of the treated rats. Rats treated using the I-neb presented higher percentage of drug in their lungs compared to the other nebulisers ($p \leq 0.05$; Table 5.6).

Similar studies were also carried out using mice inoculated with B16-F10-luc cells and treated with Luc-NIVs. In this case, the amount of luciferin inhaled was quantified both *in situ* and *ex vivo*. Similar amounts of BLI were present in the lung region of all groups of mice (Table 5.7). However, *ex vivo* imaging showed that the lungs of mice treated using the Aeroneb Go had significantly higher amounts of BLI compared to the control background group ($p \leq 0.05$; Table 5.7). In opposite, no differences were observed for the group that had Luc-NIVs nebulised with the I-neb and the control group. The amount of BLI present in the lungs before incubation in Luc-sol (BLI associated with *in vivo* luciferin delivery) and after (total amount of BLI) was used to calculate the percentage of BLI activated after Luc-NIVs inhalation. Based on this parameter, similar percentage of BLI was activated with both nebulisers delivering Luc-NIVs (Table 5.7).

**Table 5.6** AmB levels in the trachea and lungs of rats treated with inhaled AmB-NIVs (0.25 mg/ml AmB, 25 mg/ml HPγCD, 37.5 mM lipid; 1 mg/ml AmB/kg) and the percentage of AmB related to the amount of drug administered. AmB-NIVs formulation was nebulised with I-neb (continuous mode, PL6), Aeroneb Go or Aeroneb Lab, all with similar adapted mouthpiece (Figure 2.3). Rats were euthanised after 5 minutes and organs were frozen until day of *ex situ* analysis with HPLC-UV. Levels of AmB in liver, brain, spleen, kidneys and plasma were not detected (* $p \leq 0.05$ between I-neb and Aeroneb Go).

| Vibrating-mesh nebuliser | AmB levels (ng/mg tissue ± SE; n=4) | | AmB recovered (% ± SE; n=4) | |
|---|---|---|---|---|
| | Trachea | Lungs | Trachea | Lungs |
| **I-neb** | 13.55 ± 11.51 | 1.83 ± 0.70* | 0.29 ± 0.21 | 0.73 ± 0.26* |
| **Aeroneb Go** | 0.84 ± 0.84 | 0.19 ± 0.11 | 0.05 ± 0.05 | 0.09 ± 0.05 |
| **Aeroneb Lab** | 9.36 ± 7.75 | 0.62 ± 0.19 | 0.51 ± 0.45 | 0.27 ± 0.08 |

**Table 5.7** Bioluminescence (BLI) associated to the nebulisation of Luc-NIVs (freeze-dried empty-NIVs, 50 mM lipid concentration, rehydrated with 20.8 mg/ml D-luciferin with PBS pH 7.4) to a mice model of B16-F10-luc was assessed *in situ*. B16-F10-luc were injected (5 x $10^5$ cells/mice) and twenty days after, Luc-NIVs (0.5 ml/group) were nebulised with I-neb (continuous mode and PL6) and Aeroneb Go. Luc-NIVs was also nebulised with Aeroneb Go to a healthy group of mice to obtain the control BLI values. The BLI values of the *in vivo* lung area (6 minutes after complete nebulisation), the *ex vivo* lungs BLI and the *ex vivo* lungs submerged in Luc-sol (150 µg/ml) for 10 minutes prior imaging are represented. The percentage of BLI activated was calculated as stated in Equation 2.13 (* $p \leq 0.05$ compared to control; n=4).

| Lungs parameters | Group | | |
|---|---|---|---|
| | Control | I-neb | Aeroneb Go |
| **Lung area *in vivo* (BLI x $10^5$ p/s ± SE)** | 0.35 ± 0.10 | 0.30 ± 0.10 | 1.70 ± 0.39 |
| **Lungs *ex vivo* (BLI x $10^5$ p/s ± SE)** | 0.03 ± 0.06 | 9.99 ± 6.27 | 26.87 ± 9.15* |
| **Lungs *ex vivo* with Luc (BLI x $10^5$ p/s ± SE)** | 0.04 ± 0.03 | 36.84 ± 21.67 | 110.70 ± 35.80 |
| **BLI activated (% ± SE)** | n.a | 28.92 ± 3.37 | 23.79 ± 1.11 |

## 5.6. Discussion

AmB-NIVs were successfully nebulised using both active and passive vibrating-mesh nebulisers. Nebulisation had no significant effect on AmB-NIVs polydispersity index, ζ-potential or entrapment efficiency but did cause a significant decrease in vesicle size. The vibration produced by the piezoelectric element of the nebulisers could have caused fragmentation of the particles. Due to reduction in vesicle size, the vesicular system would have thought to release some of the encapsulated drug as reported by others. Elhissi *et al.* (2007) described salbutamol sulphate liposomes that decreased in size by 45 % upon air-jet nebulisation with a consequently loss of encapsulated drug up to 88 %. Kleemann *et al.* (2007) nebulised iloprost liposomes with three different nebulisers and all of them presented a minimum decrease of vesicle size of 44 % and a loss of encapsulated drug of 50 % minimum. Nonetheless, despite the fragmentation of AmB-NIVs vesicles upon nebulisation, the drug encapsulated within the NIVs was maintained within the structure. This could be related to the lipophilic nature of AmB, as the drug may be associated to the bilayer. Therefore, even with significant vesicle disruption, very little drug was released due to poor water solubility in aqueous solutions (Alexander *et al.*, 2011).

In this study, incorporation of lyoprotectant sucrose to the AmB-NIVs formulation protected against changes in vesicle size, since only 8.54 ± 1.52 % reduction occurred compared to 16.52 ± 0.67 % decrease for the formulisation without sucrose. Therefore, the sucrose added, was believed to provide extra NIVs resistance to the shear applied by the vibrating-mesh. This results correlated with Bridges and Taylor (2001), whose liposomes containing the cryoprotectant trehalose maintained vesicle size after air-jet nebulisation better than the liposomes without the additive.

In this study, there was a linear relationship between lipid concentration and the apparent viscosity of AmB-NIVs formulations. Whereas other rheological

properties, such as flow index or hysteresis loop, were not affected by the lipid concentration. For this reason, diluted samples of AmB-NIVs were ideal to investigate the effect of apparent viscosity in the performance of vibrating-mesh nebulisers. Apparent viscosity had a direct effect on aerosol output and percentage of drug delivered in other studies (Ghazanfari *et al.*, 2007; Hardaker and Hatley, 2010; Abdelkader *et al.*, 2012). In this study, Aeroneb Go could nebulise more viscous AmB-NIVs formulations than the I-neb or Aeroneb Lab nebulisers. All three nebulisers could aerosolise AmB-NIVs formations with a viscosity up to 2.13 mPa·s. Thicker NIVs formulations could be nebulised but there was intermittent production of an aerosol, or in some cases, the device simply stopped. This relation is particularly important when vesicular formulations are nebulised, like NIVs or liposomes, as these generally present higher levels of viscosity compared to the drug in solution. Therefore, when developing a nano-vesicle formulation for vibrating-mesh nebulisation, the apparent viscosity of the final product should be taken into consideration.

Aerosol droplet size between 1 and 5 μm are in the optimal range to reach the lower respiratory airways (Byron, 1986). The aerodynamic aerosol diameter of AmB-NIVs nebulised with I-neb was slightly outside the desirable 5 μm limit by *circa* 0.3 μm. However the aerosol size of AmB-NIVs nebulised with either Aeroneb Go or Aeroneb Lab was within the advisable range. Those differences observed in the MMAD were not observed with the MMD detected by laser diffraction (all nebulised < 5 μm MMD). The speed at which the aerosol was produced with the I-neb did not influence the aerodynamic diameter of the nebulised AmB-NIVs. Moreover, formulations with vesicle size in the range of 200 nm to 700 nm did not affect the final aerosol MMAD or MMD. However, higher aerosol dispersity levels were related to larger AmB-NIVs vesicles. Cipolla *et al.* (2013) extensible reviewed vesicular formulations used for inhaled therapy with different particle size. They observed a correlation between high vesicle particle size and high aerosol droplet diameter with special difference observed between nanometre and micrometre range (Elhissi *et al.*, 2007).

Therefore, AmB-NIVs vesicles between 200 nm and 700 nm, might have not been different enough to present variation in aerosol particle size but it might have been enough to provide deviation in aerosol polydispersity values.

The results of this study indicated that the aerosol size produced for Cis-NIVs were all below the 5 μm limit. The two active vibrating-mesh nebulisers produced smaller MMAD than the I-neb. However, this difference was not found for the geometric diameter of the aerosols droplets. In the case of Luc-NIVs, the I-neb produced an aerosol with the largest fine particle fraction of the three nebulisers used in this study.

The MMAD for the individual ingredient of the NIVs were also determined. These were obtained using the HPLC validated to quantify the different constituents of NIVs and the ability to separate the aerosol droplet into specific particles ranges using the NGI. All three ingredients had a similar MMAD, indicating that NIVs travelled as a single unit through the air stream. Moreover, no difference in aerodynamic aerosol size of empty-NIVs was observed between I-neb and Aeroneb Go, although the latest presented higher polydispersity values. To our knowledge, individual MMAD for each component of a vesicular system has never been calculated before. Other studies, only determine the aerosol properties of the whole carrier entity, normally using a laser diffraction technique (Bridges and Taylor, 1998). Investigating the aerosol size for each single component could be another way to assess vesicle stability of inhaled drug vesicular systems. The aerosol particles associated to freeze-dried empty-NIVs rehydrated with water, were higher than the optimal 5 μm. On the other hand, when those freeze-dried empty-NIVs were rehydrated with cisplatin, the aerosol size decreased to desirable values. These differences could be an indication of bimodal distribution of the formulation to the lungs, perhaps related to the unentrapped and entrapped drug within the formulation. This is similar to the ciprofloxacin liposomes investigated by Serisier *et al.* (2013). A dual model provided by the presence of free ciprofloxacin along the entrapped

one, was proven to be clinically beneficial as an initial high peak was followed by sustained drug release.

Impactor systems, such as MSLI and NGI, are used to determine aerodynamic size to indicate drug deposition in the respiratory system. In this study, FPF < 5 μm data obtained using the NGI and MSLI were similar for most of the studied formulations. This is consistent with studies reported by Pilcer *et al.*, (2008). Only one formulation gave different results and this was for AmB-NIVs nebulised with I-neb. Where a significant higher FPF < 5 μm was detected using the MSLI compared to the NGI (data not shown). This difference is probably related to the fewer sections within the MSLI (4 in the MSLI *vs* 7 in the NGI), so that there is less discrimination between cut-off diameters for the MSLI. Thus the MSLI has broader cut-off ranges and therefore the calculated FPF < 5 μm or MMAD are less accurate than the NGI. The MSLI was originally designed to test pMDIs and DPIs at a higher airflow (i.e. 60 L/min) that the required for nebulisation (Taki *et al.*, 2010; Wong *et al.*, 2010). When the MSLI is used at 60 L/min the cut-off diameter of the four stages are 13.3, 6.7, 3.2 and 1.7 μm. However, when the MSLI is used at a lower flow rate, which is essential to simulate nebulisation tidal breathing, the cut-off diameter ranges increased. For example, at 20 L/min the cut-off diameter of the four stages was 23.0, 11.6, 5.5 and 2.9 suggesting that only droplets on stage 4 were in the desirable respiratory range. This also jeopardized the calculation of MMAD and GSD since the equation could not always be applied. These limitations were encountered in the present study, thence the representation of aerodynamic aerosol size for the MSLI as a FPF < 5 μm and not as an approximate MMAD. This issue was solved with the incorporation of more stages in later generations impactors. For example, the NGI at tidal breathing air flow have 7 cut-off diameter stages at 14.1, 8.6, 5.4, 3.3, 2.1, 1.4 and 1.0 μm. Meaning that aerosol droplets deposited between stage 4 and 7 are in the desirable respiratory range. In conclusion, impactors with more cut-off diameter stages, such as the NGI, are desirable for nebulisation studies, which require a low airflow.

Laser diffractometry methods are easy to use; they are fast and have automated data analysis. For example, in this study, 24 nebulisation a day could be tested in the laser compared to two nebulisation a day with the NGI impactor. The NGI aerodynamic results suggested that the active vibrating-mesh nebulisers were superior in nebulising smaller droplets of AmB-NIVs and Cis-NIVs compared to the I-neb. However, this difference was not observed when the same formulations were tested for geometric aerosol size in the laser diffraction instrument. In this case, both type of nebulisers presented similar geometric aerosol sizes. The differences between the NGI and the laser diffraction could be related to the parameter that each of the technique measures. The NGI provides information about the aerodynamic diameter of the aerosol whereas the laser measures the geometric diameter. The geometric diameter does not take into consideration the particle density and assumes that the particles are spherical. In the case of Aeroneb Go the geometric aerosol particle sizes for both AmB-NIVs and Cis-NIVs were higher than the aerodynamic size. This could have been related to either non-spherical particles or particles with a density smaller than the unity. Although, both impactor and laser techniques are widely used for inhalation characteristics, each technique has its own advantages and limitations as commented above. Thus, optimisation of the evaluation method used has to be taken into consideration before choosing an apparatus for lung delivery measurements in order to obtain meaningful outcomes.

The *in vivo* delivery of NIVs aerosol was also determined to assess whether *in vitro* studies correlated with *in vivo* experiments. Rats that inhaled AmB-NIVs from different nebulisers presented higher amounts of AmB in the lungs when I-neb was used compared to Aeroneb Go and Aeroneb Lab. And these results did not correlate with the predicted deposition *in vitro*. The NGI studies suggested that Aeroneb Go was superior than the I-neb in terms of smaller aerosol size produced. From all the AmB nebulised, less than 1 % was detected in the organs of the animals by HPLC. In the case of Luc-NIVs administered to mice with B16-

F10-luc, both Aeroneb Go and I-neb provided similar drug delivery based on *ex vivo* lung BLI i.e. both nebulisers activated the same percentage of BLI after the nebulisation of Luc-NIVs. These studies emphasise the importance of *in vivo* testing in the production of pharmaceutical formulations. *In vivo* delivery is affected by multiple factors such as anatomical, physiological and pathological conditions (Sakagami, 2006; Cryan *et al.*, 2007; Nahar *et al.*, 2013). Those play an important role in aerosol deposition *in vivo* and are difficult to mimic with *in vitro* models. For example, *in vivo* the humidity of the airways is extremely high and may affect the aerosol disposition. Moreover, the structure of the lungs presents high levels of branching and several ciliated mechanisms for particle clearance, which are not present during *in vitro* techniques (Miller *et al.*, 1993). In this study, the BLI produced by the cancer cells B16-F10-luc in the presence of luciferin was used to investigate the aerosol depositions of luciferin loaded NIVs. This method provided understanding of the drug deposition in the target site of the lungs *in situ* i.e. the cancer cells. Consequently providing a big advantage over other imaging techniques such as scintigraphy, PET or MRI, which do not provide concrete evidence of drug delivery in the site of action.

Apart from aerosol size and *in vivo* deposition profiles, other aspects should be taken into consideration when comparing devices for inhaled drug administration. Special attention has to be paid to the patient use of the device. The clinical efficacy of inhaled treatments strongly relies in patients ability to use the inhaler device (McFadden, 1995). An easy-to-use inhaler would be preferred than a sophisticated and complicated one, resulting in better patient compliance and adherence. For example, nebulisers are advantageous over DPIs and pMDIs since they are easier to handle requiring less patient breath-coordination when used (Dolovich and Dhand, 2011). Even more, some nebulisers are provided with software able to optimise the drug intake ratio. For example the AAD technology included in the I-neb provides feedback to the patient regarding the correct use of the device and adherence to the treatment (Goodman *et al.*, 2010). Moreover, the I-neb with the AAD activated (i.e. not in

continuous mode) only delivers drug during the key parts of the inhalation breath. The I-neb TIM mode gives instructions to the patients on performing more successful slow and deep inhalation (Denyer *et al.*, 2010). In the other hand, simpler nebulisers such as Aeroneb Go, only nebulise in a continue mode. Consequently affecting the amount of drug finally deposited in the human lungs.

Special safety concerns should be considered when chemotherapy agents, such as cisplatin, are nebulised. Extra protection mechanism for healthcare workers need to be adopted (Darwiche *et al.*, 2013). In this current study, all the *in vivo* work was undertaken inside a safety cabinet class II to minimise exposure. Chemotherapy studies in humans have adopted other protection mechanism. For example, Wittgen *et al.* (2007) studied the use of platinum agents to treat NSCLC and dressed medical staff and patients in full barrier protection clothing. Moreover, the treatment was done in a negative pressure room inside a vinyl enclosure tent where the air was drawn through an HEPA filter. This method provided successful effectiveness in limiting occupational exposure (Zarogoulidis *et al.*, 2012). The use of breath-actuated inhalation systems can also increased the overall safety. The smart AAD mode breathing manoeuvre included in some I-neb (Denyer *et al.*, 2010) have great potential as a breath-activated nebulisation for chemotherapy.

In conclusion, the results of this study indicated that NIVs were a suitable delivery system for vibrating-mesh nebulisation:

- AmB-NIVs vesicles decreased in size after active or passive vibrating-mesh nebulisation. However, the vesicle fragmentation did not affect other parameters such as drug entrapment efficiency, z-average or vesicle charge.

- The apparent viscosity of AmB-NIVs influenced the aerosol output and the percentage of drug delivered from the different vibrating-mesh

nebulisers. Aeroneb Go was superior in fast nebulising of more viscous NIVs than I-neb and Aeroneb Lab. However, particles with viscosity larger than 2.13 mPa·s should be nebulised with precaution.

– AmB-NIVs and Cis-NIVs had smaller aerodynamics aerosol size when nebulised with active vibrating-mesh nebulisers. Cis-NIVs nebulisation presented a bimodal distribution for entrapped and unentrapped cisplatin. This bimodal distribution could allow a rapid onset of drug action followed by a sustained release from the NIVs carrier. The three NIVs ingredients presented similar MMAD values when analysed separately, this indicated that the NIVs travelled as single aggrupation along the air-stream.

– I-neb was superior in nebulising AmB-NIVs into an individual passive treatment of rats. However, less than 1 % of the AmB nebulised was detected *ex vivo* in the lungs.

– The Luc-NIVs nebulised to mice with B16-F10-luc reached the site of action, since approximately 25 % of the total BLI was obtained from both Aeroneb Go and I-neb nebulisers.

# CHAPTER 6. NOVEL MINOR GROVE BINDERS FOR THE TREATMENT OF LUNG CANCER AND VISCERAL LEISHMANIASIS

## 6.1. Introduction

Genomic DNA is formed from two polynucleotide strains, made up from base pairs (cytosine, thymine, adenine or guanine) attached to sugar-phosphate backbones; all forming a double helix structure. These backbones are structured with two different size grooves: a major grove of 22 Å and a minor groove of 12 Å. Some proteins and drugs bind to both major and minor DNA grooves in order to modulate the cell gene expression. Compounds that specially attach to the minor groove of genomic DNA are classified as minor groove binders (MGBs; Figure 6.1). MGBs can bind irreversibly causing permanent DNA damage (e.g. mitomycin C) or reversibly, only restrained near the DNA for a certain amount of time (e.g. distamycin A). The compounds that bind to DNA can cause considerable modifications in the usual transcription of genes. Those modifications result in variations in the product from crucial genes involved in cell-cycle replications and finally induce cell apoptosis (Baraldi *et al.*, 2004).

One of the first MGBs investigated was distamycin A (Figure 6.2). Distamycin A is a tripyrrole compound initially isolated from *Streptomyces distallicus* but it is now fully chemically synthesised (Arcamone *et al.*, 1964). Another lead compound in the MGBs family is netropsin. Netropsin is naturally produced by *Streptomyces netropsis* and its structure is smaller than distamycin A as it only contains two pyrroles. These two compounds have a chemical structure that matches the curvature of the DNA minor groove, allowing a good fit in the site of action (Figure 6.1). Both, distamycin and netropsin bind preferably to the adenine-thymine rich sequence of the DNA causing suppression of bacteria, viruses and protozoa (Kopka *et al.*, 1985). Nonetheless, both antibiotics are highly toxic and cause undesirable side effects to mammalian cells, as they are not specific to pathogen DNA. However, they have allowed the development of structural analogues, which have less toxicity effects and higher selectivity (Khalaf *et al.*, 2004, 2012).

Other drugs that interfere with DNA transcription have also been developed to treat cancer. For example, the major groove of the DNA is the main target for alkylating agents such as cisplatin (Figure 1.1). In addition, the minor groove of the DNA is also the site of action of other cancer therapy under development. For example, trabectedin is the first MGB clinically approved for the treatment of soft tissues sarcomas and it is under clinical trials as an antileukemic agent (Cai *et al.*, 2009). The use of MGBs for cancer treatment has been questioned due to their potential toxicity to healthy cells but recent clinical trials have shown that their benefits outweigh the toxic side effects (Puyo *et al.*, 2014). Moreover, treatment with many traditional anticancer drugs, such as cisplatin, is related to drug resistance and MGBs may overcome those by binding to another groove of the DNA (Colella *et al.*, 1999).

MGBs have also been used to target protozoan infections such as trypanosomiasis and leishmaniasis. In this last case, the diarylamidines group are the most effective MGBs. For example, pentamidine is one of the second line drugs that can be used to treat *Leishmania donovani* infections. Nonetheless, it is not a first-line drug as it induces significant side effects, including nephrotoxicity, cardiotoxicity and hepatotoxicity (Das *et al.*, 2009).

Prior to the approval of any new therapeutic agents, preclinical studies involving animal models are necessary to guarantee safety and efficacy. In this study the melanoma cancer cell line B16-F10, which quickly metastasizes to the lungs, was used for drug screening against cancer. This cell line was derived from pulmonary metastatic cells isolated from the lungs of mice after ten successive passages of B16 sub-lines (Nakamura *et al.*, 2002). The original B16-F10 cell line was transfected with firefly luciferase gene to develop the B16-F10-luc murine melanoma cell line (Bioware® B16-F10-luc-G5, Caliper Life Sciences; Hopkinton, USA). The integration of this gene allows disease progression to be monitored *in vitro* or *in vivo* by BLI imaging, which permit sequential imagining over time (Tiffen *et al.*, 2010).

This study is focused on the compounds from a library of MGBs, which were synthesised by researchers within the Chemistry Department at the University of Strathclyde (Khalaf *et al.*, 2004, 2012; Anthony *et al.*, 2007). All these MGBs were analogues from the parent compound distamycin A (Figure 6.2). The novel synthesised MGBs had variation in their C-terminus, larger head N-terminal groups, larger alkyl side chains to substitute the methyl groups and other heterocyclic rings (Appendix Table A.1, Figure 6.2). Several of the compounds included in the library had previously shown efficacy against a variety of organisms. The most significant of those was MGB-BP3 (named in this study as $MGB_{27}$), a compound now developed by MGB Biopharma (Glasgow, UK). MGB-BP3 has recently entered clinical trials for the treatment of Gram-positive bacteria, such as *Clostridium difficile,* with no toxicity against mammalian cells (Suckling, 2015). Other MGBs are being investigated for use against gram-negative bacteria, in particular against *Pseudomonas aeruginosa* for CF patients (Barrett *et al.*, 2013). *In vitro* efficacy of some of the MGBs have been demonstrated against *Aspergillus niger* and *Candida albicans* (Anthony *et al.*, 2007). The introduction of more hydrophobic groups to the MGBs structure, led to compounds with higher efficacy against *Staphylococcus aureus* (Anthony *et al.*, 2007). Higher microorganism affinity was also associated to a decrease in mammalian toxicity (Khalaf *et al.*, 2004). Khalaf *et al.* (2012) described that MGBs with hydrophobic groups were associated with lower affinity to the ion channel associated to long QT syndrome. Nonetheless, the efficacy of the MGBs produced at the University of Strathclyde had not been tested against cancer or *Leishmania* parasites prior to this study. The development of new therapeutic agents against cancer is necessary to reduce the number of deaths associated to cancer, 7.6 million worldwide (World Health Organisation, 2013). In addition, visceral leishmaniasis patient's (50,000 deaths worldwide; World Health Organisation, 2011) are also in need of new therapeutics with high efficacy, low toxicity and affordable cost (Sundar *et al.*, 2004).

Therefore, the objective of this study was to identify hit MGBs compounds that could be used to develop novel formulations to treat lung cancer or visceral leishmaniasis. Accordingly, experiments were carried out with the following aims:

- Preliminary *in vitro* screening of a range of MGBs compounds against B16-F10-luc cells and *Leishmania* (*L. donovani* and *L. major*).

- Determine the relationship between the MGBs chemical structure and activity against B16-F10-luc.

- Study the physicochemical properties of MGBs in non-ionic surfactant vesicles formulations (MGBs-NIVs).

- Determine the *in vivo* efficacy of the lead MGB candidate in a murine model of lung cancer after intravenous and inhaled administration.

- Assess the *in vivo* efficacy of the lead MGB candidate in a murine model of visceral leishmaniasis.

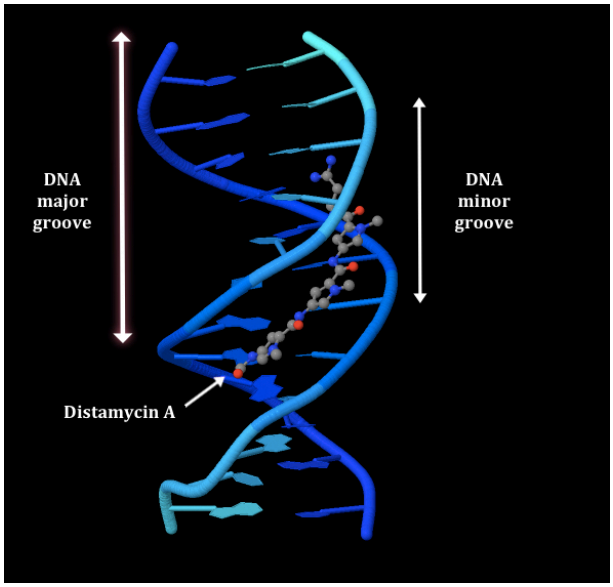


**Figure 6.1** Structural representation of the relationship between a molecule of distamycin A and the DNA. Distamycin A is attached to the minor groove of the DNA backbone (Protein Database GDL003, adapted from Coll *et al.*, 1987).

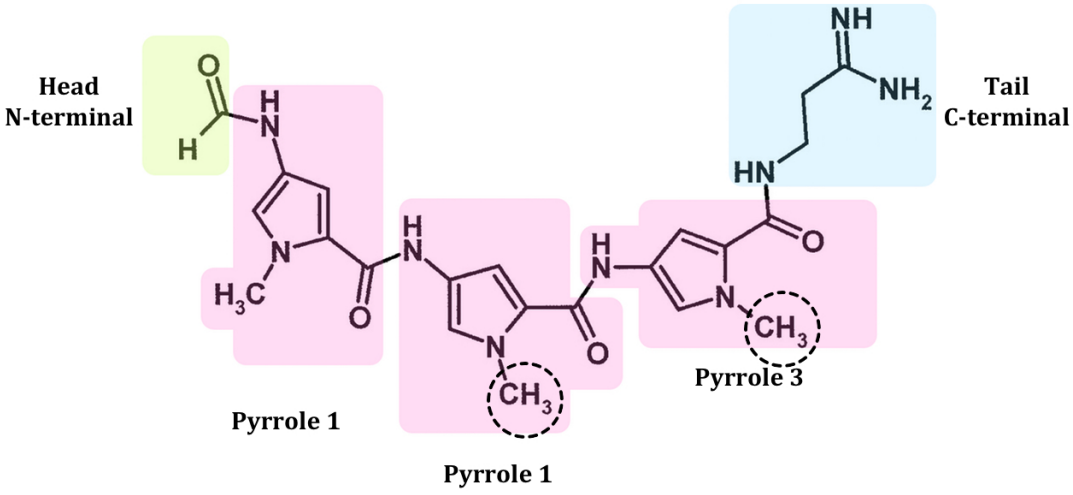


**Figure 6.2** Structural representation of the MGB parent compound distamycin A. The highlighted regions show the different parts of the compound, which were altered in the tested MGBs library: N-terminal, pyrrole 1, pyrrole 2, pyrrole 3 and C-terminal. Circled with a dotted line represent the places were alternatives to alkyl methyl groups were placed.

## 6.2. *In vitro* efficacy of MGBs against B16-F10-luc cells and *Leishmania*

Eighty-nine compounds from the MGBs library (Appendix Table A.1) were tested at a single concentration (15.36 μg/ml containing 2.44 % v/v DMSO) for their ability to inhibit the growth of B16-F10-luc cells (Table 6.1). The BLI emitted for the cells treated with MGBs was compared to the BLI emitted for the solvent control cells. This resulted in 23.47 % of the MGBs tested with significantly lower BLI than the solvent control. These were $MGB_{11, 23, 51, 54, 55, 76, 77, 83}$ ($p \leq 0.05$); $MGB_{34, 39, 50, 53, 58, 59, 62}$ ($p \leq 0.01$) and $MGB_{35 - 38, 40}$ ($p \leq 0.001$; Table 6.1).

The activity of some of these compounds was investigated in greater detail by determining their mean $IC_{50}$. In these studies, gemcitabine, a drug commonly used to treat cancer, was used as the positive control. Examples of the dose response curves used to determine the $IC_{50}$ values are shown in Figure 6.3. $MGB_{23}$, $MGB_{35}$ and $MGB_{40}$ had a smaller $IC_{50}$ than gemcitabine ($p \leq 0.05$; Table 6.2) whereas $MGB_{62}$ and $MGB_{77}$ had similar activities to gemcitabine. These studies also showed that DMSO had a significant effect on cell growth at concentrations above 0.63 % v/v (Figure 6.3.G).

The correlation between the MGBs *in vitro* efficacy (Table 6.1), the type of linked head group (alkene, amide or amidine) and the tail group (dimethylaminopropyl or morpholine) was determined (Table 6.3). The linked head group was a significant factor in influencing MGBs efficacy compared to the tail group ($p \leq 0.001$; two-way ANOVA), and these two factors acted independently. MGBs with alkene linked head groups were more effective than those with an amidine link ($p \leq 0.01$; Table 6.3).

The lipophilicity of all the tested MGBs was predicted by determining their log $D_{7.4}$ value (shown in Appendix Table A.2). There was little correlation between the log $D_{7.4}$ value and mean inhibition in cell proliferation for the 89 MGBs

compounds tested at a single concentration ($R^2$ = 0.20). However, a trend was observed for MGBs, where higher log $D_{7.4}$ values gave some correlation with a greater suppression in cell growth and *vice versa*. The head group linker influenced the correlation in a different manner. Thus the lowest correlations between log $D_{7.4}$ value and suppression in cell growth occurred if there was an amide linked head group. Whereas a bigger correlation was observed if an amidine head group was present (Figure 6.4).

An increase in percentage of cell suppression was observed in MGBs with longer alkyl side chain substituents in the pyrroles e.g. $MGB_{35}$ and $MGB_{40}$. MGBs including pyrroles with larger alkyl chains were more effective than the MGB with normal methyl pyrroles (Figure 6.5). This positive feature, observed in $MGB_{35}$ and $MGB_{40}$, was incorporated into $MGB_{23}$ to create a new analogue structure named $MGB_{93}$. $MGB_{23}$ was already very effective against B16-F10-luc *in vitro* and the addition of a further 3-carbon group in the third pyrrole ($MGB_{93}$) was investigated to increase on compound efficacy. However, $MGB_{93}$ was less effective than $MGB_{23}$, with higher $IC_{50}$ values (Figure 6.3.B,F and Table 6.2).

Parallel screening investigations indicated $MGB_{58}$ as a lead compound to treat several species of *Leishmania* (these studies were carried out by Mr Shaw, University of Strathclyde). The most effective MGB compound identified from these studies was $MGB_{58}$, which had an $IC_{50}$ of 1.05 ± 0.48 μM for *L. donovani* and 0.84 ± 0.37 μM for *L. major* (mean ± SE; n=3; cited with permission from Mr Shaw).

In conclusion, these studies identified $MGB_{23}$ as the most active compound against B16-F10-luc cells and $MGB_{58}$ as a lead compound for *L. donovani*.

**Table 6.1** The effect of treatment with different MGBs compounds on the proliferation of B16-F10-luc cells. Cells (3.7 x $10^5$ cells/well) were incubated for 24 hours in the presence of medium containing DMSO (solvent control, 2.44 % v/v DMSO) or different MGBs compounds (15.36 µg/ml with 2.44 % v/v DMSO). The effect of treatment on cell proliferation is shown as the percentage suppression compared to the mean solvent control (* $p \leq 0.05$, ** $p \leq 0.01$ and *** $p \leq 0.001$ comparing BLI of the cells treated with MGBs with the cells with solvent control).

| MGB | Suppression (% ± SD; n=3) | MGB | Suppression (% ± SD; n=3) | MGB | Suppression (% ± SD; n=3) |
|---|---|---|---|---|---|
| 1 | 0.00 ± 0.00 | 31 | 59.80 ± 10.06 | 63 | 0.00 ± 0.00 |
| 2 | 0.00 ± 0.00 | 32 | 46.53 ± 22.50 | 64 | 0.00 ± 0.00 |
| 3 | 0.00 ± 0.00 | 33 | 57.06 ± 18.58 | 65 | 0.00 ± 0.00 |
| 4 | 53.32 ± 7.34 | 34 | 77.07 ± 6.02 ** | 66 | 0.00 ± 0.00 |
| 5 | 0.00 ± 0.00 | 35 | 82.89 ± 3.45 *** | 67 | 0.00 ± 0.00 |
| 6 | 0.00 ± 0.00 | 36 | 83.60 ± 3.43 *** | 68 | 0.00 ± 0.00 |
| 7 | 0.00 ± 0.00 | 37 | 83.97 ± 3.81 *** | 69 | 0.00 ± 0.00 |
| 8 | 40.12 ± 25.96 | 38 | 84.98 ± 2.85 *** | 70 | 0.00 ± 0.00 |
| 9 | 0.00 ± 0.00 | 39 | 76.50 ± 11.72** | 71 | 0.00 ± 0.00 |
| 10 | 18.53 ± 46.80 | 40 | 87.58 ± 3.11 *** | 72 | 0.00 ± 0.00 |
| 11 | 57.12 ± 11.48 * | 41 | 33.03 ± 12.04 | 73 | 43.74 ± 10.55 |
| 12 | 30.92 ± 28.62 | 42 | 41.43 ± 23.99 | 74 | 0.00 ± 0.00 |
| 13 | 16.13 ± 8.45 | 43 | 44.00 ± 29.31 | 75 | 67.34 ± 11.74 |
| 14 | 0.00 ± 0.00 | 44 | 35.10 ± 8.56 | 76 | 69.24 ± 7.61 * |
| 15 | 0.00 ± 0.00 | 45 | 43.74 ± 31.74 | 77 | 66.35 ± 3.55 * |
| 16 | 54.10 ± 9.16 | 46 | 47.67 ± 30.02 | 78 | 0.00 ± 0.00 |
| 17 | 45.81 ± 0.43 | 47 | 50.27 ± 27.43 | 79 | 53.60 ± 9.58 |
| 18 | 36.73 ± 17.38 | 48 | 54.55 ± 26.40 | 80 | 0.00 ± 0.00 |
| 19 | 0.00 ± 0.00 | 49 | 55.18 ± 23.94 | 81 | 0.00 ± 0.00 |
| 20 | 0.00 ± 0.00 | 50 | 68.57 ± 13.66** | 82 | 0.00 ± 0.00 |
| 21 | 0.00 ± 0.00 | 51 | 57.01 ± 2.50 * | 83 | 50.93 ± 17.25 * |
| 22 | 0.00 ± 0.00 | 52 | 2.19 ± 6.89 | 84 | 6.48 (n=1) |
| 23 | 77.26 ± 5.65 * | 53 | 71.79 ± 4.38 ** | 85 | 0.00 ± 0.00 |
| 24 | 33.63 ± 4.74 | 54 | 59.36 ± 12.75 * | 86 | 22.52 ± 18.31 |
| 25 | 0.00 ± 0.00 | 55 | 64.51 ± 12.36 * | 87 | 0.00 ± 0.00 |
| 26 | 43.84 ± 10.39 | 56 | 23.09 ± 40.99 | 88 | 14.86 ± 5.91 |
| 27 | 51.47 ± 12.30 | 58 | 74.22 ± 5.14 ** | 89 | 0.00 ± 0.00 |
| 28 | 34.11 ± 5.38 | 59 | 75.67 ± 5.13 ** | 90 | 0.00 ± 0.00 |
| 29 | 46.57 ± 12.19 | 61 | 77.44 (n=1) | 91 | 0.00 ± 0.00 |
| 30 | 56.90 ± 12.65 | 62 | 73.64 ± 11.51** | 92 | 0.00 ± 0.00 |

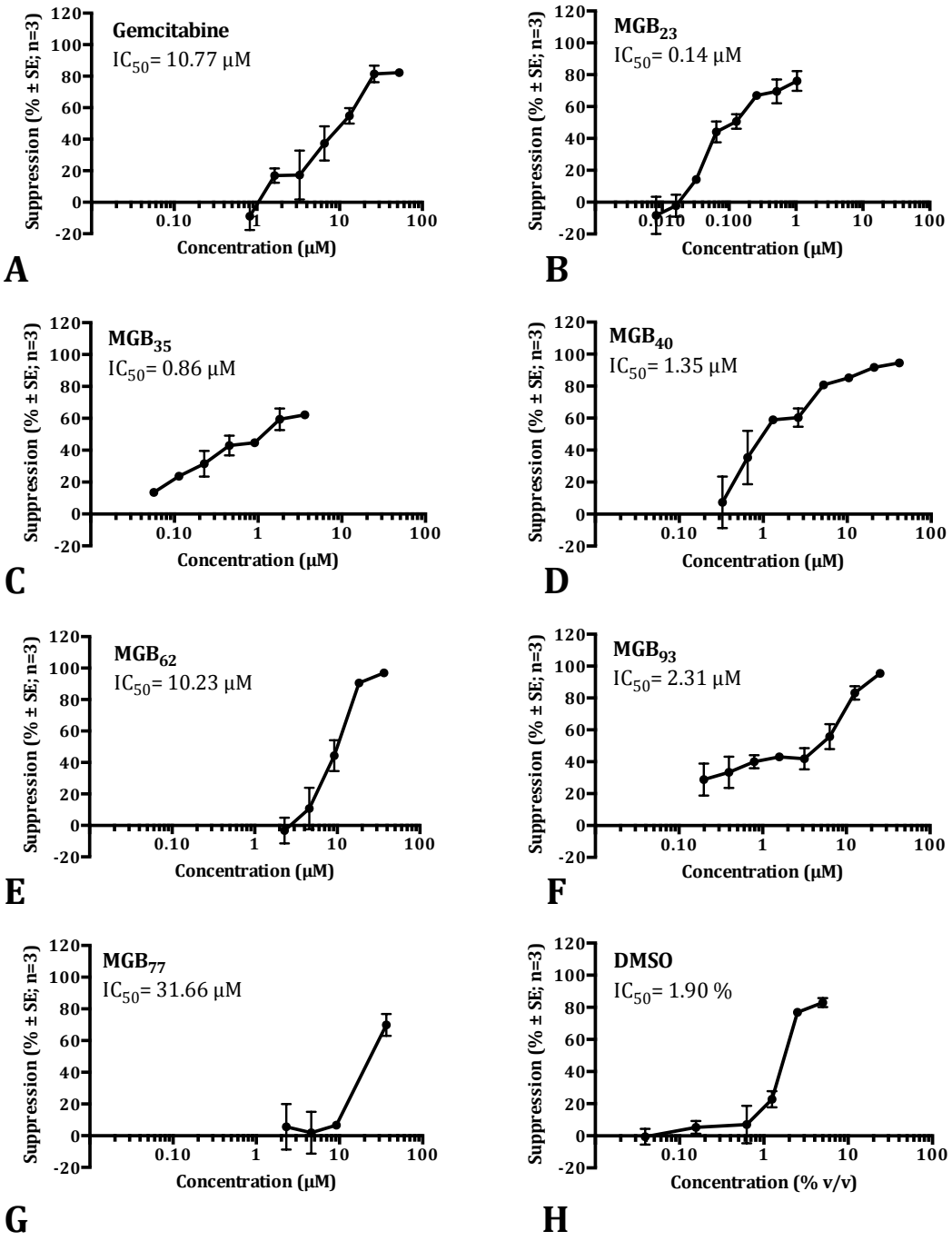


**Figure 6.3** Examples of dose response curves for different MGBs compounds against B16-F10-luc cells: A, Gemcitabine; B, $MGB_{23}$; C, $MGB_{35}$; D, $MGB_{40}$; E, $MGB_{62}$; F, $MGB_{93}$; G, $MGB_{77}$ and H, DMSO. Cells (1 x $10^5$ cells/wel) were incubated for 24 hours in the presence of medium (control) or different concentrations of MGBs compounds (stock concentration of 630 µg/ml, containing 100 % v/v DMSO). The mean half maximal inhibitory concentration ($IC_{50}$) was determined at the $50^{th}$ percentile suppression compared to the mean control value.

**Table 6.2** The mean half maximal inhibitory concentration ($IC_{50}$) values for different MGBs compounds tested against B16-F10-luc cells. The values shown are from three experiments and three replicates were used for each concentration tested in each experiment. DMSO at concentrations > 0.63 % v/v may had influenced the $IC_{50}$ of the compounds; therefore percentage of DMSO at the $IC_{50}$ concentration is shown (* $p<0.05$ compared to gemcitabine $IC_{50}$).

| **Compound** | **$IC_{50}$ (μM ± SD; n=3)** | **DMSO at $IC_{50}$ (% ± SD; n=3)** |
|---|---|---|
| Gemcitabine | 11.04 ± 1.65 | 0.52 ± 0.03 |
| $MGB_{23}$ | 0.16 ± 0.01 * | 0.01 ± 0.00 |
| $MGB_{35}$ | 0.81 ± 0.08 * | 0.11 ± 0.01 |
| $MGB_{40}$ | 1.10 ± 0.51 * | 0.13 ± 0.06 |
| $MGB_{62}$ | 10.39 ± 0.50 | 1.42 ± 0.07 |
| $MGB_{77}$ | 26.07 ± 12.64 | 2.82 ± 1.37 |
| $MGB_{93}$ | 2.16 ± 0.22 | 0.27 ± 0.03 |

**Table 6.3** Comparison between suppression cell proliferation (mean % ± SE; Table 6.1) of groups of MGBs compounds based on tail group (Dmap, dimethylaminopropyl or morpholine) and linked head group (alkene, amide or amidine; Appendix Figure A.1). A two-way ANOVA was used to identify significant differences or interactions between the tail group and the linked head group factor. The n value shows the numbers of compounds within each group tested and n.s. is not significant. The type of head linked group was a significant factor influencing cell suppression ($p \leq 0.01$).

| | | **Tail group** | | **p-value** |
|---|---|---|---|---|
| | | **Dmap** | **Morpholine** | |
| **Head linked group** | **Alkene** | 50.50 ± 17.82 (n=4) | 49.88 ± 6.24 (n=23) | $p \leq 0.01$ |
| | **Amide** | 4.08 ± 2.30 (n=19) | 0 ± 0 (n=6) | |
| | **Amidine** | 22.39 ± 7.89 (n=9) | 0 ± 0 (n=1) | |
| **p-value** | | n.s. | | n.s. |

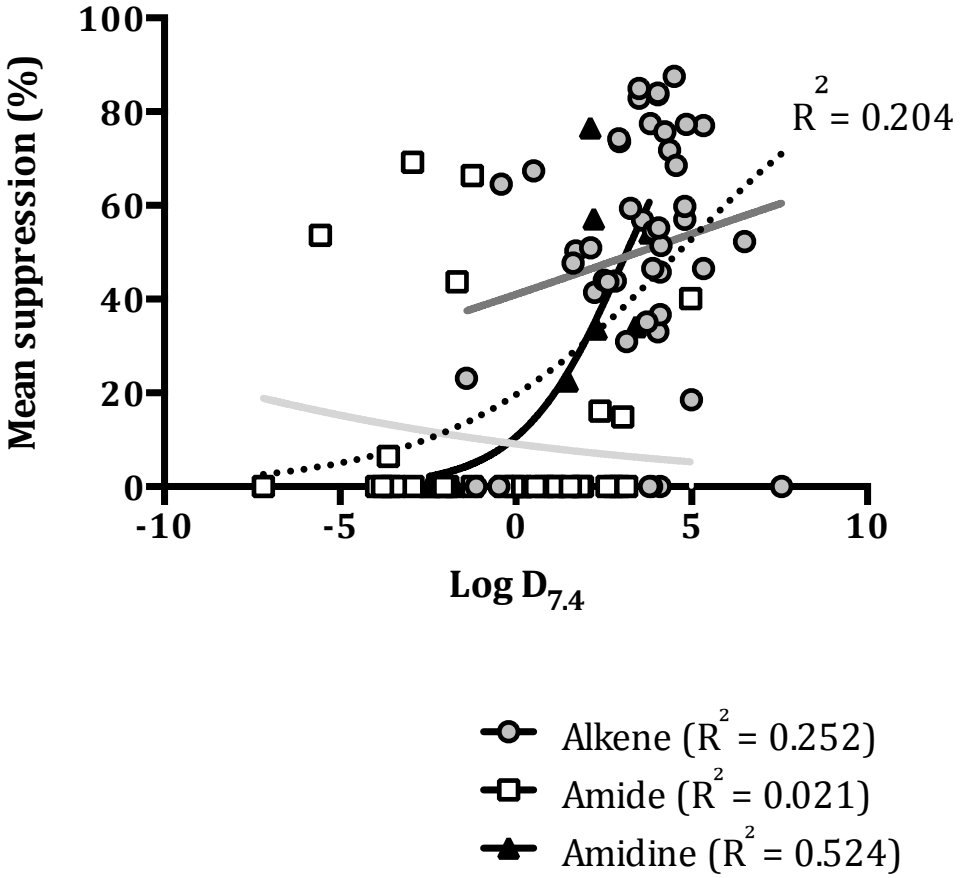


**Figure 6.4** Relation between lipophilicity of the MGBs (in terms of log $D_{7.4}$; Appendix Table A.2) and the percentage inhibition in cell proliferation for B16-10-luc cells treated with different MGBs compounds. Data for each MGBs compound was the suppression for cell proliferation (Table 6.1). The selected points were fitted to a non-linear dose response curve. The curve fitted to all MGBs together was marked in dotted points and the correlation coefficient for this line and for the specific head link groups (alkene, amide or amidine) are shown.

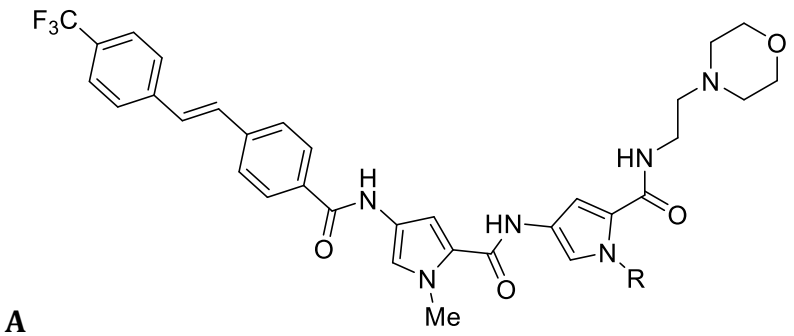


A

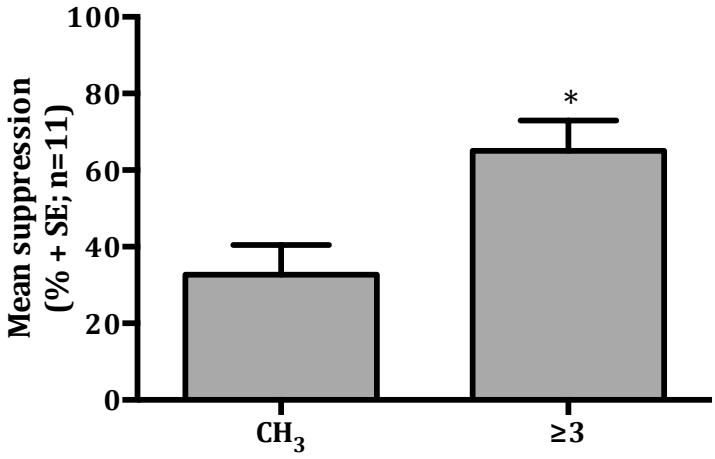


B

**Figure 6.5** Influence of alkyl side chain length on the activity of MGBs compounds against B16-F10-luc cells (Table 6.1). Only MGBs with alkene linked head and morpholine tail groups were included in this analysis. A, is an example of alkene linked head group with a morpholine tail. R indicates the pyrrole position where alkyl side chains were incorporated (i.e. R = $CH_3$ corresponded to $MGB_{23}$; R = $C_3H_7$ corresponded to $MGB_{93}$). B, is the percentage of B16-F10-luc inhibition according to the length of ramification (* $p \leq 0.05$).

## 6.3. Production of MGB-NIVs formulations

NIVs formulations of $MGB_{23}$ and $MGB_{58}$ were produced using the passive DRV method, where freeze-dried empty-NIVs were rehydrated with the relevant MGB solution to produce MGB-NIVs. The MGBs were dissolved in DMSO prior to dilution with PBS pH 7.4 (total DMSO of 2 % v/v). Compound precipitation was observed as soon as PBS pH 7.4 was incorporated into to the MGBs, probably as a consequence of poor water solubility. Nonetheless, the MGBs were formulated in MGB-NIVs (Table 6.4). All the vesicle formulations had a similar large vesicle size but the polydispersity span value was significantly higher for $MGB_{58}$-NIVs compared to empty-NIVs ($p \leq 0.05$; Table 6.4). The ζ-potential of both MGB-NIVs formulations was significantly more negative than that of empty-NIVs ($p \leq 0.01$; Table 6.4). The entrapment efficiency of $MGB_{23}$ within NIVs was calculated at 30.31 ± 0.31 % (amount $MGB_{23}$ pellet compared to whole theoretical amount, study carried out and cited with permission from Dr. Scott, University of Strathclyde).

## 6.4. Effect of different $MGB_{23}$ formulations in a murine model of lung cancer

The effect of treatment with $MGB_{23}$ solution or $MGB_{23}$-NIVs given by intravenous injection or inhalation, on the progression of lung cancer (B16 F10-luc) was determined in BALB/c mice. None of the treatments had any significant effect on body weight or animal health over the course of the studies, indicating that the $MGB_{23}$ formulation had no observed toxic effects. For intravenous administration, the average body weight gain ± SE (g; n=5/treatment) for the control group was 5.76 ± 1.20, 4.68 ± 0.26 for mice treated with empty-NIVs, 5.36 ± 3.76 (one mouse lost 6.70 % body weight) for $MGB_{23}$ solution and 2.74 ± 0.35 for $MGB_{23}$-NIVs. For the inhaled administration, the average body weight gain for control group was 0.74 ± 1.06, 0.47 ± 1.13 for mice treated with empty-NIVs, 0.84 ± 1.40 for $MGB_{23}$ solution and 1.05 ± 1.50 for $MGB_{23}$-NIVs.

As expected, the B16-F10-luc cells proliferated in mice over the course of the study, which was demonstrated as an increase in BLI in controls (Figure 6.6, Figure 6.7 and Figure 6.9). None of the formulations administered intravenously had any significant effect on cancer progression, as similar amounts of BLI were present in all mice over the course of the study (Figure 6.7). An increase of BLI in the areas outside the lungs was observed over the course of the study, indicating that the cells that originally colonised these areas grew over time or that the cells from the lungs metastasized to these sites during the study. The amount of BLI emitted *ex vivo* from the liver confirmed the presence of metastatic tumours, especially in control and empty-NIVs groups (Figure 6.6 and Figure 6.8). Mice treated with $MGB_{23}$ solution (52.6 mg/kg $MGB_{23}$) or $MGB_{23}$-NIVs (10.5 mg/kg $MGB_{23}$, 0.30 mmol/kg lipid) had significantly lower amounts of *ex vivo* BLI ($p \leq 0.01$) compared to mice treated with empty-NIVs (1.50 mmol/kg lipid; Figure 6.8). Thus, the $MGB_{23}$ could inhibit metastatic spread of the cells or inhibit B16-F10-luc cell growth in the liver. The lungs from all the mice had similar *ex vivo* BLI (Figure 6.6 and Figure 6.8). The organ weight for liver, lungs and spleen of all the mice was similar for all the treatments (Table 6.5). These results indicated that intravenous $MGB_{23}$ formulations did not have a major effect on cancer progression.

$MGB_{23}$ formulations were also tested *in vivo* by the inhalation route to determine if local delivery was more effective. There was no difference in the amount of BLI emitted by mice throughout the study or in the *ex vivo* BLI for lungs from these mice (Figure 6.9). In this case, similar *ex vivo* levels of liver BLI were observed for all treatment groups (Figure 6.10). The mean lungs and livers *ex vivo* weights were similar between groups (Table 6.5). These results indicated that the $MGB_{23}$ formulations had no effect on cancer progression when administered by inhalation.

**Table 6.4** Physicochemical properties of different MGB-NIVs formulations. Freeze-dried empty-NIVs (150 mM) were rehydrated with PBS pH 7.4 (containing 2 % v/v DMSO; empty-NIVs), $MGB_{23}$ solution (1 mg/ml $MGB_{23}$ in PBS pH 7.4 containing 2 % v/v DMSO; $MGB_{23}$-NIVs) or $MGB_{58}$ solution (1 mg/ml $MGB_{58}$ in PBS PBS pH 7.4 containing 2 % v/v DMSO; $MGB_{58}$-NIVs). The properties of the different MGB-NIVs were compared to empty-NIVs (* $p \leq 0.05$, ** $p \leq 0.01$; MMD, mass median diameter).

| Properties | Empty-NIVs | $MGB_{23}$-NIVs | $MGB_{58}$-NIVs |
|---|---|---|---|
| **MMD (µm ± SD; n=3)** | 9.40 ± 0.38 | 8.70 ± 0.89 | 12.29 ± 1.79 |
| **SPAN (± SD; n=3)** | 1.07 ± 0.16 | 2.86 ± 0.62 | 4.03 ± 1.79* |
| **ζ-potential (mV ± SD; n=3)** | -66.55 ± 4.17 | -81.16 ± 0.82** | -79.29 ± 3.02** |

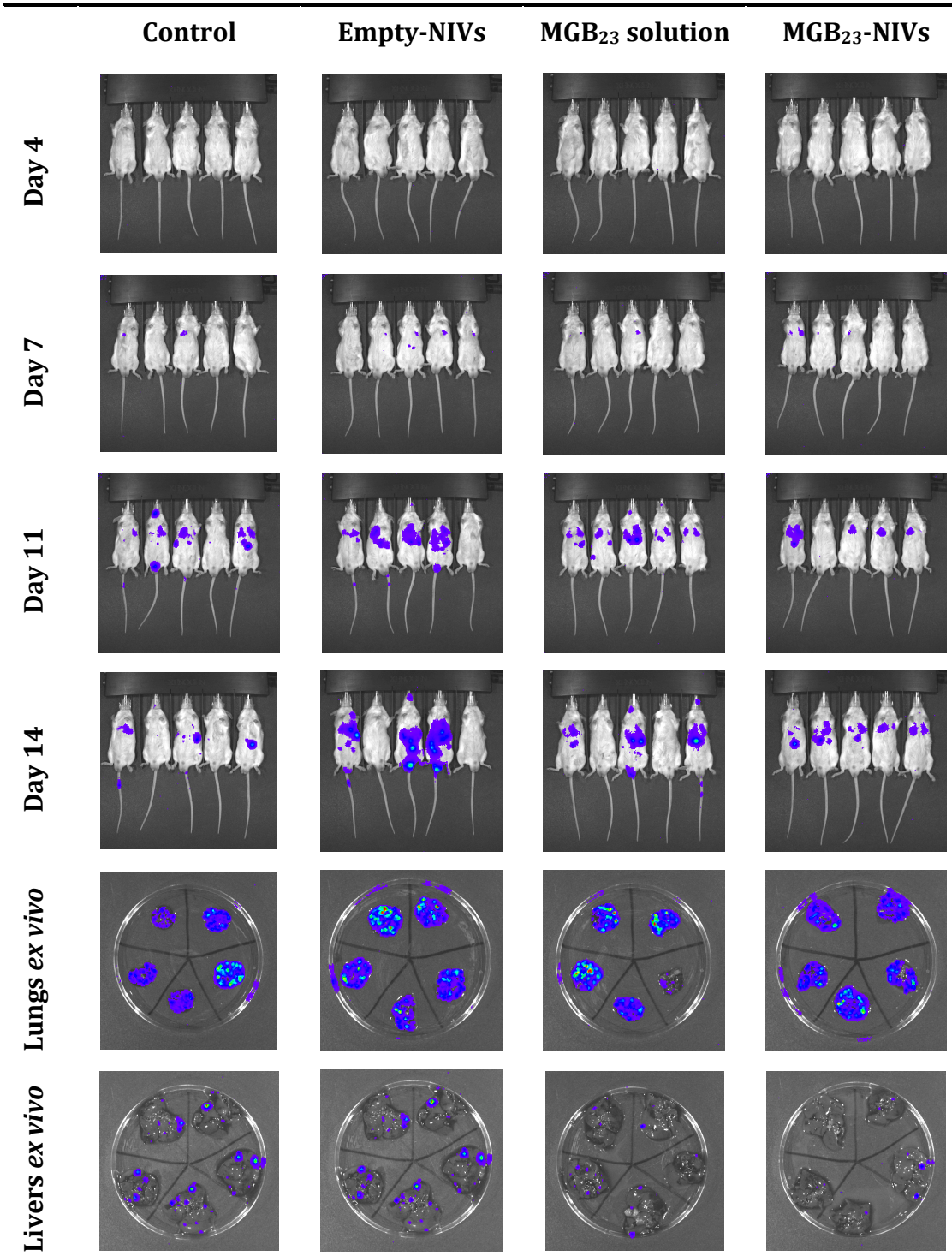


**Figure 6.6** The BLI images of BALB/c mice treated with different $MGB_{23}$ formulations as stated in Table 2.6. On day 14 of the experiment, the lungs and liver of each mouse were isolated and immersed in luciferin solution (150 µg/ml Luc in PBS pH 7.4). The organs were then removed from the solution and the amount of BLI emitted determined by IVIS imaging. All the images had similar p/s range (minimum of $1x10^4$ p/s and maximum $2x10^6$ p/s) and mice were always imaged in the same alignment order.

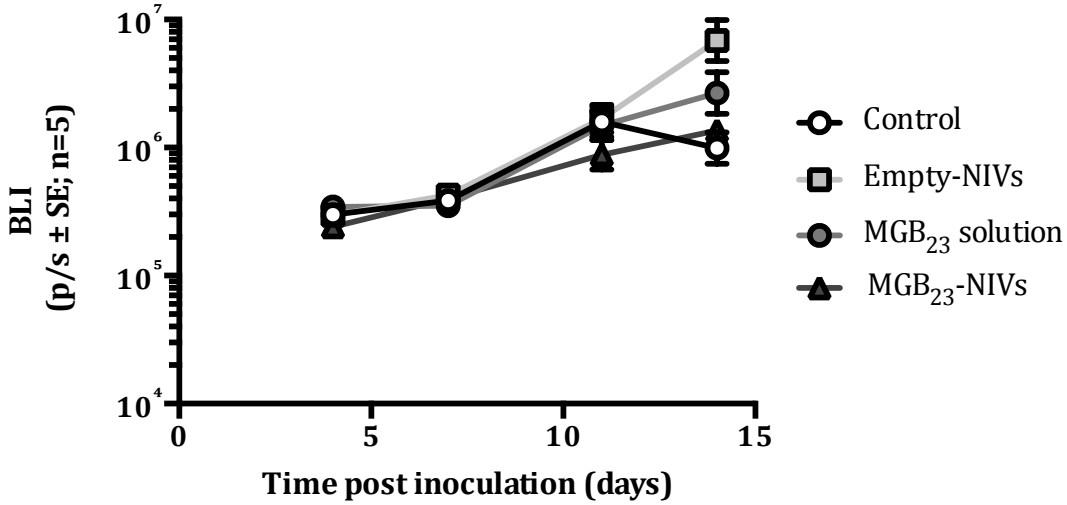


**Figure 6.7** The effect of intravenous treatment with different $MGB_{23}$ formulations on the progression of lung cancer in BALB/c mice. Mice were inoculated with B16-F10-luc cells on day 0 (5 x $10^5$ cells/mouse). On day 3, 9 and 11 mice were treated by intravenous injection (n=5/treatment) according to the dosage regiment described in Table 2.6. Cancer progression was determined by monitoring the amount of BLI emitted by the whole mice body over the course of the experiment.

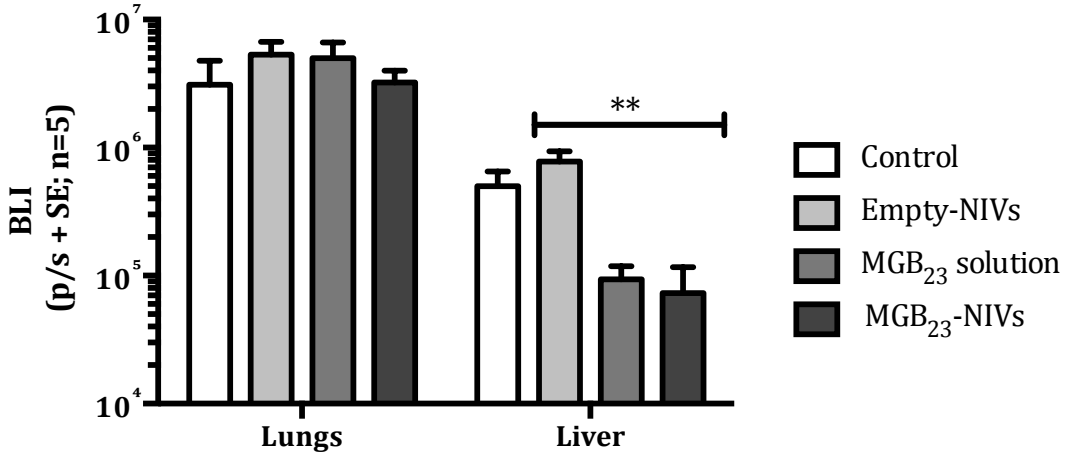


**Figure 6.8** The effect of treatment with different $MGB_{23}$ formulations (Table 2.6.) on the *ex vivo* organs BLI. On day 14 of the experiment, the lungs and liver of each mouse was isolated and immersed in luciferin solution (150 μg/ml Luc in PBS pH 7.4). The organs were then removed from the solution and the amount of BLI emitted determined by IVIS imaging (** $p \leq 0.01$ compared to empty-NIVs).

**Table 6.5** Mice were inoculated with B16-F10-luc cells on day 0 and treated by the intravenous route (iv) or inhalation (inh) on days 3, 9 and 11 (Table 2.6.). On day 14, the experiment was terminated and the liver, lungs and spleen (only for intravenous route) were removed and weighed (n.d., non-determined).

| Groups | Organ weight (g ± SE; n=5) | | | | | |
|---|---|---|---|---|---|---|
| | Liver | | Lungs | | Spleen | |
| | Iv | Inh | Iv | Inh | Iv | Inh |
| **Control** | 1.88 ± 0.18 | 1.60 ± 0.04 | 0.49 ± 0.04 | 0.23 ± 0.05 | 0.17 ± 0.02 | n.d. |
| **Empty-NIVs** | 2.00 ± 0.09 | 1.95 ± 0.22 | 0.54 ± 0.03 | 0.30 ± 0.01 | 0.25 ± 0.02 | n.d. |
| **$MGB_{23}$ solution** | 1.76 ± 0.07 | 1.82 ± 1.72 | 0.46 ± 0.05 | 0.22 ± 0.02 | 0.14 ± 0.01 | n.d. |
| **$MGB_{23}$-NIVs** | 1.68 ± 0.53 | 2.20 ± 0.21 | 0.61 ± 0.04 | 0.30 ± 0.05 | 0.25 ± 0.02 | n.d. |

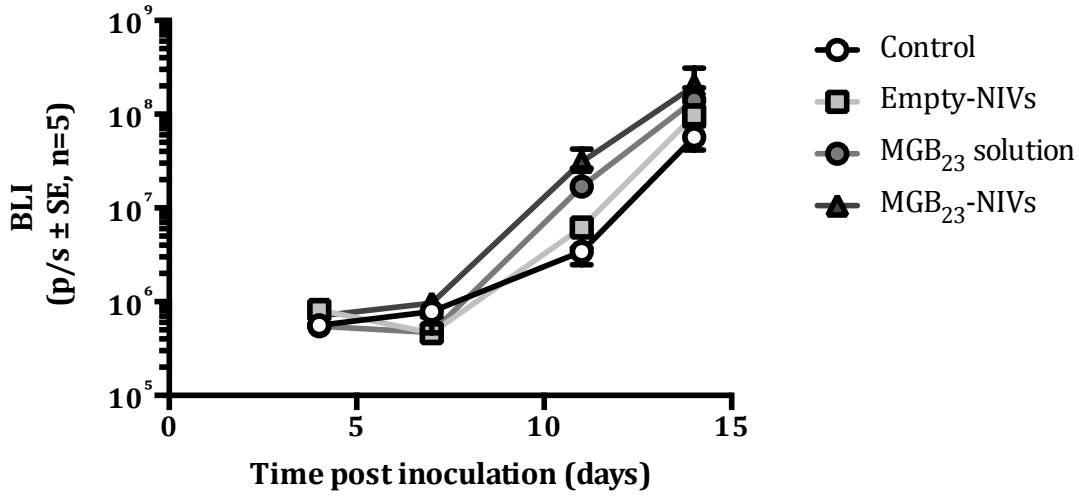


**Figure 6.9** The effect of inhaled treatment with different $MGB_{23}$ formulations on the progression of lung cancer in BALB/c mice. Mice were inoculated with B16-F10-luc cells on day 0 (5 x $10^5$ cells/mouse). On day 3, 9 and 11 mice were treated by inhalation (n=5/treatment; Aeroneb Lab) as described in Table 2.6. Cancer progression was determined by monitoring the amount of BLI emitted by the whole mice body over the course of the experiment.

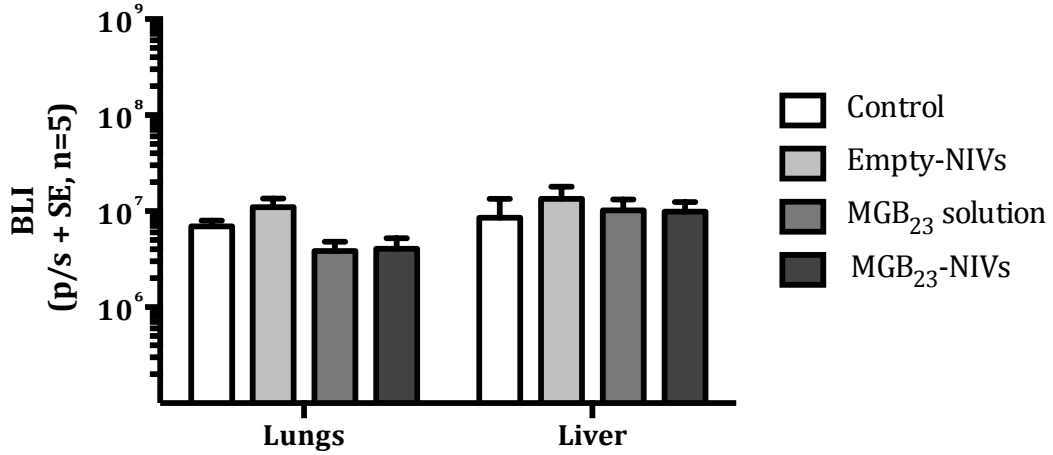


**Figure 6.10** The effect of inhaled treatment with different $MGB_{23}$ formulations (Table 2.6) on the *ex vivo* BLI of lungs and livers. On day 14 of the experiment, the lungs and liver of each mouse was isolated and immersed in luciferin solution (150 µg/ml Luc in PBS pH 7.4). The organs were then removed from the solution and the amount of BLI emitted determined by IVIS imaging.

## 6.5. Efficacy of different $MGB_{58}$ formulations in a mice model of *Leishmania donovani*

The effect of treatment with $MGB_{58}$ solution or $MGB_{58}$-NIVs given by the intravenous route to outcome *L. donovani* infection was determined in BALB/c mice. Treatments with empty-NIVs, $MGB_{58}$ solution or $MGB_{58}$-NIVs (150 mM lipid) had no significant effect on parasite burdens in any of the sites investigated i.e. the spleen, liver or bone marrow (Table 6.6). Only treatment with diluted $MGB_{58}$-NIVs (10 mg/kg $MGB_{58}$, 0.30 mmol/kg lipid) caused a significant reduction in liver parasite burdens ($p \leq 0.05$; 40.20 ± 16.26 % suppression; Table 6.6). Treatments with the higher concentration of $MGB_{58}$-NIVs (50 mg/kg $MGB_{58}$, 1.50 mmol/kg lipid) or empty-NIVs (1.50 mmol/kg lipid) were associated with significant increase in spleen weight on day 14. However, this was not present in animal given lower lipidic doses of NIVs (0.30 mmol/kg lipid; Table 6.6).

The inflammatory response associated to $MGB_{58}$-NIVs or empty-NIVs treatment was determined in mice uninfected and infected with *L. donovani*. The CLI associated with the neutrophil recruitment during the inflammatory response was imaged after treatment with luminol by intraperitoneal injection (Figure 6.11 and Figure 6.12). Intravenous injection of PBS into uninfected and *L. donovani* infected mice had a minimal effect on neutrophil activation based on the amount of CLI emitted from the whole mice. However, the intravenous injection of empty-NIVs and $MGB_{58}$-NIVs resulted in a significant increase of the neutrophil activation in both infected and uninfected mice ($p \leq 0.05$; Figure 6.12). Images suggested localised recruitment of neutrophils in the spleen and lungs based on the site of the CLI emitted (Figure 6.11.B-C). There was no difference in the amount of CLI emitted by uninfected and *L. donovani* infected mice treated with empty-NIVs or $MGB_{58}$-NIVs.

**Table 6.6** The effect of treatment of different $MGB_{58}$ formulations on the organ weights and parasite burdens of *L. donovani* infected BALB/c mice. Mice were infected with *L. donovani* (LV82 strain, 1 x $10^7$ parasites/mouse) and treated on day 7 by intravenous injection with the treatment dosage described in Table 2.7. On day 14 the experiment was terminated. The livers and spleens were removed and weighed and parasite burdens in the spleen, liver and bone marrow determined (* $p \leq 0.05$, 40.20 ± 16.26 % reduction compared to control; ** $p \leq 0.01$; H, high dose; L, low dose).

| Treatment | Organ weight (g ± SE; n=5) | | Parasite burdens (mean ± SE; n=5) | | |
|---|---|---|---|---|---|
| | Spleen | Liver | Spleen | Liver | Bone marrow |
| **Control** | 0.20 ± 0.01 | 1.35 ± 0.05 | 7.60 ± 2.91 | 184.40 ± 21.57 | 25.00 ± 9.01 |
| **Empty-NIVs** | 0.36 ± 0.03** | 1.73 ± 0.15 | 13.20 ± 1.88 | 235.00 ± 27.94 | 15.40 ± 1.44 |
| **$MGB_{58}$ sol** | 0.22 ± 0.01 | 1.29 ± 0.04 | 8.40 ± 2.98 | 244.60 ± 39.03 | 15.60 ± 5.74 |
| **$MGB_{58}$-NIVs (H)** | 0.48 ± 0.04** | 1.74 ± 0.09 | 20.75 ± 7.86 | 155.80 ± 36.66 | 32.25 ± 19.02 |
| **$MGB_{58}$-NIVs (L)** | 0.23 ± 0.02 | 1.44 ± 0.08 | 6.80 ± 1.93 | 92. 75 ± 37.14* | 12.40 ± 5.35 |

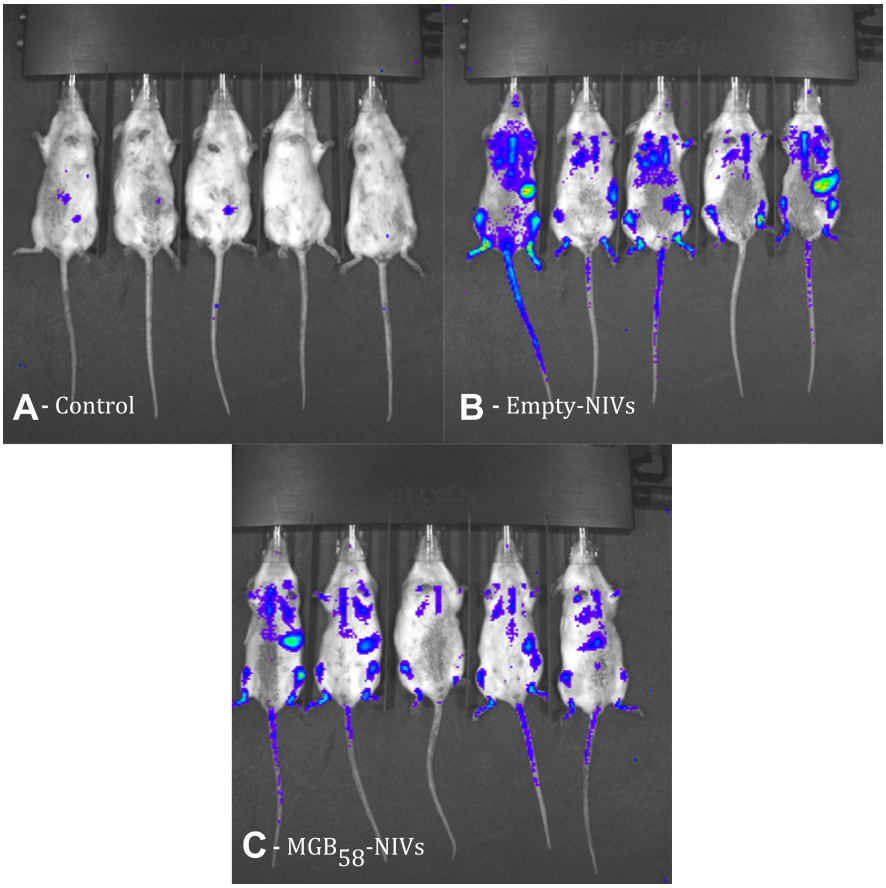


**Figure 6.11** Examples of neutrophil levels (based on luminol CLI) in uninfected BALB/c after intravenous treatment with PBS pH 7.4 containing 0.40 % v/v DMSO (control; A), empty-NIVs (0.30 mmol/kg lipid in PBS pH 7.4 containing 0.40 % v/v DMSO; B) or $MGB_{58}$-NIVs (10.00 mg/kg $MGB_{58}$, 0.30 mmol/kg in PBS pH 7.4 containing 0.40 % v/v DMSO; C). Images corresponding to 4 minute after treatment (colour scale minimum of 1.01 x $10^4$ p/s and maximum of 1.69 x $10^5$ p/s).

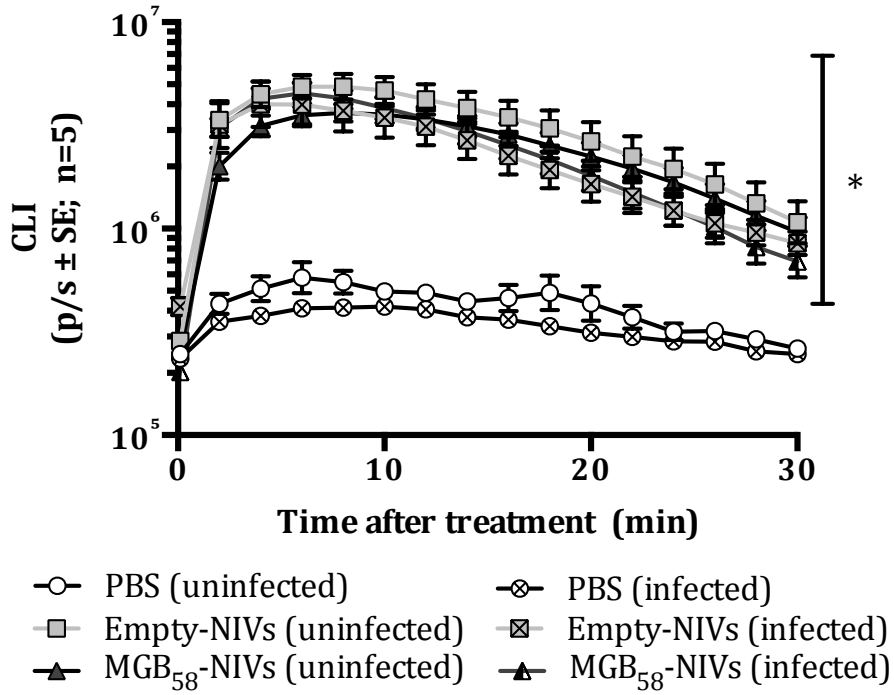


**Figure 6.12** CLI emitted from uninfected (mice shown in Figure 6.11) and *L. donovani* infected mice (day 7 post infection with LV82 $1x10^7$ parasites/mouse). Uninfected and infected mice were injected intravenously with PBS pH 7.4 containing 0.40 % v/v DMSO (control), empty-NIVs (0.30 mmol/kg lipid in PBS pH 7.4 containing 0.40 % v/v DMSO) or $MGB_{58}$-NIVs (10.00 mg/kg $MGB_{58}$, 0.30 mmol/kg in PBS pH 7.4 containing 0.40 % v/v DMSO). Images of the mice whole body were obtained under the IVIS system and luminol (ip, 100 mg/kg) was injected after 2 minutes of imaging (* $p \leq 0.05$ compared to PBS control).

## 6.6. Discussion

In this study, various compounds from the MGBs library synthesised in the Chemistry Department at the University of Strathclyde (Khalaf *et al.*, 2004, 2012; Anthony *et al.*, 2007) were tested for their potential anti-cancer and *L. donovani* activity. A preliminary screen to test the efficacy of MGBs against B16-F10-luc cancer cells indicated that 23% of the compounds had a significant effect on this cancer cell suppression. All the tested MGBs were analogues of distamycin A and structurally differed from each other. A two-way variation study suggested that the type of linked head group influenced the MGBs activity against B16-F10-luc more than the type of tail group. The lipophilicity values of the MGBs (log $D_{7.4}$) were also related to the percentage of cell suppression. In order to bind to the intracellular DNA, the MGBs compounds require penetration through the cell bilayer (Camenisch *et al.*, 1998). Therefore it is not surprising that hydrophobic drugs are more active since those cross the bilayer with ease compared to hydrophilic drugs. Compounds with an amidine head group presented the highest correlation between log $D_{7.4}$ and percentage cell suppression. Others have demonstrated the interaction between lipophilicity and MGBs efficacy based on bacterial diseases (Anthony *et al.*, 2007). More lipophilic compounds were also associated with less mammalian toxicological effects (Khalaf *et al.*, 2012).

Another factor that presented significant improvement in cell suppression was related to the pyrrole alkyl chains. Larger alkyl pyrrole chains in the MGBs structure were associated with higher efficacy against B16-F10-luc cells. However, when larger chains were used in custom synthesised $MGB_{93}$, this compound was not effective as others. Therefore, it is believed that other structural factors influenced the activity of the compounds. For a deeper understanding of the relation between MGBs structure and efficacy, a controlled fully multifactorial design should be considered. Other factors that should be studied are the effects of compound ionicity, other types of tail group, the types

of head group, the type of pyrrole groups and the binding site of the MGBs in the DNA groove (Dervan and Edelson, 2003). Any relationship between structure and activity is likely to be multifactorial with interactions between factors; therefore this should be taken into account in designing a suitable factorial design.

In this study, MGBs were formulated into NIVs as this drug delivery system can improve bioavailability. The precipitation of the MGBs upon NIVs formulation was not ideal and would require further studies. Changing the formulation to increase solubility e.g. by using CDs, could help address this problem (Jansook *et al.*, 2010). $MGB_{23}$ and $MGB_{58}$ compounds were successfully formulated into NIVs to produce MGBs-NIVs. The MGB-NIVs formulations had vesicle size in the range of micrometres, which was considerably large for a vesicular delivery system but not unexpected for NIVs produced from freeze-dried empty-NIVs that did not contain cryoprotectant (see Section 4.4). The entrapment efficiency of $MGB_{58}$ could not be determined due to solubility or instability issues (oral communication from Dr. Scott, University of Strathclyde).

Treatment with $MGB_{23}$ was tested *in vivo* in a murine model of lung cancer caused by intravenous injection of B16-F10-luc. There was only one indication that the compound had anticancer activity. Thus, intravenous treatment with $MGB_{23}$ solution or with $MGB_{23}$-NIVs significantly decreased the levels of BLI in the liver *ex vivo*, perhaps indicating an ability of the compound to reduce liver metastasis. The incorporation of $MGB_{23}$ into the NIVs enhanced the drug's anti-metastatic effect as a similar reduction in liver BLI was observed after treatment with a five fold lower drug dose ($MGB_{23}$ solution was administered at 52.60 mg/kg and $MGB_{23}$-NIVs at 10.52 mg/kg with 0.30 mmol/kg lipid). Administration of the same formulations by inhalation did not show a significant difference from control groups. Slightly smaller BLI levels in the lungs were observed for inhaled $MGB_{23}$ treated groups (solution and NIVs) although that was not significant different with a Kruskal-Wallis one-way

analysis of variance statistical test. It is important to note that $MGB_{23}$ is a very hydrophobic compound, which could be related to very low bioavailability, even encapsulated within NIVs. To corroborate this hypothesis, further experiments should focus on obtaining pharmacokinetic data.

Nonetheless, these results reflected the importance to perform *in vivo* studies in order to fully assess the effect of a drug towards its intended target. Here, *in vitro* studies against B16-F10-luc indicated that $MGB_{23}$ was the most active MGBs compound within the library and more effective that the commercialised gemcitabine. Nonetheless, in this case, the *in vivo* results did not compare to the *in vitro* data. Discrepancies between *in vitro* and *in vivo* correlations are multifactorial. Within *in vitro* studies, those factors are simplified, i.e. focus in the cell line to target within the enclosure of a well. However, the *in vivo* reality includes more factors such as the absorption, distribution, metabolism and excretion of the drug and the target of the cancer cells within a tissue tumour mass (Cardot and Davit, 2012). This study demonstrated the usefulness of using B16-F10-luc cells for drug screening studies. The BLI associated to this cell line is well correlated to cell proliferation (Craft *et al.*, 2005) and it is an accurate sensitive method for *in vitro* screening (Al-Gawhari, 2013). The same type of cells can be used to establish a metastatic lung cancer in mice with fully working immunity system, which is more relevant to clinical conditions than nude mice. The fact that this is an aggressive cell line that grows quickly in mice makes it a stringent system to test potential anticancer drugs. If $MGB_{23}$ had been active on B16-F10-luc, additional studies using human cell lines would have been carried out. In particular A549 human adenocarcinoma cell line (Jung *et al.*, 2010) that can be used as a xenograft in nude mice (Yamori *et al.*, 1999).

In contrast, the lead MGB compound against *L. donovani*, $MGB_{58}$ did have *in vivo* activity. However, $MGB_{58}$ in a solution form did not suppress parasite burdens in any of the infection sites. Though the treatment with $MGB_{58}$-NIVs caused a significant reduction in the liver parasite burdens. Interestingly, only the diluted

form of $MGB_{58}$-NIVs (10.00 mg/kg $MGB_{58}$ and 0.30 mmol/kg lipid) had significant effects but not the higher dose of $MGB_{58}$-NIVs (50.00 mg/kg $MGB_{58}$ and 1.50 mmol/kg lipid). The difference between both dosages efficacies of $MGB_{58}$-NIVs could have been related to different factors. One being the low solubility associated with the $MGB_{58}$ compound. Hence more diluted forms presented higher efficacy whereas more concentrated forms could have been deposited somewhere in the organism. Furthermore, the amount of lipids present also varied between high and low dosage forms. Higher concentration of lipids might have influenced the DNA targeting of the $MGB_{58}$. Perhaps the lipids interfered with the MGB traversing through the parasitophorous vacuole and the nucleus membrane, hence affecting the MGB binding to the parasite's DNA. Moreover, only parasite reduction in the liver were observed whilst parasite burdens in the spleen and bone marrow were kept constant. This results correlated with previous published (Abra and Hunt, 1981) and discussed data (Section 3.4 and Section 4.5) where NIVs facilitate drug target delivery to the liver.

Similar inflammatory response was observed for $MGB_{58}$-NIVs and empty-NIVs, which indicated that the $MGB_{58}$ compound, was not directly associated with the recruitment of inflammatory neutrophils. Further studies, with increased dose of $MGB_{58}$ in the NIVs with reduced lipidic content (0.30 mmol/kg lipid) could lead to more accentuated and spread parasite burden reduction i.e. including bone marrow and spleen.

In conclusion, novel MGBs for the treatment of lung cancer and visceral leishmaniasis were identified and the main objectives covered:

- Two MGBs compounds within the presented library were determined as lead candidates for B16-F10-luc cancer treatment and *L. donovani* parasite inhibition, being $MGB_{23}$ and $MGB_{58}$ respectively.

- A preliminary study determined that several structural properties on the MGBs were responsible for its activity against B16-F10-luc inhibition. MGBs with alkene linked head groups, high lipophilicity and branched alkyl pyrroles presented better efficacy against the murine cell line than other MGBs.

- $MGB_{23}$ and $MGB_{58}$ were successfully formulated in NIVs with a vesicle size within the micrometre range.

- Intravenous administration of $MGB_{23}$ did not prevent the proliferation of B16-F10-luc but affected the cancer progression in the *ex vivo* livers. This anti-metastatic effect was attributed to the compound, especially when encapsulated in NIVs.

- $MGB_{58}$ encapsulated in NIVs with low lipid concentration presented anti-leishmaniasis effect as the mean parasite burdens in the liver were significantly suppressed. The observed inflammatory effect was not attributed to the $MGB_{58}$ but to the vesicular formulation.

# CHAPTER 7. CONCLUSIONS AND FURTHER WORK

## 7.1. General outcomes

The main aim of this project was to investigate the use of NIVs as a stable and versatile drug delivery system, especially for the inhaled route of administration. Firstly, the research gap recognised in the general introduction, established that further optimisation of AmB-NIVs was required. Special focus was set on increasing stability of the formulation and further characterisation of the inhalation profile, in order to treat visceral leishmaniasis. In this case, a stable and scalable freeze-dried AmB-NIVs formulation was produced. The incorporation of the lyoprotectant sucrose and the optimisation of the freeze-drying procedure permitted the maintenance of the physicochemical properties of AmB-NIVs. The lyophilised formulation was proven stable for a 4 months stability study and up to 21 days after rehydration when stored at 4°C. AmB-NIVs were able to supress the progress of *in vivo* visceral leishmaniasis when administered both intravenously or by inhalation to different strains of *L. donovani* (LV82-luc, LV82 or 200015). AmB encapsulated within NIVs was significantly more effective supressing the parasite burdens than the drug alone (AmB-CD), especially in the liver. Inhaled AmB-NIVs demonstrated to target intracellular infections in the mononuclear phagocytic system in a systemic level. From those, AmB-NIVs with larger particle size in the range of 800 nm were superior to the smaller range of the particles (200 nm) in terms of leishmaniasis burden inhibition.

It was observed, that scaled-up empty-NIVs could not maintain their physicochemical properties upon freeze-drying. Hence, the rehydration of the lyophilisate with different drug solutions resulted in considerably enlarged particles. Several lyoprotectants were studied to impair the particle damage upon freeze-drying, with only HPγCD presenting successful results. The novel use of HPγCD, to protect the vesicles of empty-NIVs upon lyophilisation also included better lyoprotectant characteristics compared to other additives. HPγCD had a higher $T_g$' than other lyoprotectants, which would reduce

considerably the primary drying time and therefore cost of production. The optimised freeze-dried empty-NIVs (with HPγCD) was able to encapsulate different drugs by the passive DRV method such as cisplatin, gemcitabine and AmB. Those could be formulated *in situ* evading unwanted drug instability issues. Moreover, the substrate luciferin incorporated within NIVs by passive DRV, demonstrated increased *in vivo* contact with the luciferase expressing parasites (LV82-luc) than the solution alone.

An extensive study of AmB-NIVs suggested that the NIVs particles decreased in diameter upon nebulisation but other characteristics, such as entrapment efficiency were maintained for both active and passive vibrating-mesh nebulisers. The apparent viscosity of the formulations influenced the nebulisers aerosol output and percentage of drug delivered, with a maximum allowed of 2 mPa·s. Active vibrating-mesh nebulisers produced smaller MMAD when AmB-NIVs or Cis-NIVs were nebulised (< 4 μm) compared to passive vibrating-mesh nebulisers. All the NIVs components were demonstrated to travel in conjunction through the airstream upon nebulisation. *In vivo* administration of AmB-NIVs presented less than 1 % of the inhaled drug in the lungs. Inhaled luciferin (Luc-NIVs) was demonstrated to reach the site of action, since the BLI of the cancer cells in the lungs was induced.

Already commercialised drugs benefited from the NIVs delivery system, such as AmB, cisplatin or gemcitabine. Moreover, the technology was further investigated for novel MGBs compounds. Those MGBs were screened against B16-F10-luc to identify the most successful candidates against lung cancer. Several MGBs structures were identified as responsible for the compounds inhibitory profile. MGBs with alkene-linked group between the main body and the head, high lipophilicity compounds and MGBs with branched pyrroles were significantly superior against the murine cell line. $MGB_{23}$ and $MGB_{58}$ were identified *in vitro* as candidates for lung cancer and *L. donovani* treatment.

$MGB_{23}$ presented no major efficacy against the *in vivo* model. However, $MGB_{58}$-NIVs was effective against *in vivo L. donovani*.

This work pointed towards several novel knowledge characteristics related to NIVs delivery system. Moreover, the initial stated objectives were carefully met during the study:

- The production of freeze-dried AmB-NIVs was scalable and the formulation was stable upon four-month storage at 4°C. Inhaled AmB-NIVs demonstrated to inhibit the progression of visceral leishmaniasis, an intracellular and systemic disease.

- Empty-NIVs were successfully freeze-dried with the use of HPγCD as a lyoprotectant. This allowed the encapsulation of various drugs whilst maintaining NIVs physicochemical characteristics. Therefore the freeze-dried empty-NIVs technology has the vast potential to be used as a delivery system for different applications.

- NIVs were successfully nebulised with active and passive vibrating-mesh nebulisers maintaining the structure through the airstream. Nebulised AmB-NIVs decreased in vesicle size but maintained the drug entrapment efficiency, presented respirable aerosol particle size (< 5 μm) and were detected in the lungs of treated rats.

- $MGB_{23}$ was identified *in vitro* as a lead compound to treat lung cancer but had little efficacy in the *in vivo* model. Whereas, $MGB_{58}$ encapsulated within NIVs was effective against *in vivo L. donovani*.

## 7.2. Further work

The presented study covered the most significant experiments to gain novel knowledge of the NIVs technology. Nonetheless, further lines of work are suggested for following investigations on the subject.

The freeze-drying optimisation of NIVs particles could benefit from further investigations with different equipment. For instance, the Epsilon 2-4 LSC freeze dryer used in these studies did not have a sample thief hatch or a system for accurate determination of process end-point. Hence, the approximation of end-point was noted when product thermocouples of the product were similar to the chamber atmosphere temperature. However, the vials containing the thermocouples are not representative of the whole batch and those vials are likely to nucleate at higher temperature and dry faster. Therefore, due to the variability associated to this type of end-point determination, extra time was incorporated to the primary drying in order to avoid collapse or melt-back during the increase of shelf temperature in the secondary drying. As a consequence, the time of primary drying and the process cost was increased. Further optimisation could be archived using a freeze-drier with a sample thief hatch followed by residual moisture measurement either gravimetrically or by Karl Fischer. Other techniques such as comparative pressure measurements between drying chamber and condenser are more suitable for continuous manufacturing or process analytical technology implementation (Van Arnum, 2013). Patel *et al.* (2010) established that the Pirani gauge was the best choice between those methods in order to evaluate the end of primary drying. Pirani controls the thermal conductivity of the gas in the drying chamber associated to water vapour. When the Pirani pressure decreases it is an accurate indication of complete sublimation. Further freeze-drying optimisation would benefit from more accurate identification of collapse temperatures. In this study, the different thermal events during freeze thawing were investigated using a conventional DSC. However, some samples contained a subtle $T_g$' and sample

concentration was the only option to increase the signal of the phase transition. The use of a temperature-modulated DSC (TMDSC) is believed to overcome those difficulties. The total heat flow obtained in conventional DSC is separated in TMDSC which allows more precise determination of $T_g$' (Santoveña *et al.*, 2010). Moreover, the use of freeze-drying microscopy would be beneficial to observe the intrinsic collapse events (Pikal and Shah, 1990).

Maintaining AmB at 70°C for more than 1 hour affected the integrity of AmB and this was observed in the validated HPLC method. However, the use of other detection methods such as mass spectroscopy would specifically indicate the different species of the degradation reaction. The production of AmB-NIVs could also benefit from a HPH final step, as used in scaled-up studies for empty-NIVs. This would further reduce the vesicle size at a cooler temperature and facilitate the final filtration step. Further studies should tackle the sterilisation of AmB-NIVs since it is necessary to consider this step as an integral part of the production of a formulations for respiratory delivery (Cipolla *et al.*, 2014). Since filter-sterilisation was not suitable for AmB-NIVs, different approaches could be: using dynamic HPH or freeze-drying in a sterile environment. Other sterilisation procedures have been shown to be effective for freeze-dried liposomes, such as γ-irradiation. Studies showed that the radiation was not detrimental to the lyophilised formulation since the major source of damaging radicals were attributed to water content (Mohammed *et al.*, 2006).

The addition of sucrose increased the vesicle size stability of AmB-NIVs formulations both in the freeze-drying process and the vibrating-mesh nebulisation. The freeze-dried formulation was proven to be chemically stable when stored in the fridge for almost 6 months. Nonetheless, the formulation was not stable at the accelerated stability study conditions proposed by the ICH guidelines (40°C for 6 months; ICH, 2003). AmB-NIVs could benefit of further freeze-drying optimisation studies, as discussed previously. Hence, repeating

the stability study in compliance with the long-term storage conditions of the ICH guidelines would be advisable (25°C for 12 months).

*In vivo* administration of NIVs with the highest concentrations of lipids (1.50 mmol/kg) resulted in increase of spleen weight and neutrophil induced CLI. This indicates that an inflammatory response was induced, probably due to the lipid components. Nonetheless, this reaction was unnoticeable when the amount of lipids was reduced by dilution of the formulations. Therefore, further NIVs formulation studies should include the minimum lipidic components whilst maintaining the NIVs enhanced properties. A reduction in lipid content may also lead to a more isotonic formulation, especially benefiting NIVs containing high levels of lyoprotectant.

AmB-NIVs maintained their critical physicochemical properties upon vibrating mesh nebulisation. Even though the vesicle size decreased through the mesh, the entrapment efficiency of the AmB formulation remained stable. This could have been attributed to the lipophilic nature of AmB. To deeply investigate this hypothesis, further vibrating-mesh nebulisation studies, including different hydrophilic drugs within the NIVs, should be characterised in terms of vesicle size and entrapment efficiency variation.

Several drugs were encapsulated in NIVs using the passive DRV method by rehydrating freeze-dried empty-NIVs with HPγCD. Lyophilised empty-NIVs with HPγCD have the potential to increase the bioavailability and target delivery of a vast number of drugs. In this study, NIVs have demonstrated to specifically target the mononuclear phagocytic system where *Leishmania* parasites are located. Other intracellular diseases, such as tuberculosis or toxoplasmosis, could benefit of this delivery system. Further *in vitro* and *in vivo* investigations of NIVs encapsulating drugs such as rifampicin, pyrimethamine or sulfadiazine may lead to innovative results to treat those different diseases. An example of a novel drug that benefited from the NIVs technology was $MGB_{58}$. $MGB_{58}$-NIVs

decreased the *Leishmania* parasite burthens. Further experiments, should investigate the $MGB_{58}$ solubility so DMSO is completely removed from the formulation. Furthermore, the addition of HPγCD in the freeze-dried empty-NIVs used to produce $MGB_{58}$-NIVs would produce smaller and more homogeneous particle size. Moreover, additional $MGB_{58}$ studies should focus on investigating its mechanism of action against different *Leishmania* species.

# REFERENCES

Abd-Elbary A, El-laithy HM, Tadros MI. 2008. Sucrose stearate-based proniosome-derived niosomes for the nebulisable delivery of cromolyn sodium. International Journal of Pharmaceutics 357: 189–98.

Abdelkader H, Wu Z, Al-Kassas R, Alany RG. 2012. Niosomes and discomes for ocular delivery of naltrexone hydrochloride: Morphological, rheological, spreading properties and photo-protective effects. International Journal of Pharmaceutics 433: 142–8.

Abra R, Hunt C. 1981. Liposome disposition in vivo. III. Dose and vesicle-size effects. Biochimica et Biophysica Acta 666: 493–503.

Abra R, Szoka FC. 1988. Stabilized liposome/ amphotericin composition and method. USA patent number 4,766,046.

Abra R, Hunt C, Lau D. 1984. Liposome Disposition in vivo VI: Delivery to the Lung. Journal of Pharmaceutical Sciences 73: 203–6.

Abramowicz M, Zuccotti G, Pflomm J-Ma. 2015. An Inhaled Insulin (Afrezza). The Journal of the American Medical Association 313: 2176–7.

Aerogen. 2014. Aeroneb Lab. http://www.aerogen.com/products/aeroneb-lab.html [Accessed June 2014].

Al-Gawhari FJ. 2013. Development of a non-ionic surfactant vesicles formulation of gemcitabine for pulmonary delivery. University of Strathclyde, PhD thesis.

Alexander BD, Winkler TP, Shi S, Dodds Ashley ES, Hickey AJ. 2011. In vitro characterization of nebulizer delivery of liposomal amphotericin B aerosols. Pharmaceutical Development and Technology 16: 577–82.

Alsaadi M. 2011. Non-Ionic Surfactant Vesicles as a Delivery System for Cisplatin. University of Strathclyde, PhD thesis.

Alsaadi M, Carter K, Mullen A. 2013. High performance liquid chromatography with evaporative light scattering detection for the characterisation of a vesicular delivery system during stability studies. Journal of Chromatography. A 1320: 80–5.

Alsaadi M, Italia J, Mullen M, *et al.*, 2012. The efficacy of aerosol treatment with non-ionic surfactant vesicles containing amphotericin B in rodent models of leishmaniasis and pulmonary aspergillosis infection. Journal of Controlled Release 160: 685–91.

Amidon GL, Lennernäs H, Shah VP, Crison JR. 1995. A Theoretical Basis for a Biopharmaceutic Drug Classification: The Correlation of in vitro Drug Product

Dissolution and in Vivo Bioavailability. Pharmaceutical Research 12: 413–20.

Anabousi V. 2006. Liposomal Drug Carrier Systems for Inhalation Treatment of Lung Cancer. University of Saarlandes, PhD thesis.

Andersen P, Doherty TM. 2005. Tuberculosis vaccine. Nature Reviews Microbiology 3: 656–62.

Anthony NG, Breen D, Clarke J, *et al.,* 2007. Antimicrobial lexitropsins containing amide, amidine, and alkene linking groups. Journal of Medicinal Chemistry 50: 6116–25.

Arcamone F, Penco S, Orezzi P, Nicolella V, Pirelli A. 1964. Structure and Synthesis of Distamycin A. Nature 203: 1064–5.

Ardizzoni A, Tiseo M, Boni L. 2014. Validation of standard definition of sensitive versus refractory relapsed small cell lung cancer: a pooled analysis of topotecan second-line trials. European Journal of Cancer 50: 2211–8.

Van Arnum. 2013. Advances in PAT for Parenteral Drug Manufacturing. BioPharm International 26: 18–22.

Arunothayanun P, Bernard MS, Craig DQ, Uchegbu IF, Florence a. T. 2000. The effect of processing variables on the physical characteristics of non-ionic surfactant vesicles (niosomes) formed from a hexadecyl diglycerol ether. International Journal of Pharmaceutics 201: 7–14.

Asking L, Olsson B. 1997. Calibration at Different Flow Rates of a Multistage Liquid Impinger. Aerosol Science and Technology 27: 39–49.

Ayensu I, Mitchell JC, Boateng JS. 2012. Development and physico-mechanical characterisation of lyophilised chitosan wafers as potential protein drug delivery systems via the buccal mucosa. Colloids and Surfaces B: Biointerfaces 91: 258–65.

Azarmi S, Roa WH, Löbenberg R. 2008. Targeted delivery of nanoparticles for the treatment of lung diseases. Advanced Drug Delivery Reviews 60: 863–75.

Baalousha M, Lead JR. 2012. Rationalizing nanomaterial sizes measured by AFM, FlFFF and DLS: sample preparation, polydispersity and particle structure. Environmental Science Technology 46: 6134–42.

Bai S, Ahsan F. 2010. Inhalable Liposomes of Low Molecular Weight Heparin for the Treatment of Venous Thromboembolism. Journal of Pharmaceutical Sciences 99: 4554–64.

Bailey C, Barnett A. 2010. Inhaled insulin: new formulation, new trial. The

Lancet 375: 2199–201.

Bakker EM, Volpi S, Salonini E, *et al.,* 2011. Improved treatment response to dornase alfa in cystic fibrosis patients using controlled inhalation. European Respiratory Journal 38: 1328–35.

Baraldi PG, Bovero A, Fruttarolo F, *et al.,* 2004. DNA minor groove binders as potential antitumor and antimicrobial agents. Medicinal Research Reviews 24: 475–528.

Barratt G, Bretagne S. 2007. Optimizing efficacy of Amphotericin B through nanomodification. International Journal of Nanomedicine 2: 301–13.

Barrett MP, Gemmell CG, Suckling CJ. 2013. Minor groove binders as anti-infective agents. Pharmacology and Therapeutics 139: 12–23.

Barry PW, O'Callaghan C. 1996. Inhalational drug delivery from seven different spacer devices. Thorax 51: 835–40.

Bates DW, Su L, Yu DT, *et al.,* 2001. Mortality and costs of acute renal failure associated with amphotericin B therapy. Clinical Infectious Diseases 32: 686–93.

Bayindir ZS, Yuksel N. 2010. Characterization of Niosomes Prepared With Various Nonionic Surfactants for Paclitaxel Oral Delivery. Journal of Pharmaceutical Sciences 99: 2049–60.

Besteiro S, Williams RAM, Coombs GH, Mottram JC. 2007. Protein turnover and differentiation in Leishmania. International Journal for Parasitology 37: 1063–75.

Beyer J, Schwartz S, Barzen G, *et al.,* 1994. Use of amphotericin B aerosols for the prevention of pulmonary aspergillosis. Infection 22: 143–8.

Bitonti AJ, Dumont J a, Low SC, *et al.,* 2004. Pulmonary delivery of an erythropoietin Fc fusion protein in non-human primates through an immunoglobulin transport pathway. Proceedings of the National Academy of Sciences of the United States of America 101: 9763–8.

Boer AH, Gjaltema D, Hagedoorn P, Frijlink HW. 2002. Characterization of inhalation aerosols: a critical evaluation of cascade impactor analysis and laser diffraction technique. International Journal of Pharmaceutics 249: 219–31.

Bridges PA, Taylor KMG. 1998. Nebulisers for the generation of liposomal aerosols. International Journal of Pharmaceutics 173: 117–25.

Bridges PA, Taylor KMG. 2001. The effects of freeze-drying on the stability of

liposomes to jet nebulization. The Journal of Pharmacy and Pharmacology 53: 393–8.

Brime B, Moreno MA, Frutos G, Ballesteros MP, Frutos P. 2002. Amphotericin B in oil-water lecithin-based microemulsions: formulation and toxicity evaluation. Journal of Pharmaceutical Sciences 91: 1178–85.

British Lung Foundation. 2014. British Lung Foundation, about us. www.blf.org.uk [Accessed January 2014].

Brody H, Grayson M, Carmichael M, Piper W, Silao R. 2012. Chronic obstructive pulmonary disease. Nature 489: S1.

Byron R. 1986. Prediction of drug residence times in regions of the human respiratory tract following aerosol inhalation. Journal of Pharmaceutical Sciences 7: 433–8.

Cai X, Gray PJ, Von Hoff DD. 2009. DNA minor groove binders: Back in the groove. Cancer Treatment Reviews 35: 437–50.

Camenisch G, Alsenz J, Van De Waterbeemd H, Folkers G. 1998. Estimation of permeability by passive diffusion through Caco-2 cell monolayers using the drugs' lipophilicity and molecular weight. European Journal of Pharmaceutical Sciences 6: 313–9.

Cardot J-M, Davit BM. 2012. In vitro–In Vivo Correlations: Tricks and Traps. The AAPS Journal 14: 491–9.

Carstensen JT, Rhodes CT. 2000. Drug stability, principles and practices, Marcel Dekker Inc. (ed). Third edition: New York.

Carter K, Baillie A, Williams D. 1997. Vesicle formulation comprising non-ionic surfactant. EU patent number: EP 0 774 958 B1.

Carter KC, Baillie AJ, Mullen AB. 1999. The cured immune phenotype achieved by treatment of visceral leishmaniasis in the BALB/c mouse with a nonionic surfactant vesicular formulation of sodium stibogluconate does not protect against reinfection. Clinical and Diagnostic Laboratory Immunology 6: 61–5.

Carter KC, Hutchison S, Boitelle A, Murray HW, Sundar S, Mullen AB. 2005. Sodium stibogluconate resistance in Leishmania donovani correlates with greater tolerance to macrophage antileishmanial responses and trivalent antimony therapy. Parasitology 131: 747–57.

Carter KC, Mullen AB, Ferro VA. 2009. Pulmonary drug delivery. US patent number: 0324743 A1.

Carter KC, Mullen AB, Sundar S, Kenney RT. 2001. Efficacies of Vesicular and Free Sodium Stibogluconate Formulations against Clinical Isolates of Leishmania donovani. Antimicrobial Agents and Chemotherapy 45: 3555–9.

Casal J, Varela S, Anido U, *et al.,* 2011. Induction Chemotherapy With Docetaxel (D) and Cisplatin (C) Followed by Concurrent Thoracic Radiotherapy With Biweekly D and C for Stage III Non-Small Cell Lung Cancer (NSCLC) – a Galician Lung Cancer Group Study. European Journal of Cancer 47: S603.

Casares C, Ramírez-Camacho R, Trinidad A, Roldán A, Jorge E, García-Berrocal J. 2012. Reactive oxygen species in apoptosis induced by cisplatin: Review of physiopathological mechanisms in animal models. European Archives of Oto-Rhino-Laryngology 269: 2455–9.

Cassidy JP, Amin N, Marino M, *et al.,* 2011. Insulin lung deposition and clearance following technosphere insulin inhalation powder administration. Pharmaceutical Research 28: 2157–64.

Chakrabarty US, Pal TK. 2011. Rapid and Sensitive High Performance Liquid Chromatography Method for The Determination of Amphotericin B in Rat Plasma. Journal of Pharmacy Research 4: 3194–7.

Chattopadhyay A, Jafurulla M. 2011. A novel mechanism for an old drug: Amphotericin B in the treatment of visceral leishmaniasis. Biochemical And Biophysical Research Communications 416: 7–12.

Chen C, Han D, Cai C, Tang X. 2010. An overview of liposome lyophilization and its future potential. Journal of Controlled Release 142: 299–311.

Cheng Y, Irshand H, Kuehl P, Holmes T, Sherwood R, Hobbs C. 2008. Lung deposition of droplet aerosols in monkeys. Inhalation Toxicology 11: 1029–36.

Chono S, Fukuchi R, Seki T, Morimoto K. 2009. Aerosolized liposomes with dipalmitoyl phosphatidylcholine enhance pulmonary insulin delivery. Journal of Controlled Release 137: 104–9.

Christopher D, Dey M, Lyapustina L, *et al.,* 2013. Alternative approches for MMAD determination. http://ipacrs.com/PDFs/Posters/Alternative MMAD.pdf [Accessed June 2013].

Cipolla D, Gonda I, Chan H-K. 2013. Liposomal formulations for inhalation. Therapeutic Delivery 4: 1047–72.

Cipolla D, Shekunov B, Blanchard J, Hickey A. 2014. Lipid-based carriers for pulmonary products: Preclinical development and case studies in humans.

Advanced Drug Delivery Reviews 75: 53–80.

Clancy JP, Dupont L, Konstan MW, *et al.,* 2013. Phase II studies of nebulised Arikace in CF patients with Pseudomonas aeruginosa infection. Thorax 68: 818–25.

Clarke SW. 1988. Inhaler therapy. The Quarterly Journal Of Medicine 67: 355–68.

Clerc S, Barenholz Y. 1995. Loading of amphipathic weak acids into liposomes in response to transmembrane calcium acetate gradients. Biochimica Et Biophysica Acta 1240: 257–65.

Colella G, Marchini S, D'Incalci M, Brown R, Broggini M. 1999. Mismatch repair deficiency is associated with resistance to DNA minor groove alkylating agents. British Journal of Cancer 80: 338–43.

Coll M, Frederick CA, Wang AH, Rich A. 1987. A bifurcated hydrogen-bonded conformation in the d(A.T) base pairs of the DNA dodecamer d(CGCAAATTTGCG) and its complex with distamycin. Proceedings of the National Academy of Sciences of the United States of America 84: 8385–9.

Collins N. 2009. Nebulizer therapy in cystic fibrosis: an overview. Journal of the Royal Society of Medicine 102: S11–7.

Colombo P, Traini D, Buttini F. 2012. Inhalation Drug Delivery, Wiley-Blackwell (ed). First edition: Chichester, West Sussex.

Cook RO, Pannu RK, Kellaway IW. 2005. Novel sustained release microspheres for pulmonary drug delivery. Journal of Controlled Release 104: 79–90.

Craft N, Bruhn KW, Nguyen BD, *et al.,* 2005. Bioluminescent imaging of melanoma in live mice. Journal of Investigative Dermatology 125: 159–65.

Crowe JH, Hoekstra FA, Nguyen KHN, Crowe LM. 1996. Is vitrification involved in depression of the phase transition temperature in dry phospholipids? Biochimica et Biophysica Acta - Biomembranes 1280: 187–96.

Cryan S-A, Sivadas N, Garcia-Contreras L. 2007. In vivo animal models for drug delivery across the lung mucosal barrier. Advanced Drug Delivery Reviews 59: 1133–51.

Dalby RN, Eicher J, Zierenberg B. 2011. Development of Respimat soft mist inhaler and its clinical utility in respiratory disorders. Medical Devices: Evidence and Research 4: 145–55.

Darwiche K, Zarogoulidis P, Karamanos NK, *et al.,* 2013. Efficacy versus safety

concerns for aerosol chemotherapy in non-small-cell lung cancer: a future dilemma for micro-oncology. Future oncology (London, England) 9: 505–25.

Darwis Y, Kellaway IW. 2001. Nebulisation of rehydrated freeze-dried beclomethasone dipropionate liposomes. International Journal of Pharmaceutics 215: 113–21.

Das VNR, Siddiqui NA, Pandey K, *et al.,* 2009. A controlled, randomized nonblinded clinical trial to assess the efficacy of amphotericin B deoxycholate as compared to pentamidine for the treatment of antimony unresponsive visceral leishmaniasis cases in Bihar, India. Therapeutics and Clinical Risk Management 5: 117–24.

Deimann W. 1984. Endogenous peroxidase activity in mononuclear phagocytes. Progress in Histochemistry and Cytochemistry 15: 1–59.

Denyer J, Black A, Nikander K, Dyche T, Prince I. 2010. Domiciliary experience of the Target Inhalation Mode (TIM) breathing maneuver in patients with cystic fibrosis. Journal of Aerosol Medicine and Pulmonary Drug Delivery 23: S45–54.

Dershwitz M, Walsh J, Morishige R, *et al.,* 2000. Pharmacokinetics and pharmacodynamics of inhaled versus intravenous morphine in healthy volunteers. Anesthesiology 93: 619–28.

Dervan PB, Edelson BS. 2003. Recognition of the DNA minor groove by pyrrole-imidazole polyamides. Current Opinion in Structural Biology 13: 284–99.

Desai TR, Finlay WH. 2002. Nebulization of niosomal all-trans-retinoic acid: An inexpensive alternative to conventional liposomes. International Journal of Pharmaceutics 241: 311–7.

Desjeux. 1996. Leishmaniasis, public health aspects and control. Clinics in Dermatology 14: 417–23.

Dhand R. 2010. Intelligent nebulizers in the age of the Internet: The I-neb Adaptive Aerosol Delivery (AAD) system. Journal o Aerosol Medicine and Pulmonary Drug Delivery 23: III – V.

Doherty MM, Hughes PJ, Kim SR, Mainwaring DE, Charman WN. 1994. Effect of lyophilization on the physical characteristics of medium molecular mass hyaluronates. International Journal of Pharmaceutics 111: 205–11.

Dolovich M, Sanchis J, Rossman C, Newhouse M. 1976. Aerosol penetrance: a sensitive index of peripheral airways obstruction. Journal of Applied Physiology 40: 468–71.

Dolovich MB, Dhand R. 2011. Aerosol drug delivery: developments in device design and clinical use. Lancet 377: 1032–45.

Dong MM. 2006. Modern HPLC for practicing scientists, John Wiley and Sons (ed). First edition: New Jersey.

Doro B. 2014. Development of a gamma glutamylcysteine synthetase vaccine to protect against Leishmania infection. University of Strathclyde, PhD thesis.

Dufes C, Gaillard F, Uchegbu IF, Schätzlein AG, Olivier J-C, Muller J-M. 2004. Glucose-targeted niosomes deliver vasoactive intestinal peptide (VIP) to the brain. International Journal of Pharmaceutics 285: 77–85.

Duman O, Tunç S. 2009. Electrokinetic and rheological properties of Na-bentonite in some electrolyte solutions. Microporous and Mesoporous Materials 117: 331–8.

Dutcher J, Gold W, Pagano J, J V. 1959. Amphotericin B, its production and its salts. US patent number: 2,908,611.

Edwards KA, Baeumner AJ. 2006. Analysis of liposomes. Talanta 68: 1432–41.

Eldem T, Arican-Cellat N. 2001. Determination of amphotericin B in human plasma using solid-phase extraction and high-performance liquid chromatography. Journal of Pharmaceutical and Biomedical Analysis 25: 53–64.

Elhissi A, Brar J, Roberts S, Taylor K. 2005. Enhanced fine particle dose of nebulised salbutamol sulphate using a proliposome approach. The Journal of Pharmacy And Pharmacology 57: 48–57.

Elhissi A, Faizi M, Naji W, Gill H, Taylor K. 2007. Physical stability and aerosol properties of liposomes delivered using an air-jet nebulizer and a novel micropump device with large mesh apertures. International Journal of Pharmaceutics 334: 62–70.

Elhissi A, Giebultowicz J, Stec A, *et al.,* 2012. Nebulization of ultradeformable liposomes: the influence of aerosolization mechanism and formulation excipients. International Journal of Pharmaceutics 436: 519–26.

Elhissi A, Hidayat K, Phoenix D, *et al.,* 2013. Air-jet and vibrating-mesh nebulization of niosomes generated using a particulate-based proniosome technology. International Journal of Pharmaceutics 444: 193–9.

Elhissi A, Karnam K, Danesh-Azari M, Gill HS, Taylor K. 2006. Formulations generated from ethanol-based proliposomes for delivery via medical nebulizers. The Journal of Pharmacy And Pharmacology 58: 887–94.

Espada R, Valdespina S, Alfonso C, Rivas G, Ballesteros MP, Torrado JJ. 2008. Effect of aggregation state on the toxicity of different amphotericin B preparations. International Journal of Pharmaceutics 361: 64–9.

Esposito E, Bortolotti F, Menegatti E, Cortesi R. 2003. Amphiphilic association systems for Amphotericin B delivery. International Journal of Pharmaceutics 260: 249–60.

Van Etten EW, ten Kate MT, Stearne LE, Bakker-woudenberg IA. 1995. Amphotericin B liposomes with prolonged circulation in blood : in vitro antifungal activity , toxicity , and efficacy in systemic candidiasis in leukopenic mice. Antimicrobial Agents and Chemotherapy 39: 1954–8.

European Medicines Agency. 1995. ICH Topic Q2 (R1) Note for guidance on validation of analytical procedures. http://www.ema.europa.eu/docs/en_GB/document_library/Scientific_guideline/2009/09/WC500002662.pdf [Accessed September 2015].

European Pharmacopeia. 2005. 2.9.18 Preparations for inhalation: aerodynamic assessment of fine particles. Preparations for Inhalation 5.1: 2799–811.

European Pharmacopoeia. 2004. Section 5.1. General Texts On Sterility. The Directorate for the Quality of Medicines and Healthcare of the Council of Europe 5.0.

European Pharmacopoeia. 2008. Section 2.9.44 Preparations for Nebulisation: Characterisation. The Directorate for the Quality of Medicines and Healthcare of the Council of Europe 6.0.

European Respiratory Society. 2012. The Burden Of Lung Disease, European Respiratory Society (ed). Chapter 1.

Fauvel M, Farrugia C, Tsapis N, *et al.,* 2012. Aerosolized liposomal amphotericin B : Prediction of lung deposition , in vitro uptake and cytotoxicity. International Journal of Pharmaceutics 436: 106–10.

Fittler A, Mayer A, Kocsis B, Gerlinger I, Fónay F, Botz L. 2007. Stability testing of amphotericin B nasal spray solutions with chemical and biological analysis. Acta Pharmaceutica Hungarica 77: 159–64.

Food and Drug Administration. 2015. Liposome Drug Products - Guidance for Industry. Pharmaceutical Quality Revision 1: 1–13.

Franks F. 2007. Freeze-drying of Pharmaceuticals and Biopharmaceuticals, principles and practice, The Royal Society of Chemistry (ed). First edition:

Cambridge.

Fresta M, Villari A, Puglisi G, Cavallaro G. 1993. 5-Fluorouracil: Various kinds of loaded liposomes: Encapsulation efficiency, storage stability and fusogenic properties. International Journal of Pharmaceutics 99: 145–56.

Gan KH, Bruttini R, Crosser OK, Liapis AI. 2005. Freeze-drying of pharmaceuticals in vials on trays: effects of drying chamber wall temperature and tray side on lyophilization performance. International Journal of Heat and Mass Transfer 48: 1675–87.

Gandhi NR, Nunn P, Dheda K, *et al.,* 2010. Multidrug-resistant and extensively drug-resistant tuberculosis: a threat to global control of tuberculosis. The Lancet 375: 1830–43.

Gaspar MM, Gobbo O, Ehrhardt C. 2010. Generation of liposome aerosols with the Aeroneb Pro and AeroProbe nebulizers. Journal of Liposome Research 20: 55–61.

Gately DP, Howell SB. 1993. Cellular accumulation of the anticancer agent cisplatin: a review. British Journal of Cancer 67: 1171–6.

Gentile L, Mortensen K, Rossi CO, Olsson U, Ranieri G a. 2011a. Multi-lamellar vesicle formation in a long-chain nonionic surfactant: C16E4/D2O system. Journal of Colloid and Interface Science 362: 1–4.

Gentile L, Rossi CO, Olsson U, Ranieri GA. 2011b. Effect of shear rates on the MLV formation and MLV stability region in the C12E5/D2O System: Rheology and Rheo-NMR and Rheo-SANS experiments. Langmuir 27: 2088–92.

Ghanbarzadeh S, Valizadeh H, Zakeri-Milani P. 2013. The effects of lyophilization on the physico-chemical stability of sirolimus liposomes. Advanced Pharmaceutical Bulletin 3: 25–9.

Ghazanfari T, Elhissi A, Ding Z, Taylor K. 2007. The influence of fluid physicochemical properties on vibrating-mesh nebulization. International Journal of Pharmaceutics 339: 103–11.

Gilead Sciences Limited. 2012. AmBisome Liposomal Amphotericin B. http://www.biopharma-mea.com/products/hepatology/ [Access August 2015].

Gilpin RK. 2011. Pharmaceuticals and related drugs. Analytical Chemistry 83: 4489–507.

Goldstraw P, Ball D, Jett JR, *et al.,* 2011. Non-small-cell lung cancer. The Lancet 378: 1727–40.

Goodman N, Morgan M, Nikander K. 2010. Evaluation of Patient-Reported Outcomes and Quality of Life with the I-neb AAD System. Journal of Aerosol Medicine and Pulmonary Drug Delivery 23: S61–70.

Gradzielski M. 2011. The rheology of vesicle and disk systems — Relations between macroscopic behaviour and microstructure. Current Opinion in Colloid & Interface Science 16: 13–7.

Graham-Rowe D. 2012. Therapeutics: Strength in numbers. Nature 489: S16–7.

Grevelink S, Lerner E. 1996. Leishmaniasis. Journal of the American Academy of Dermatology 34: 257–72.

Gridelli C, Manzione L, Perrone F, *et al.,* 2001. Carboplatin plus paclitaxel in extensive small cell lung cancer: a multicentre phase 2 study. British Journal of Cancer 84: 38–41.

Groll AH, Walsh TJ. 2002. Antifungal chemotherapy : advances and perspectives. Swiss Medical Weekly 132: 303–12.

Groneberg DA, Witt C, Wagner U, Chung KF, Fischer A. 2003. Fundamentals of pulmonary drug delivery. Respiratory Medicine 97: 382–7.

Gross S, Gammon ST, Moss BL, Rauch D, Harding J, Jay W. 2009. Bioluminescence imaging of myeloperoxidase activity in vivo. Nature Medicine 15: 455–61.

Guerin PJ, Olliaro P, Sundar S, *et al.,* 2002. Visceral leishmaniasis: current status of control, diagnosis, and treatment, and a proposed research and development agenda. The Lancet Infectious Diseases 2: 494–501.

Hadj-Mohammadi MR, Chaichi MJ. 1996. Separation, identification and determination of luciferin in the Iranian firefly, Lampyris turkestanicus by HPLC and spectroscopic methods. Photochemistry and Photobiology 64: 821–2.

Hajos F, Stark B, Hensler S, Prassl R, Mosgoeller W. 2008. Inhalable liposomal formulation for vasoactive intestinal peptide. International Journal of Pharmaceutics 357: 286–94.

Hardaker L, Hatley R. 2010. In vitro characterization of the I-neb Adaptive Aerosol Delivery (AAD) system. Journal of Aerosol Medicine and Pulmonary Drug Delivery 23: S11–20.

Hastings, Grady, Sakuma, Matthay. 1992. Clearance of different-sized proteins space in humans and rabbits from the alveolar. Journal of Applied Physiology 73: 1310–6.

Hawksworth R, Sykes A, Faris M, Mant T, Lee T. 2002. Albuterol HFA is as effective as albuterol CFC in preventing exercise-induced bronchoconstriction. Annals Allergy Asthma Immunology 88: 473–7.

He Y, Fu P, Shen X, Gao H. 2008. Cyclodextrin-based aggregates and characterization by microscopy. Micron 39: 495–516.

Heimann M, Käsermann HP, Pfister R, Roth DR, Bürki K. 2009. Blood collection from the sublingual vein in mice and hamsters: a suitable alternative to retrobulbar technique that provides large volumes and minimizes tissue damage. Laboratory Animals 43: 255–60.

Hillery AM, Lloyd AW, Swarbrick. J. 2001. Drug delivery and targeting for pharmacists and pharmaceutical scientists, CRC Press Inc (ed). First edition: London and New York.

Hincha DK, Rennecke P, Oliver AE. 2008. Protection of liposomes against fusion during drying by oligosaccharides is not predicted by the calorimetric glass transition temperatures of the dry sugars. European Biophysics Journal 37: 503–8.

Hirsh AJ. 2002. Altering airway surface liquid volume: Inhalation therapy with amiloride and hyperosmotic agents. Advanced Drug Delivery Reviews 54: 1445–62.

Hoffman PC, Mauer a M, Vokes EE. 2000. Lung cancer. The Lancet 355: 479–85.

Home Office. 2014. Code of Practice for the housing and care of animals used in scientific procedures, Williams Lea Group (ed).

Hossann M, Wang T, Wiggenhorn M, *et al.,* 2010. Size of thermosensitive liposomes influences content release. Journal of Controlled Release 147: 436–43.

van den Hoven JM, Metselaar JM, Storm G, Beijnen JH, Nuijen B. 2012. Cyclodextrin as membrane protectant in spray-drying and freeze-drying of PEGylated liposomes. International Journal of Pharmaceutics 438: 209–16.

Hu T, Wang J, Shen Z, Chen J. 2008. Engineering of drug nanoparticles by HGCP for pharmaceutical applications. Particulogy 6: 239–51.

Hughes V. 2012. Where there's smoke. Nature 489: S18–20.

Hung CT, Lam F., Perrier D., Souter A. 1988. A stability study of amphotericin B in aqueous media using factorial design. International Journal of Pharmaceutics 44: 117–23.

International Conference on Harmonisation. 2003. Q1A(R2) Stability testing of new drug substances and products. http://www.fda.gov/downloads/drugs/guidancecomplianceregulatoryinformation/guidances/ucm073369.pdf [Access September 2015] Version 4.

International Union Against Cancer. 2009. TNM Classification of Malignant Tumours, Wiley-Blackwell (ed). 7th Edition.

Italia JL, Singh D, Ravi Kumar MN V. 2009a. High-performance liquid chromatographic analysis of amphotericin B in rat plasma using alpha-naphthol as an internal standard. Analytica Chimica Acta 634: 110–4.

Italia JL, Yahya M, Singh D, Kumar M. 2009b. Biodegradable nanoparticles improve oral bioavailability of amphotericin B and show reduced nephrotoxicity compared to intravenous Fungizone. Pharmaceutical Research 26: 1324–31.

Jahn A, Vreeland WN, Devoe DL, Locascio LE, Gaitan M. 2007. Microfluidic directed formation of liposomes of controlled size. Langmuir 23: 6289–93.

Jain, Kumar. 2010. Development of amphotericin B loaded polymersomes based on (PEG)(3)-PLA co-polymers: Factors affecting size and in vitro evaluation. European Journal of Pharmaceutical Sciences 40: 456–65.

Jain PP, Leber R, Nagaraj C, *et al.,* 2014. Liposomal nanoparticles encapsulating iloprost exhibit enhanced vasodilation in pulmonary arteries. International Journal of Nanomedicine 9: 3249–61.

Jansook P, Kurkov S V, Loftsson T. 2010. Cyclodextrins as Solubilizers : Formation of Complex Aggregates. Journal of Pharmaceutical Sciences 99: 719–29.

Jee J-P, McCoy A, Mecozzi S. 2012. Encapsulation and release of Amphotericin B from an ABC triblock fluorous copolymer. Pharmaceutical Research 29: 69–82.

Jha TK, Sundar S, Thakur CP, Felton JM, Sabin AJ, Horton J. 2005. A phase II dose-ranging study of sitamaquine for the treatment of visceral leishmaniasis in India. The American Society of Tropical Medicine and Hygiene 73: 1005–11.

Johnson MA, Newman SP, Bloom R, Talaee N, Clarke SW. 1989. Delivery of albuterol and ipratropium bromide from two nebulizer systems in chronic stable asthma. Efficacy and pulmonary deposition. Efficacy Pulmonary Deposition Chest 96: 6–10.

Jung SY, Lee SH, Kang HB, *et al.,* 2010. Antitumor activity of 3,4-

dihydroquinazoline dihydrochloride in A549 xenograft nude mice. Bioorganic and Medicinal Chemistry Letters 20: 6633–6.

Katial R, Reisner C, Buchmeier A, Barteison B, Nelson H. 2000. Comparison of three commercial ultrasonic nebulizers. Annals Allergy Asthma Immunology 84: 255–61.

Kaur I, Rana C, Singh M, Bhushan S, Singh H, Kakkar S. 2012. Development and evaluation of novel surfactant-based elastic vesicular system for ocular dlivery of fluconazole. Journal of Ocular Pharmacology and Therapeutics 28: 484–96.

Kayser O, Olbrich C, Yardley V, Fiderlen A., Croft, S L. 2003. Formulation of amphotericin B as nanosuspension for oral administration. International Journal of Pharmaceutics 254: 73–5.

Kesser KC, Geller DE. 2009. New aerosol delivery devices for cystic fibrosis. Respiratory Care 54: 754–67.

Khalaf AI, Bourdin C, Breen D, *et al.,* 2012. Design, synthesis and antibacterial activity of minor groove binders: the role of non-cationic tail groups. European Journal of Medicinal Chemistry 56: 39–47.

Khalaf AI, Waigh RD, Drummond AJ, *et al.,* 2004. Distamycin analogues with enhanced lipophilicity: synthesis and antimicrobial activity. Journal of Medicinal Chemistry 47: 2133–56.

Kheirolomoom A, Kruse DE, Qin S, *et al.,* 2010. Enhanced in vivo bioluminescence imaging using liposomal luciferin delivery system. Journal of Controlled Release 141: 128–36.

Kilkenny C, Browne WJ, Cuthill IC, Emerson M, Altman DG. 2010. Improving bioscience research reporting: The arrive guidelines for reporting animal research. PLoS Biology 8: 1–5.

Kim, Shin B-K, Garripelli VK, *et al.,* 2010. A thermosensitive vaginal gel formulation with HPgammaCD for the pH-dependent release and solubilization of amphotericin B. European Journal of Pharmaceutical Sciences 41: 399–406.

Kirby C, Gregoriadis G. 1984. Dehydration-rehydration vesicles: a simple method for high yield drug entrapment in liposomes. Nature Biotechnology 2: 979–84.

Kleemann E, Schmehl T, Gessler T, Bakowsky U, Kissel T, Seeger W. 2007. Iloprost-containing liposomes for aerosol application in pulmonary arterial hypertension: Formulation aspects and stability. Pharmaceutical Research 24:

277–87.

Kopka ML, Yoon C, Goodsell D, Pjura P, Dickerson RE. 1985. The molecular origin of DNA-drug specificity in netropsin and distamycin. Proceedings of the National Academy of Sciences of the United States of America 82: 1376–80.

Koster KL, Lei YP, Anderson M, Martin S, Bryant G. 2000. Effects of vitrified and nonvitrified sugars on phosphatidylcholine fluid-to-gel phase transitions. Biophysical Journal 78: 1932–46.

Koudelka S, Masek J, Neuzil J, Turanek J. 2010. Lyophilised Liposome-Based Formulations of alpha-Tocopheryl Succinate : Preparation and Physico-Chemical Characterisation. Journal of Pharmaceutical Sciences 99: 2434–43.

Kumar R, Engwerda C. 2014. Vaccines to prevent leishmaniasis. Clinical & Translational Immunology 3: 1–6.

Kundu AK, Chandra PK, Hazari S, *et al.,* 2012. Stability of lyophilized siRNA nanosome formulations. International Journal of Pharmaceutics 423: 525–34.

de La Llave E, Lecoeur H, Besse A, Milon G, Prina E, Lang T. 2011. A combined luciferase imaging and reverse transcription polymerase chain reaction assay for the study of Leishmania amastigote burden and correlated mouse tissue transcript fluctuations. Cellular Microbiology 13: 81–91.

Labiris NR, Dolovich MB. 2003. Pulmonary drug delivery. Part I: Physiological factors affecting therapeutic effectiveness of aerosolized medications. British Journal of Clinical Pharmacology 56: 588–99.

Lambros MP, Bourne DW, Abbas SA, Johnson DL. 1997. Disposition of aerosolized liposomal amphotericin B. Journal of Pharmaceutical Sciences 86: 1066–9.

Lamprou DA, Venkatpurwar V, Kumar MNVR. 2013. Atomic Force Microscopy Images Label-Free, Drug Encapsulated Nanoparticles In Vivo and Detects Difference in Tissue Mechanical Properties of Treated and Untreated: A Tip for Nanotoxicology. PLoS ONE 8: 8–12.

Landsman L, Jung S. 2007. Lung Macrophages Serve as Obligatory Intermediate between Blood Monocytes and Alveolar Macrophages. Journal of Immunology 179: 3488–94.

Lasic DD. 1998. Novel applications of liposomes. Trends In Biotechnology 16: 307–21.

Lavorini F, Fontana G a., Usmani OS. 2014. New inhaler devices - The good, the

bad and the ugly. Respiration 88: 3–15.

Lawn SD, Zumla AI. 2011. Tuberculosis. The Lancet 378: 57–72.

Lehofer B, Bloder F, Jain PP, *et al.,* 2014. Impact of atomization technique on the stability and transport efficiency of nebulized liposomes harboring different surface characteristics. European Journal Of Pharmaceutics And Biopharmaceutics 88: 1076–85.

Lemke A, Kiderlen AF, Kayser O. 2005. Amphotericin B. Applied Microbiology and Biotechnology 68: 151–62.

Lestner JM, Howard SJ, Goodwin J, *et al.,* 2010. Pharmacokinetics and pharmacodynamics of amphotericin B deoxycholate, liposomal amphotericin B, and amphotericin B lipid complex in an in vitro model of invasive pulmonary aspergillosis. Antimicrobial Agents and Chemotherapy 54: 3432–41.

Lewis D, Copley M. 2013. Inhaled Product Characterization. http://www.copleyscientific.com/files/ww/news/COP%20JOB%20147_Inhaled%20Product%20Characterization.pdf [Access September 2015].

Lian T, Ho R. 2001. Trends and developments in liposome drug delivery systems. Journal of Pharmaceutical Sciences 90: 667–80.

Liesenborghs L, Verhaegen J, Peetermans WE, Vandeven J, Flamaing J. 2013. Trends in serotype prevalence in invasive pneumococcal disease before and after infant pneumococcal vaccination in Belgium, 2002-2010. Vaccine 31: 1529–34.

Lippert B. 1999. Cisplatin : chemistry and biochemistry of a leading anticancer drug, Verlag Helvetica Chimica Acta (ed). First edition: New York.

Liu L, Dahlgren C, Elwing H, Lundqvist H. 1996. A simple chemiluminescence assay for the determination of reactive oxygen species produced by human neutrophils. Journal of Immunological Methods 192: 173–8.

Llambrich A, Zaballos P, Terrasa F, Torne I, Puig S, Malvehy J. 2009. Dermoscopy of cutaneous leishmaniasis. The British Journal of Dermatology 160: 756–61.

Lo CT, Jahn A, Locascio LE, Vreeland WN. 2010. Controlled Self-Assembly of Monodisperse Niosomes by Microfluidic Hydrodynamic Focusing. Langmuir 26: 8559–66.

Loftsson T, Duchêne D. 2007. Cyclodextrins and their pharmaceutical applications. International Journal Of Pharmaceutics 329: 1–11.

Lönnroth K, Castro KG, Chakaya JM, *et al.,* 2010. Tuberculosis control and

elimination 2010-50: cure, care, and social development. The Lancet 375: 1814–29.

Lopez-Flores A, Jurado R, Garcia-Lopez P. 2005. A high-performance liquid chromatographic assay for determination of cisplatin in plasma, cancer cell, and tumor samples. Journal of Pharmacological and Toxicological Methods 52: 366–72.

Low SC, Nunes SL, Bitonti AJ, Dumont JA. 2005. Oral and pulmonary delivery of FSH-Fc fusion proteins via neonatal Fc receptor-mediated transcytosis. Human Reproduction 20: 1805–13.

Lucangelo U, Pelosi P, Walter AZ, Aliverti A. 2008. Respiratory System and Artificial Ventilation, Springer-Verlag Italia (ed). First edition: New York.

Lue L, Hadman S, Vancura A. 2002. Liquid chromatographic determination of amphotericin B in different pharmaceuticals. Journal of AOAC International 85: 15–9.

Mahale NB, Thakkar PD, Mali RG, Walunj DR, Chaudhari SR. 2012. Niosomes: Novel sustained release nonionic stable vesicular systems - An overview. Advances in Colloid and Interface Science 183-184: 46–54.

Mahalingam V, Onclin S, Péter M, Ravoo BJ, Huskens J, Reinhoudt DN. 2004. Directed self-assembly of functionalized silica nanoparticles on molecular printboards through multivalent supramolecular interactions. Langmuir : the ACS Journal of Surfaces and Colloids 20: 11756–62.

Maltezou HC. 2010. Drug resistance in visceral leishmaniasis. Journal of Biomedicine and Biotechnology 2010: 1–8.

Manca ML, Manconi M, Nacher A, *et al.,* 2014. Development of novel diolein–niosomes for cutaneous delivery of tretinoin: Influence of formulation and in vitro assessment. International Journal of Pharmaceutics 477: 176–86.

Manca ML, Manconi M, Valenti D, *et al.,* 2012a. Liposomes Coated with Chitosan – Xanthan Gum ( Chitosomes ) as Potential Carriers for Pulmonary Delivery of Rifampicin. Journal of Pharmaceutical Sciences 101: 566–75.

Manca ML, Sinico C, Maccioni AM, Diez O, Fadda AM, Manconi M. 2012b. Composition influence on pulmonary delivery of rifampicin liposomes. Pharmaceutics 4: 590–606.

Marianecci C, Di Marzio L, Rinaldi F, *et al.,* 2014. Niosomes from 80s to present: The state of the art. Advances in Colloid and Interface Science 205: 187–206.

Marianecci C, Paolino D, Celia C, Fresta M, Carafa M, Alhaique F. 2010. Non-ionic surfactant vesicles in pulmonary glucocorticoid delivery : Characterization and interaction with human lung fibroblasts. Journal of Controlled Release 147: 127–35.

Martinez FD, Vercelli D. 2013. Asthma. The Lancet 382: 1360–72.

Masson LMP, Rosenthal A, Calado VM, Deliza R, Tashima L. 2011. Effect of ultra-high pressure homogenization on viscosity and shear stress of fermented dairy beverage. LWT - Food Science and Technology 44: 495–501.

Mastrandrea LD, Quattrin T. 2006. Clinical evaluation of inhaled insulin. Advanced Drug Delivery Reviews 58: 1061–75.

Mather LE, Woodhouse A, Ward ME, Farr SJ, Rubsamen RA, Eltherington LG. 1998. Pulmonary administration of aerosolised fentanyl: Pharmacokinetic analysis of systemic delivery. British Journal of Clinical Pharmacology 46: 37–43.

Mathias NR, Hussain MA. 2010. Non-invasive Systemic Drug Delivery: Developability Considerations for Alternate Routes of Administration. Journal of Pharmaceutical Sciences 99: 1–20.

McFadden ER. 1995. Improper patient techniques with metered dose inhalers: clinical consequences and solutions to misuse. The Journal of Allergy and Clinical Immunology 96: 278–83.

McNamara PS, McCormack P, McDonald AJ, Heaf L, Southern KW. 2009. Open adherence monitoring using routine data download from an adaptive aerosol delivery nebuliser in children with cystic fibrosis. Journal of Cystic Fibrosis 8: 258–63.

Van Meerbeeck JP, Fennell DA, De Ruysscher DKM. 2011. Small-cell lung cancer. The Lancet 378: 1741–55.

Miller FJ, Mercer RR, Crapo JD. 1993. Lower Respiratory Tract Structure of Laboratory Animals and Humans: Dosimetry Implications. Aerosol Science and Technology 18: 257–71.

Min YG, Lee KS, Yun JB, *et al.,* 2001. Hypertonic saline decreases ciliary movement in human nasal epithelium in vitro. Otolaryngology - Head and Neck Surgery 124: 313–6.

Misra A, Hickey AJ, Rossi C, *et al.,* 2011. Inhaled drug therapy for treatment of tuberculosis. Tuberculosis 91: 71–81.

Mißlitz A, Mottram JC, Overath P, Aebischer T. 2000. Targeted integration into a rRNA locus results in uniform and high level expression of transgenes in Leishmania amastigotes. Molecular and Biochemical Parasitology 107: 251–61.

Miyajima K. 1997. Role of saccharides for the freeze-thawing and freeze drying of liposome. Advanced Drug Delivery Reviews 24: 151–9.

Moazeni E, Gilani K, Sotoudegan F, *et al.,* 2010. Formulation and in vitro evaluation of ciprofloxacin containing niosomes for pulmonary delivery. Journal of Microencapsulation 27: 618–27.

Moghassemi S, Hadjizadeh A. 2014. Nano-niosomes as nanoscale drug delivery systems: An illustrated review. Journal of Controlled Release 185: 22–36.

Mohammed AI, Abboud ZH, Alghanimi AHO. 2012. Synthesis of d-mannitol substituted ether-linked bis-1,2,3-triazoles as models of gemini surfactants. Tetrahedron Letters 53: 5081–3.

Mohammed AR, Bramwell VW, Coombes AGA, Perrie Y. 2006. Lyophilisation and sterilisation of liposomal vaccines to produce stable and sterile products. Methods 40: 30–8.

Mohammed AR, Coombes AGA, Perrie Y. 2007. Amino acids as cryoprotectants for liposomal delivery systems. European Journal of Pharmaceutical Sciences 30: 406–13.

Morand K, Bartoletti AC, Bochot A, Barratt G, Brandely ML, Chast F. 2007. Liposomal amphotericin B eye drops to treat fungal keratitis: physico-chemical and formulation stability. International Journal of Pharmaceutics 344: 150–3.

Moreno, Frutos P, Ballesteros MP. 2001. Lyophilized Lecithin Based Oil-Water Microemulsions as a New and Low Amphotericin B. Pharmaceutical research 18: 344–51.

Mufamadi MS, Pillay V, Choonara YE, *et al.,* 2011. A review on composite liposomal technologies for specialized drug delivery. Journal of Drug Delivery 2011: 939851.

Mullen AB, Baillie AJ, Carter KC. 1998. Visceral leishmaniasis in the BALB/c mouse: a comparison of the efficacy of a nonionic surfactant formulation of sodium stibogluconate with those of three proprietary formulations of amphotericin B. Antimicrobial Agents and Chemotherapy 42: 2722–5.

Mullen AB, Carter KC, Baillie AJ. 1997. Comparison of the efficacies of various formulations of amphotericin B against murine visceral leishmaniasis .

Antimicrobial Agents and Chemotherapy 41: 2089–92.

Murray, Berman JD, Davies CR, Saravia NG. 2005. Advances in leishmaniasis. The Lancet 366: 1561–77.

Musa AM, Younis B, Fadlalla A, *et al.,* 2010. Paromomycin for the treatment of visceral leishmaniasis in Sudan: A randomized, open-label, dose-finding study. PLoS Neglected Tropical Diseases 4: 4–10.

Nagayasu A, Uchiyama K, Kiwada H. 1999. The size of liposomes: a factor which affects their targeting efficiency to tumors and therapeutic activity of liposomal antitumor drugs. Advanced Drug Delivery Reviews 40: 75–87.

Nahar K, Gupta N, Gauvin R, *et al.,* 2013. In vitro, in vivo and ex vivo models for studying particle deposition and drug absorption of inhaled pharmaceuticals. European Journal of Pharmaceutical Sciences 49: 805–18.

Nakamura K, Yoshikawa N, Yamaguchi Y, Kagota S, Shinozuka K, Kunitomo M. 2002. Characterization of mouse melanoma cell lines by their mortal malignancy using an experimental metastatic model. Life Sciences 70: 791–8.

Nasseri B. 2005. Effect of cholesterol and temperature on the elastic properties of niosomal membranes. International Journal Of Pharmaceutics 300: 95–101.

Newman S. 1993. Scintigraphic assessment of therapeutic aerosols. Critical Reviews in Therapeutic Drug Carrier Systems 10: 65–109.

Newman SP, Clark AR, Talaee N, Clarke SW. 1991. Lung deposition of 5 mg Intal from a pressurised metered dose inhaler assessed by radiotracer technique. International Journal of Pharmaceutics 74: 203–8.

Ng AWK, Wasan KM, Lopez-berestein G. 2003. Development of liposomal polyene antibiotics : an historical perspective . Journal of Pharmaceutical Sciences 6: 67–83.

Nieto J, Alvar J, Mullen AB, *et al.,* 2003. Pharmacokinetics , Toxicities , and Efficacies of Sodium Stibogluconate Formulations after Intravenous Administration in Animals. Antimicrobial agents and chemotherapy 47: 2781–7.

Niven RW, Brain JD. 1994. Some functional aspects of air-jet nebulizers. International Journal of Pharmaceutics 104: 73–85.

Noble S, Goa KL. 1997. Gemcitabine. A review of its pharmacology and clinical potential in non-small cell lung cancer and pancreatic cancer. Adis Drug Evaluation 54: 447–72.

Noormandi A, Pardakhty A, Torabifard H. 2012. Formulation and in vitro

characterization of amphotericin B. Research in Pharmaceutical Sciences 7: S344.

O'Sullivan BP, Freedman SD. 2009. Cystic fibrosis. The Lancet 373: 1891–904.

Oller AR, Oberdörster G. 2010. Incorporation of particle size differences between animal studies and human workplace aerosols for deriving exposure limit values. Regulatory Toxicology and Pharmacology 57: 181–94.

Ong HX, Benaouda F, Traini D, *et al.,* 2014. In vitro and ex vivo methods predict the enhanced lung residence time of liposomal ciprofloxacin formulations for nebulisation. European Journal of Pharmaceutics and Biopharmaceutics 86: 83–9.

Osaka K, Ritov VB, Bernardo JF, Branch R a, Kagan VE. 1997. Amphotericin B protects cis-parinaric acid against peroxyl radical-induced oxidation: amphotericin B as an antioxidant. Antimicrobial Agents and Chemotherapy 41: 743–7.

Paranjpe M, Müller-Goymann C. 2014. Nanoparticle-Mediated Pulmonary Drug Delivery: A Review. International Journal of Molecular Sciences 15: 5852–73.

Pardakhty A, Varshosaz J, Rouholamini A. 2007. In vitro study of polyoxyethylene alkyl ether niosomes for delivery of insulin. International Journal of Pharmaceutics 328: 130–41.

Parshina NA, Pleteneva T V., Baikova VN, Narimanov MN, Tyulyandin SA. 2008. Quantitative estimation of gemcitabine by HPLC in plasma. Pharmaceutical Chemistry Journal 42: 288–90.

Parveen S, Kaur S, David SAW, Kenney JL, McCormick WM, Gupta RK. 2011. Evaluation of growth based rapid microbiological methods for sterility testing of vaccines and other biological products. Vaccine 29: 8012–23.

Patel B, Gauvin R, Absar S, *et al.,* 2012. Computational and bioengineered lungs as alternatives to whole animal, isolated organ, and cell-based lung models. American Journal of Physiology, Lung Cellular and Molecular Physiology 303: 733–47.

Patel SM, Doen T, Pikal MJ. 2010. Determination of end point of primary drying in freeze-drying process control. AAPS PharmSciTech 11: 73–84.

Patton J, Byron P. 2007. Inhaling medicines: delivering drugs to the body through the lungs. Nature Reviews. Drug discovery 6: 67–74.

Patton J, McCabe, Hansen, Daugherty. 1989. Absorption of human growth

hormone from the rat lung. Biotechnology 1: 213–8.

Pérez-Campaña C, Gómez-Vallejo V, Puigivila M, *et al.,* 2014. Assessing lung inflammation after nanoparticle inhalation using 2-deoxy-2-[18F]Fluoro-d-glucose positron emission tomography imaging. Molecular Imaging and Biology 16: 264–73.

Perfect JR, Dodds Ashley E, Drew R. 2004. Design of aerosolized amphotericin B formulations for prophylaxis trials among lung transplant recipients. Clinical infectious Diseases 39: S207–10.

Pestana KC, Formariz TP, Franzini CM, *et al.,* 2008. Colloids and Surfaces B : Biointerfaces Oil-in-water lecithin-based microemulsions as a potential delivery system for amphotericin B. Colloids and Surfaces 66: 253–9.

Pikal MJ, Shah S. 1990. The collapse temperature in freeze drying: Dependence on measurement methodology and rate of water removal from the glassy phase. International Journal of Pharmaceutics 62: 165–86.

Pilcer G, Vanderbist F, Amighi K. 2008. Correlations between cascade impactor analysis and laser diffraction techniques for the determination of the particle size of aerosolised powder formulations. International Journal of Pharmaceutics 358: 75–81.

Poncet JM, Lebel JM. 2003. Influence of cryoprotective agent and cooling rate on frozen and thawed hemocytes from the Mollusk Haliotis tuberculata. Cryobiology 47: 184–9.

Proffitt RT, Adler-Moore J, Chiang S-M. 1999. Amphotericin B liposome preparation, US patent number: 5,965,156.

Puig-Sellart M. 2013. Non-ionic surfactant vesicles as an Amphotericin B inhaled delivery system for the treatment of leishmaniasis. University of Strathclyde, MRes in Drug Delivery Systems Thesis.

Puyo S, Montaudon D, Pourquier P. 2014. From old alkylating agents to new minor groove binders. Critical Reviews in Oncology/Hematology 89: 43–61.

Rabinowitz JD, Wensley M, Lloyd P, *et al.,* 2004. Fast onset medications through thermally generated aerosols. The Journal of Pharmacology and Experimental Therapeutics 309: 769–75.

Rahman M, Ahmed BN, Faiz MA, *et al.,* 2011. Phase IV trial of miltefosine in adults and children for treatment of visceral leishmaniasis (kala-azar) in Bangladesh. American Journal of Tropical Medicine and Hygiene 85: 66–9.

Rajagopalan N, Chen SC, Chow W-S. 1986. A study of the inclusion complex of amphotericin-B with γ-cyclodextrin. International Journal of Pharmaceutics 29: 161–8.

Rao MA. 1999. Flow and Functional Models for Rheological Properties of Fluid Foods. In: Rheology of Fluid and Semisolid Foods, 27–58.

Rey L, May JC. 2010. Freeze Drying/Lyophilization of Pharmaceutical and Biological Products. Informa healthcare: London.

Rigon RB, Oyafuso MH, Fujimura AT, *et al.,* 2015. Nanotechnology-Based Drug Delivery Systems for Melanoma Antitumoral Therapy : A Review. BioMed Research International 2015: 1–22.

Rijnders BJ, Cornelissen JJ, Slobbe L, *et al.,* 2008. Aerosolized liposomal amphotericin B for the prevention of invasive pulmonary aspergillosis during prolonged neutropenia: a randomized, placebo-controlled trial. Clinical Infectious Diseases 46: 1401–8.

Rinaldi M, Crinò L, Scagliotti G V., *et al.,* 2000. A three-week schedule of gemcitabine-cisplatin in advanced non-small-cell lung cancer with two different cisplatin dose levels: A phase II randomized trial. Annals of Oncology 11: 1295–300.

Ritmeijer K, Dejenie A, Assefa Y, *et al.,* 2006. A comparison of miltefosine and sodium stibogluconate for treatment of visceral leishmaniasis in an Ethiopian population with high prevalence of HIV infection. Clinical Infectious Diseases 43: 357–64.

Sakagami M. 2006. In vivo, in vitro and ex vivo models to assess pulmonary absorption and disposition of inhaled therapeutics for systemic delivery. Advanced Drug Delivery Reviews 58: 1030–60.

Salem LB, Bosquillon C, Dailey LA, *et al.,* 2009. Sparing methylation of B-cyclodextrin mitigates cytotoxicity and permeability induction in respiratory epithelial cell layers in vitro. Journal of Controlled Release 136: 110–6.

Santangelo R, Paderu P, Delmas G, *et al.,* 2000. Efficacy of Oral Cochleate-Amphotericin B in a Mouse Model of Systemic Candidiasis. Antimicrobial Agents and Chemotherapy 44: 256–2360.

Santos Cavaiola T, Edelman S. 2014. Inhaled Insulin: A Breath of Fresh Air? A Review of Inhaled Insulin. Clinical Therapeutics 36: 1275–89.

Santoveña A, Piñero MJ, Llabrés M. 2010. Comparison between DSC and TMDSC

in the investigation into frozen aqueous cryoprotectants solutions. Drug Development and Industrial Pharmacy 36: 1413–21.

Schick MJ. 1987. Nonionic Surfactants: Physical Chemistry. In: Marcel Dekker (ed). Surfactant Science Series volume 23. New York

Schlesinger RB. 1985. Comparative deposition of inhaled aerosols in experimental animals and humans: a review. Journal of Toxicology and Environmental Health 15: 197–214.

Schmittel A, Sebastian M, Fischer von Weikersthal L, *et al.,* 2011. A German multicenter, randomized phase III trial comparing irinotecan-carboplatin with etoposide-carboplatin as first-line therapy for extensive-disease small-cell lung cancer. Annals of Oncology 22: 1798–804.

Schreief H, Bouwstra J. 1994. Liposomes and niosomes as topical drug carriers : dermal and transdermal drug delivery. Journal of Controlled Release 30: 1–15.

Schreier H, Gonzalez-rothib RJ, Stecenkoc AA. 1993. Pulmonary delivery of liposomes. Journal of Controlled Release 24: 209–23.

Schuster BS, Suk JS, Woodworth GF, Hanes J. 2013. Nanoparticle diffusion in respiratory mucus from humans without lung disease. Biomaterials 34: 3439–46.

Schuster J, Rubsamen R, Lloyd P, Lloyd J. 1997. The AER aerosol delivery system. Pharmaceutical Research 14: 354–7.

Sears MR. 2014. Trends in the prevalence of asthma. Chest 145: 219–25.

Segal B. 2009. Medical progress Aspergillosis. The New England Journal of Medicine 360: 1870–84.

Serisier D, Bilton D, De Soyza A, *et al.,* 2013. Inhaled, dual release liposomal ciprofloxacin in non-cystic fibrosis bronchiectasis (ORBIT-2): a randomised, double-blind, placebo-controlled trial. Thorax 68: 812–7.

Shaw CD, Carter KC. 2014. Drug Delivery : Lessons to Be Learnt From Leishmania Studies. Nanomedicine 9: 1531–44.

Singh, Malviya R, Sharma PK. 2011. Novasome-A Breakthrough in Pharmaceutical Technology a Review Article. Advances in Biological Research 5: 184–9.

Singh B, Sundar S. 2012. Leishmaniasis: Vaccine candidates and perspectives. Vaccine 30: 3834–42.

Singhal SS, Wickramarachchi D, Singhal J, Yadav S, Awasthi YC, Awasthi S. 2006. Determinants of differential doxorubicin sensitivity between SCLC and NSCLC. FEBS Letters 580: 2258–64.

Siow LF, Rades T, Lim MH. 2007. Characterizing the freezing behavior of liposomes as a tool to understand the cryopreservation procedures. Cryobiology 55: 210–21.

Siow LF, Rades T, Lim MH. 2008. Cryo-responses of two types of large unilamellar vesicles in the presence of non-permeable or permeable cryoprotecting agents. Cryobiology 57: 276–85.

Sivak O, Gershkovich P, Lin M, *et al.,* 2011. Tropically stable novel oral lipid formulation of amphotericin B (iCo-010): biodistribution and toxicity in a mouse model. Lipids in Health and Disease 10: 135.

Smyth HDC, Hickey AJ. 2011. Controlled pumonary drug delivery, Springer (ed). First edition: New York.

Snyder LR, Kirkland JJ, Glajch JL. 1997. Practical HPLC method development, John Wiley and Sons (ed). Second edition: New Jersey.

Sorensen SF, Carus A, Meldgaard P. 2015. Intravenous or oral administration of vinorelbine in adjuvant chemotherapy with cisplatin and vinorelbine for resected NSCLC. Lung Cancer 88: 167–73.

Srividya G, Kulshrestha A, Singh R, Salotra P. 2011. Diagnosis of visceral leishmaniasis: developments over the last decade. Parasitology Research.

Stark B, Pabst G, Prassl R. 2010. Long-term stability of sterically stabilized liposomes by freezing and freeze-drying: Effects of cryoprotectants on structure. European Journal of Pharmaceutical Sciences 41: 546–55.

Stein SW, Sheth P, Hodson PD, Myrdal PB. 2014. Advances in Metered Dose Inhaler Technology: Hardware Development. AAPS PharmSciTech 15: 326–38.

Suckling CJ. 2015. The antibacterial drug MGB-BP3: from discovery to clinical trial. Chemistry and Biology Interface 5: 166–74.

Sundar S, Mehta H, Suresh a V, Singh SP, Rai M, Murray HW. 2004. Amphotericin B treatment for Indian visceral leishmaniasis: conventional versus lipid formulations. Clinical infectious diseases 38: 377–83.

Taki M, Marriott C, Zeng X-M, Martin GP. 2010. Aerodynamic deposition of combination dry powder inhaler formulations in vitro: a comparison of three impactors. International Journal of Pharmaceutics 388: 40–51.

Tan SW, Billa N, Roberts CR, Burley JC. 2010. Surfactant effects on the physical characteristics of Amphotericin B-containing nanostructured lipid carriers. Colloids and Surfaces A: Physicochemical and Engineering Aspects 372: 73–9.

Tandon V, Bhagavatula SK, Nelson WC, Kirby BJ. 2008. Zeta potential and electroosmotic mobility in microfluidic devices fabricated from hydrophobic polymers : 1 . The origins of charge. Electrophoresis 29: 1092–101.

Tang X, Pikal MJ. 2004. Design of freeze-drying processes for pharmaceuticals: practical advice. Pharmaceutical Research 21: 191–200.

Tavano L, Alfano P, Muzzalupo R, de Cindio B. 2011. Niosomes vs microemulsions: new carriers for topical delivery of Capsaicin. Colloids and Surfaces. B, Biointerfaces 87: 333–9.

Terzano C, Allegra L, Alhaique F, Marianecci C, Carafa M. 2005. Non-phospholipid vesicles for pulmonary glucocorticoid delivery. European Journal of Pharmaceutics and Biopharmaceutics 59: 57–62.

Testa M, Simonson D. 2007. Satisfaction and Quality of Life With Premeal Inhaled Versus Injected Insulin in Adolescents and Adults With Type 1 Diabetes. Diabetes Care 30: 1399–405.

Thompson R, Finlay W. 2012. Using MRI to measure aerosol deposition. Journal of Aerosol Medicine and Pulmonary Drug Delivery 25: 55–62.

Tiffen JC, Bailey CG, Ng C, Rasko JEJ, Holst J. 2010. Luciferase expression and bioluminescence does not affect tumor cell growth in vitro or in vivo. Molecular Cancer 9: 299.

Tiyaboonchai W, Woiszwillo J, Middaugh CR. 2001. Formulation and Characterization of Amphotericin B - Polyethylenimine - Dextran Sulfate Nanoparticles. Journal of Pharmaceutical Sciences 90: 902–14.

Torrado JJ, Espada R, Ballesteros MP, Torrado-Santiago S. 2008. Amphotericin B Formulations and Drug Targeting. Journal of Pharmaceutical Sciences 97: 2405–25.

Triballier K, Dumouchel C, Cousin J. 2003. A technical study on the Spraytec performances: influence of multiple light scattering and multi-modal drop-size distribution measurements. Experiments in Fluids 35: 347–56.

Uchegbu IF. 1999. Synthetic surfactant vesicles: niosomes and other non-phospholipid vesicular systems, Harwood Academic, Abingdon M (ed). First edition: Amsterdam.

Uchegbu IF, Vyas SP. 1998. Non-ionic surfactant based vesicles (niosomes) in drug delivery. International Journal of Pharmaceutics 172: 33–70.

United States Pharmacopoeia. 2008. Section 601, Aerosols, nasal sprays, metered-dose inhalers, and dry powder inhalers. http://www.pharmacopeia.cn/v29240/usp29nf24s0_c601_viewall.html [Access May 2013].

VanDevanter DR, Geller DE. 2011. Tobramycin administered by the TOBI Podhaler for persons with cystic fibrosis: A review. Medical Devices: Evidence and Research 4: 179–88.

Verhamme KMC, Afonso A, Romio S, Stricker BC, Brusselle GGO, Sturkenboom MCJM. 2013. Use of tiotropium Respimat Soft Mist Inhaler versus HandiHaler and mortality in patients with COPD. European Respiratory Journal 42: 606–15.

Verwey EJW. 1947. Theory of the stability of lyophobic colloids. The Journal of Physical and Colloid Chemistry 51: 631–6.

Vyas SP, Quraishi S, Gupta S, Jaganathan KS. 2005. Aerosolized liposome-based delivery of amphotericin B to alveolar macrophages. International Journal of Pharmaceutics 296: 12–25.

Wang J, Yadav V, Smart AL, Tajiri S, Basit AW. 2015. Stability of peptide drugs in the colon. European Journal of Pharmaceutical Sciences 78: 31–6.

Wang X, Guo L. 2008. Effect of sucrose on rheological properties of aqueous zirconia suspensions with polyacrylate. Powder Technology 186: 107–12.

Wasan EK, Gershkovich P, Zhao J, *et al.,* 2010. A novel tropically stable oral amphotericin B formulation (iCo-010) exhibits efficacy against visceral Leishmaniasis in a murine model. PLoS Neglected Tropical Diseases 4: e913.

Wasan KM, Wasan EK, Gershkovich P, *et al.,* 2009. Highly effective oral amphotericin B formulation against murine visceral leishmaniasis. The Journal of Infectious Diseases 200: 357–60.

Wasunna MK, Rashid JR, Mbui J, *et al.,* 2005. A phase II dose-increasing study of sitamaquine for the treatment of visceral leishmaniasis in Kenya. American Journal of Tropical Medicine and Hygiene 73: 871–6.

Wauthoz N, Amighi K. 2014. Phospholipids in pulmonary drug delivery. European Journal of Lipid Science and Technology 116: 1114–28.

Westphalen K, Gusarova G a., Islam MN, *et al.,* 2014. Sessile alveolar macrophages communicate with alveolar epithelium to modulate immunity.

Nature, Letter Research: 1–5.

Wexler A. 1977. Vapor pressure formulation for ice. Journal of Research of the National Bureau of Standards 81A: 5–20.

Wittgen BPH, Kunst PW a, Van Der Born K, *et al.,* 2007. Phase I study of aerosolized SLIT cisplatin in the treatment of patients with carcinoma of the lung. Clinical Cancer Research 13: 2414–21.

Wong W, Crapper J, Chan H-K, Traini D, Young PM. 2010. Pharmacopeial methodologies for determining aerodynamic mass distributions of ultra-high dose inhaler medicines. Journal of Pharmaceutical and Biomedical Analysis 51: 853–7.

Woo J, Chiu GNC, Karlsson G, *et al.,* 2008. Use of a passive equilibration methodology to encapsulate cisplatin into preformed thermosensitive liposomes. International Journal of Pharmaceutics 349: 38–46.

World Health Organisation. 2010. Control of the leishmaniases. In: Report of a meeting of the WHO Expert Committee on the Control of Leishmaniases. Geneva

World Health Organisation. 2011a. Leishmaniasis, burden of the disease, magnitude of the problem. http://www.who.int/leishmaniasis/burden/en/ [Access November 2011].

World Health Organisation. 2011b. Leishmaniasis. http://www.who.int/leishmaniasis/en/ [Access, September 2013].

World Health Organisation. 2013. Cancer fact sheet number 297. http://www.who.int/mediacentre/factsheets/fs297/en/ [Access May 2015].

Yamori T, Matsunaga A, Sato S, *et al.,* 1999. Potent antitumor activity of MS-247, a novel DNA minor groove binder, evaluated by an in vitro and in vivo human cancer cell line panel. Cancer Research 59: 4042–9.

Yang S, Liu C, Liu W, *et al.,* 2013. Preparation and characterization of nanoliposomes entrapping medium-chain fatty acids and vitamin C by lyophilization. International Journal of Molecular Sciences 14: 19763–73.

Yang T, Cui F-D, Choi M-K, *et al.,* 2007. Enhanced solubility and stability of PEGylated liposomal paclitaxel: in vitro and in vivo evaluation. International Journal of Pharmaceutics 338: 317–26.

Yi D, Naqwi A, Panoskaltsis-Mortari A, Wiedmann TS. 2012. Distribution of aerosols in mouse lobes by fluorescent imaging. International Journal of Pharmaceutics 426: 108–15.

Zanen P, Go LT, Lammers J-WJ. 1994. The optimal particle size for β-adrenergic aerosols in mild asthmatics. International Journal of Pharmaceutics 107: 211–7.

Zarogoulidis P, Eleftheriadou E, Sapardanis I, *et al.,* 2012. Feasibility and effectiveness of inhaled carboplatin in NSCLC patients. Investigational New Drugs 30: 1628–40.

Zhang, Zhu X, Ke F, *et al.,* 2009. Preparation and self-assembly of amphiphilic triblock copolymers with polyrotaxane as a middle block and their application as carrier for the controlled release of Amphotericin B. Polymer 50: 4343–51.

Zhigaltsev I V, Maurer N, Akhong Q, *et al.,* 2005. Liposome-encapsulated vincristine, vinblastine and vinorelbine: A comparative study of drug loading and retention. Journal of Controlled Release 104: 103–11.

# APPENDIX

**Table A.1** Chemical structure of the minor groove binders (MGBs) studied together with the molecular weight (MW)

| MGB | MW (g/mol) | Structure |
|---|---|---|
| **1** | 697.80 | 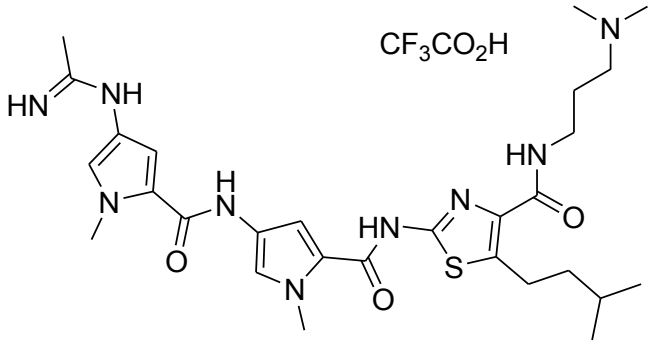 |
| **2** | 737.30 | 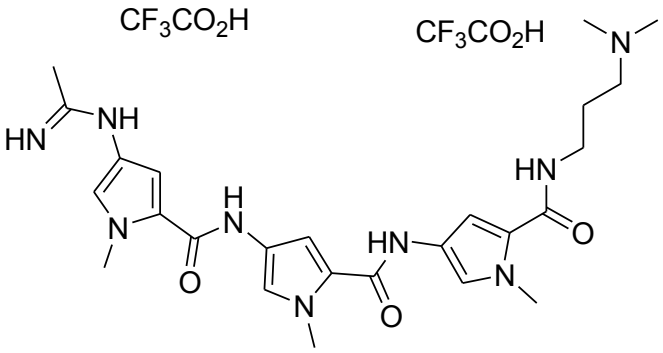 |
| **3** | 762.80 | 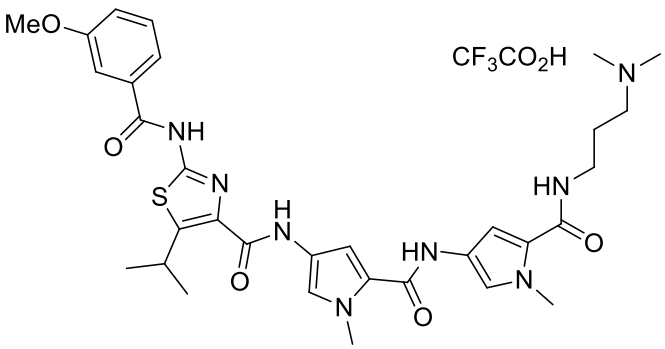 |
| **4** | 819.90 | 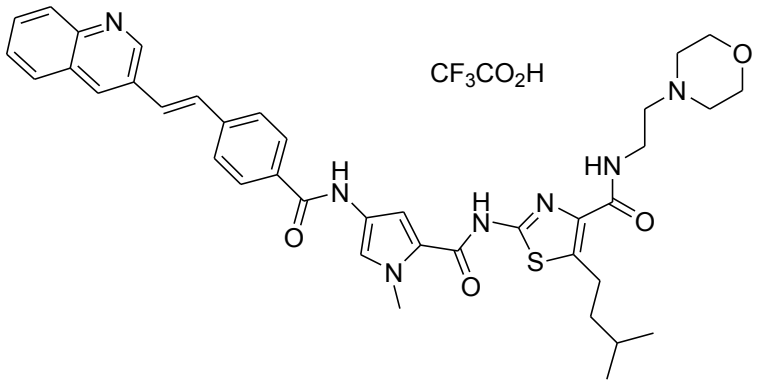 |

| MGB | MW (g/mol) | Structure |
|---|---|---|
| **5** | 854.30 | 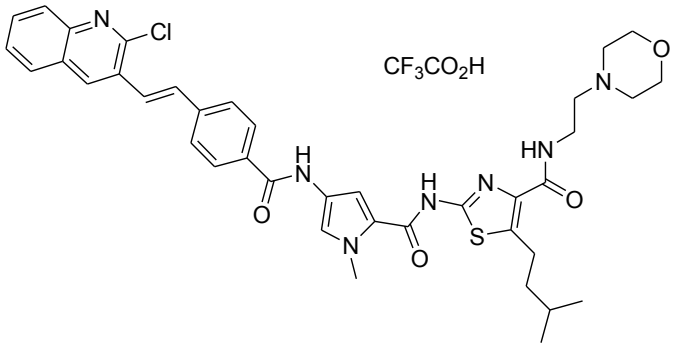 |
| **6** | 766.80 | 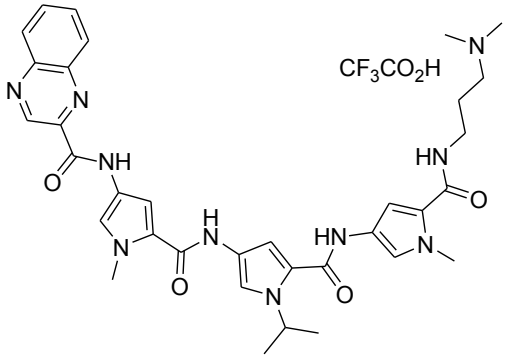 |
| **7** | 802.80 | 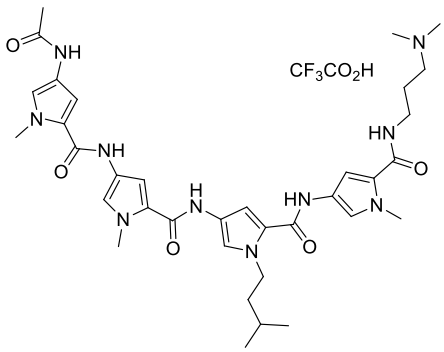 |
| **8** | 889.90 | 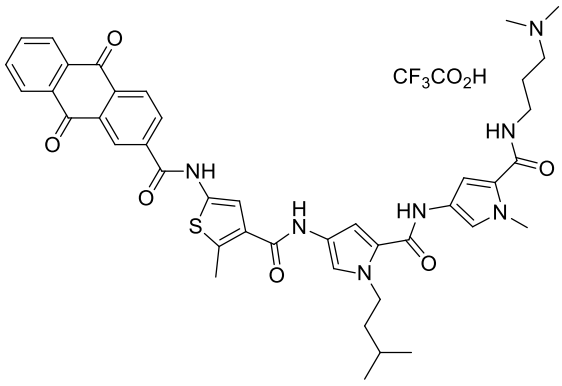 |

| MGB | MW (g/mol) | Structure |
|---|---|---|
| **9** | 641.70 | 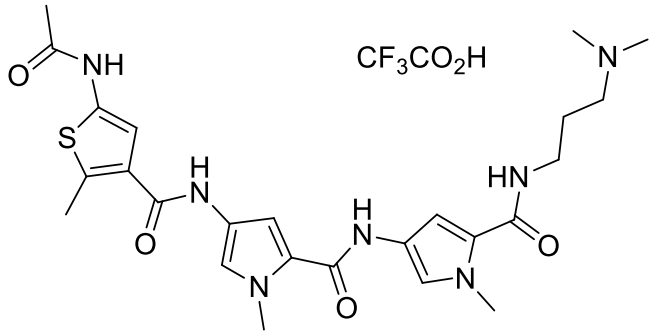 |
| **10** | 791.80 | 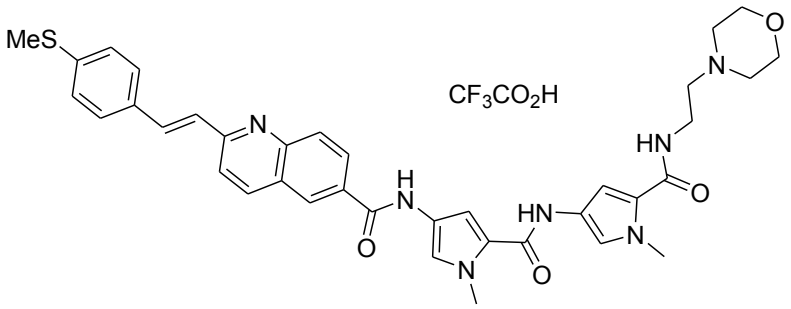 |
| **11** | 845.80 | 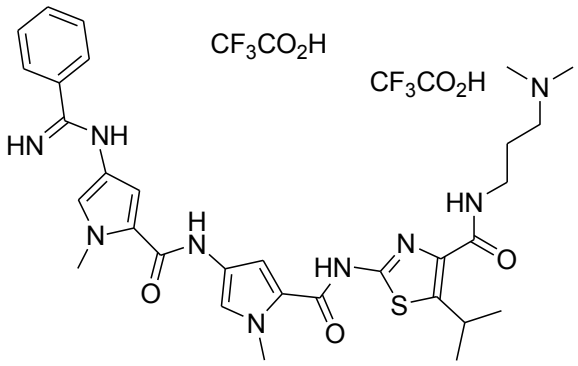 |
| **12** | 736.70 | 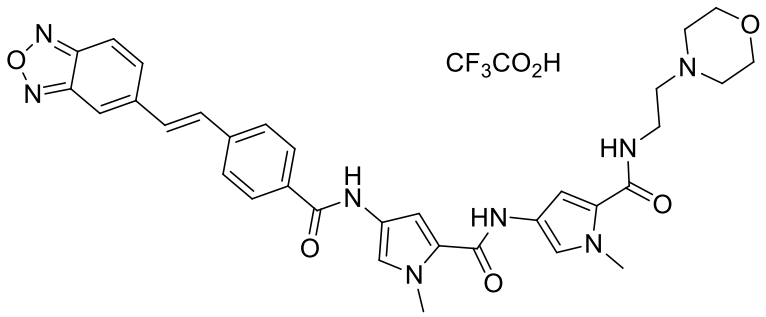 |

| MGB | MW (g/mol) | Structure |
|---|---|---|
| **13** | 784.60 | 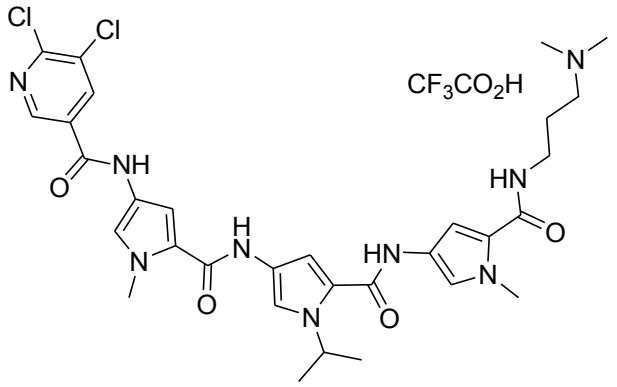 |
| **14** | 797.60 | 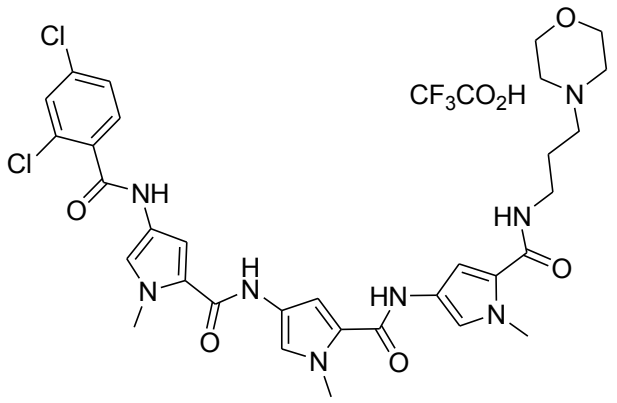 |
| **15** | 871.70 | 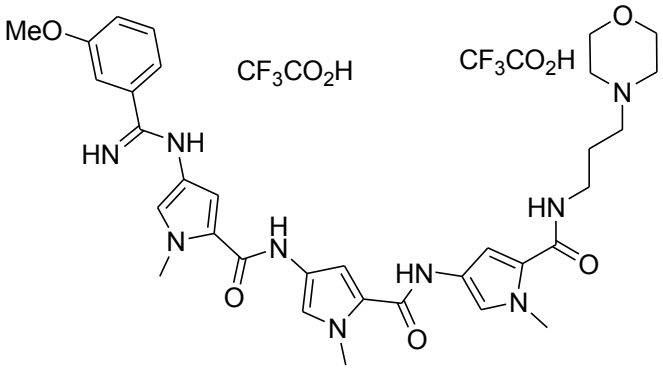 |
| **16** | 924.9 | 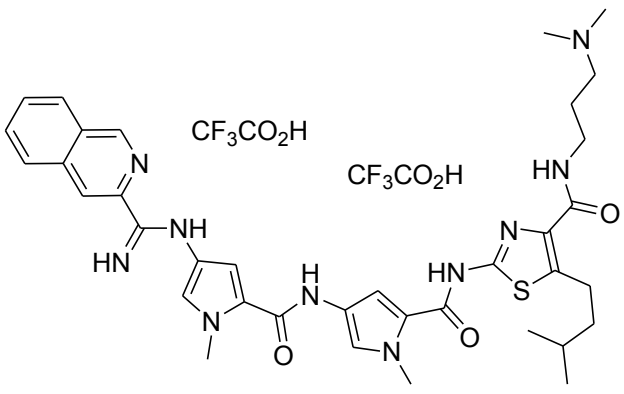 |

| MGB | MW (g/mol) | Structure |
|---|---|---|
| **17** | 742.7 | 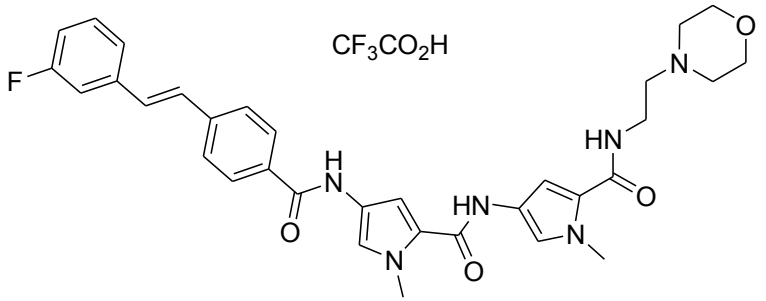 |
| **18** | 752.8 | 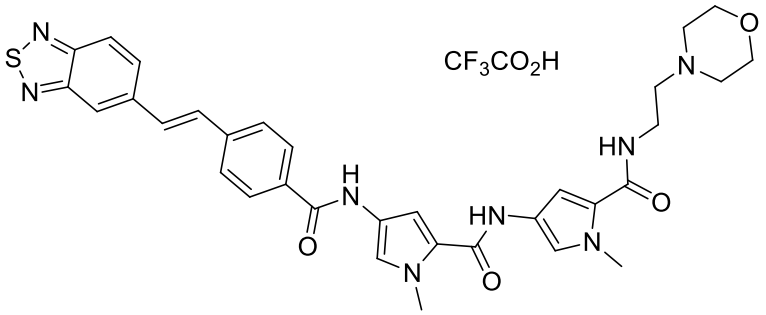 |
| **19** | 742.7 | 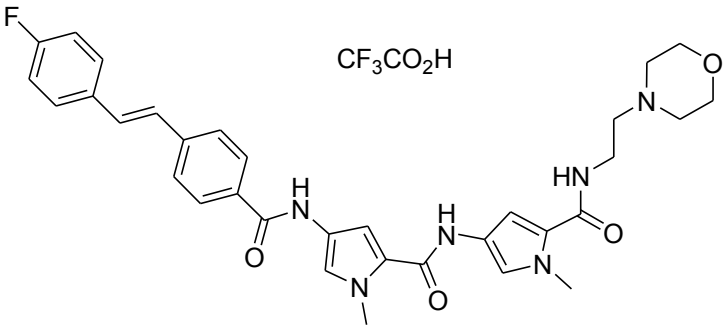 |
| **20** | 726.70 | 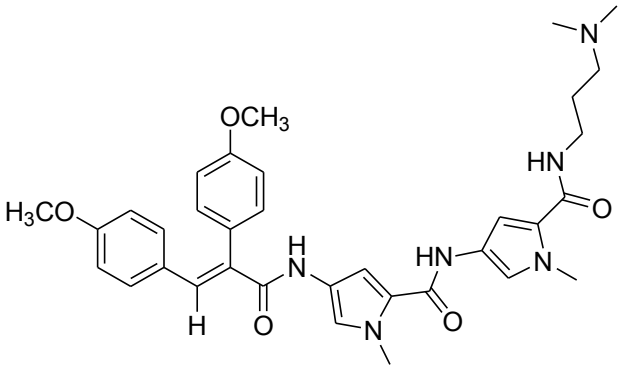 |

| MGB | MW (g/mol) | Structure |
|---|---|---|
| **21** | 738.70 | 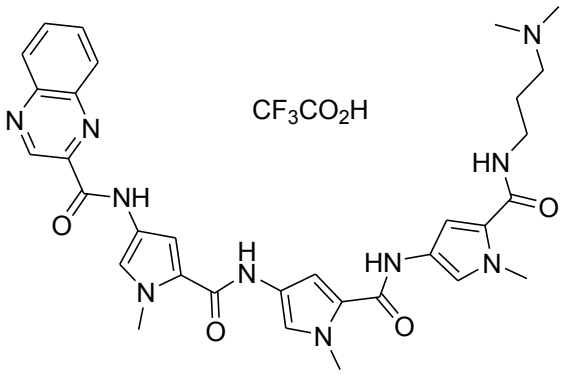 |
| **22** | 763.70 | 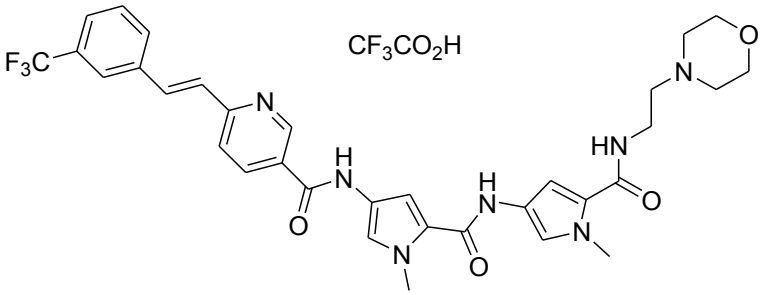 |
| **23** | 762.7 | 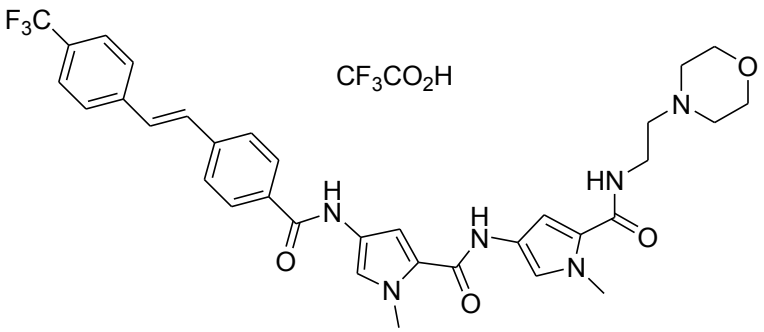 |
| **24** | 865.8 | 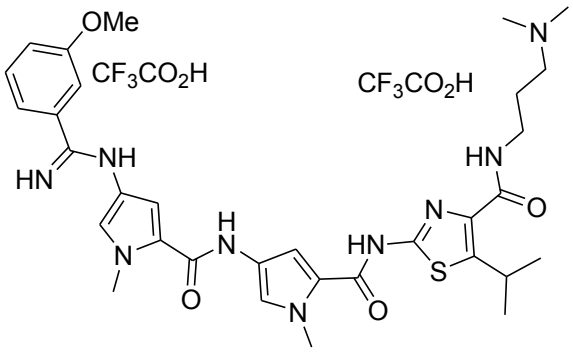 |

| MGB | MW (g/mol) | Structure |
|---|---|---|
| **25** | 610.80 | 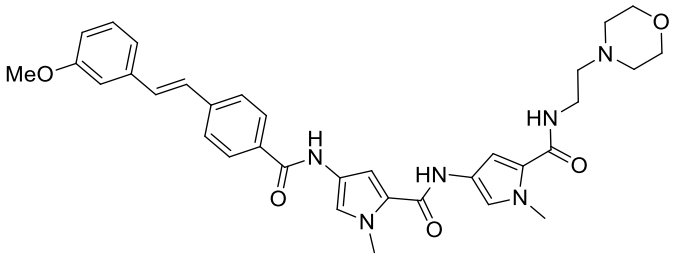 |
| **26** | 611.69 | 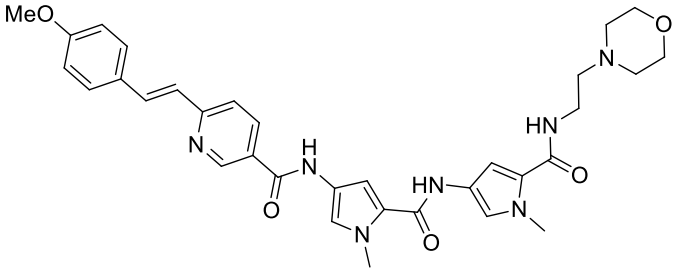 |
| **27** | 631.72 | 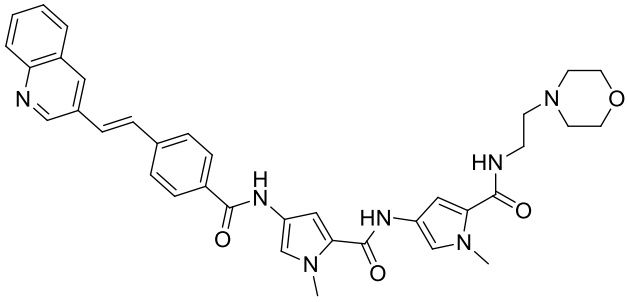 |
| **28** | 903.89 | 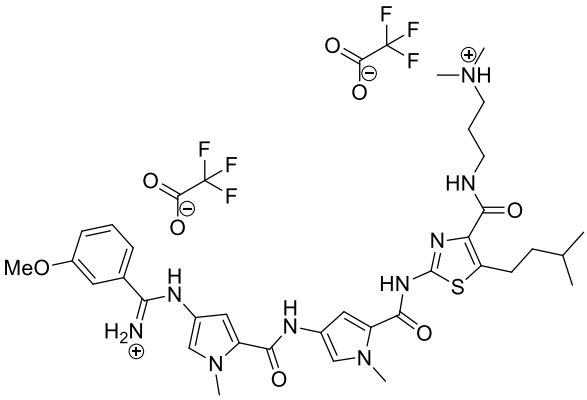 |

| MGB | MW (g/mol) | Structure |
|---|---|---|
| **29** | 775.73 | 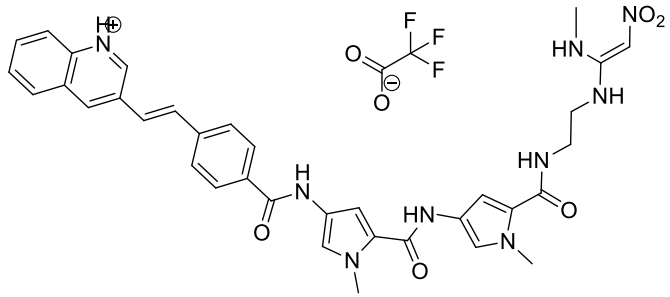 |
| **30** | 756.73 | 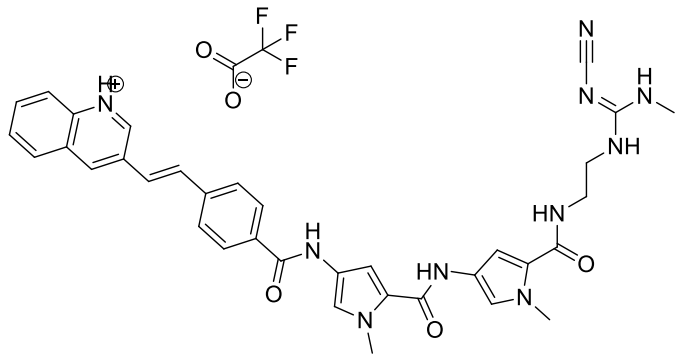 |
| **31** | 887.82 | 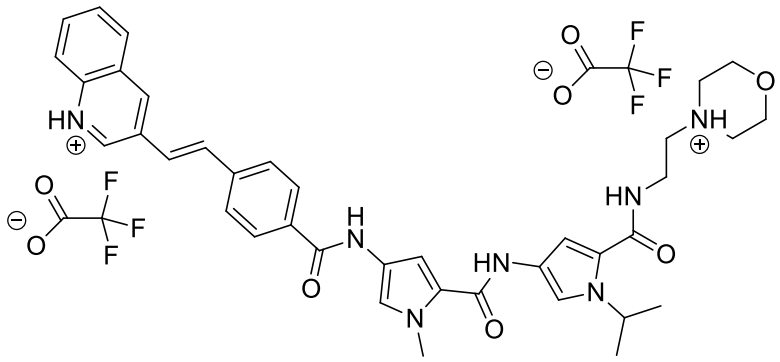 |
| **32** | 901.84 | 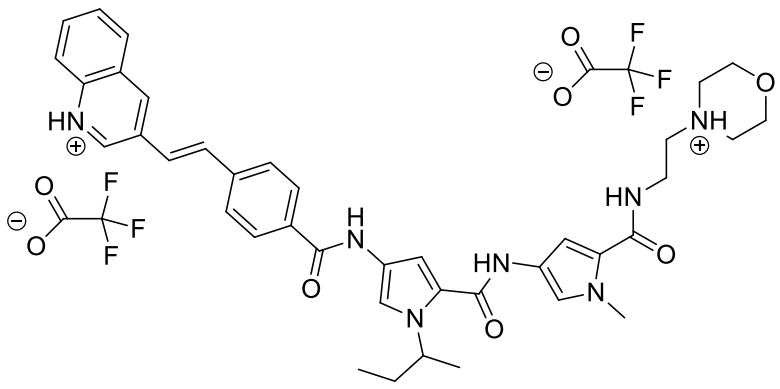 |

| MGB | MW (g/mol) | Structure |
|---|---|---|
| **33** | 887.82 | 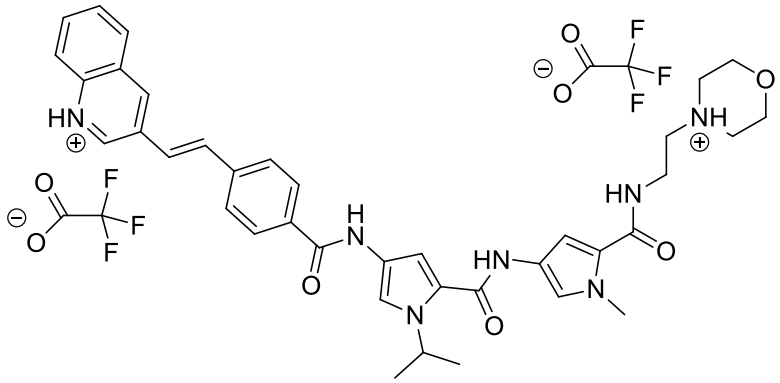 |
| **34** | 901.85 | 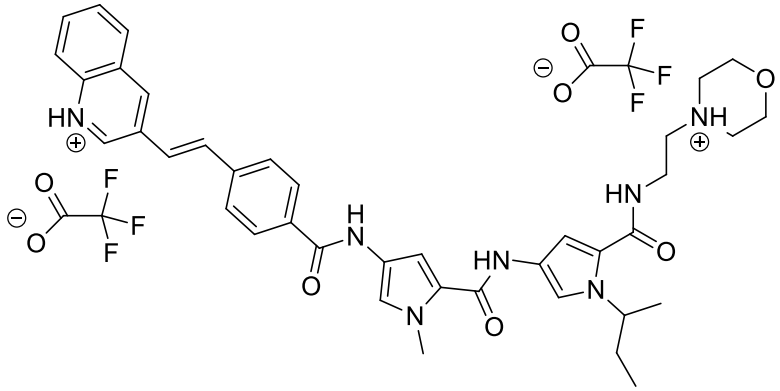 |
| **35** | 867.79 | 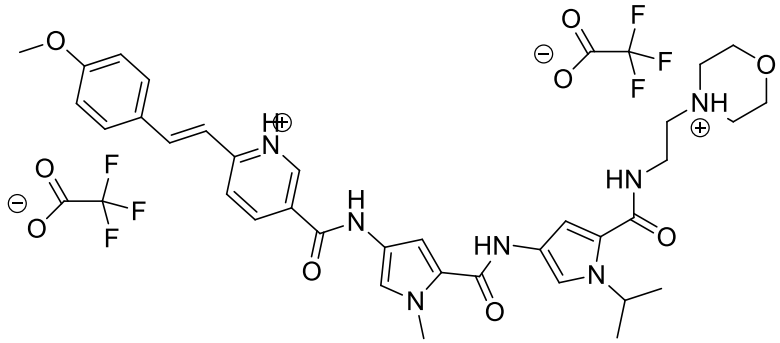 |
| **36** | 881.82 | 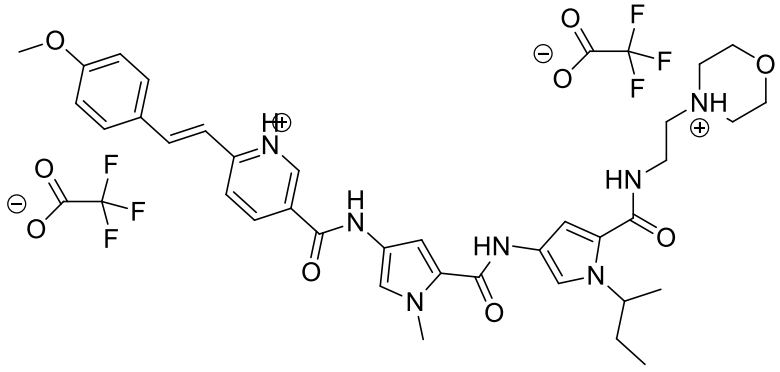 |

| MGB | MW (g/mol) | Structure |
|---|---|---|
| **37** | 881.82 | 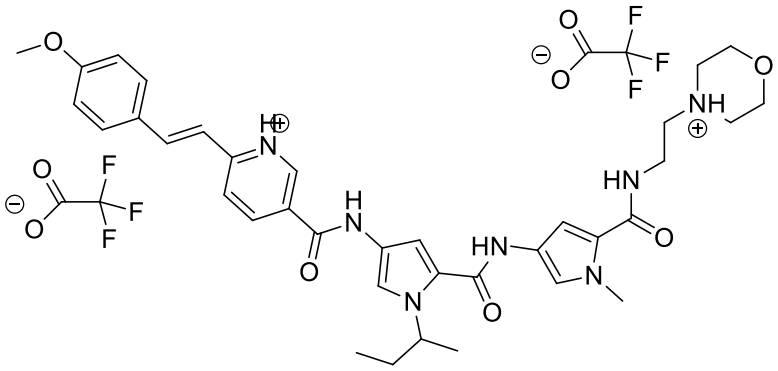 |
| **38** | 867.79 | 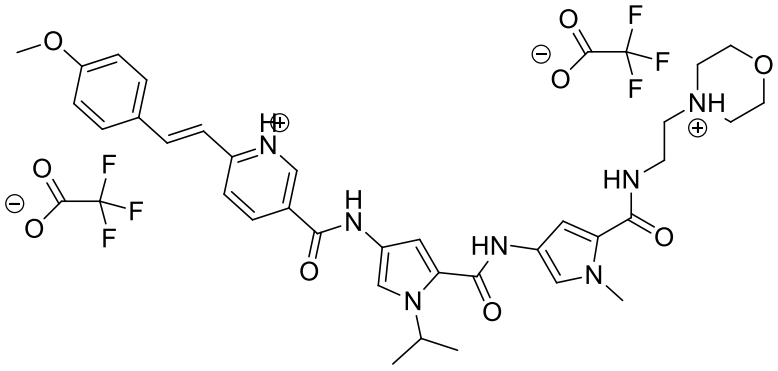 |
| **39** | 354.75 | 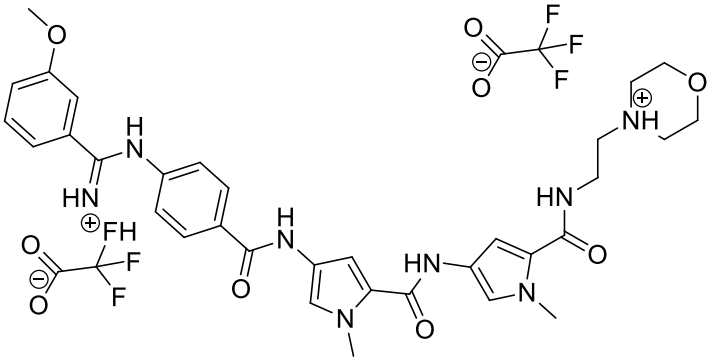 |
| **40** | 752.78 | 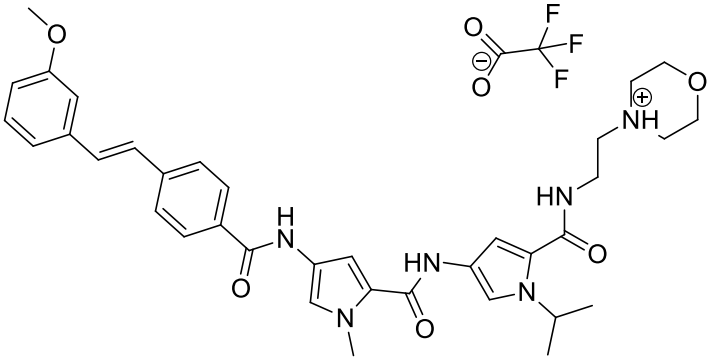 |

| MGB | MW (g/mol) | Structure |
|---|---|---|
| **41** | 773.66 | 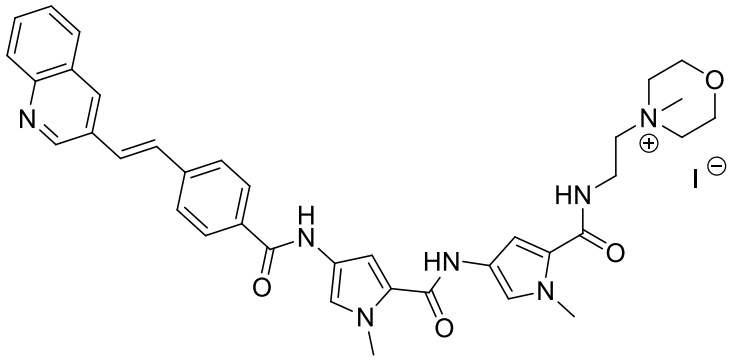 |
| **42** | 649.74 | 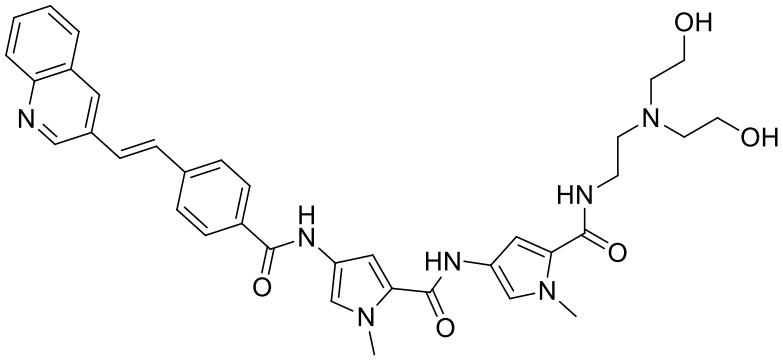 |
| **43** | 592.64 | 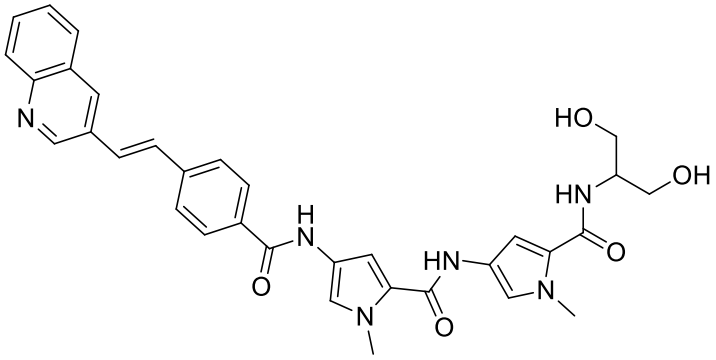 |
| **44** | 629.71 | 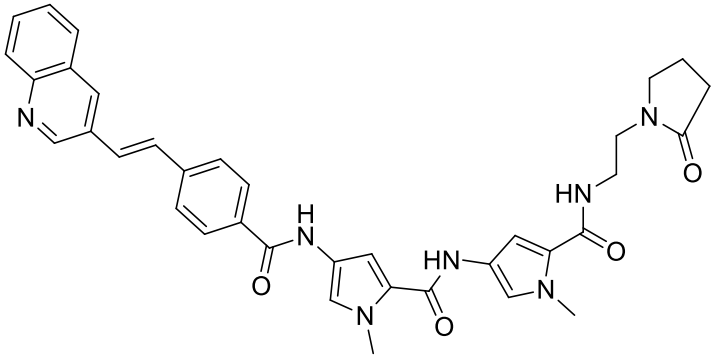 |

| MGB | MW (g/mol) | Structure |
|---|---|---|
| **45** | 626.70 | 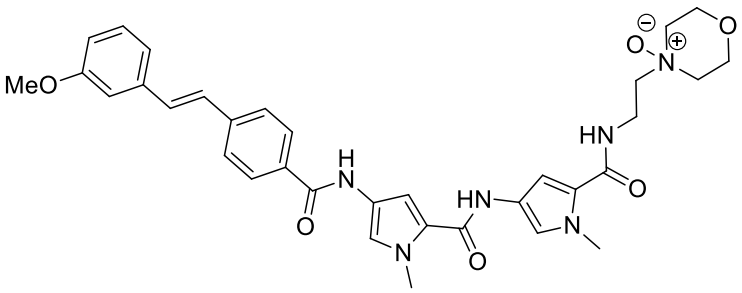 |
| **46** | 741.71 | 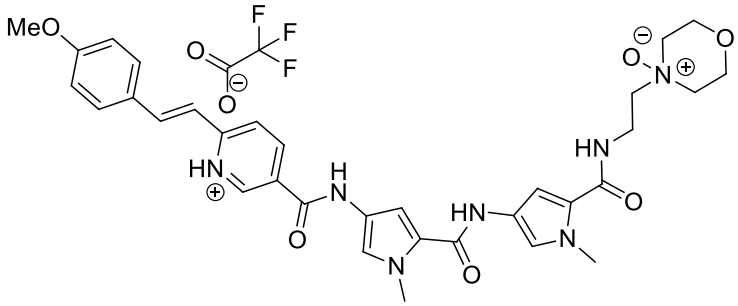 |
| **47** | 789.68 | 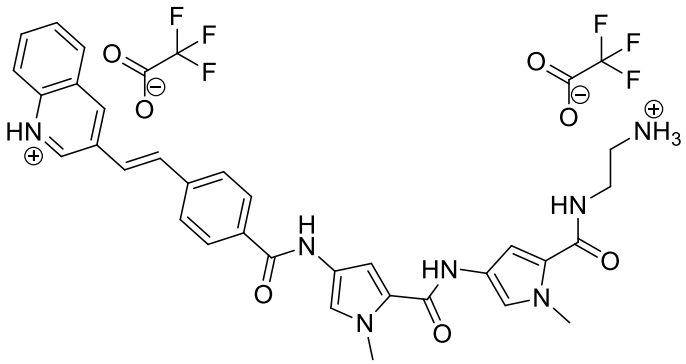 |
| **48** | 532.52 | 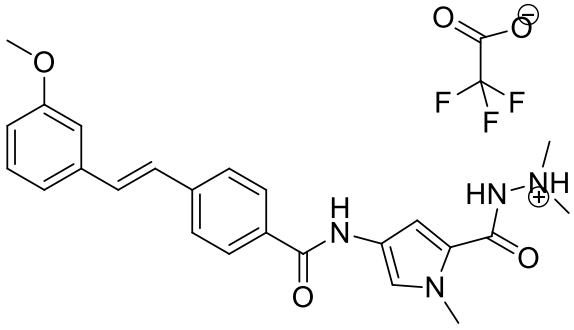 |

| MGB | MW (g/mol) | Structure |
|---|---|---|
| **49** | 602.60 | 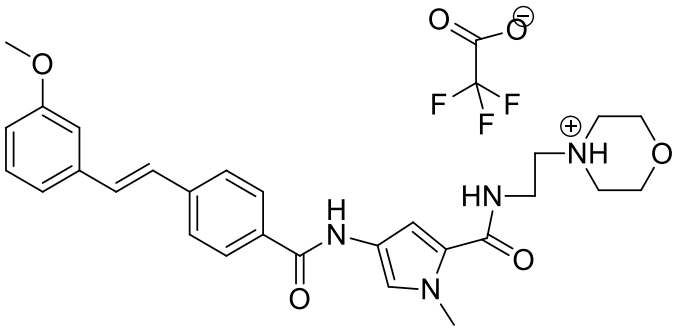 |
| **50** | 707.62 | 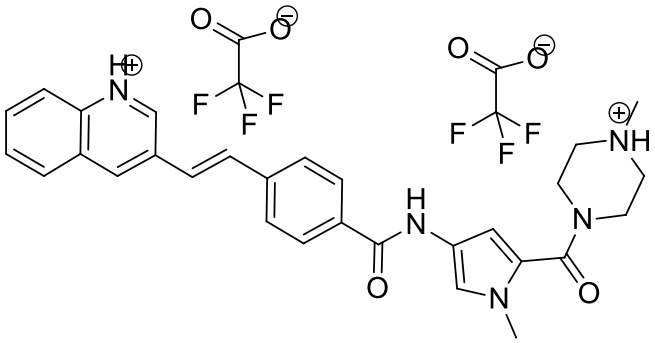 |
| **51** | 656.68 | 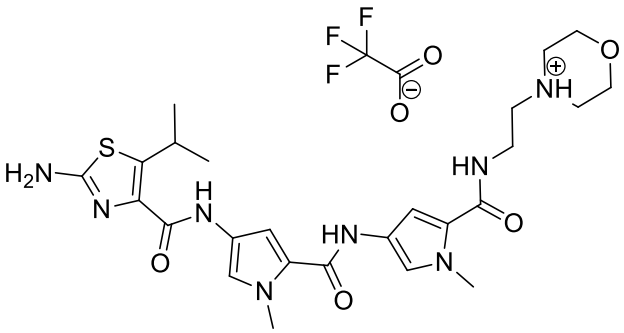 |
| **52** | 534.55 | 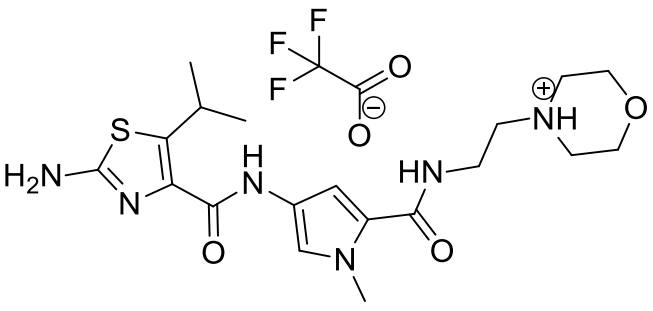 |

| MGB | MW (g/mol) | Structure |
|---|---|---|
| **53** | 737.65 | 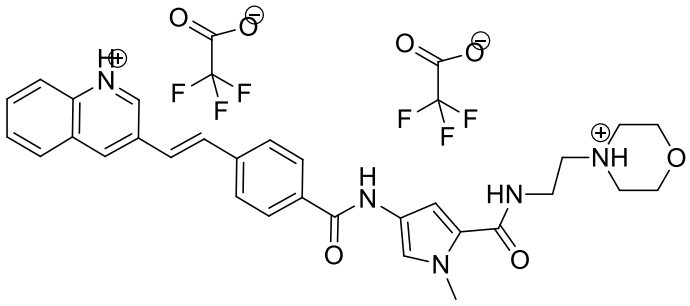 |
| **54** | 573.56 | 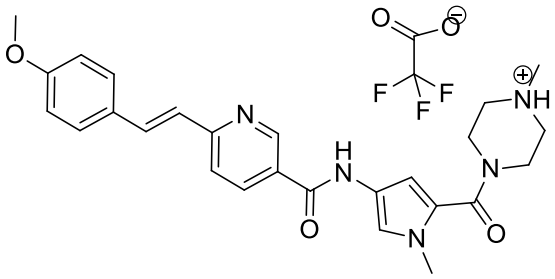 |
| **55** | 738.75 | 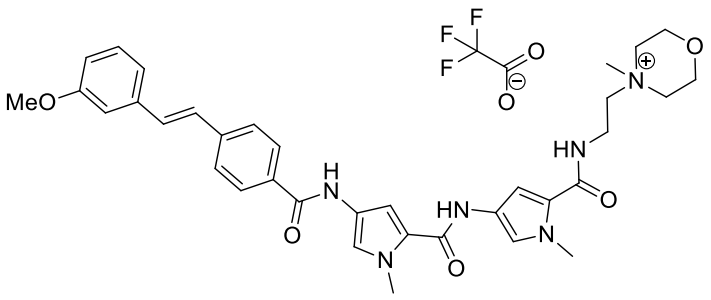 |
| **56** | 853.76 | 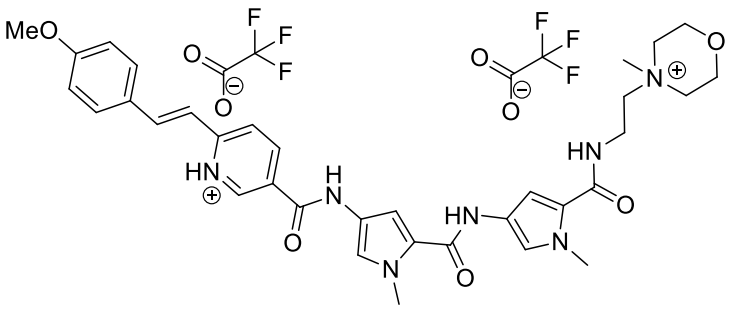 |

| MGB | MW (g/mol) | Structure |
|---|---|---|
| **58** | 761.74 | 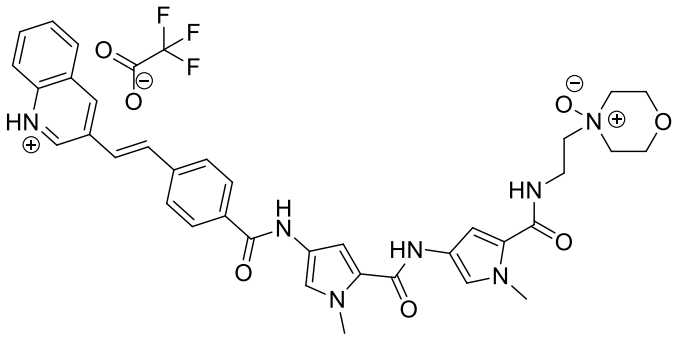 |
| **59** | 572.58 | 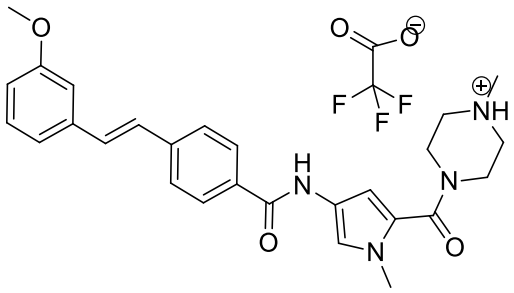 |
| **61** | 885.87 | 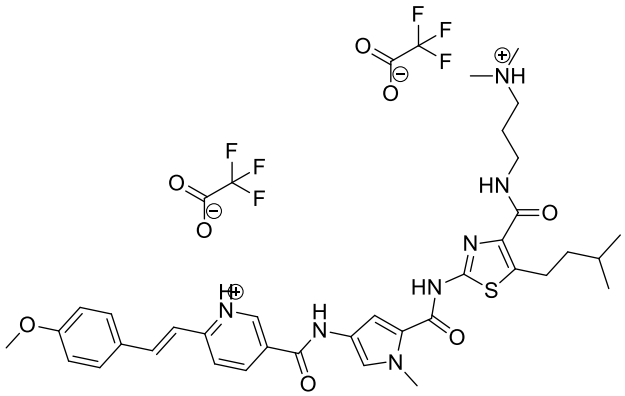 |
| **62** | 857.82 | 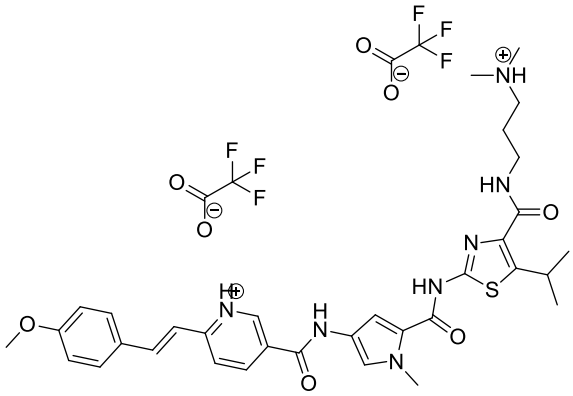 |

| MGB | MW (g/mol) | Structure |
|---|---|---|
| **63** | 917.92 | 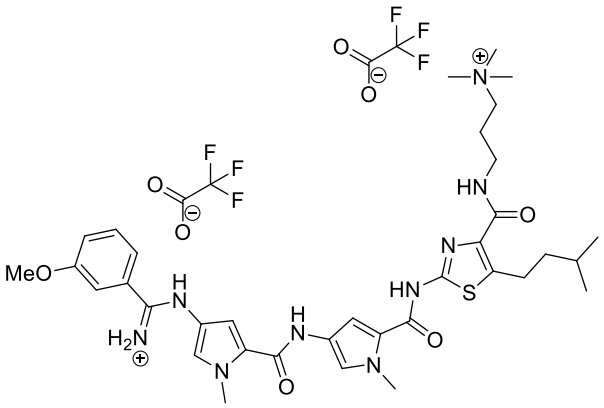 |
| **64** | 826.74 | 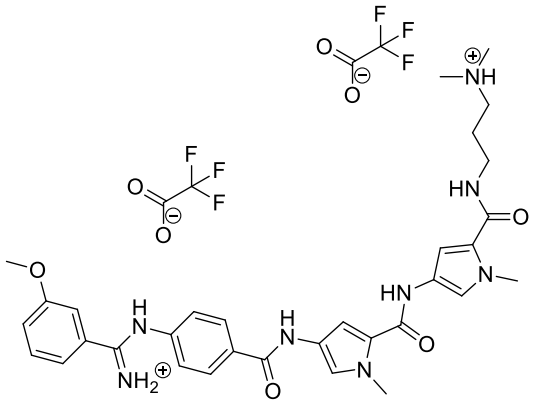 |
| **65** | 811.73 | 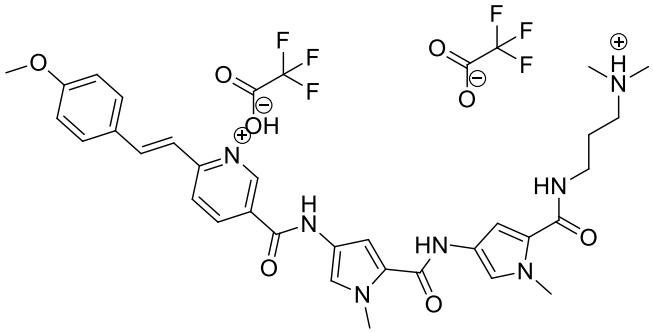 |
| **66** | 701.58 | 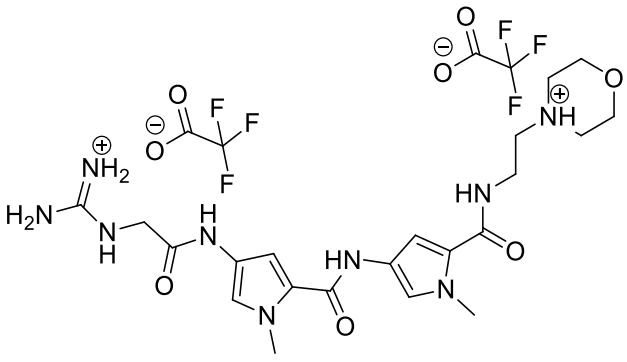 |

| MGB | MW (g/mol) | Structure |
|---|---|---|
| **67** | 650.60 | 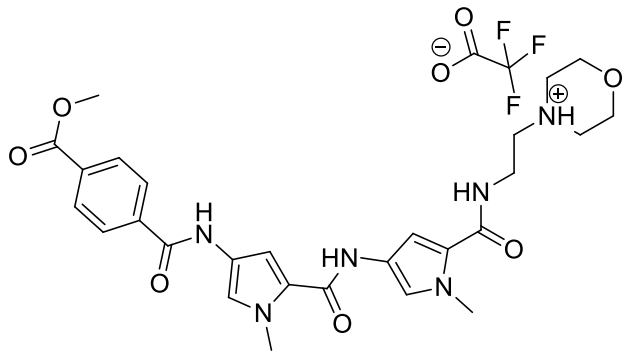 |
| **68** | 636.58 | 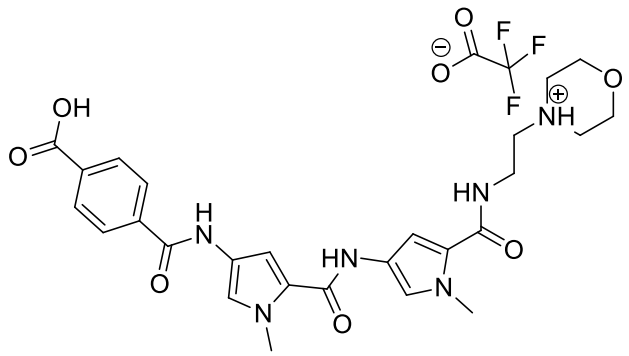 |
| **69** | 602.56 | 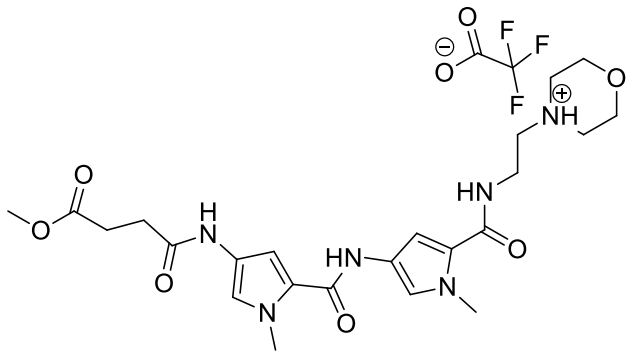 |
| **70** | 588.53 | 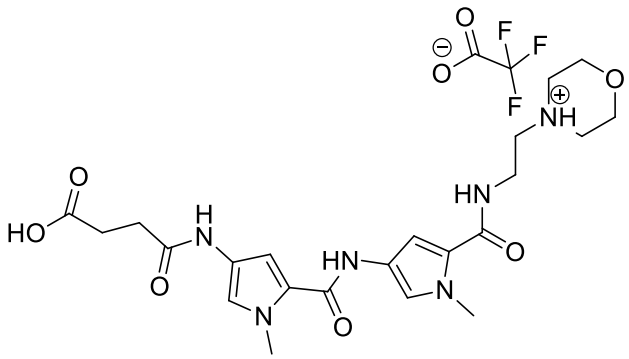 |

| MGB | MW (g/mol) | Structure |
|---|---|---|
| **71** | 559.50 | 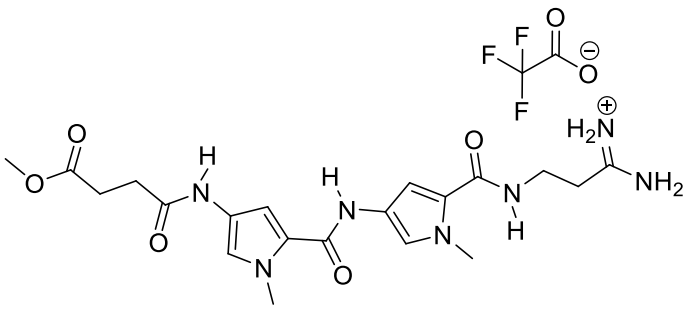 |
| **72** | 658.52 | 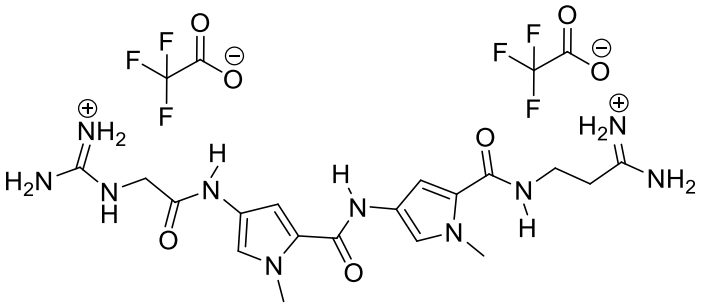 |
| **73** | 607.54 | 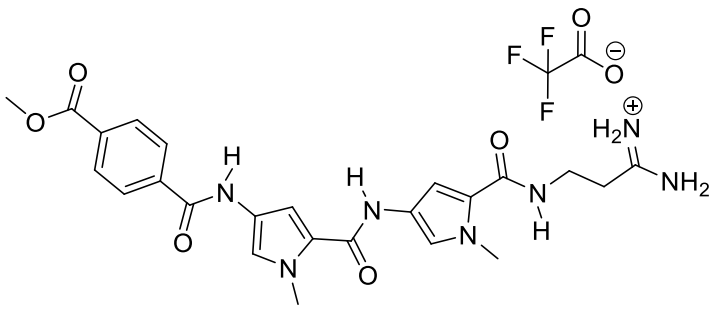 |
| **74** | 796.67 | 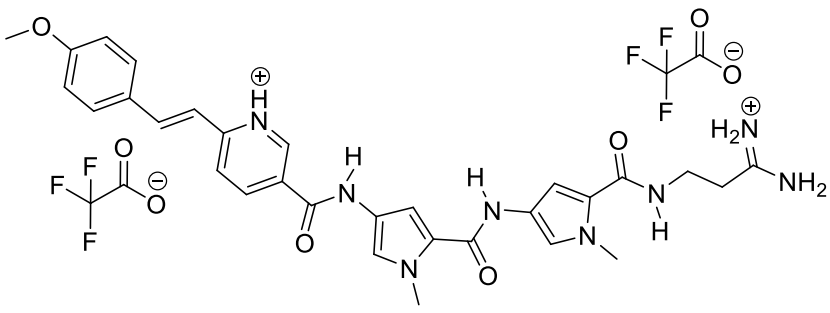 |

| MGB | MW (g/mol) | Structure |
|---|---|---|
| **75** | 681.66 | 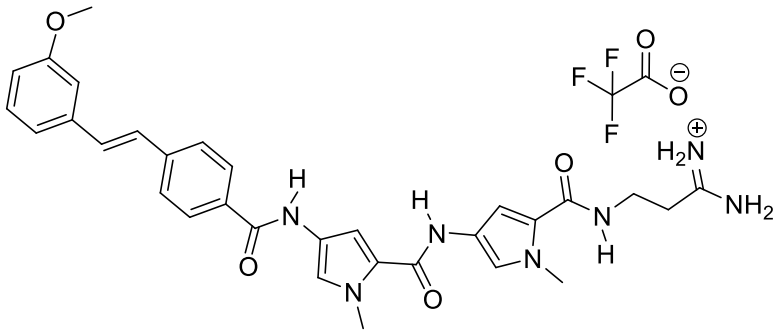 |
| **76** | 545.50 | 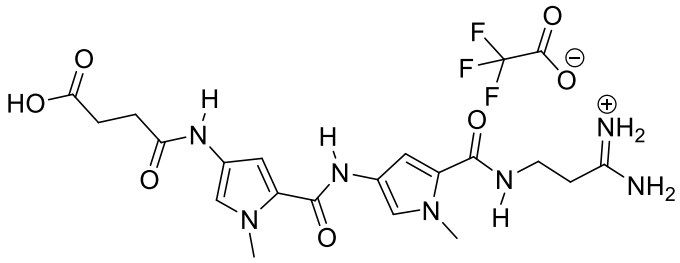 |
| **77** | 593.52 | 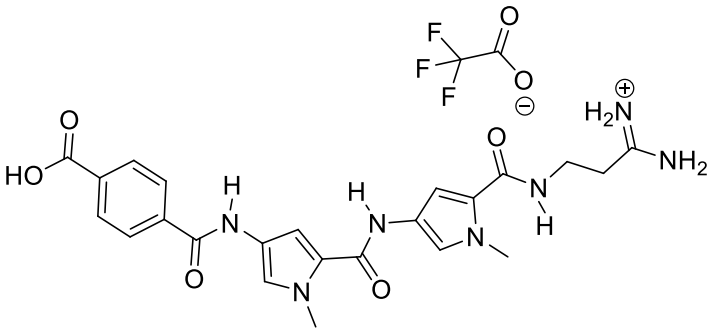 |
| **78** | 622.59 | 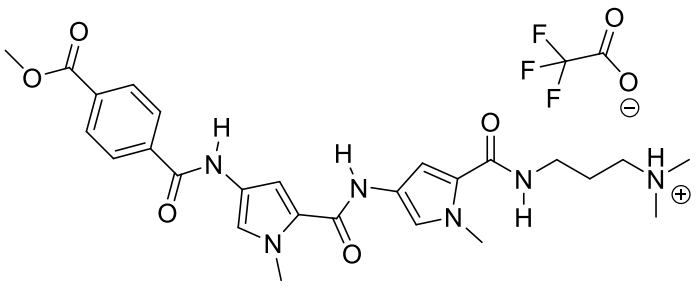 |

| MGB | MW (g/mol) | Structure |
|---|---|---|
| **79** | 673.57 | 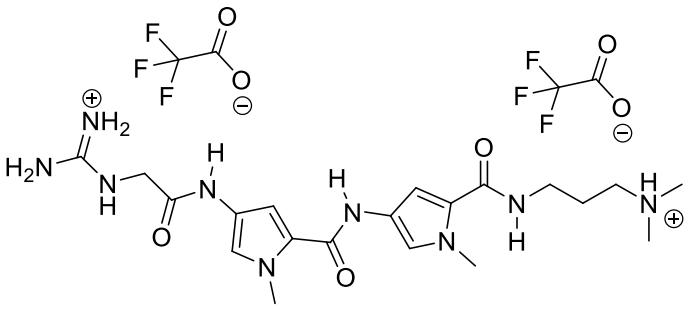 |
| **80** | 574.55 | 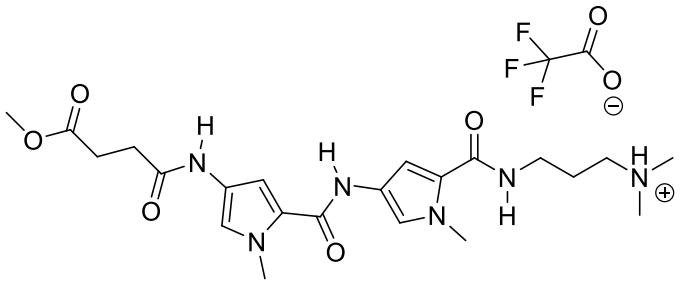 |
| **81** | 608.56 | 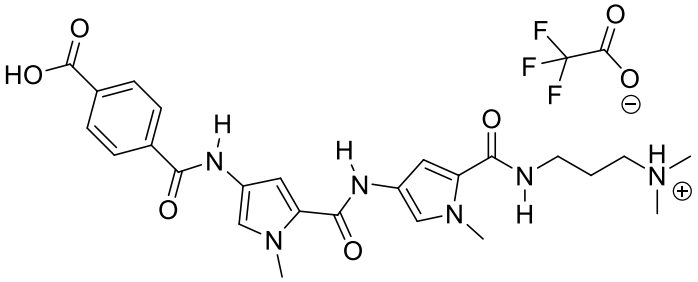 |
| **82** | 560.52 | 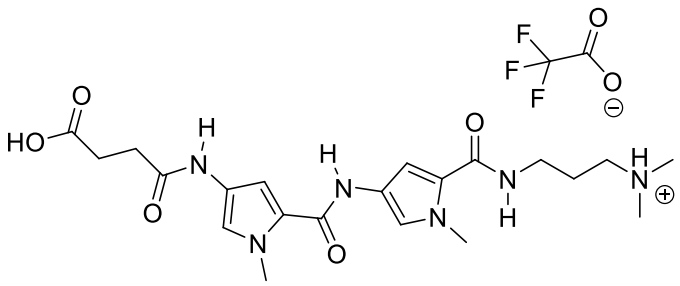 |

| MGB | MW (g/mol) | Structure |
|---|---|---|
| **83** | 696.72 | 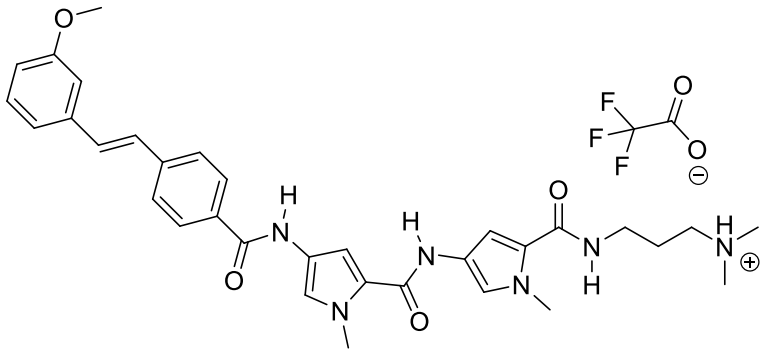 |
| **84** | 653.57 | 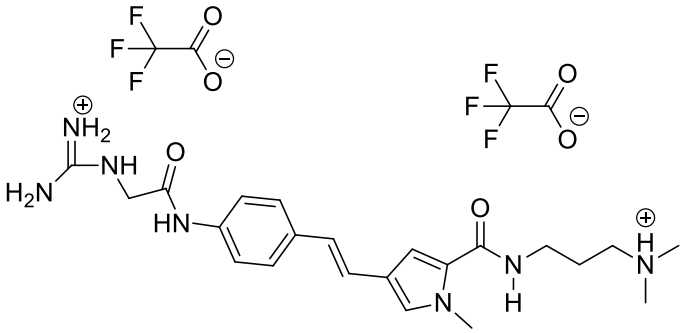 |
| **85** | 655.59 | 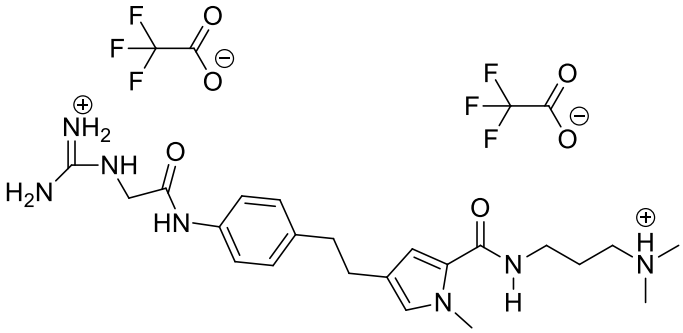 |
| **86** | 812.78 | 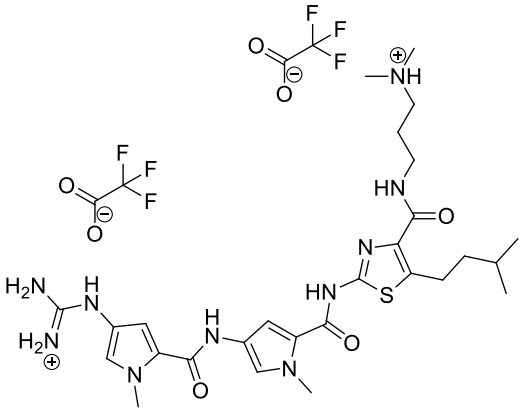 |

| MGB | MW (g/mol) | Structure |
|---|---|---|
| **87** | 804.84 | 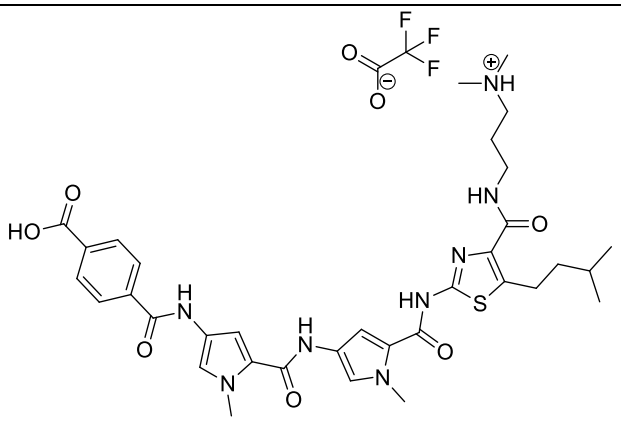 |
| **88** | 818.86 | 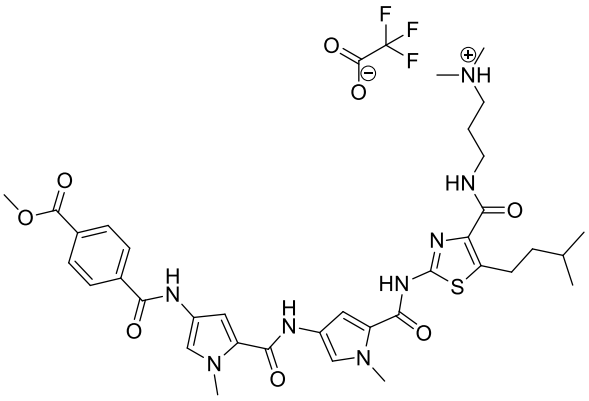 |
| **89** | 880.82 | 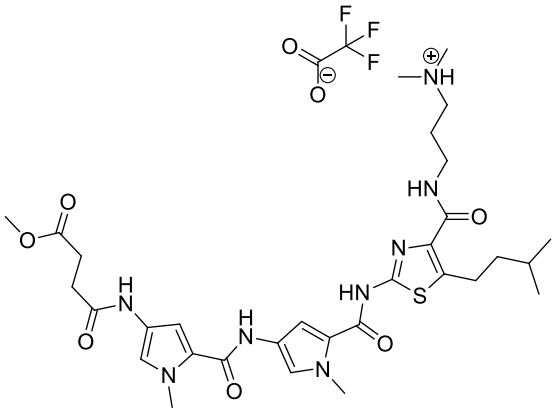 |
| **90** | 756.79 | 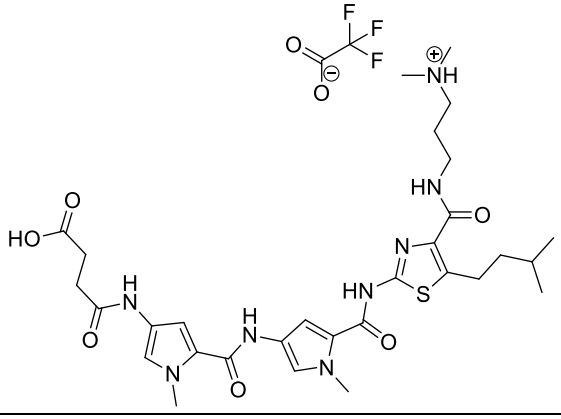 |

| MGB | MW (g/mol) | Structure |
|---|---|---|
| **91** | 869.84 | 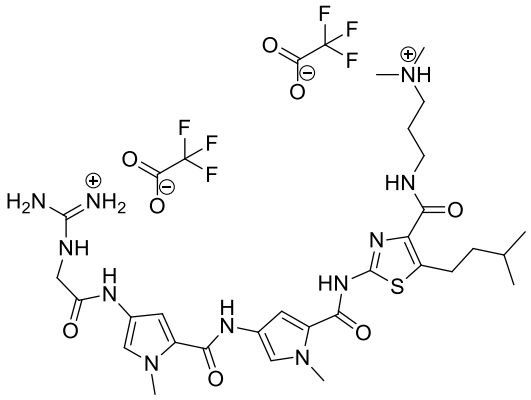 |
| **92** | 964.88 | 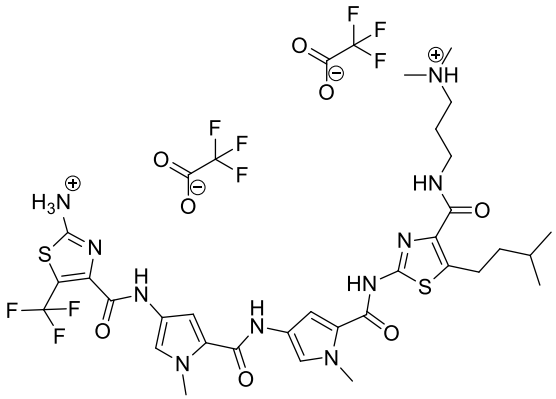 |
| **93** | 676.30 | 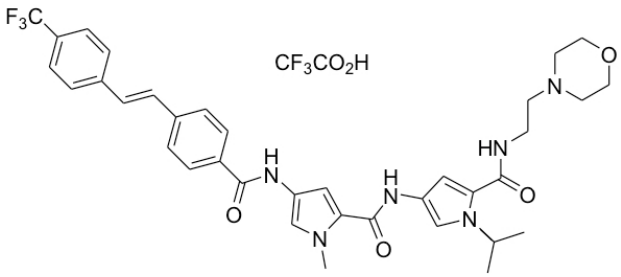 |

**Table A.2** Abbreviated structures of MGBs compounds studied together with lipophilicity measures by Log $D_{7.4}$, the head group link, number and type of heterocycles, tail groups and maxim number of carbons in the alkyl chains attached to the heterocycles (Figure 6.2). Abbreviations used: Ake, alkene; Ade, amide; Adi, amidine; Ane, amine; Cyg, cyanoguanidine; Dha, dihydroxyalkyl; Dmap, dimethylaminopropyl; Dmh, dimethylhydrazine; Mdmap, methylated dimethylaminopropyl; Mmor, methylated morpholine; Mor, morpholine; Omor, N-oxide morpholine; Nalk, nitro alkene; Pip, piperazine; Pyri, pyridine; Pyr, pyrrole; Pyol, pyrrolidine and Thz, thiazole.

| MGB | Head | Cycles | Pyr1 | Pyr2 | Pyr3 | Tail | Alkyl chains | Log $D_{7.4}$ |
|---|---|---|---|---|---|---|---|---|
| **1** | Adi | 3 | Pyr | Pyr | Thz | Dmap | 5 | 0.18 |
| **2** | Adi | 3 | Pyr | Pyr | Pyr | Dmap | 1 | -2.42 |
| **3** | Ade | 3 | Thz | Pyr | Pyr | Dmap | 3 | 2.77 |
| **4** | Ake | 3 | Ben | Pyr | Thz | Mor | 5 | 6.51 |
| **5** | Ake | 3 | Ben | Pyr | Thz | Mor | 5 | 7.56 |
| **6** | Ade | 3 | Pyr | Pyr | Pyr | Dmap | 3 | 1.90 |
| **7** | Ade | 4 | Pyr | Pyr/Pyr | Pyr | Dmap | 5 | 0.80 |
| **8** | Ade | 3 | Thz | Pyr | Pyr | Dmap | 5 | 4.97 |
| **9** | Ade | 3 | Thz | Pyr | Pyr | Dmap | 1 | 0.56 |
| **10** | Ake | 3 | Ben | Pyr | Pyr | Mor | 1 | 4.99 |
| **11** | Adi | 3 | Pyr | Pyr | Thz | Dmap | 3 | 2.22 |
| **12** | Ake | 3 | Ben | Pyr | Pyr | Mor | 1 | 3.15 |
| **13** | Ade | 3 | Pyr | Pyr | Pyr | Dmap | 3 | 2.39 |
| **14** | Ade | 3 | Pyr | Pyr | Pyr | Mor | 1 | 3.15 |
| **15** | Adi | 3 | Pyr | Pyr | Pyr | Mor | 1 | 1.48 |
| **16** | Adi | 3 | Pyr | Pyr | Thz | Dmap | 5 | 3.81 |
| **17** | Ake | 3 | Ben | Pyr | Pyr | Mor | 1 | 4.11 |
| **18** | Ake | 3 | Ben | Pyr | Pyr | Mor | 1 | 4.11 |
| **19** | Ake | 3 | Ben | Pyr | Pyr | Mor | 1 | 4.11 |
| **20** | Ade | 2 | Pyr | Pyr | - | Dmap | 1 | 2.59 |
| **21** | Ade | 3 | Pyr | Pyr | Pyr | Dmap | 1 | 1.08 |
| **22** | Ake | 3 | Ben | Pyr | Pyr | Mor | 1 | 3.86 |
| **23** | Ake | 3 | Ben | Pyr | Pyr | Mor | 1 | 4.85 |
| **24** | Adi | 3 | Pyr | Pyr | Thz | Dmap | 3 | 2.29 |
| **25** | Ake | 3 | Ben | Pyr | Pyr | Mor | 1 | 3.81 |
| **26** | Ake | 3 | Pyri | Pyr | Pyr | Mor | 1 | 2.83 |
| **27** | Ake | 3 | Ben | Pyr | Pyr | Mor | 1 | 4.13 |
| **28** | Adi | 3 | Pyr | Pyr | Thz | Dmap | 5 | 3.41 |
| **29** | Ake | 3 | Ben | Pyr | Pyr | Nalk | 1 | 3.90 |
| **30** | Ake | 3 | Ben | Pyr | Pyr | Cyg | 1 | 3.61 |
| **31** | Ake | 3 | Ben | Pyr | Pyr | Mor | 3 | 4.81 |
| **32** | Ake | 3 | Ben | Pyr | Pyr | Mor | 4 | 5.34 |
| **33** | Ake | 3 | Ben | Pyr | Pyr | Mor | 3 | 4.81 |
| **34** | Ake | 3 | Ben | Pyr | Pyr | Mor | 4 | 5.34 |
| **35** | Ake | 3 | Pyri | Pyr | Pyr | Mor | 3 | 3.51 |
| **36** | Ake | 3 | Pyri | Pyr | Pyr | Mor | 4 | 4.04 |

| MGB | Head | Cycles | Pyr1 | Pyr2 | Pyr3 | Tail | Alkyl chains | Log $D_{7.4}$ |
|---|---|---|---|---|---|---|---|---|
| **37** | Ake | 3 | Pyri | Pyr | Pyr | Mor | 4 | 4.04 |
| **38** | Ake | 3 | Pyri | Pyr | Pyr | Mor | 3 | 3.51 |
| **39** | Adi | 3 | Ben | Pyr | Pyr | Mor | 1 | 2.12 |
| **40** | Ake | 3 | Ben | Pyr | Pyr | Mor | 3 | 4.50 |
| **41** | Ake | 3 | Ben | Pyr | Pyr | Mmor | 1 | 4.04 |
| **42** | Ake | 3 | Ben | Pyr | Pyr | Dha | 1 | 2.24 |
| **43** | Ake | 3 | Ben | Pyr | Pyr | Dha | 1 | 2.52 |
| **44** | Ake | 3 | Ben | Pyr | Pyr | Pyol | 1 | 3.73 |
| **45** | Ake | 3 | Ben | Pyr | Pyr | Omor | 1 | 2.62 |
| **46** | Ake | 3 | Ben | Pyr | Pyr | Omor | 1 | 1.63 |
| **47** | Ake | 3 | Ben | Pyr | Pyr | Ane | 1 | 1.71 |
| **48** | Ake | 2 | Ben | Pyr | - | Dmh | 1 | 3.92 |
| **49** | Ake | 2 | Ben | Pyr | - | Mor | 1 | 4.06 |
| **50** | Ake | 2 | Ben | Pyr | - | Pip | 1 | 4.56 |
| **51** | Ane | 3 | Thz | Pyr | Pyr | Mor | 3 | 0.93 |
| **52** | Ane | 2 | Thz | Pyr | - | Mor | 3 | 1.27 |
| **53** | Ake | 2 | Ben | Pyr | - | Mor | 1 | 4.37 |
| **54** | Ake | 2 | Ben | Pyr | - | Pip | 1 | 3.26 |
| **55** | Ake | 3 | Ben | Pyr | Pyr | Mmor | 1 | -0.42 |
| **56** | Ake | 3 | Ben | Pyr | Pyr | Mmor | 1 | -1.41 |
| **58** | Ake | 3 | Ben | Pyr | Pyr | Omor | 1 | 2.93 |
| **59** | Ake | 2 | Ben | Pyr | - | Pip | 1 | 4.24 |
| **61** | Ake | 3 | Pyri | Pyr | Thz | Dmap | 5 | 3.83 |
| **62** | Ake | 3 | Pyri | Pyr | Thz | Dmap | 3 | 2.95 |
| **63** | Adi | 3 | Pyr | Pyr | Thz | Mdmap | 5 | 0.21 |
| **64** | Adi | 3 | Ben | Pyr | Pyr | Dmap | 1 | -1.74 |
| **65** | Ake | 3 | Pyri | Pyr | Pyr | Dmap | 1 | -1.13 |
| **66** | Ade | 2 | Pyr | Pyr | - | Mor | 1 | -3.96 |
| **67** | Ade | 2 | Pyr | Pyr | - | Mor | 1 | 1.55 |
| **68** | Ade | 2 | Pyr | Pyr | - | Mor | 1 | -2.05 |
| **69** | Ade | 2 | Pyr | Pyr | - | Mor | 1 | -0.34 |
| **70** | Ade | 2 | Pyr | Pyr | - | Mor | 1 | -3.79 |
| **71** | Ade | 2 | Pyr | Pyr | - | Adi | 1 | -3.56 |
| **72** | Ade | 2 | Pyr | Pyr | - | Adi | 1 | -7.18 |
| **73** | Ade | 2 | Pyr | Pyr | - | Adi | 1 | -1.67 |
| **74** | Ake | 3 | Pyri | Pyr | Pyr | Adi | 1 | -0.48 |
| **75** | Ake | 3 | Ben | Pyr | Pyr | Adi | 1 | 0.50 |
| **76** | Ade | 2 | Pyr | Pyr | - | Adi | 1 | -2.94 |
| **77** | Ade | 2 | Pyr | Pyr | - | Adi | 1 | -1.24 |
| **78** | Ade | 2 | Pyr | Pyr | - | Dmap | 1 | -0.05 |
| **79** | Ade | 2 | Pyr | Pyr | - | Dmap | 1 | -5.56 |
| **80** | Ade | 2 | Pyr | Pyr | - | Dmap | 1 | -1.94 |
| **81** | Ade | 2 | Pyr | Pyr | - | Dmap | 1 | -1.24 |

| MGB | Head | Cycles | Pyr1 | Pyr2 | Pyr3 | Tail | Alkyl chains | Log $D_{7.4}$ |
|---|---|---|---|---|---|---|---|---|
| **82** | Ade | 2 | Pyr | Pyr | - | Dmap | 1 | -2.93 |
| **83** | Ake | 3 | Ben | Pyr | Pyr | Dmap | 1 | 2.13 |
| **84** | Ade | 2 | Ben | Pyr | - | Dmap | 1 | -3.63 |
| **85** | Ade | 2 | Ben | Pyr | - | Dmap | 1 | -3.43 |
| **86** | Adi | 3 | Pyr | Pyr | Thz | Dmap | 1 | 1.47 |
| **87** | Ade | 3 | Ben | Pyr | Thz | Dmap | 5 | 1.84 |
| **88** | Ade | 3 | Ben | Pyr | Thz | Dmap | 5 | 3.04 |
| **89** | Ade | 3 | Ben | Pyr | Thz | Dmap | 5 | 1.15 |
| **90** | Ade | 3 | Ben | Pyr | Thz | Dmap | 5 | 0.16 |
| **91** | Adi | 3 | Ben | Pyr | Thz | Dmap | 5 | -2.47 |
| **92** | Ade | 3 | Ben | Pyr | Thz | Dmap | 5 | 2.94 |